frontiers | Research Topics

Community series in biology of C-reactive protein, volume II

Edited by
Alok Agrawal and Yi Wu

Published in
Frontiers in Immunology

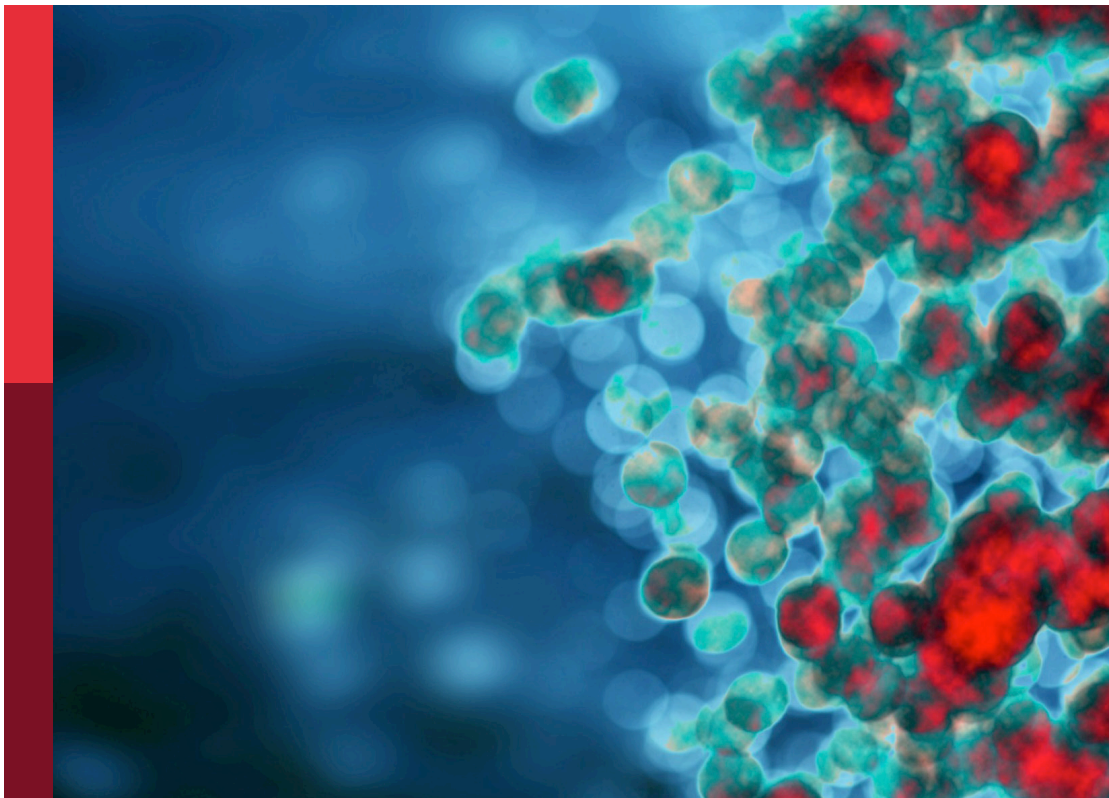

ISSN 1664-8714
ISBN 978-2-8325-7350-1
DOI 10.3389/978-2-8325-7350-1

Generative AI statement
Any alternative text (Alt text) provided alongside figures in the articles in this ebook has been generated by Frontiers with the support of artificial intelligence and reasonable efforts have been made to ensure accuracy, including review by the authors wherever possible. If you identify any issues, please contact us.

About Frontiers

Frontiers is more than just an open access publisher of scholarly articles: it is a pioneering approach to the world of academia, radically improving the way scholarly research is managed. The grand vision of Frontiers is a world where all people have an equal opportunity to seek, share and generate knowledge. Frontiers provides immediate and permanent online open access to all its publications, but this alone is not enough to realize our grand goals.

Frontiers journal series

The Frontiers journal series is a multi-tier and interdisciplinary set of open-access, online journals, promising a paradigm shift from the current review, selection and dissemination processes in academic publishing. All Frontiers journals are driven by researchers for researchers; therefore, they constitute a service to the scholarly community. At the same time, the *Frontiers journal series* operates on a revolutionary invention, the tiered publishing system, initially addressing specific communities of scholars, and gradually climbing up to broader public understanding, thus serving the interests of the lay society, too.

Dedication to quality

Each Frontiers article is a landmark of the highest quality, thanks to genuinely collaborative interactions between authors and review editors, who include some of the world's best academicians. Research must be certified by peers before entering a stream of knowledge that may eventually reach the public - and shape society; therefore, Frontiers only applies the most rigorous and unbiased reviews. Frontiers revolutionizes research publishing by freely delivering the most outstanding research, evaluated with no bias from both the academic and social point of view. By applying the most advanced information technologies, Frontiers is catapulting scholarly publishing into a new generation.

What are Frontiers Research Topics?

Frontiers Research Topics are very popular trademarks of the *Frontiers journals series*: they are collections of at least ten articles, all centered on a particular subject. With their unique mix of varied contributions from Original Research to Review Articles, Frontiers Research Topics unify the most influential researchers, the latest key findings and historical advances in a hot research area.

Find out more on how to host your own Frontiers Research Topic or contribute to one as an author by contacting the Frontiers editorial office: frontiersin.org/about/contact

Community series in biology of C-reactive protein, volume II

Topic editors

Alok Agrawal — Retired, Johnson City, United States

Yi Wu — Xi'an Jiaotong University, China

Citation

Agrawal, A., Wu, Y., eds. (2026). *Community series in biology of C-reactive protein, volume II*. Lausanne: Frontiers Media SA. doi: 10.3389/978-2-8325-7350-1

Table of contents

frontiers | Frontiers in Immunology

TYPE Editorial
PUBLISHED 18 December 2025
DOI 10.3389/fimmu.2025.1751020

OPEN ACCESS

EDITED AND REVIEWED BY
Francesca Granucci,
University of Milano-Bicocca, Italy

*CORRESPONDENCE
Alok Agrawal
avds_99@yahoo.com
Yi Wu
wuyi_med@xjtu.edu.cn

†PRESENT ADDRESS
Alok Agrawal,
Retired, Johnson City, TN, United States

RECEIVED 21 November 2025
ACCEPTED 10 December 2025
PUBLISHED 18 December 2025

CITATION
Agrawal A and Wu Y (2025)
Editorial: Community series in
biology of C-reactive protein, volume II.
Front. Immunol. 16:1751020.
doi: 10.3389/fimmu.2025.1751020

Editorial: Community series in biology of C-reactive protein, volume II

Alok Agrawal[1*†] and Yi Wu[2*]

[1]Department of Biomedical Sciences, College of Medicine, East Tennessee State University, Johnson City, TN, United States, [2]MOE Key Laboratory of Environment and Genes Related to Diseases, School of Basic Medical Sciences, Xi'an Jiaotong University, Xi'an, China

KEYWORDS

C-reactive protein, amyloidosis, pneumococcal infection, Fc receptors, biomarkers of inflammation

Editorial on the Research Topic
Community series in biology of C-reactive protein, volume II

C-reactive protein (CRP) is an evolutionarily conserved protein with pattern recognition receptor-like activities (1). Experiments performed *in vitro* and employing mouse models of human diseases have revealed that CRP possesses anti-bacterial, anti-atherosclerotic, anti-arthritic and anti-amyloidogenic activities (2–8). In addition to executing host-defense functions, CRP also serves as a biomarker of inflammation (9). This Research Topic includes nine articles: four of these articles report latest findings on the structure-function relationships of CRP and the other five articles cover the developments in the clinical utility of CRP.

CRP exists and is active in three different structural conformations: native pentameric CRP, monomeric CRP (mCRP) and intermediate or non-native or transitional or modified or loosened pentameric CRP (pCRP*) (10). The abbreviation CRP represents native pentameric CRP. Potempa et al. reviewed the literature on the three forms of CRP and re-evaluated their roles in the tissue repair processes and thereby resolving some controversies on the structure-function relationships of CRP.

It has been shown previously that CRP binds to Fcγ receptors (FcγR); neither the complexing of CRP with a ligand nor a conformational change in the native pentameric structure of CRP was required for CRP to bind to FcγRs (11, 12). Henning et al. thoroughly investigated the CRP-FcγR interactions by employing both CRP and mCRP in both free and immobilized forms. They found that both forms of immobilized CRP engaged both the activating and inhibitory FcγRs. Activation of FcγRs by fluid-phase CRP was considerably lower than with immobilized CRP but was enhanced in the presence of streptococci. Immobilization of CRP exposed mCRP epitopes, suggesting that pCRP*, not CRP, is the major FcγR-activating conformation.

The primary ligand-binding specificity of CRP is for phosphocholine (PCh)-containing substances such as cell wall C-polysaccharide of pneumococci. CRP has been shown to protect mice against lethal pneumococcal infection but only when CRP is administered to mice during the early stages of infection. Employing CRP-deficient mice in pneumococcal infection experiments, Agrawal et al. found that CRP was protective against late-stage

infection also; however, the protection against late-stage infection involved structural changes in CRP and subsequent binding of CRP to PCh and of structurally altered CRP to both PCh and amyloids present on the bacterial surface. In addition, their data also suggested that the amyloid-binding protein, serum amyloid P component, cooperated with CRP in reducing bacteremia and bacterial load in mice infected with pneumococci. The PCh-binding function of CRP has been conserved throughout evolution from arthropods to humans. However, it was not known whether the amyloid-binding function of structurally altered CRP has also been evolutionarily conserved. Agrawal et al. isolated arthropod CRP from American horseshoe crab *Limulus polyphemus* (Li-CRP) and investigated the anti-amyloidogenic activity of Li-CRP. They report that Li-CRP binds to amyloids and prevents the formation of amyloid fibrils, and unlike human CRP, Li-CRP does not require any changes in its overall structure to bind to amyloids. Their data further suggested that a variety of Li-CRP molecules of different subunit compositions were present in *Limulus* hemolymph, raising the possibility that the presence of various Li-CRP species in hemolymph facilitates the recognition of a range of proteins with differing amyloidogenicity. It was concluded that the binding of CRP to amyloids is also an ancient function of CRP. In invertebrates, the amyloid-binding function of CRP can protect the host from toxicity caused by amyloidogenic and pathogenic proteins. In humans, the amyloid-binding function of CRP can protect against inflammatory diseases in which the host proteins are ectopically deposited on either host cells or foreign cells in an inflammatory milieu since immobilized proteins may expose amyloid-like structures after deposition at places where they are not supposed to be.

Since the serum level of CRP rises in inflammatory states, serum CRP is used as a non-specific biomarker of inflammation. In this Research Topic, there are five reports on the use of CRP as a co-biomarker for specific diseases. Chen et al. investigated whether CRP could be used as a co-biomarker to improve the prediction of venous thromboembolism in patients with bladder cancer. They found that the combined model of elevated CRP and elevated D-Dimer levels offers superior predictive performance. Chen et al. investigated whether CRP could be used as a co-biomarker for predicting severity in acute pancreatitis. They report that the ratio of serum CRP to serum calcium levels is a novel biomarker for predicting severity in acute pancreatitis in their retrospective cross-sectional study. However, further multicenter prospective cohort studies are needed to confirm its clinical utility. Huang et al. performed a cross-sectional study and investigated whether CRP could be used as a co-biomarker for the prevalence of hyperuricemia in adults with diabetes or prediabetes. They found that an elevated CRP to high-density lipoprotein cholesterol ratio was significantly associated with a higher risk of hyperuricemia in adults with diabetes or prediabetes. Wu et al. investigated the association of CRP with hepatic fibrosis in US and Chinese patients with metabolic dysfunction-associated steatotic liver disease (MASLD) and assessed its predictive efficacy. They found a significant correlation between elevated CRP levels and increased risk of fibrosis and cirrhosis in US MASLD patients and between elevated CRP levels and hepatic fibrosis in Chinese MASLD patients. Finally, Xu et al. reviewed the published literature and performed meta-analysis of the data to compare the diagnostic accuracy of resistin and CRP levels for sepsis in neonates and children. They found that both CRP and resistin levels could be used as biomarkers for detecting pediatric and neonatal sepsis.

In summary, recent data indicate that the native pentameric structure of CRP is flexible and that the structural changes in CRP is a key mechanism for CRP to be protective against inflammatory diseases. Appropriately designed animal models can be used to further understand the conformation-dependent actions of CRP *in vivo* (1). Potempa et al. provides a review of the shortcomings of the currently available diagnostic tests for CRP and highlight the need for change in how CRP is currently utilized in clinical practice.

Author contributions

AA: Writing – original draft, Writing – review & editing. YW: Writing – review & editing, Writing – original draft.

Conflict of interest

The author(s) declared that this work was conducted in the absence of any commercial or financial relationships that could be construed as a potential conflict of interest.

The author(s) declared that AA and YW were an editorial board member of Frontiers, at the time of submission. This had no impact on the peer review process and the final decision.

Generative AI statement

The author(s) declared that generative AI was not used in the creation of this manuscript.

Any alternative text (alt text) provided alongside figures in this article has been generated by Frontiers with the support of artificial intelligence and reasonable efforts have been made to ensure accuracy, including review by the authors wherever possible. If you identify any issues, please contact us.

Publisher's note

References

1. Ji S-R, Zhang S-H, Chang Y, Li H-Y, Wang M-Y, Lv J-M, et al. C-reactive protein: The most familiar stranger. *J Immunol*. (2023) 210:699–707. doi: 10.4049/jimmunol.2200831

2. Ngwa DN, Agrawal A. Structure-function relationships of C-reactive protein in bacterial infection. *Front Immunol.* (2019) 10:166. doi: 10.3389/fimmu.2019.00166

3. Chen D, Hu J, Zhu M, Xie Y, Yao H, An H, et al. C-reactive protein is a broad-spectrum capsule-binding receptor for hepatic capture of blood-borne bacteria. *EMBO J*. (2025). doi: 10.1038/s44318-025-00623-w

4. Agrawal A, Ngwa DN, Simons JP, Singh SK. Protection against prolonged pneumococcal infection involves structural changes in C-reactive protein and subsequent binding to both phosphocholine and amyloids on the pneumococcal surface. *Front Immunol*. (2025) 16:1631409.

5. Pathak A, Singh SK, Thewke DP, Agrawal A. Conformationally altered C-reactive protein capable of binding to atherogenic lipoproteins reduces atherosclerosis. *Front Immunol*. (2020) 11:1780. doi: 10.3389/fimmu.2020.01780

6. Singh SK, Prislovsky A, Ngwa DN, Munkhsaikhan U, Abidi AH, Brand DD, et al. C-reactive protein lowers the serum level of IL-17, but not TNF-a, and decreases the incidence of collagen-induced arthritis in mice. *Front Immunol*. (2024) 15:1385085. doi: 10.3389/fimmu.2024.1385085

7. Ngwa DN, Agrawal A. Structurally altered, not wild-type, pentameric C-reactive protein inhibits formation of amyloid-b fibrils. *J Immunol*. (2022) 209:1180–8. doi: 10.4049/jimmunol.2200148

8. Liu C, Huang X, Huang Y, Jin H. Mendelian randomization analysis: The causal relationship between C-reactive protein and amyloidosis and between C-reactive protein and atherosclerosis. *PloS One*. (2025) 20:0329612. doi: 10.1371/journal.pone.0329612

9. Gabay C, Kushner I. Acute-phase proteins and other systemic responses to inflammation. *N Engl J Med*. (1999) 340:448–54. doi: 10.1056/NEJM199902113400607

10. McFadyen JD, Zeller J, Potempa LA, Pietersz GA, Eisenhardt SU, Peter K. C-reactive protein and its structural isoforms: An evolutionary conserved marker and central player in inflammatory diseases and beyond. *Subcell Biochem*. (2020) 94:499–520.

11. Lu J, Marjon KD, Mold C, Du Clos TW, Sun PD. Pentraxins and fc receptors. *Immunol Rev*. (2012) 250:230–8. doi: 10.1111/j.1600-065X.2012.01162.x

12. Feng J-R, Li X, Han C, Chang Y, Fu Y, Feng G-C, et al. C-reactive protein induces immunosuppression by activating FcgRIIB in pulmonary macrophages to promote lung metastasis. *Cancer Res*. (2024) 84:4184–98. doi: 10.1158/0008-5472.CAN-24-0253

frontiers | Frontiers in Immunology

TYPE Original Research
PUBLISHED 16 September 2024
DOI 10.3389/fimmu.2024.1466865

OPEN ACCESS

EDITED BY
Liwu Li,
Virginia Tech, United States

REVIEWED BY
Alessandra Zarantonello,
University of Copenhagen, Denmark
Swathy Sajja,
New York University, United States

*CORRESPONDENCE
Sanjay K. Singh
singhs@etsu.edu
Alok Agrawal
avds_99@yahoo.com

†PRESENT ADDRESS
Alok Agrawal,
Retired, Johnson City, TN, United States
Asmita Pathak,
Department of Molecular and Cellular Pharmacology, Miller School of Medicine, University of Miami, Miami, FL, United States

RECEIVED 18 July 2024
ACCEPTED 28 August 2024
PUBLISHED 16 September 2024

CITATION
Agrawal A, Pathak A, Ngwa DN, Thirumalai A, Armstrong PB and Singh SK (2024) An evolutionarily conserved function of C-reactive protein is to prevent the formation of amyloid fibrils.
Front. Immunol. 15:1466865.
doi: 10.3389/fimmu.2024.1466865

An evolutionarily conserved function of C-reactive protein is to prevent the formation of amyloid fibrils

Alok Agrawal[1*†], Asmita Pathak[1†], Donald N. Ngwa[1], Avinash Thirumalai[1], Peter B. Armstrong[2] and Sanjay K. Singh[1*]

[1]Department of Biomedical Sciences, Quillen College of Medicine, East Tennessee State University, Johnson City, TN, United States, [2]Marine Biological Laboratory, Woods Hole, MA, United States

C-reactive protein (CRP) binds to phosphocholine (PCh)-containing substances and subsequently activates the complement system to eliminate the ligand. The PCh-binding function of CRP has been conserved throughout evolution from arthropods to humans. Human CRP, in its structurally altered conformation at acidic pH, also binds to amyloid-β (Aβ) and prevents the formation of Aβ fibrils. It is unknown whether the Aβ-binding function of CRP has also been evolutionarily conserved. The aim of this study was to determine whether CRP isolated from American horseshoe crab *Limulus polyphemus* was also anti-amyloidogenic and whether this function required structural alteration of *Limulus* CRP (Li-CRP). Two CRP species Li-CRP-I and Li-CRP-II were purified from hemolymph by employing PCh-affinity chromatography and phosphoethanolamine-affinity chromatography, respectively. Both Li-CRP-I and Li-CRP-II bound to immobilized Aβ at physiological pH. Unlike human CRP, Li-CRP did not require any changes in its overall structure to bind to Aβ. Both Li-CRP-I and Li-CRP-II bound to Aβ in the fluid phase also and prevented the fibrillation of Aβ. Additionally, ion-exchange chromatography of purified Li-CRP indicated that a variety of Li-CRP molecules of different subunit compositions were present in *Limulus* hemolymph, raising the possibility that the presence of various Li-CRP species in hemolymph facilitates the recognition of a range of proteins with differing amyloidogenicity. We conclude that the binding of CRP to Aβ is an ancient function of CRP. In invertebrates, the Aβ-binding function of CRP can protect the host from toxicity caused by amyloidogenic and pathogenic proteins. In humans, the Aβ-binding function of CRP can protect against inflammatory diseases in which the host proteins are ectopically deposited on either host cells or foreign cells in an inflammatory milieu since immobilized proteins may expose Aβ-like structures after deposition at places where they are not supposed to be.

KEYWORDS

C-reactive protein, *Limulus polyphemus*, American horseshoe crab, amyloidosis, protein toxicity

Introduction

C-reactive protein (CRP) is characterized by its ability to bind to phosphocholine (PCh) or to both PCh and phosphoethanolamine (PEt) in a Ca^{2+}-dependent manner (1–6). Human CRP is encoded by a single gene producing a non-glycosylated polypeptide of 206 amino acid residues and is a cyclic pentamer of five identical non-covalently attached subunits (7). The molecular weights of the pentamer and subunits are ~115 kDa and ~23 kDa, respectively. The interfaces of the CRP pentamer are flexible (8–10). Human CRP also has the ability to multimerize as a stack of two pentamers in the presence of zinc ions or high levels of NaCl (10–12).

Human CRP functions in two different conformations: as a native pentamer at physiological pH and as a non-native pentamer at acidic pH (13). When exposed to acidic pH, the native pentameric conformation of CRP is altered (8, 10, 14–17). Such non-native pentameric CRP is also generated by exposure of native CRP to H_2O_2 (16, 18). Native CRP binds primarily to PCh-containing substances and subsequently activates the complement system to eliminate the ligand (19, 20). Non-native CRP binds to amyloid-β peptide 1-42 (Aβ) and to Aβ-like structures displayed on immobilized, denatured and aggregated proteins, in addition to retaining the ability to bind to PCh (15, 21–24). It has also been recently shown that non-native pentameric CRP binds to Aβ in the fluid phase, subsequently preventing their fibrillation (21). Thus, human CRP is an anti-amyloidogenic protein; however, an inflammatory milieu and subsequent conformational changes in native CRP are required for human CRP to be anti-amyloidogenic.

CRP has been conserved throughout evolution (25–27). The earliest known CRP is reported from arthropods American horseshoe crab *Limulus polyphemus* (28), Japanese horseshoe crab *Tachypleus tridentatus* (29) and South Asian horseshoe crab *Carcinoscorpius rotundicauda* (30). CRP has also been isolated and characterized from the mollusk *Achatina fulica* (31, 32). It is unknown whether the anti-amyloidogenic function of human CRP has been evolutionarily conserved and whether CRP from invertebrates exhibits structure-based ligand-binding properties.

CRP from *L. polyphemus* which diverged from the vertebrate lineage ~500 million years ago (35) has been previously investigated in greater detail (28, 33–38): *Limulus* CRP (Li-CRP) is encoded by three homologous genes producing three types of subunits (34). All three subunit types have 218 amino acid residues and are present approximately in equimolar amounts (35). They also share an identical N-terminal sequence of 44 amino acid residues and an identical C-terminal sequence of 13 amino acid residues (35). There is only 10% microheterogeneity amongst the rest of the amino acid sequences. There are six half-cystines that form the three intrachain disulfide bonds in all subunits (35). The positions of six half-cystines are constant in all subunits. All three types of subunits are glycosylated although the glycosylation is variable (35). The sites of glycosylation are also constant in all three subunits. Each type of subunit forms a hexagonal structure as revealed by electron microscopy and two hexamers are stacked together to form the Li-CRP dodecamer. The molecular weights of Li-CRP dodecamer and subunits are ~300 kDa and ~25 kDa, respectively (36). Thus, there are twelve subunits in each Li-CRP molecule. Each type of subunit binds to both PCh and PEt in a Ca^{2+}-dependent manner (34). There is no immunological cross-reactivity between Li-CRP and human CRP (28, 39).

There are two other proteins similar to Li-CRP present in *Limulus* hemolymph. One has been named human serum amyloid P component (SAP)-like protein which has an affinity for PEt and carbohydrate moieties but not PCh (33, 40–42). The N-terminal amino acid sequences of Li-CRP and SAP-like protein are different. The first ten N-terminal amino acid residues of Li-CRP are LEEGEITSKV/I and of SAP-like protein are AVDIRDVKIS (34, 35, 41). The other protein similar to Li-CRP in hemolymph has been named limulin which binds to fetuin or sialic acid (28, 33, 43–45).

The aim of this study was to determine whether Li-CRP was an anti-amyloidogenic protein like human CRP and whether this function of Li-CRP required acidic pH. Since Li-CRP is known to bind to both PCh and PEt, we isolated Li-CRP from the hemolymph employing two different affinity chromatography methods. Li-CRP isolated by PCh-affinity chromatography was named Li-CRP-I and Li-CRP isolated by PEt-affinity chromatography was named Li-CRP-II. Both CRP species, Li-CRP-I and Li-CRP-II, were then characterized and investigated for their effects on Aβ fibrillation.

Materials and methods

Purification of human CRP

Human CRP was purified from discarded body fluids employing PCh-affinity chromatography, exactly as described previously (46).

Purification of Li-CRP-I and Li-CRP-II

Limulus hemolymph was obtained from Marine Biological Laboratory. Li-CRP was purified from the hemolymph as described previously, with some modifications (33). Hemolymph was first centrifuged at 15,000 g for 15 min to collect the clear blue plasma. The plasma was passed through a Sepharose 4B (MilliporeSigma, 4B200) column in 10 mM Tris-HCl, pH 7.2, containing 150 mM NaCl (TBS) and 2 mM $CaCl_2$ to remove carbohydrate-binding proteins. Next, polyethylene glycol-8000 was added to the plasma at a final concentration of 3% and incubated at 4°C for 16 h with shaking to remove hemocyanin. The plasma was then centrifuged at 30,000 g for 30 min. The blue pellet was discarded, and the transparent plasma was recovered and used to purify Li-CRP by employing two different affinity chromatography methods, as follows.

Abbreviations: Aβ, Amyloid-β peptide 1-42; CRP, C-reactive protein; Li-CRP, *Limulus* CRP (I + II); Li-CRP-I, Li-CRP purified by PCh-affinity chromatography; Li-CRP-II, Li-CRP purified by PEt-affinity chromatography; PCh, phosphocholine; PEt, phosphoethanolamine; PnC, pneumococcal C-polysaccharide; SAP, serum amyloid P component; TBS, 10 mM Tris-HCl, pH 7.2, containing 140 mM NaCl; TBS-Ca, TBS containing 0.1% gelatin, 0.02% Tween-20 and 2 mM $CaCl_2$; ThT, Thioflavin T; WT, wild-type.

Method 1: Li-CRP was isolated from plasma by employing Ca^{2+}-dependent PCh-affinity chromatography as described previously for purification of human CRP (46). Briefly, plasma was passed through a PCh-Sepharose column in a Ca^{2+}-containing buffer. After washing the column, Li-CRP was eluted by using EDTA. The EDTA eluate was concentrated and Li-CRP was further purified by using gel filtration chromatography on a Superose 12 column in TBS containing 5 mM EDTA. Fractions containing Li-CRP were pooled and dialyzed against TBS containing 2 mM $CaCl_2$. This preparation of pure Li-CRP which involved purification by PCh-affinity chromatography was named Li-CRP-I.

Method 2: Li-CRP was isolated from plasma by employing Ca^{2+}-dependent PEt-affinity chromatography as described previously for purification of recombinant human CRP mutants (46). Briefly, plasma was passed through a PEt-Sepharose column in a Ca^{2+}-containing buffer. After washing the column, Li-CRP was eluted by EDTA. The EDTA eluate was concentrated and Li-CRP was further purified as described above in method 1. This preparation of pure Li-CRP which involved purification by PEt-affinity chromatography was named Li-CRP-II.

The purity of Li-CRP preparations was determined by using denaturing SDS-PAGE under reducing conditions in a 4-20% gradient gel and by N-terminal sequencing. The N-terminal amino acid sequencing of Li-CRP was performed at the Molecular Structure Facility, University of California, Davis. The concentrations of Li-CRP-I and Li-CRP-II were determined by using the extinction coefficient of 15.49 at A_{280} (36).

Determination of the overall structure of Li-CRP

The molecular weight of native Li-CRP was determined by employing gel filtration chromatography on a calibrated Superose 12 column (10/300 GL, GE healthcare), as described previously for human CRP (46). The gel filtration column was equilibrated with TBS containing 5 mM EDTA. Li-CRP was injected into the column and eluted with TBS containing 5 mM EDTA at a flow rate of 0.3 ml/min. Fractions (60 fractions, 250 µl each) were collected and absorbance at 280 nm measured to locate the elution volume of Li-CRP. The molecular weight of the subunits of Li-CRP was determined by employing denaturing SDS-PAGE under reducing conditions in a 4-20% gradient gel. The composition of Li-CRP was further evaluated by employing anion exchange chromatography on a MonoQ column (5/50 GL, GE healthcare), as described previously for human CRP (46). The fractions collected after the chromatography were subjected to denaturing SDS-PAGE under reducing conditions in a 4-20% gradient gel.

Deglycosylation of Li-CRP

Deglycosylation of Li-CRP was performed using the Glycoprofile IV Chemical Deglycosylation kit (MilliporeSigma, PP0510) according to manufacturer's instructions. Briefly, 150 µl of chilled trifluoromethanesulfonic acid (MilliporeSigma, 34781-7) was added to 1 mg of cold lyophilized Li-CRP and incubated on ice for 25 min with occasional shaking. Bromophenol blue (0.2%; 4 µl) was added to the reaction followed by dropwise addition of 60% pyridine solution (MilliporeSigma, P5496) in a methanol-dry ice bath until the color of the reaction changed from red to light purple or blue. Samples were then dialyzed against TBS overnight. The deglycosylation of Li-CRP was verified and the molecular weight of the deglycosylated subunits determined by employing denaturing SDS-PAGE under reducing conditions in a 4-20% gradient gel.

Generation of polyclonal anti-Li-CRP-I antibodies

Li-CRP-I was purified as described above. Rabbit polyclonal antibodies against purified Li-CRP-I were generated commercially by Thermo Fisher Scientific. The antiserum obtained from the company was used as such after titrating to determine the dilution to be used in the assays.

Immunological cross-reactivity assay

The immunological cross-reactivity between Li-CRP-I and Li-CRP-II was determined by employing anti-Li-CRP-I antibodies and purified Li-CRP-I and Li-CRP-II, as follows. Microtiter wells were coated with increasing amounts of Li-CRP-I or Li-CRP-II and incubated at 37°C for 2 h. The unreacted sites in the wells were blocked with TBS containing 0.5% gelatin for 45 min at room temperature. Next, anti-Li-CRP-I antibodies diluted in TBS was added to the wells and incubated at 37°C for 1 h. HRP-conjugated donkey anti-rabbit IgG, diluted in TBS, was used as the secondary antibody. Color was developed using ABTS as the substrate and the OD was read at 405 nm in a microtiter plate reader.

PCh-binding assay

Binding activity of Li-CRP for PCh was measured by using pneumococcal C-polysaccharide (PnC; purchased from Statens Serum Institut) as the PCh-containing ligand, exactly as described previously (9).

Preparation of Aβ peptides, monomers and fibrils

Lyophilized Aβ peptide 1-42 was purchased from Bachem (H-1368) and reconstituted according to manufacturer's instructions. Reconstituted Aβ peptide solution should contain Aβ monomers; however, oligomers of Aβ monomers are also present in the reconstituted Aβ peptide solution (47). Aβ monomers were prepared from Aβ peptides according to a published method (48) and exactly as described previously (21). In brief, lyophilized Aβ peptides were dissolved in hexafluoroisopropanol (MilliporeSigma) and incubated at 37°C for 2 h for monomerization of the oligomers present in the Aβ peptide solution. After removing hexafluoroisopropanol by evaporation overnight, the vials containing the film of Aβ monomers were stored at -20°C. Aβ fibrils were prepared from Aβ peptides according to a published method (48) and exactly as described previously (21). In brief, when

needed, ice-cold TBS was added to a vial containing the film of Aβ monomers to obtain a 200 µg/ml solution of Aβ monomers. To prepare Aβ fibrils, the Aβ monomers were vortexed and transferred to a 96-well microtiter plate (Immunochemistry Technologies, Costar 266). The plate was incubated at 37°C for 3 h with shaking at 300 rpm. The resulting Aβ fibrils were stored at -20°C until needed.

Li-CRP-Aβ binding assay

Binding activity of Li-CRP for immobilized Aβ was evaluated as described earlier (21). Briefly, lyophilized Aβ peptides were reconstituted in TBS. Microtiter wells were coated with 10 µg/ml of Aβ at 4°C overnight. The unreacted sites in the wells were blocked with TBS containing 0.5% gelatin. Li-CRP, diluted in TBS containing 0.1% gelatin, 0.02% Tween-20 and 2 mM $CaCl_2$ (TBS-Ca), was added in duplicate wells and incubated at 37°C overnight. After washing the wells, rabbit polyclonal anti-Li-CRP-I antibody was used to detect bound Li-CRP. HRP-conjugated donkey anti-rabbit IgG (GE Healthcare) was used as the secondary antibody. Color was developed, and the OD was read at 405 nm.

Human SAP-Aβ binding assay

Binding activity of human SAP (Calbiochem, 565190) for immobilized Aβ was evaluated as follows. Microtiter wells were coated with 10 µg/ml of Aβ peptide, monomer and fibrils diluted in TBS. The unreacted sites in the wells were blocked with TBS containing 0.5% gelatin for 45 min at room temperature. SAP, diluted in TBS-Ca was then added in duplicate wells and incubated for 2 h at 37°C. Bound SAP was detected by using rabbit anti-human SAP (Calbiochem, 565191) by adding the antibody (5 µg/ml) to the wells and incubating at 37°C for 1 h. HRP- conjugated donkey anti-rabbit antibody (Southern Biotech, 6441-05) was used as the secondary antibody. Color was developed, and the OD was read at 405 nm.

Thioflavin T assay for Aβ fibrillation

The fibrillation of Aβ monomers was monitored by employing ThT assay according to a published method (49, 50) and exactly as described previously (21). In brief, the effects of Li-CRP on Aβ fibrillation were determined by adding CRP to Aβ at time zero, that is, CRP and Aβ were mixed together before the beginning of the fibrillation reaction. The fibrillation reaction mix was prepared with and without CRP. In CRP-containing mixture, the final concentrations of CRP were 1, 10 and 100 µg/ml. After vortexing, 240 µl of each mixture was transferred in triplicate wells in a 96-well microtiter plate (Immunochemistry Technologies, Costar 266). Fluorescence was measured by using the Synergy H1 microplate reader (BioTek) with excitation at 440 nm and emission at 480 nm. After the first measurement at 5 min, the plate was incubated at 37°C for 3 h with shaking at 300 rpm; fluorescence was measured every 15 min for 3 h.

Results

Verification of the composition and characteristics of Li-CRP-I and Li-CRP-II

Gel filtration and SDS-PAGE were performed to determine the molecular weight of native Li-CRP, the number of subunits in each molecule and the molecular weight of the subunits. As shown in Figure 1A, the elution volumes from the calibrated gel filtration column for both Li-CRP-I purified by PCh-affinity chromatography and Li-CRP-II purified by PEt-affinity chromatography were 10 ml. The molecular weights of both Li-CRP-I and Li-CRP-II were calculated to be ~300 kDa. SDS-PAGE (Figure 1B) revealed that Li-CRP-I was composed of two types of subunits of molecular weight 27.3 ± 1.7 kDa (band A) and 25.8 ± 2.7 kDa (band B). The band A was a doublet of two bands. Li-CRP-II was also composed of two types of subunits of molecular weight 29.6 ± 2.6 kDa (band C) and 24.7 ± 2.5 kDa (band D), although a third subunit of molecular weight 28.2 ± 2.5 kDa was also seen as a faint band in between bands C and D. In another preparation of Li-CRP-II, there was an additional faint band of molecular weight 54.8 ± 0.01 (band E, Figure 1D). Thus, both Li-CRP-I and Li-CRP-II were composed of twelve subunits, assuming an average molecular weight of 25 kDa for each subunit.

We checked the purity of Li-CRP-I eluted by using either EDTA (lane 2) or PCh (lane 3) from the PCh-affinity column (Figure 1C). We also compared the purity of Li-CRP-I purified by either affinity chromatography (lanes 2-3) only or by affinity chromatography followed by gel filtration (lanes 4-5). As shown, there was no difference in the purity of Li-CRP-I eluted by either EDTA or PCh from the affinity column. Similarly, there was no difference in the purity of Li-CRP-I purified by just affinity chromatography or by affinity chromatography followed by gel filtration. These results indicated that the affinity-purified Li-CRP-I was pure; there was no need for further purification.

The purity of Li-CRP-II eluted by using either EDTA (lanes 2-4) or PEt (lanes 5-7) from the PEt-affinity column was also investigated (Figure 1D). As shown, when Li-CRP-II was eluted from the affinity column by using PEt (lane 5), the top band C (as shown in Figure 1B) was absent; instead, there was a doublet of the middle band. We also compared the purity of Li-CRP-II purified by either affinity chromatography (lanes 2 and 5) alone or by affinity chromatography followed by ion-exchange chromatography (lanes 3 and 6) or by affinity chromatography followed by gel filtration (lanes 4 and 7). There was no difference in the purity of Li-CRP-II purified by just affinity chromatography or by affinity chromatography followed by either ion-exchange chromatography or gel filtration. These results indicated that the affinity-purified Li-CRP-II was also pure; there was no need for further purification.

To remove the contaminant protein (band E) present in Li-CRP-II, each fraction collected after ion-exchange chromatography was subjected to SDS-PAGE individually (Figure 2A), instead of pooling the fractions (lane 2, Figure 1D). As shown in Figure 2A, the intensity of band E was directly proportional to the intensity of band C and that the compositions of Li-CRP-II present in each

10.3389/fimmu.2024.1466865

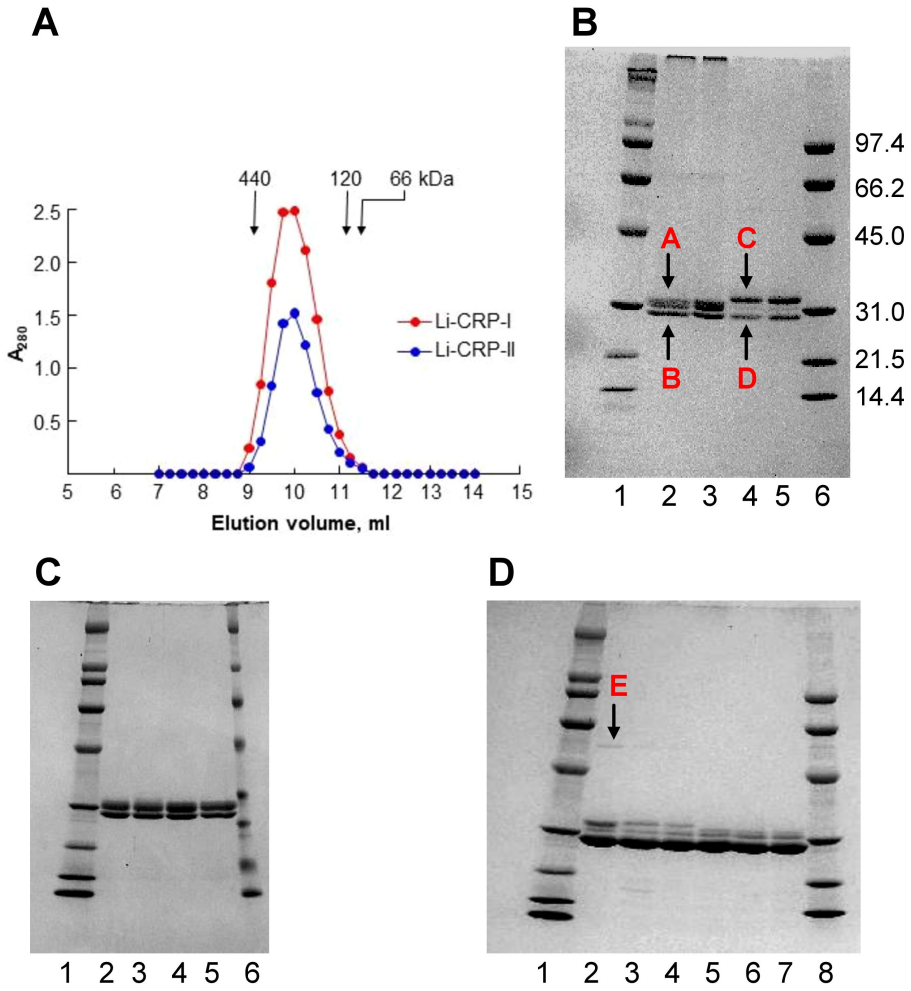

FIGURE 1
Purification of Li-CRP-I and Li-CRP-II. **(A)** Elution profiles of Li-CRP-I and Li-CRP-II from the gel filtration column are shown. The arrows point to the elution volumes of molecular weight markers: apoferritin (440 kDa), human CRP (120 kDa) and BSA (66 kDa). A representative of three chromatograms is shown. **(B)** Li-CRP-I and Li-CRP-II were subjected to SDS-PAGE. Lane 1, Bio-Rad broad-range molecular weight markers; Lane 2, Li-CRP-I eluted from the PCh-affinity column by using EDTA; Lane 3, Li-CRP-I eluted from the PCh-affinity column by using PCh; Lane 4, Li-CRP-II eluted from the PEt-affinity column by using EDTA; Lane 5, Li-CRP-II eluted from the PEt-affinity column by using PEt; Lane 6, Bio-Rad low-range molecular weight markers. The molecular weights of the CRP subunits were calculated from three separate gels and presented as average ± SEM (see the Results section). **(C)** Lane 1, molecular weight markers; Lane 2, Li-CRP-I eluted from the PCh-affinity column by using EDTA; Lane 3, Li-CRP-I eluted from the PCh-affinity column by using EDTA, followed by gel filtration chromatography; Lane 4, Li-CRP-I eluted from the PCh-affinity column by using PCh; Lane 5, Li-CRP-I eluted from the PCh-affinity column by using PCh, followed by gel filtration chromatography; Lane 6, molecular weight markers. **(D)** Lane 1, molecular weight marker; Lane 2, Li-CRP-II eluted from the PEt-affinity column by using EDTA; Lane 3, Li-CRP-II eluted from the PEt-column by using EDTA, followed by ion-exchange chromatography; Lane 4, Li-CRP-II eluted from the PEt-column by using EDTA, followed by gel filtration chromatography; Lane 5, Li-CRP-II eluted from the PEt-affinity column by using PEt; Lane 6, Li-CRP-II eluted from the PEt-column by using PEt, followed by ion-exchange chromatography; Lane 7, Li-CRP-II eluted from the PEt-column by using PEt, followed by gel filtration chromatography; Lane 8, molecular weight markers. A representative of three Coomassie brilliant blue-stained gels is shown for each panel.

fraction were different from each other. Some fractions had more of subunit C and some had more of subunit D. That was not the case with Li-CRP-I (Figure 2B); when individual fractions of Li-CRP-I after ion-exchange chromatography were subjected to SDS-PAGE, the composition of Li-CRP-I in each fraction was the same.

Deglycosylation of Li-CRP followed by SDS-PAGE were performed to determine whether each type of subunit present in Li-CRP-I and Li-CRP-II was glycosylated. As shown in Figure 2C, deglycosylation of Li-CRP-I resulted in a single band of molecular weight 23.2 kDa (lanes 1 and 2). Similarly, deglycosylation of Li-CRP-II also resulted in a single band of molecular weight 23.2 kDa (lanes 4 and 5). These data suggest that the difference in the electrophoretic mobility between subunits A and B and between subunits C and D was due to the difference in the extent of glycosylation of each type of subunit. Bands A and B were the products of a single gene and bands C and D were also the products of a single gene.

Native PAGE was also performed to check the purity of Li-CRP preparations. As shown in Figure 2D, there was only one band for Li-CRP-I, further indicating that it was a pure preparation of Li-CRP-I. In contrast, two bands were observed in the native PAGE of Li-CRP-II. This was not expected. Likely, the top band seen in Li-

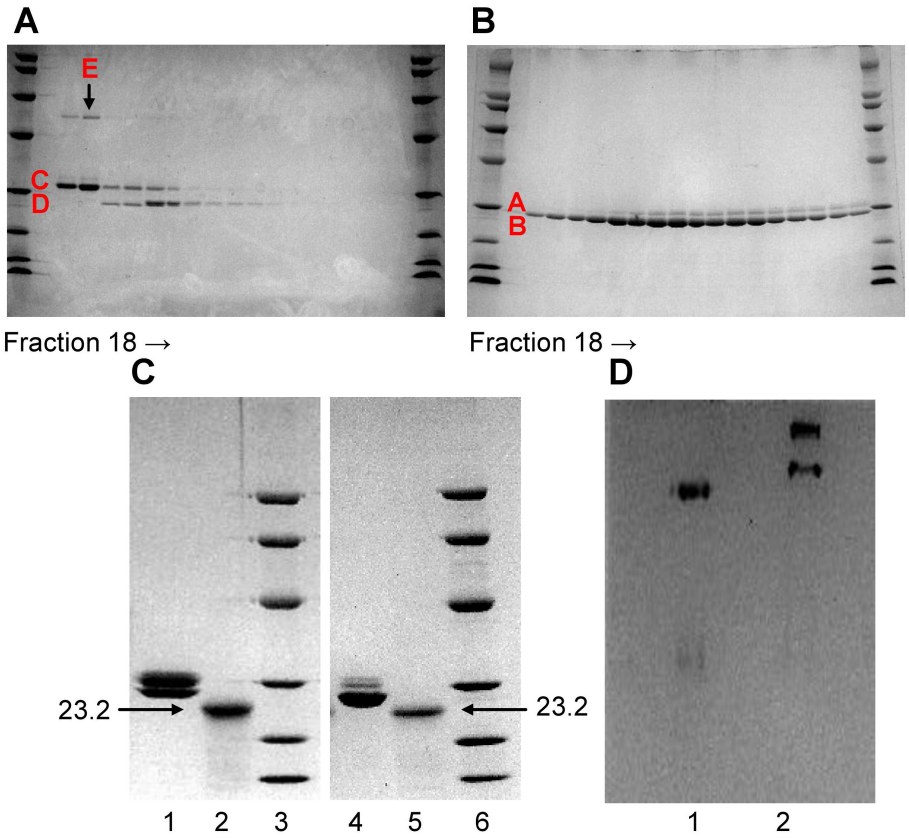

FIGURE 2
Characterization of Li-CRP-I and Li-CRP-II. **(A)** Li-CRP-II, purified by affinity chromatography and gel filtration, was subjected to ion-exchange chromatography on a MonoQ column (chromatogram not shown). Fractions (18-35) collected from the MonoQ column were subjected to SDS-PAGE. **(B)** Li-CRP-I, purified by affinity chromatography and gel filtration, was subjected to ion-exchange chromatography on a MonoQ column (chromatogram not shown). Fractions (18-35) collected from the MonoQ column were subjected to SDS-PAGE. **(C)** Native and deglycosylated Li-CRP-I and Li-CRP-II were subjected to SDS-PAGE. Lane 1, Li-CRP-I (10 µg); Lane 2, deglycosylated Li-CRP-I (80 µg); Lane 3, molecular weight markers; Lane 4, Li-CRP-II (10 µg); Lane 5, deglycosylated Li-CRP-II; Lane 6, molecular weight markers. **(D)** Li-CRP-I and Li-CRP-II were subjected to native PAGE. Lane 1, Li-CRP-I; Lane 2, Li-CRP-II. A representative of two Coomassie brilliant blue-stained gels is shown for each panel.

CRP-II lane contained ligand-bound Li-CRP-II and the ligand could be the protein seen as band E in SDS-PAGE gels.

The N-terminal sequences of the first ten amino acids of Li-CRP-I and Li-CRP-II were LEEGEITSKV and LEEGEITSKI, respectively. The amino acid sequences of Li-CRP-I and Li-CRP-II were identical for the first nine residues. Sequencing of Li-CRP-II, however, revealed an additional protein with the sequence MLTTKVRFFH of the first 10 residues, probably reflecting the band E in Li-CRP-II.

The preparations of Li-CRP-I and Li-CRP-II purified by affinity chromatography and gel filtration as shown in Figure 1B were used in the subsequent experiments involving Li-CRP.

Li-CRP-II reacts with polyclonal antibodies to Li-CRP-I

Immunological cross-reactivity assays for Li-CRP-I and Li-CRP-II showed that the antibodies to Li-CRP-I reacted with both Li-CRP-I and Li-CRP-II with almost equal affinity (Figure 3). These data suggested that anti-Li-CRP-I antibodies could be used to detect both Li-CRP-I and Li-CRP-II. These results were not surprising considering the similarity in the amino acid sequences of Li-CRP-I and Li-CRP-II.

Li-CRP binds to PCh but not as avidly as human CRP does

We next evaluated whether Li-CRP-II which was purified by PEt-affinity chromatography bound to PCh also and, if so, then whether the PCh-binding ability of Li-CRP-II was different from that of Li-CRP-I and human CRP. As shown in Figure 4, both Li-CRP-I and Li-CRP-II and human CRP bound to PCh in a CRP concentration-dependent manner. However, the binding of Li-CRP-I and Li-CRP-II to PCh was not comparable to each other and was different from human CRP. For equivalent binding (OD at 405 nm equal to 1) of Li-CRP-I, Li-CRP-II and human CRP to PCh, the required concentrations of Li-CRP-I, Li-CRP-II and human CRP were 1.2 µg/ml, 12 µg/ml and 0.009 µg/ml, respectively. Thus, for equivalent binding of Li-CRP-II and Li-CRP-I to PCh, 10-times more of Li-CRP-II was required compared to Li-CRP-I, indicating

10.3389/fimmu.2024.1466865

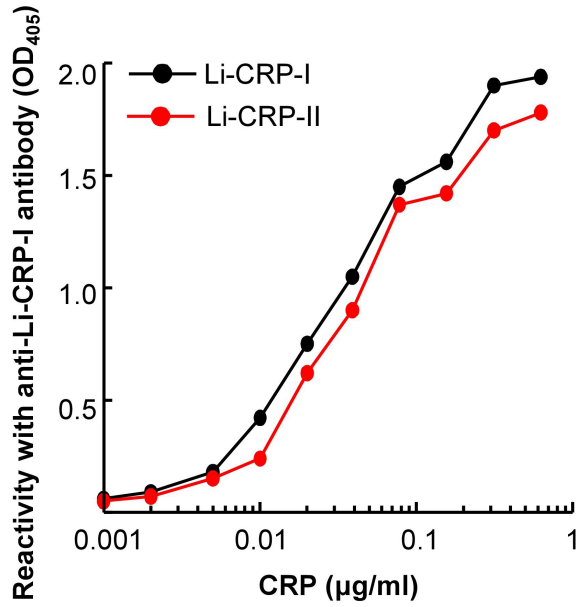

FIGURE 3
Reactivity of anti-Li-CRP-I antibodies with Li-CRP-II. Microtiter wells were coated with Li-CRP-I and Li-CRP-II. After blocking the unreacted sites in the wells, rabbit polyclonal anti-Li-CRP-I antibody was added to the wells. Bound antibody was detected by HRP-conjugated donkey anti-rabbit IgG. Color was developed and the OD was read at 405 nm. The experiment was performed three times and comparable results were obtained each time. Results of a representative experiment are shown.

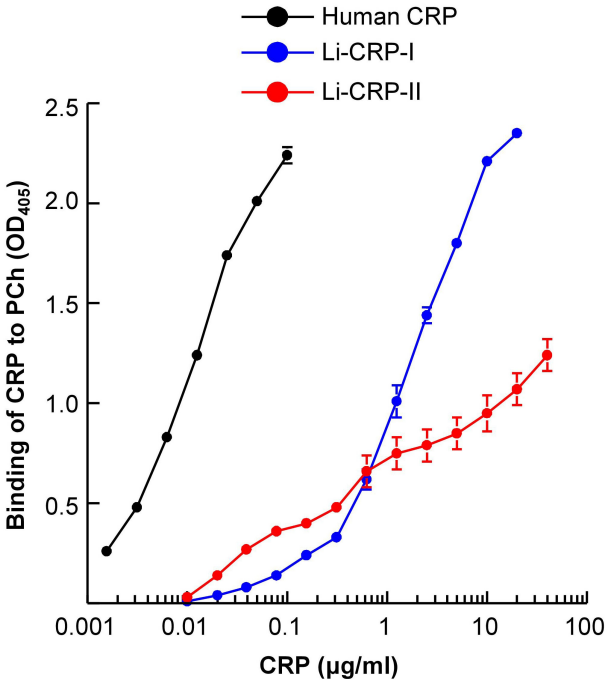

FIGURE 4
PCh-binding activity of Li-CRP-I and Li-CRP-II. Microtiter wells were coated with PnC. After blocking the unreacted sites in the wells, human CRP and Li-CRP diluted in TBS-Ca were added to the wells. Bound human CRP was detected by using rabbit anti-human CRP antibody and bound Li-CRP was detected by using anti-Li-CRP-I antibody. HRP-conjugated donkey anti-rabbit IgG was used as the secondary antibody. Color was developed and the OD was read at 405 nm. Data shown are mean ± SEM of three experiments.

that the PCh-binding avidity of Li-CRP-II was 90% less than that of Li-CRP-I. For equivalent binding of Li-CRP-II and human CRP to PCh, ~1300-times more of Li-CRP-II was required compared to human CRP, indicating that the PCh-binding avidity of Li-CRP-II was ~99% less than that of human CRP. Similarly, for equivalent binding of Li-CRP-I and human CRP to PCh, ~130-times more of Li-CRP-I was required compared to human CRP, indicating that the PCh-binding avidity of Li-CRP-I was also ~99% less than that of human CRP.

Like human SAP, both Li-CRP-I and Li-CRP-II bind to immobilized Aβ at physiological pH

Employing solid-phase Aβ-binding assays, the binding of Li-CRP to immobilized Aβ, in the presence and absence of Ca^{2+}, was determined. As shown in Figure 5, Li-CRP-I bound to immobilized Aβ peptides, monomers and fibrils, at physiological pH, in a CRP concentration-dependent manner. The binding of Li-CRP-I to Aβ did not require Ca^{2+} since the binding also occurred in the absence of Ca^{2+}. Similarly, Li-CRP-II also bound to Aβ peptides, monomers and fibrils, at physiological pH, in a CRP concentration-dependent manner. However, in contrast to Li-CRP-I, the binding of Li-CRP-II to Aβ was Ca^{2+}-dependent since the binding of Li-CRP-II to Aβ was either absent or drastically reduced in the absence of Ca^{2+}. These data suggest that Aβ is a ligand of both native Li-CRP-I and native Li-CRP-II although the undefined Aβ-binding site may be located on different regions in Li-CRP-I and Li-CRP-II.

Next, to compare Li-CRP with human SAP, the binding of human SAP to immobilized Aβ, in the presence and absence of Ca^{2+}, was investigated (Figure 6). As shown, human SAP bound to immobilized Aβ peptides, monomers and fibrils, at physiological pH, in the presence of Ca^{2+} and in an SAP concentration-dependent manner. However, like Li-CRP-II, human SAP did not bind to Aβ in the absence of Ca^{2+}, suggesting that Li-CRP-II and human SAP recognize Aβ in similar environment.

Both Li-CRP-I and Li-CRP-II prevent fibrillation of Aβ

Next, we investigated whether Li-CRP capable of binding to immobilized Aβ can also bind to Aβ when both Li-CRP and Aβ are in the fluid phase and inhibit the formation of Aβ fibrils. Aβ monomers were employed in the fibrillation assays (Figure 7). In the absence of Li-CRP, the fibrillation of Aβ began within 5 min and continued until ~2 h when further fibrillation stopped (black curves in both panels). Both Li-CRP-I and Li-CRP-II inhibited the fibrillation of Aβ in a CRP concentration-dependent manner. In case of Li-CRP-I, there was no statistically significant difference in fibrillation with or without 1 μg/ml of Li-CRP-I and there was no

10.3389/fimmu.2024.1466865

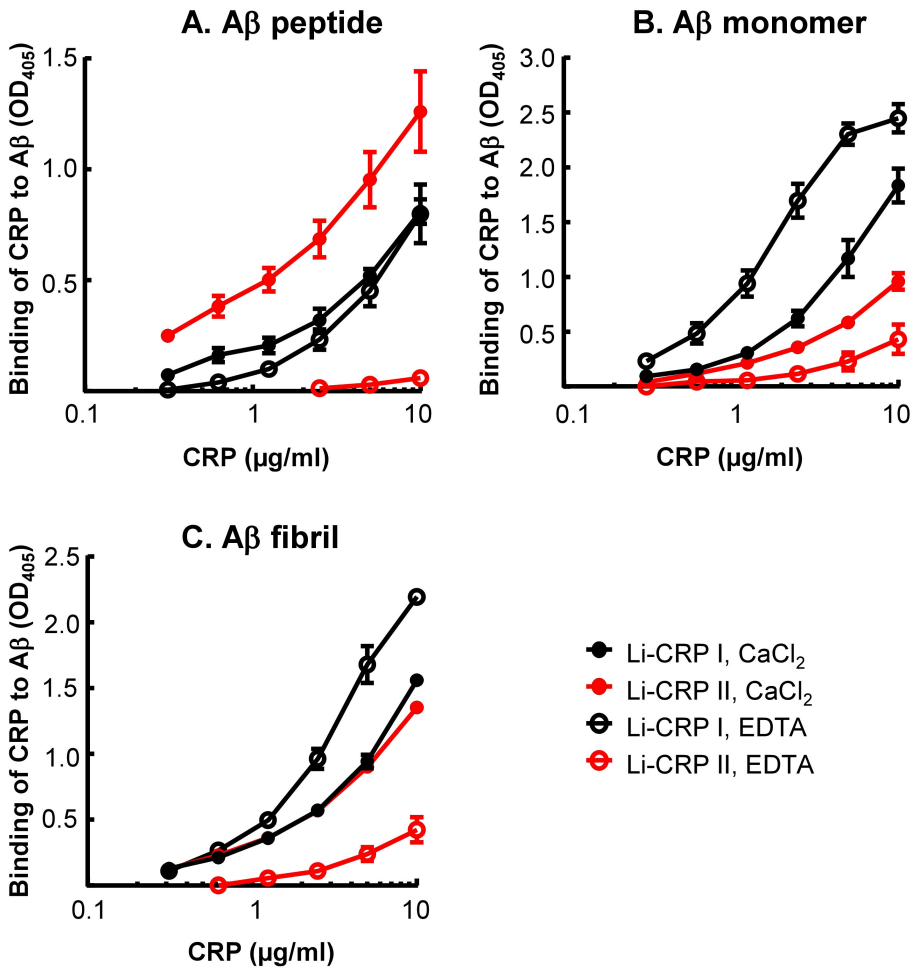

FIGURE 5
Aβ-binding activity of Li-CRP-I and Li-CRP-II. **(A)** Microtiter wells were coated with Aβ peptides. The unreacted sites in the wells were blocked with gelatin. Li-CRP, diluted in TBS-Ca and TBS-EDTA, was added to the wells. Bound CRP was detected by using anti-Li-CRP-I antibody as the primary antibody and HRP-conjugated donkey anti-rabbit IgG as the secondary antibody. Color was developed and the OD was read at 405 nm. Data shown are mean ± SEM of three experiments. **(B)** As in *A*, except that the microtiter wells were coated with Aβ monomers. **(C)** As in **(A)**, except that the microtiter wells were coated with Aβ fibrils.

statistically significant difference in fibrillation with 1 μg/ml and 10 μg/ml of Li-CRP-I. There were statistically significant differences in the fibrillation when Li-CRP-I was used at 10 μg/ml and 100 μg/ml. In case of Li-CRP-II, the inhibition of fibrillation was more efficient; even 1 μg/ml of Li-CRP-II was able to significantly inhibit the fibrillation of Aβ and the inhibition of fibrillation was significantly more at higher concentrations of Li-CRP-II. Thus, both Li-CRP-I and Li-CRP-II bound to Aβ in the fluid phase, inhibited the rate of fibrillation of Aβ over time, and also inhibited the total amount of the fibrils formed by the end of the fibrillation reaction.

Discussion

In this study, we tested the hypothesis that the recently reported function of human CRP to bind to Aβ peptides and prevent their fibrillation (21) has been evolutionarily conserved. Two different CRP species, termed as Li-CRP-I and Li-CRP-II, were isolated from hemolymph of *L. polyphemus* and investigated for their anti-amyloidogenic activity. Our major findings were: 1. A variety of Li-CRP molecules of different subunit compositions are present in *Limulus* hemolymph. 2. Both Li-CRP-I and Li-CRP-II bound to both immobilized and fluid-phase Aβ. 3. The binding of both Li-CRP-I and Li-CRP-II to Aβ did not require acidic pH or any structural alteration of the Li-CRP dodecamers. 4. Both Li-CRP-I and Li-CRP-II prevented the formation of Aβ fibrils. These findings indicate that Li-CRP is an anti-amyloidogenic protein and raise the possibility that the presence of various Li-CRP species in hemolymph facilitates the recognition of a range of proteins with differing amyloidogenicity.

Before purifying Li-CRP by employing affinity chromatography, the SAP-like protein was removed by passing the hemolymph through a Sepharose column. Also, purified Li-CRP-I and Li-CRP-II did not bind to fetuin when passed through a fetuin-sepharose column (sialic acid affinity chromatography) indicating that both Li-CRP preparations did not contain limulin either (data not shown). The results of the N-terminal sequencing of Li-CRP-I and Li-CRP-II verified the purity of Li-CRP preparations. Both Li-

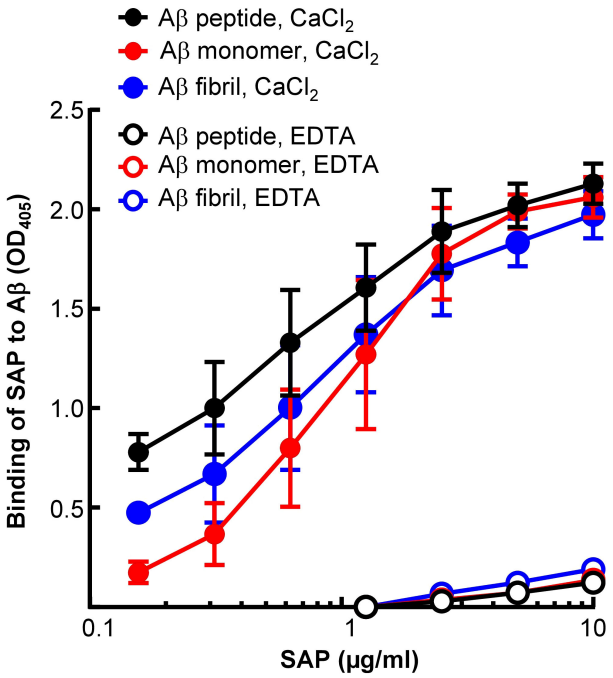

FIGURE 6
Aβ-binding activity of human SAP. Microtiter wells were coated with Aβ peptides, monomers and fibrils. The unreacted sites in the wells were blocked with gelatin. Human SAP, diluted in TBS-Ca and TBS-EDTA, was added to the wells. Bound SAP was detected by using rabbit polyclonal anti-SAP antibody as the primary antibody and HRP-conjugated donkey anti-rabbit IgG as the secondary antibody. Color was developed and the OD was read at 405 nm. Data shown are mean ± SEM of three experiments.

CRP-I and Li-CRP-II were dodecamers with a molecular weight of ~300 kDa consisting of two types of glycosylated subunits, six copies of each, with the same N-terminal amino acid residues as reported previously (33–36). The results of the deglycosylation experiments, combined with the amino acid sequencing data, indicated that the two types of subunits of Li-CRP-I were differentially glycosylated forms of a single gene product. Similarly, the two types of subunits of Li-CRP-II were also differentially glycosylated products of another homologous gene. It is not clear whether the PCh-binding and PEt-binding activities of Li-CRP-I and Li-CRP-II were due to the differences in the extent of glycosylation or due to being the products of homologous genes.

The data obtained from the PCh-binding assays suggested that Li-CRP-II, which was purified by PEt-affinity chromatography, bound to PCh also, although purified Li-CRP-II did not bind to PCh on the PCh-Sepharose column (data not shown). Similarly, Li-CRP-I, which was purified by PCh-affinity chromatography, either did not bind or bound poorly to PEt on the PEt-Sepharose column

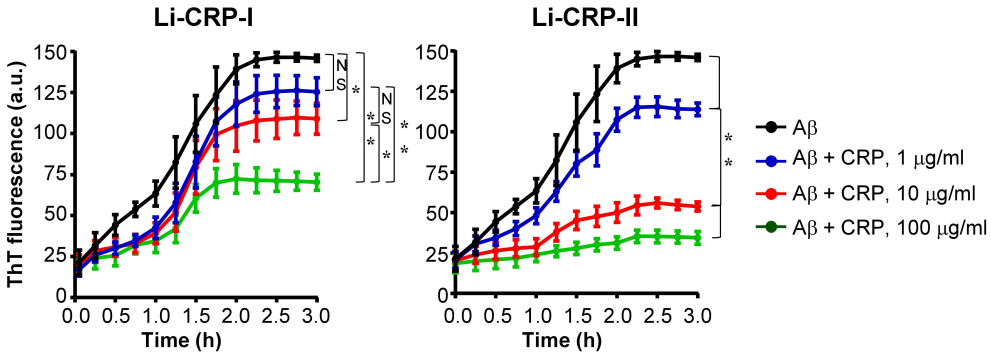

FIGURE 7
Effects of Li-CRP-I and Li-CRP-II on the formation of Aβ fibrils. The fibrillation of Aβ was measured by ThT fluorescence in the absence (black) or presence of 1 μg/ml (blue), 10 μg/ml (red) and 100 μg/ml (green) of Li-CRP. Li-CRP-I and Aβ monomers were mixed at time zero and added to microtiter wells. After the first measurement at 5 min, the plate was incubated at 37°C with shaking; fluorescence was measured every 15 min. Results are plotted as mean arbitrary units (a.u.) ± SEM of three experiments. For the time period of 5 min to 2 h, *p* values were determined by employing linear regression analysis of the slopes. For the time period of 2.25 h to 3 h, *p* values were determined by taking the mean of all points and employing student unpaired *t* test. NS, not significant ($p>0.05$); * < 0.05; ** <0.008.

(data not shown). The PEt-binding activity of Li-CRP-I could not be assessed by using immobilized biotinylated PEt as the PEt-containing ligand (18) since Li-CRP bound to biotin itself. It is possible that Li-CRP-II preparations contained some Li-CRP-I and that Li-CRP-I preparations contained some Li-CRP-II.

Our data indicate that the anti-amyloidogenic function of CRP has been conserved from arthropods to humans. The difference between Li-CRP and human CRP in exerting their anti-amyloidogenic function is that Li-CRP does not require any change in its dodecameric structure while human CRP requires an inflammatory milieu that can change its pentameric structure (8). In this regard, Li-CRP, specifically Li-CRP-II, is more like human SAP. Human SAP also bound to Aβ peptides and fibrils without any structural alteration of SAP and needed Ca^{2+} (23, 51–53). The binding of SAP to Aβ is known to prevent fibrillation and the binding of SAP to the fibrils of Aβ prevents further fibrillation (51–55). The findings that both, Li-CRP which is a dodecamer and human CRP which is a pentamer, bind to Aβ suggest that an Aβ-binding site is located on each subunit. This is reasonable to assume since the Aβ and Aβ-like structures can be accommodated by a single CRP subunit.

To determine the role of the carbohydrate component of Li-CRP in binding to their ligands, Li-CRP was deglycosylated by employing two methods: chemical deglycosylation (Figure 2C) and enzymatic deglycosylation (data not shown). Enzymatic deglycosylation was performed under both denaturing and non-denaturing conditions using the Protein Deglycosylation Mix II kit (New England Biolabs, P6044). Both deglycosylation procedures resulted in the denaturation of the protein. Therefore, the role of the carbohydrate moieties present on Li-CRP-I and Li-CRP-II in binding to their ligands could not be evaluated in functional assays.

The data obtained from the biochemical analyses of Li-CRP indicated that Li-CRP-II existed in both free and ligand-bound form in hemolymph. This interpretation is based on the finding that the intensity of the contaminant band E in the gels, possibly a Li-CRP-II ligand, was proportional to the intensity of one of the two Li-CRP-II bands. Also, the protein seen as band E could not be removed by gel filtration and ion-exchange chromatography. The presence of two bands for Li-CRP-II in the native PAGE gels supported the presence of ligand-bound Li-CRP-II in hemolymph. If the protein present in band E is a ligand of Li-CRP-II and could be co-purified with Li-CRP-II by PEt-affinity chromatography, then the data suggest that the PEt-binding site in liganded Li-CRP-II was vacant. Combined data suggest that there are two functional ligand-binding sites on Li-CRP, one site for binding to PEt and the other site for covalent binding to a protein ligand that has amyloid-like structures.

Previously, Li-CRP has been shown to protect against xenobiotic insults and to chelate the heavy metals mercury and cadmium, and hence playing a role in detoxification of heavy metals (56). Li-CRP has also been shown to exhibit Ca^{2+}-independent binding to membranes mimicking the outer membrane of gram-negative bacteria and then create pores in the lipid bilayer (57). In addition, Li-CRP also bound to any protein immobilized on microtiter wells which could be due to the exposure of amyloid-like structures on the immobilized proteins (58). We report here that Li-CRP exerts anti-amyloidogenic function. Thus, Li-CRP is a polyfunctional protein. Li-CRP is one of the most abundant constitutively expressed proteins in hemolymph (28, 33–36). The average concentration of Li-CRP in hemolymph is ~2.0 mg/ml. The presence of high concentration of Li-CRP in hemolymph at all times suggests an important function for the protein and a function that is needed at all times. This can be attributed to the fact that these animals are constantly exposed to harsh environments which can induce the formation of amyloidogenic proteins in hemolymph. It is likely that constitutive expression of Li-CRP helps protecting the animals from microbial pathogens and pathogenic proteins by utilizing its PCh-binding and Aβ-binding properties, respectively.

Purified Li-CRP-II was a mixture of dodecamers composed of different types of subunits and hexamers, as suggested by the data obtained from ion-exchange chromatography. If the function of Li-CRP depended upon their glycosylation (35–37), then the random assembly of various types of subunits and hexamers into dodecamers will generate a repertoire of native Li-CRP species where the functional efficiency of each dodecamer will be different. At least nine different Li-CRP species were found to be present in hemolymph in an earlier study (36). Our findings raise the possibility that the presence of various Li-CRP species in hemolymph facilitates the recognition of a range of proteins with differing amyloidogenicity. In a mouse model of amyloidosis, it has been shown previously that injected human SAP was deposited in amyloidotic mice while Li-CRP was not (59). It is possible that Li-CRP was not deposited on amyloids in mice significantly since Li-CRP might have been the mixture of a variety of dodecamers, each being specific for a particular Aβ. Although the cross-reactivity against human CRP and rabbit CRP is weak (28, 39), Li-CRP exhibits immunological cross-reactivity against snail CRP (31), suggesting that CRP performs anti-amyloidogenic functions in invertebrates in general. A mechanism for the generation of many structurally-altered variants of human CRP pentamers has also been reported: both, a wide range of acidic pH and the treatment of CRP with H_2O_2 have all been shown to generate CRP pentamers capable of binding to Aβ (8, 9, 18). It is unlikely that the structures of acidic pH-modified CRP molecules and H_2O_2-modified CRP (8, 18) will have identical structures.

We conclude that the anti-amyloidogenic function of CRP through the recognition of Aβ is an ancient function of CRP. Our findings that the PCh-binding avidity of Li-CRP was more than 90% lower than that of human CRP suggest that the anti-amyloidogenic function of CRP is its most basic function. In invertebrates, the Aβ-binding function of CRP can protect the host against toxicity caused by amyloidogenic and pathogenic proteins (60). It has been shown previously that the blocking a region in Aβ blocks Aβ toxicity (61). In humans, where CRP is an acute phase protein produced during inflammatory states (62), this property of CRP can protect the host against inflammatory diseases involving malfunctioning proteins such as atherosclerosis in which LDL is ectopically deposited in the arteries, in pneumococcal infection where complement inhibitor factor H is deposited on pneumococci and in inflammatory arthritis in which immune

complexes are formed, assuming that these proteins expose Aβ-like structures after deposition at places where they are not supposed to be (63–65).

Data availability statement

The original contributions presented in the study are included in the article/supplementary material. Further inquiries can be directed to the corresponding authors.

Ethics statement

The manuscript presents research on animals that do not require ethical approval for their study.

Author contributions

AA: Writing – review & editing, Writing – original draft, Validation, Supervision, Project administration, Funding acquisition, Formal Analysis, Conceptualization. AP: Writing – review & editing, Investigation. DN: Writing – review & editing, Investigation. AT: Writing – review & editing, Investigation. PA: Writing – review & editing, Methodology, Investigation. SS: Writing – review & editing, Investigation.

Funding

The author(s) declare financial support was received for the research, authorship, and/or publication of this article. This work was supported by National Institutes of Health Grants AR068787 and R01AI151561.

Conflict of interest

The authors declare that the research was conducted in the absence of any commercial or financial relationships that could be construed as a potential conflict of interest.

The author(s) declared that they were an editorial board member of Frontiers, at the time of submission. This had no impact on the peer review process and the final decision.

Publisher's note

References

1. Ji S-R, Zhang S-H, Chang Y, Li H-Y, Wang M-Y, Lv J-M, et al. C-reactive protein: The most familiar stranger. *J Immunol.* (2023) 210:699–707. doi: 10.4049/jimmunol.2200831

2. Volanakis JE, Kaplan MH. Specificity of C-reactive protein for choline phosphate residues of pneumococcal C-polysaccharide. *Proc Soc Exp Biol Med.* (1971) 136:612–4. doi: 10.3181/00379727-136-35323

3. Schwalbe RA, Dahlbäck B, Coe JE, Nelsestuen GL. Pentraxin family of proteins interacts specifically with phosphorylcholine and/or phosphorylethanolamine. *Biochemistry.* (1992) 31:4907–15. doi: 10.1021/bi00135a023

4. Agrawal A, Simpson MJ, Black S, Carey M-P, Samols D. A C-reactive protein mutant that does not bind to phosphocholine and pneumococcal C-polysaccharide. *J Immunol.* (2002) 169:3217–22. doi: 10.4049/jimmunol.169.6.3217

5. Mikolajek H, Kolstoe SE, Pye VE, Mangione P, Pepys MB, Wood SP. Structural basis of ligand specificity in the human pentraxins, C-reactive protein and serum amyloid P component. *J Mol Recognit.* (2011) 24:371–7. doi: 10.1002/jmr.1090

6. Mattecka S, Bock C, Vogt B, Yapici G, Schrödl W, Janko C, et al. CRP and SAP from different species have different membrane ligand specificities. *Autoimmunity.* (2013) 46:347–50. doi: 10.3109/08916934.2013.780601

7. Shrive AK, Cheetham GMT, Holden D, Myles DAA, Turnell WG, Volanakis JE, et al. Three-dimensional structure of human C-reactive protein. *Nat Struct Biol.* (1996) 3:346–54. doi: 10.1038/nsb0496-346

8. Hammond DJ Jr, Singh SK, Thompson JA, Beeler BW, Rusiñol AE, Pangburn MK, et al. Identification of acidic pH-dependent ligands of pentameric C-reactive protein. *J Biol Chem.* (2010) 285:36235–44. doi: 10.1074/jbc.M110.142026

9. Singh SK, Thirumalai A, Hammond DJ Jr., Pangburn MK, Mishra VK, Johnson DA, et al. Exposing a hidden functional site of C-reactive protein by site-directed mutagenesis. *J Biol Chem.* (2012) 287:3550–8. doi: 10.1074/jbc.M111.310011

10. Noone DP, van der Velden TT, Sharp TH. Cryo-electron microscopy and biochemical analysis offer insights into the effects of acidic pH, such as occur during acidosis, on the complement binding properties of C-reactive protein. *Front Immunol.* (2021) 12:757633. doi: 10.3389/fimmu.2021.757633

11. Guillon C, Bigouagou UM, Folio C, Jeannin P, Delneste Y, Gouet P. A staggered decameric assembly of human C-reactive protein stabilized by zinc ions revealed by X-ray crystallography. *Protein Pept Lett.* (2014) 22:248–55. doi: 10.2174/0929866522666141231111226

12. Okemefuna AI, Stach L, Rana S, Buetas AJ, Gor J, Perkins SJ. C-reactive protein exists in an NaCl concentration-dependent pentamer-decamer equilibrium in physiological buffer. *J Biol Chem.* (2010) 285:1041–52. doi: 10.1074/jbc.M109.044495

13. Agrawal A, Gang TB, Rusiñol AE. Recognition functions of pentameric C-reactive protein in cardiovascular disease. *Mediators Inflammation.* (2014) 2014:319215. doi: 10.1155/2014/319215

14. Suresh MV, Singh SK, Agrawal A. Interaction of calcium-bound C-reactive protein with fibronectin is controlled by pH: *In vivo* implications. *J Biol Chem.* (2004) 279:52552–7. doi: 10.1074/jbc.M409054200

15. Singh SK, Hammond DJ Jr., Beeler BW, Agrawal A. The binding of C-reactive protein, in the presence of phosphoethanolamine, to low-density lipoproteins is due to phosphoethanolamine-generated acidic pH. *Clin Chim Acta.* (2009) 409:143–4. doi: 10.1016/j.cca.2009.08.013

16. Li S-L, Feng J-R, Zhou H-H, Zhang C-M, Lv G-B, Tan Y-B, et al. Acidic pH promotes oxidation-induced dissociation of C-reactive protein. *Mol Immunol.* (2018) 104:47–53. doi: 10.1016/j.molimm.2018.09.021

17. Ullah N, Ma F-R, Han J, Liu X-L, Fu Y, Liu Y-T, et al. Monomeric C-reactive protein regulates fibronectin mediated monocyte adhesion. *Mol Immunol.* (2020) 117:122–30. doi: 10.1016/j.molimm.2019.10.013

18. Singh SK, Thirumalai A, Pathak A, Ngwa DN, Agrawal A. Functional transformation of C-reactive protein by hydrogen peroxide. *J Biol Chem.* (2017) 292:3129–36. doi: 10.1074/jbc.M116.773176

19. Kaplan MH, Volanakis JE. Interaction of C-reactive protein complexes with the complement system. I. Consumption of human complement associated with the reaction of C-reactive protein with pneumococcal C-polysaccharide and with the choline phosphatides, lecithin, and sphingomyelin. *J Immunol.* (1974) 112:2135–47. doi: 10.4049/jimmunol.112.6.2135

20. Singh SK, Ngwa DN, Agrawal A. Complement activation by C-reactive protein is critical for protection of mice against pneumococcal infection. *Front Immunol.* (2020) 11:1812. doi: 10.3389/fimmu.2020.01812

21. Ngwa DN, Agrawal A. Structurally altered, not wild-type, pentameric C-reactive protein inhibits formation of amyloid-β fibrils. *J Immunol*. (2022) 209:1180–8. doi: 10.4049/jimmunol.2200148

22. Strang F, Scheichl A, Chen Y-C, Wang X, Htun N-M, Bassler N, et al. Amyloid plaques dissociate pentameric to monomeric C-reactive protein: A novel pathomechanism driving cortical inflammation in Alzheimer's disease? *Brain Pathol*. (2012) 22:337–46. doi: 10.1111/j.1750-3639.2011.00539.x

23. Dorta-Estremera SM, Cao W. Human pentraxins bind to misfolded proteins and inhibit production of type I interferon induced by nucleic acid-containing amyloid. *J Clin Cell Immunol*. (2015) 6:332. doi: 10.4172/2155-9899

24. Ozawa D, Nomura R, Mangione PP, Hasegawa K, Okoshi T, Porcari R, et al. Multifaceted anti-amyloidogenic and pro-amyloidogenic effects of C-reactive protein and serum amyloid P component *in vitro*. *Sci Rep*. (2016) 6:29077. doi: 10.1038/srep29077

25. Pathak A, Agrawal A. Evolution of C-reactive protein. *Front Immunol*. (2019) 10:943. doi: 10.3389/fimmu.2019.00943

26. Torzewski M. C-reactive protein: Friend or foe? Phylogeny from heavy metals to modified lipoproteins and SARS-CoV-2. *Front Cardiovasc Med*. (2022) 9:797116. doi: 10.3389/fcvm.2022.797116

27. Wang Y, Chen W, Ding S, Wang W, Wang C. Pentraxins in invertebrates and vertebrates: From structure, function and evolution to clinical applications. *Dev Comp Immunol*. (2023) 149:105064. doi: 10.1016/j.dci.2023.105064

28. Robey FA, Liu T-Y. Limulin: A C-reactive protein from *Limulus polyphemus*. *J Biol Chem*. (1981) 256:969–75. doi: 10.1016/S0021-9258(19)70074-X

29. Iwaki D, Osaki T, Mizunoe Y, Wai SN, Iwanaga S, Kawabata S-I. Functional and structural diversities of C-reactive proteins present in horseshoe crab hemolymph plasma. *Eur J Biochem*. (1999) 264:314–26. doi: 10.1046/j.1432-1327.1999.00588.x

30. Li Y, Ng PML, Ho B, Ding JL. A female-specific pentraxin, CrOctin, bridges pattern recognition receptors to bacterial phosphoethanolamine. *Eur J Immunol*. (2007) 37:3477–88. doi: 10.1002/eji.200737078

31. Agrawal A, Mitra S, Ghosh N, Bhattacharya S. C-reactive protein in hemolymph of a mollusc, *Achatina fulica* Bowdich. *Indian J Exp Biol*. (1990) 28:788–9.

32. Mukherjee S, Barman S, Mandal NC, Bhattacharya S. Anti-bacterial activity of *Achatina* CRP and its mechanism of action. *Indian J Exp Biol*. (2014) 52:692–704.

33. Armstrong PB. Comparative biology of the pentraxin protein family: Evolutionarily conserved component of innate immune system. *Int Rev Cell Mol Biol*. (2015) 316:1–47. doi: 10.1016/bs.ircmb.2015.01.002

34. Nguyen NY, Suzuki A, Cheng SM, Zon G, Liu T-Y. Isolation and characterization of *Limulus* C-reactive protein genes. *J Biol Chem*. (1986) 261:10450–5. doi: 10.1016/S0021-9258(18)67545-3

35. Nguyen NY, Suzuki A, Boykins RA, Liu T-Y. The amino acid sequence of *Limulus* C-reactive protein: Evidence of polymorphism. *J Biol Chem*. (1986) 261:10456–65. doi: 10.1016/S0021-9258(18)67546-5

36. Tennent GA, Bulter PJG, Hutton T, Woolfitt AR, Harvey DJ, Rademacher TW, et al. Molecular characterization of *Limulus polyphemus* C-reactive protein. I. Subunit composition. *Eur J Biochem*. (1993) 214:91–7. doi: 10.1111/j.1432-1033.1993.tb17900.x

37. Tennent GA, Pepys MB. Glycobiology of the pentraxins. *Biochem Soc Trans*. (1994) 22:74–9. doi: 10.1042/bst0220074

38. Fernández-Morán H, Marchalonis JJ, Edelman GM. Electron microscopy of a hemagglutinin from *Limulus polyphemus*. *J Mol Biol*. (1968) 32:467–9. doi: 10.1016/0022-2836(68)90023-5

39. Ying S-C, Marchalonis JJ, Gewurz AT, Siegel JN, Jiang H, Gewurz BE, et al. Reactivity of anti-human C-reactive protein (CRP) and serum amyloid P component (SAP) monoclonal antibodies with limulin and pentraxins of other species. *Immunology*. (1992) 76:324–30.

40. Shrive AK, Metcalfe AM, Cartwright JR, Greenhough TJ. C-reactive protein and SAP-like pentraxin are both present in *Limulus polyphemus* haemolymph: Crystal structure of *Limulus* SAP. *J Mol Biol*. (1999) 290:997–1008. doi: 10.1006/jmbi.1999.2956

41. Tharia HA, Shrive AK, Mills JD, Arme C, Williams GT, Greenhough TJ. Complete cDNA sequence of SAP-like pentraxin from *Limulus polyphemus*: Implications for pentraxin evolution. *J Mol Biol*. (2002) 316:583–97. doi: 10.1006/jmbi.2001.5356

42. Shrive AK, Burns I, Chou H-T, Stahlberg H, Armstrong PB, Greenhough TJ. Crystal structures of *Limulus* SAP-like pentraxin reveal two molecular aggregations. *J Mol Biol*. (2009) 386:1240–54. doi: 10.1016/j.jmb.2009.01.008

43. Srimal S, Quigley JP, Armstrong PB. Limulin and C-reactive protein from the plasma of *Limulus polyphemus* are different proteins. *Biol Bull*. (1993) 185:325. doi: 10.1086/BBLv185n2p325

44. Quigley J, Misquith S, Surolia A, Srimal S, Armstrong P. Preliminary investigation of the molecular basis for the functional differences between the two pentraxins limulin and C-reactive protein from the plasma of the American horseshoe crab, *Limulus polyphemus*. *Biol Bull*. (1994) 187:229–30. doi: 10.1086/BBLv187n2p229

45. Armstrong PB, Swarnakar S, Srimal S, Misquith S, Hahn EA, Aimes RT, et al. A cytolytic function for a sialic acid-binding lectin that is a member of the pentraxin family of proteins. *J Biol Chem*. (1996) 271:14717–21. doi: 10.1074/jbc.271.25.14717

46. Thirumalai A, Singh SK, Hammond DJ Jr, Gang TB, Ngwa DN, Pathak A, et al. Purification of recombinant C-reactive protein mutants. *J Immunol Methods*. (2017) 443:26–32. doi: 10.1016/j.jim.2017.01.011

47. Sawaya MR, Hughes MP, Rodriguez JA, Riek R, Eisenberg DS. The expanding amyloid family: Structure, stability, function, and pathogenesis. *Cell*. (2021) 184:4857–73. doi: 10.1016/j.cell.2021.08.013

48. Stine WB, Jungbauer L, Yu C, LaDu MJ. Preparing synthetic Aβ in different aggregation states. *Methods Mol Biol*. (2011) 670:13–32. doi: 10.1007/978-1-60761-744-0_2

49. Blancas-Mejia LM, Misra P, Dick CJ, Marin-Argany M, Redhage KR, Cooper SA, et al. Assays for light chain amyloidosis formation and cytotoxicity. *Methods Mol Biol*. (2019) 1873:123–53. doi: 10.1007/978-1-4939-8820-4_8

50. Xue C, Lin TY, Chang D, Guo Z. Thioflavin T as an amyloid dye: Fibril quantification, optimal concentration and effect on aggregation. *R Soc Open Sci*. (2017) 4:160696. doi: 10.1098/rsos.160696

51. Danielsen B, Sørensen IJ, Nybo M, Nielsen EH, Kaplan B, Svehag S-E. Calcium-dependent and -independent binding of the pentraxin serum amyloid P component to glycosaminoglycans and amyloid proteins: Enhanced binding at slightly acid pH. *Biochim Biophys Acta*. (1997) 1339:73–8. doi: 10.1016/S0167-4838(96)00218-X

52. Hamazaki H. Ca^{2+}-dependent binding of human serum amyloid P component to Alzheimer's β-amyloid peptide. *J Biol Chem*. (1995) 270:10392–4. doi: 10.1074/jbc.270.18.10392

53. Pepys MB, Dyck RF, de Beer FC, Skinner M, Cohen AS. Binding of serum amyloid P-component (SAP) by amyloid fibrils. *Clin Exp Immunol*. (1979) 38:284–93.

54. Janciauskiene S, de Frutos PG, Carlemalm E, Dahlbäck B, Eriksson S. Inhibition of Alzheimer β-peptide fibril formation by serum amyloid P component. *J Biol Chem*. (1995) 270:26041–4. doi: 10.1074/jbc.270.44.26041

55. Tennent GA, Lovat LB, Pepys MB. Serum amyloid P component prevents proteolysis of the amyloid fibrils of Alzheimer disease and systemic amyloidosis. *Proc Natl Acad Sci USA*. (1995) 92:4299–303. doi: 10.1073/pnas.92.10.4299

56. Agrawal A, Bhattacharya S. Binding property of rat and *Limulus* C-reactive proteins (CRP) to mercury. *Experientia*. (1989) 45:567–70. doi: 10.1007/BF01990509

57. Harrington JM, Chou H-T, Gutsmann T, Gelhaus C, Stahlberg H, Leippe M, et al. Membrane activity of a C-reactive protein. *FEBS Lett*. (2009) 583:1001–5. doi: 10.1016/j.febslet.2009.02.019

58. Pathak A, Singh SK, Thirumalai A, Armstrong PB, Agrawal A. Evolution of a host-defense function of C-reactive protein from horseshoe crab to humans. *J Immunol*. (2016) 196:132.5. doi: 10.4049/jimmunol.196.Supp.132.5

59. Hawkins PN, Myers MJ, Epenetos AA, Caspi D, Pepys MB. Specific localization and imaging of amyloid deposits *in vivo* using ^{123}I-labeled serum amyloid P component. *J Exp Med*. (1988) 167:903–13. doi: 10.1084/jem.167.3.903

60. Chiti F, Dobson CM. Protein misfolding, amyloid formation, and human disease: A summary of progress over the last decade. *Annu Rev Biochem*. (2017) 86:27–68. doi: 10.1146/annurev-biochem-061516-045115

61. Nelson TJ, Alkon DL. Protection against β-amyloid-induced apoptosis by peptides interacting with β-amyloid. *J Biol Chem*. (2007) 282:31238–49. doi: 10.1074/jbc.M705558200

62. Kushner I. The phenomenon of the acute phase response. *Ann N Y Acad Sci*. (1982) 389:39–48. doi: 10.1111/j.1749-6632.1982.tb22124.x

63. Ngwa DN, Singh SK, Gang TB, Agrawal A. Treatment of pneumococcal infection by using engineered human C-reactive protein in a mouse model. *Front Immunol*. (2020) 11:586669. doi: 10.3389/fimmu.2020.586669

64. Pathak A, Singh SK, Thewke DP, Agrawal A. Conformationally altered C-reactive protein capable of binding to atherogenic lipoproteins reduces atherosclerosis. *Front Immunol*. (2020) 11:1780. doi: 10.3389/fimmu.2020.01780

65. Singh SK, Prislovsky A, Ngwa DN, Munkhsaikhan U, Abidi AH, Brand DD, et al. C-reactive protein lowers the serum level of IL-17, but not TNF-α, and decreases the incidence of collagen-induced arthritis in mice. *Front Immunol*. (2024) 15:1385085. doi: 10.3389/fimmu.2024.1385085

frontiers | Frontiers in Medicine

TYPE Original Research
PUBLISHED 07 February 2025
DOI 10.3389/fmed.2025.1506543

OPEN ACCESS

EDITED BY
Alok Agrawal,
Retired, Johnson City, TN, United States

REVIEWED BY
Bhowmick Mithu,
Apollo Hospitals, India
Faisal Ismail,
Aga Khan University, Pakistan

*CORRESPONDENCE
Yisen Huang
✉ 18159503331@163.com

†These authors have contributed equally to this work

RECEIVED 10 October 2024
ACCEPTED 29 January 2025
PUBLISHED 07 February 2025

CITATION
Chen X, Huang Y, Xu Q, Zhang B, Wang Y and Huang M (2025) C-reactive protein to serum calcium ratio as a novel biomarker for predicting severity in acute pancreatitis: a retrospective cross-sectional study.
Front. Med. 12:1506543.
doi: 10.3389/fmed.2025.1506543

C-reactive protein to serum calcium ratio as a novel biomarker for predicting severity in acute pancreatitis: a retrospective cross-sectional study

Xinqi Chen†, Yisen Huang*†, Qiaoli Xu, Bifeng Zhang, Yubin Wang and Meixue Huang

Department of Gastroenterology, First Hospital of Quanzhou Affiliated to Fujian Medical University, Quanzhou, Fujian, China

Background: Acute pancreatitis (AP) is a prevalent gastrointestinal emergency with a wide spectrum of clinical outcomes, varying from mild cases to severe forms. The early identification of high-risk patients is essential for improving prognosis. However, the predictive and prognostic potential of the C-reactive protein to serum calcium ratio (CCR) in AP has not been investigated. This study aims to explore the association between CCR and disease severity in patients with AP.

Methods: This retrospective cross-sectional study included 476 AP patients. The CCR was calculated from C-reactive protein and serum calcium levels within the first 24 h of admission. Multivariable logistic regression models were used to evaluate the relationship between CCR and AP severity, with restricted cubic spline analysis and receiver operating characteristic (ROC) analysis to assess dose–response and predictive performance, respectively.

Results: Of the 476 patients, 176 (37%) had mild acute pancreatitis (MAP) and 300 (63%) had moderate to severe AP. The CCR distribution had a median value of 17.5, with an interquartile range (IQR) of 3.0 to 60.2. Each unit increase in CCR was associated with a 7% increase in the risk of developing moderate to severe AP (OR: 1.07; 95% CI: 1.06–1.09). In fully adjusted models, this association remained statistically significant. The area under the curve (AUC) for CCR in predicting moderate to severe AP was 86.9%, with a sensitivity of 73.7% and specificity of 89.2%.

Conclusion: The CCR measured within the first 24 h of admission shows promise as a valuable biomarker for predicting the severity of AP. However, further multicenter prospective cohort studies are needed to confirm its clinical utility and investigate its role in improving treatment strategies and patient management.

KEYWORDS

acute pancreatitis, C-reactive protein to serum calcium ratio, severity, biomarker, cross-sectional study

1 Introduction

Acute pancreatitis (AP) is a prevalent gastrointestinal emergency, with an annual incidence ranging from 13 to 45 cases per 100,000 individuals, marked by its rapid onset and potential for severe complications (1). The primary causes of AP comprise biliary tract disease, excessive alcohol consumption, and hypertriglyceridemia (2–4). The pathophysiology of AP involves the premature activation of pancreatic enzymes, leading to autodigestion of pancreatic tissue and triggering an inflammatory cascade that extends beyond the pancreas to affect distant organs (5). While the majority of AP cases resolve with supportive care, approximately 20% of patients progress to moderate to severe AP, characterized by persistent organ failure and local complications such as necrosis or abscess formation (6–8). Early identification of high-risk patients and appropriate adjustment of therapeutic strategies are crucial for improving patient outcomes. Consequently, the discovery of simple, accurate indicators to predict AP severity is of significant clinical value.

Since the 1970s, multifactorial scoring systems, such as the AP-specific Ranson score (9), Bedside Index of Acute Pancreatitis Severity (BISAP) (10), computed tomography severity index (CTSI) (11), and the broader Acute Physiology and Chronic Health Examination (APACHE)-II (12), have been widely employed to assess the severity of acute pancreatitis (AP). These scoring systems have become critical tools in evaluating AP severity and guiding clinical decision-making. However, systems with a greater number of indicators can be challenging to apply in real-time due to their complexity and the need for multiple parameters. As a result, there is growing interest in simpler laboratory markers that can effectively evaluate AP severity, predict complications, and assess potential mortality risks.

Recently, novel combined indicators, such as the lactate to albumin Ratio (LAR) (1), C-reactive protein to lymphocyte ratio (CLR) (13), and neutrophil to lymphocyte ratio (NLR) (14), have been utilized for prognostic evaluation in patients with AP. Despite these advances, research on the predictive and prognostic potential of the C-reactive protein to serum calcium ratio (CCR) in AP remains limited. This study aims to explore the association between CCR and disease severity in AP patients, addressing a critical gap in current research.

2 Methods

2.1 Study population

This retrospective cross-sectional study involved in-patients with AP who were admitted to the First Hospital of Quanzhou Affiliated to Fujian Medical University between January 2018 and December 2019. All enrolled patients fulfilled the diagnostic criteria set by the Atlanta classification (15). Mild acute pancreatitis (MAP) is defined by the lack of organ failure and absence of local or systemic complications. Moderately severe acute pancreatitis (MSAP) involves transient organ failure or local/systemic complications without persistent organ failure. Severe acute pancreatitis (SAP) is marked by persistent organ failure. The exclusion criteria were as follows: (1) chronic pancreatitis, (2) malignant tumors, (3) pregnancy, and (4) incomplete data. In total, 476 patients with AP were included in the analysis, comprising 176 with MAP and 300 with moderate to severe AP. This study adhered to the Declaration of Helsinki and received approval from our institution's Ethics Committee (QYL 2021–199). Given its retrospective nature and use of anonymized data, informed consent was waived.

2.2 Data collection

All patient demographic and laboratory information was extracted from our hospital's electronic medical records. The collected data encompassed age, gender, smoking and alcohol consumption, preexisting conditions, disease severity, length of hospital stay, and laboratory results from the first 24 h after admission.

2.3 Measurement of CCR

The CCR was determined using the formula: CCR (mg/mmol) = C-reactive protein (CRP) level (mg/L)/serum calcium (mmol/L).

2.4 Statistical analysis

Continuous variables were reported as the mean and standard deviation (SD) for data following a normal distribution, or as the median and interquartile range (IQR) for non-normally distributed data. Categorical variables were reported as percentages (%). Differences between groups were analyzed using one-way ANOVA for normally distributed continuous variables, and chi-square or trend tests for categorical variables.

Multivariate logistic regression models were employed to evaluate the odds ratios (OR) and 95% confidence intervals (CI) for the relationship between CCR and the incidence of moderate to severe AP. Variables included in the model were chosen based on their clinical relevance, statistical significance in univariable analyses, and a change in the estimated effect of at least 10% that could influence potential confounding effects (16). The regression analysis involved four models. Model 1 had no adjustments, while Model 2 was adjusted for age and gender. In Model 3, additional adjustments were made for smoking status, alcohol use, diabetes, fatty liver, etiology, and length of hospital stay. Model 4 further adjusted for hemoglobin and albumin levels on top of the factors in Model 3.

Restricted cubic spline analyses were used to explore the dose–response relationship between CCR and the incidence of moderate to severe AP.

Subgroup analyses were performed by stratifying according to relevant covariates, including age, gender, smoking status, alcohol use, diabetes, fatty liver disease, and etiology.

Receiver Operating Characteristic (ROC) analysis was employed to evaluate the predictive performance, sensitivity, and specificity of CCR for moderate to severe AP incidence. The optimal threshold for CCR was established using the Youden Index.

All analyses were conducted with the statistical software R 3.3.2 (http://www.R-project.org, The R Foundation) and Free Statistics software version 1.9. A p-value of less than 0.05 (two-sided) was considered statistically significant.

3 Results

3.1 Baseline characteristics

The study population selection is illustrated in Figure 1, with a total of 476 patients being included. The baseline characteristics of the participants, categorized by CCR tertiles, are presented in Table 1. The enrolled patients were stratified into three tertiles based on their CCR levels: Q1 with 2.0 (1.0, 3.0) mg/mmol, Q2 with 17.5 (9.9, 30.0) mg/mmol, and Q3 with 82.8 (60.4, 99.3) mg/mmol. Among the 476 patients, the average age was 44 ± 13.2 years, with 364 (76.5%) of the participants being male. The CCR distribution had a median value of 17.5, with an IQR of 3.0 to 60.2. The CCR levels were higher in men compared to women (133 [83.6%] vs. 115 [72.3%]), in smokers compared to non-smokers (67 [42.1%] vs. 49 [30.8%]), and in drinkers compared to non-drinkers (81 [50.9%] vs. 61 [38.4%]). Additionally, a higher CCR was associated with prolonged hospitalizations, increased rates of diabetes and fatty liver disease, as well as a higher incidence of moderate to severe AP.

3.2 Relationship between CCR and the incidence of moderate to severe AP

Table 2 displays the findings from a multivariable logistic regression analysis, which assessed the association between CCR and the incidence of moderate to severe AP. When CCR was analyzed as a continuous variable, each one-unit rise (1 mg/mmol) was associated with a 7% increase in the risk of developing moderate to severe AP (OR: 1.07; 95% CI: 1.06–1.09). This relationship remained statistically significant after adjusting for covariates in models 2 and 3. In the fully adjusted model (Model 4), which included all covariates, each unit increase in CCR was still linked to a 7% higher risk of developing moderate to severe AP (OR: 1.07; 95% CI: 1.05–1.09).

Additionally, in the fully adjusted model (Model 4), when CCR was treated as a categorical variable, a clear trend was observed. Compared to the lowest CCR group (Q1), the adjusted OR for the second (Q2) and third quartiles (Q3) were 4.78 (95% CI: 2.70–8.45) and 74.95 (95% CI: 24.14–232.73), respectively. The trend analysis showed a statistically significant result ($p < 0.001$).

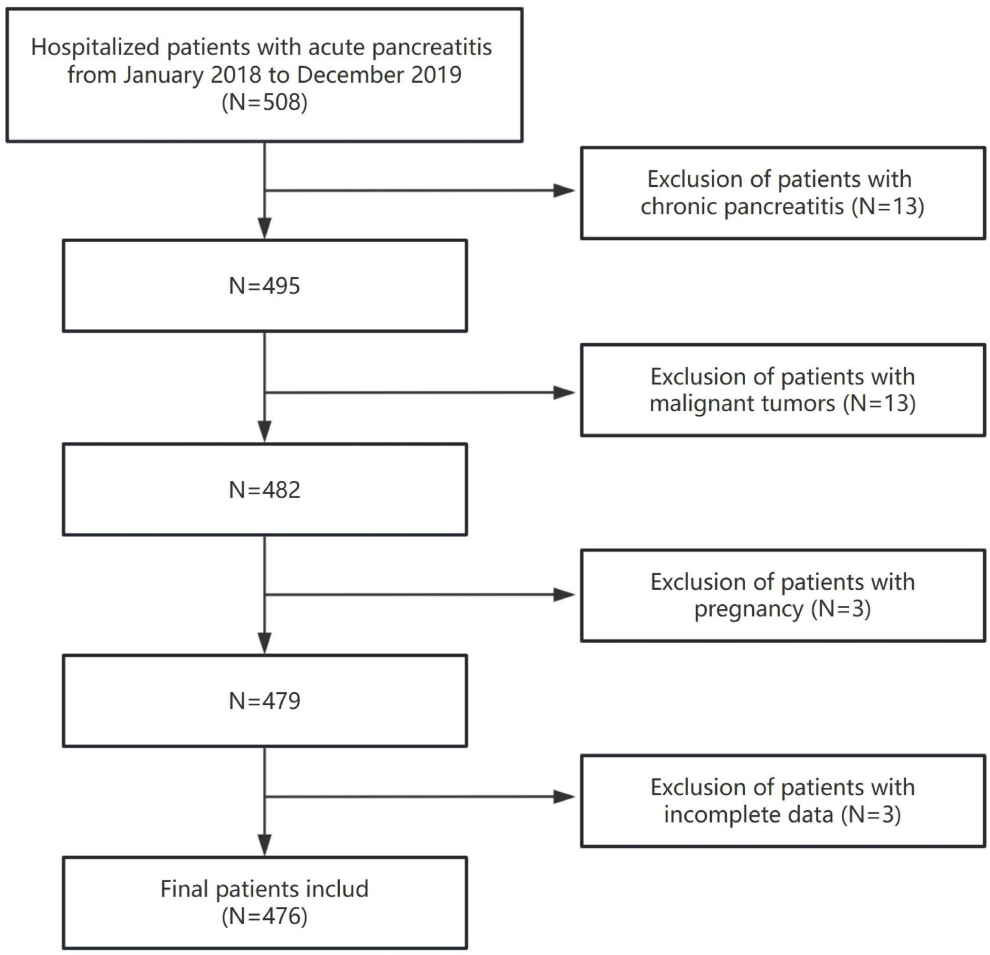

FIGURE 1
The flow chart of patient selection.

TABLE 1 Baseline characteristics of the patients with acute pancreatitis.

Covariates	Total (n = 476)	Q1 (n = 159)	Q2 (n = 158)	Q3 (n = 159)	p value
CCR, mg/mmol	17.5 (3.0, 60.2)	2.0 (1.0, 3.0)	17.5 (9.9, 30.0)	82.8 (60.4, 99.3)	< 0.001
Age, years	44.0 ± 13.2	45.3 ± 13.1	45.1 ± 14.0	41.7 ± 12.2	0.026
Gender					0.032
Male	364 (76.5)	115 (72.3)	116 (73.4)	133 (83.6)	
Female	112 (23.5)	44 (27.7)	42 (26.6)	26 (16.4)	
Smoking	161 (33.8)	49 (30.8)	45 (28.5)	67 (42.1)	0.023
Alcohol consumption	196 (41.2)	61 (38.4)	54 (34.2)	81 (50.9)	0.007
Diabetes	154 (32.4)	31 (19.5)	57 (36.1)	66 (41.5)	< 0.001
Fatty live	280 (58.8)	67 (42.1)	101 (63.9)	112 (70.4)	< 0.001
Etiology					< 0.001
Hypertriglyceridemia	277 (58.2)	68 (42.8)	94 (59.5)	115 (72.3)	
Biliary	92 (19.3)	36 (22.6)	34 (21.5)	22 (13.8)	
Alcohol	53 (11.1)	26 (16.4)	14 (8.9)	13 (8.2)	
Other	54 (11.3)	29 (18.2)	16 (10.1)	9 (5.7)	
Hospitalization days, days	6.0 (5.0, 9.0)	5.0 (4.0, 7.0)	6.0 (5.0, 8.0)	8.0 (6.0, 11.0)	< 0.001
Moderate to severe AP	300 (63.0)	40 (25.2)	105 (66.5)	155 (97.5)	< 0.001
WBC, 10^9/L	11.9 (9.3, 15.4)	10.1 (7.6, 12.0)	11.9 (9.8, 15.4)	14.3 (11.6, 17.1)	< 0.001
Hemoglobin, g/L	151.0 ± 22.9	146.9 ± 22.0	152.5 ± 23.8	153.8 ± 22.4	0.017
Platelets, 10^9/L	220.0 (181.0, 261.0)	225.0 (182.0, 268.0)	218.5 (171.2, 257.8)	220.0 (186.5, 253.5)	0.576
Serum amylase, U/L	246.5 (120.8, 627.5)	286.0 (132.0, 696.0)	234.0 (109.0, 676.0)	245.0 (117.5, 528.5)	0.189
Albumin, g/L	38.8 ± 16.9	41.8 ± 28.0	38.5 ± 5.2	36.0 ± 5.6	0.008
AST, U/L	27.0 (19.8, 44.0)	28.0 (20.0, 40.0)	27.5 (21.0, 47.0)	26.0 (19.0, 47.0)	0.459
ALT, U/L	27.0 (18.0, 45.2)	27.0 (18.5, 47.5)	30.0 (19.0, 54.0)	27.0 (17.0, 38.5)	0.287
Creatinine, umol/L	65.0 (55.0, 78.0)	64.4 (55.0, 76.0)	67.0 (56.2, 79.0)	64.0 (53.8, 79.0)	0.615
Sodium, mmol/L	133.6 ± 12.9	135.6 ± 11.3	133.4 ± 11.3	131.9 ± 15.5	0.041
Calcium, mmol/L	2.2 (2.1, 2.3)	2.3 (2.2, 2.3)	2.2 (2.2, 2.3)	2.1 (2.0, 2.3)	< 0.001
CRP, mg/L	38.2 (7.0, 126.0)	5.0 (2.4, 7.0)	38.2 (22.0, 67.0)	183.0 (126.0, 200.0)	< 0.001

CCR, C-reactive protein/serum calcium ratio; AP, acute pancreatitis; WBC, white blood cell; ALT, alanine transaminase; AST, aspartate transaminase; CRP, C-reactive protein.

TABLE 2 Association between C-reactive protein/serum calcium ratio and the incidence of moderate to severe acute pancreatitis.

Exposure	Model 1		Model 2		Model 3		Model 4	
	OR (95% CI)	P value	OR (95% CI)	P value	OR (95% CI)	P value	OR (95% CI)	P value
CCR	1.07 (1.06 ~ 1.09)	<0.001	1.07 (1.06 ~ 1.09)	<0.001	1.07 (1.05 ~ 1.09)	<0.001	1.07 (1.05 ~ 1.09)	<0.001
CCR tertiles								
Q1(1.0, 3.0)	Reference		Reference		Reference		Reference	
Q2(9.9, 30.0)	5.89 (3.62 ~ 9.59)	<0.001	6.36(3.84 ~ 10.53)	<0.001	5.10 (2.91 ~ 8.94)	<0.001	4.78 (2.70 ~ 8.45)	<0.001
Q3(60.4, 99.3)	115.28(40.13 ~ 331.16)	<0.001	115.53(39.76 ~ 335.66)	<0.001	78.7(25.57 ~ 242.24)	<0.001	74.95 (24.14 ~ 232.73)	<0.001
P for trend		<0.001		<0.001		<0.001		<0.001

Model 1: no covariates were adjusted. Model 2: adjusted for age and gender. Model 3: adjusted for age, gender, smoking, alcohol consumption, diabetes, fatty liver, etiology and hospitalization days. Model 4: adjusted for age, gender, smoking, alcohol consumption, diabetes, fatty liver, etiology, hospitalization days, hemoglobin and albumin. CCR, C-reactive protein/serum calcium ratio; OR, odds ratios; CI, confidence intervals.

3.3 Dose–response relationships

The study applied a logistic regression model with a cubic spline function to investigate how CCR relates to the incidence of moderate to severe AP. Figure 2 presents the distributions of variables (depicted as blue histograms), the relationship between CCR and the incidence of moderate to severe AP (shown by the solid red line), and the 95% confidence interval (marked by red

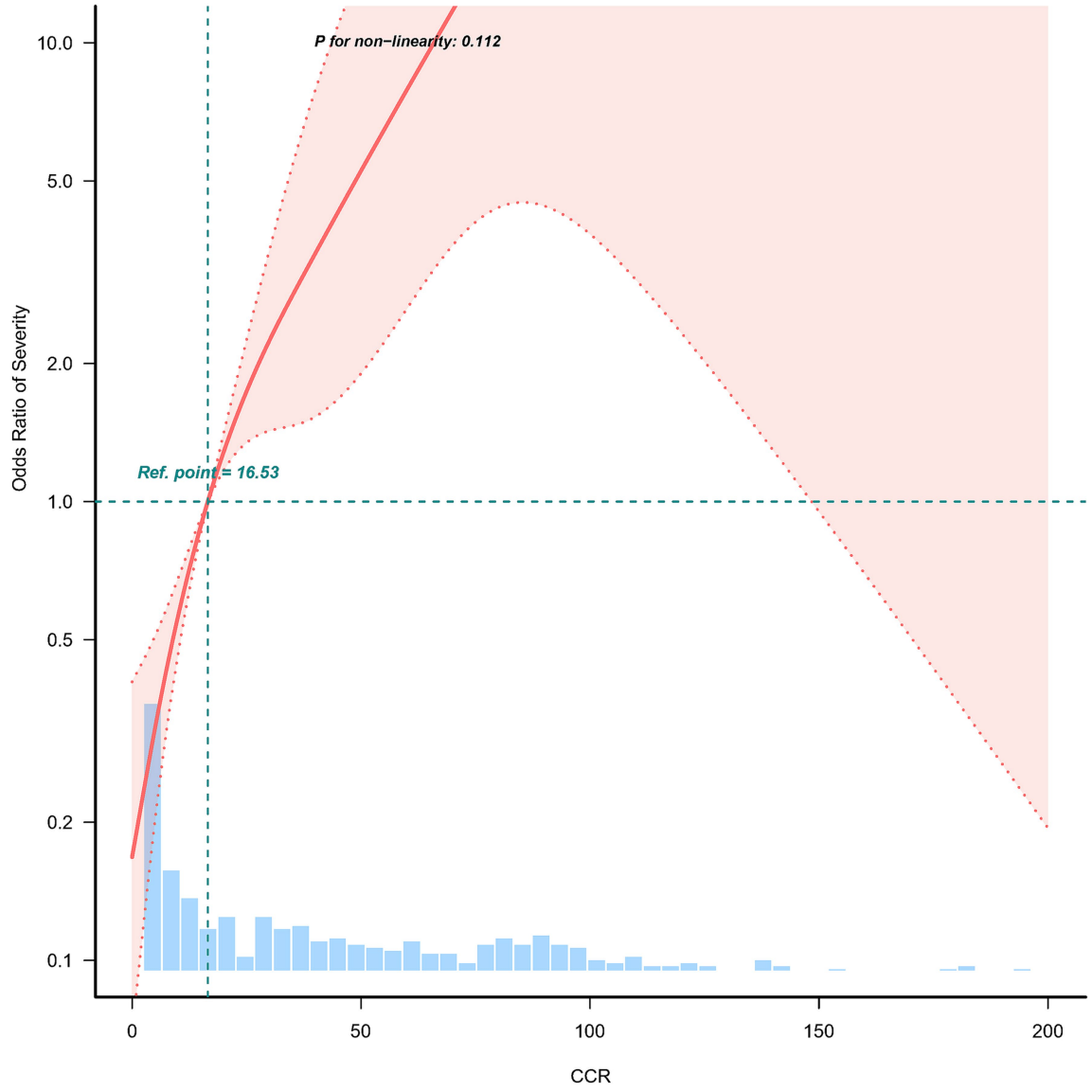

FIGURE 2
Nonlinear relationship between C-reactive protein/serum calcium ratio and the incidence of moderate to severe acute pancreatitis. Adjusted for age, gender, smoking, alcohol consumption, diabetes, fatty liver, etiology, hospitalization days, hemoglobin and albumin. The red line and the area between the red dashed lines represents the estimated values and their corresponding 95% confidence intervals, respectively.

dashed lines). After adjusting for confounding factors, a significant linear correlation between CCR and moderate to severe AP was found.

3.4 Subgroup analyses

The study further assessed possible modifiers that might influence the relationship between CCR and the incidence of moderate to severe AP. Stratification was performed based on variables like age, gender, smoking, alcohol consumption, diabetes, fatty liver, and etiology (Figure 3). Nonetheless, no significant interactions were detected.

3.5 ROC curve analysis

ROC curves were created to evaluate CCR's predictive accuracy for moderate to severe AP, with detailed results provided in Table 3 and illustrated in Figure 4. The CCR had an area under the curve (AUC) of 86.933% (95% CI: 83.765% ~ 90.100%), and the optimal cut-off value was found to be 16.733. This cut-off achieved a sensitivity of 73.7% and a specificity of 89.2%.

4 Discussion

This study demonstrated that the CCR is significantly associated with the severity of AP. Our results show that higher

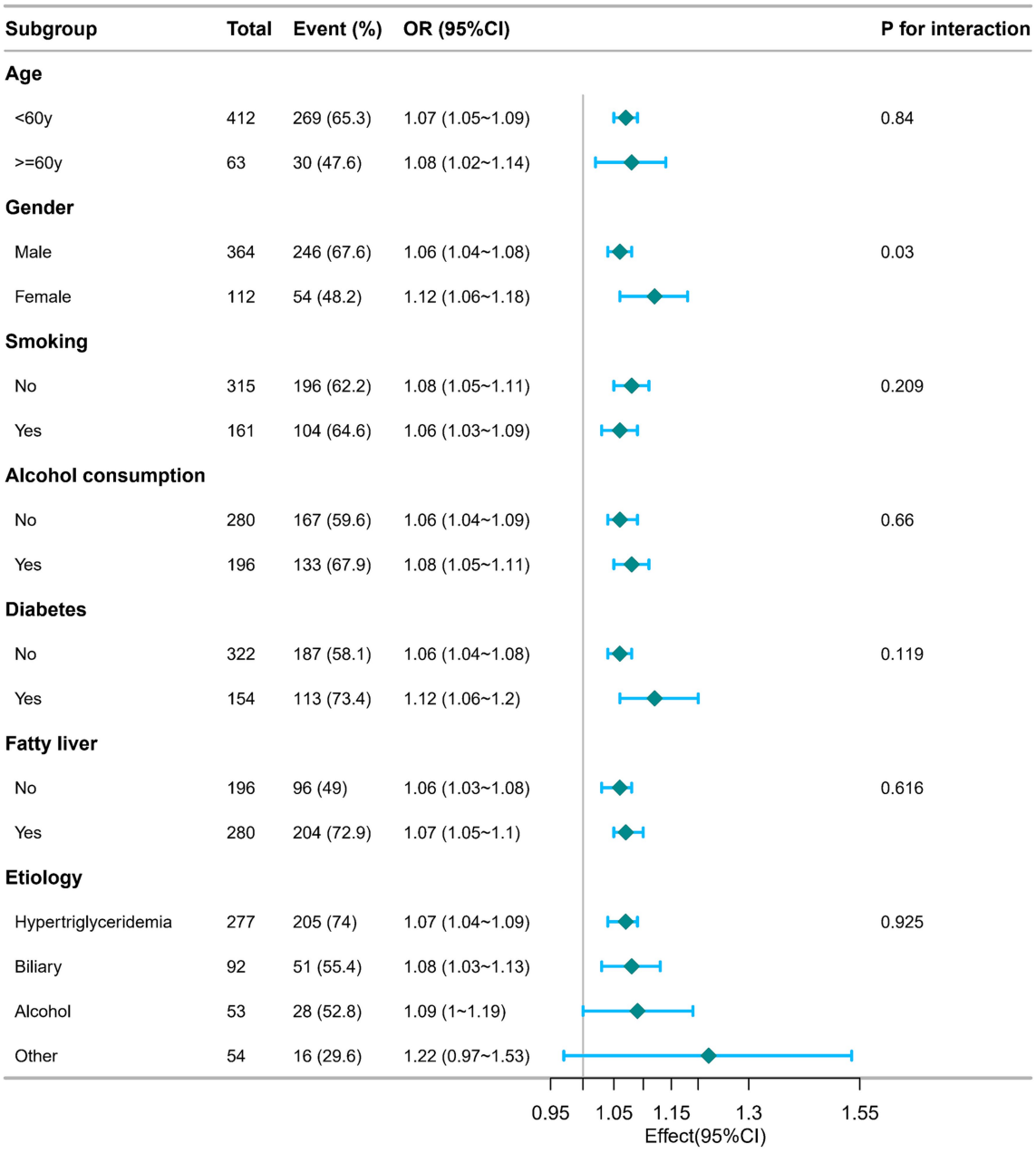

FIGURE 3
Subgroup analysis of the relationship between C-reactive protein/serum calcium ratio and the incidence of moderate to severe acute pancreatitis. Adjusted for age, gender, smoking, alcohol consumption, diabetes, fatty liver, etiology, hospitalization days, hemoglobin and albumin. OR, odds ratios; CI, confidence intervals.

TABLE 3 Information of receiver operating characteristic curve in Figure 4.

Variables	AUC	95%CI	Threshold	Sensitivity	Specificity
CCR	86.933%	83.765% ~ 90.100%	16.733	0.737	0.892

CCR, C-reactive protein/serum calcium ratio; AUC, area under the curve; CI, confidence intervals.

CCR levels are strongly correlated with an increased risk of moderate to severe AP. Specifically, each one-unit increase in CCR was associated with a 7% higher likelihood of developing moderate to severe AP, even after adjusting for relevant confounding factors. Additionally, when patients were stratified into tertiles based on their CCR levels, those in the highest tertile demonstrated a markedly higher risk of moderate to severe AP compared to those in the lowest tertile. These findings suggest

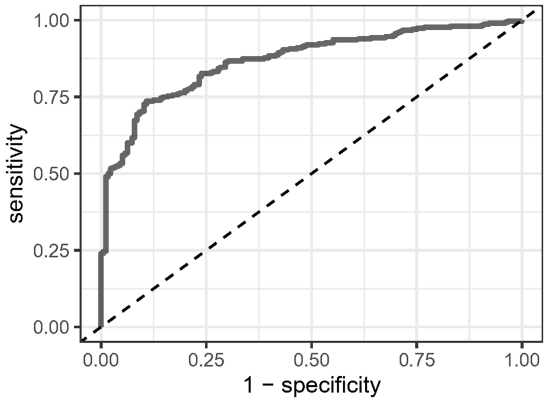

FIGURE 4
Receiver operating characteristic analysis of C-reactive protein/serum calcium ratio in predicting the onset of moderate to severe acute pancreatitis.

that CCR could be a valuable biomarker in predicting AP severity, providing clinicians with a tool for early risk stratification in AP patients. Furthermore, the dose–response relationship between CCR and AP severity, as demonstrated by the restricted cubic spline analysis, underscores the potential clinical utility of CCR in managing this condition.

AP is an inflammatory condition with diverse clinical presentations, varying progression, and different patient outcomes. While mild cases often resolve rapidly, severe cases can induce both local and systemic inflammatory responses, increasing the risk of organ dysfunction or failure, which can be life-threatening. Therefore, promptly identifying high-risk patients who could benefit from intensive care and close monitoring is crucial for effective management. In recent years, researchers have focused on developing systemic inflammatory biomarkers to predict the prognosis of AP patients at an early stage. Prominent biomarkers include the red blood cell distribution width to serum calcium ratio (RDW/Ca) (17), glycemic to lymphocyte ratio (GLR) (18), LAR (1), CLR (13), and NLR (14, 19). These biomarkers are being explored for their potential to offer early insights into disease progression and outcomes. However, no studies have yet explored the association between CCR and AP severity. Thus, this study is the first to evaluate the clinical relevance of CCR in AP.

The association between CRP and AP severity is well-documented, with higher CRP levels consistently linked to worse outcomes, such as necrotizing pancreatitis, organ failure, and increased mortality (20–22). However, CRP alone may not fully capture the metabolic alterations associated with severe AP, particularly hypocalcemia, which is a known marker of poor prognosis in this condition. Previous studies have shown that low serum calcium levels are correlated with increased mortality and disease severity in AP (20, 23, 24). Combining CRP and calcium into a single ratio (CCR) adds a metabolic dimension to the inflammatory marker, providing a more comprehensive assessment of disease severity.

Biologically, the interplay between inflammation and calcium metabolism in AP provides a plausible mechanism for the observed predictive power of CCR. CRP is produced in response to pro-inflammatory cytokines, such as interleukin-6 (IL-6), which are elevated in AP (25). The inflammatory response in severe AP is further exacerbated by the release of pancreatic enzymes that cause local tissue damage and fat necrosis, leading to the consumption of calcium for the formation of calcium soaps (26). This dual process of inflammation and calcium consumption likely drives the progression to more severe disease. The CCR, by combining CRP and serum calcium, effectively reflects both of these pathological processes, making it a robust marker of disease severity. We further evaluated the predictive power of CCR within the first 24 h for determining moderate to severe AP, finding an AUC of 86.933%, indicating strong discriminative ability. Given the simplicity and widespread availability of both CRP and serum calcium measurements in clinical practice, CCR could offer a more practical alternative to complex scoring systems.

The strengths of this study lie in the use of CCR, a novel composite biomarker that evaluates AP severity by integrating inflammation and metabolic disturbances. Furthermore, the large sample size and rigorous multivariable adjustments used in our study enhance the robustness and reliability of our findings. However, there are several limitations to our study. First, the cross-sectional design of the study precludes the establishment of a causal relationship between CCR and the development of moderate to severe AP. Second, as this is a single-center study conducted solely within a Chinese population, the generalizability of our findings to other populations may be limited. Lastly, although we adjusted for several key confounding factors, unmeasured variables may still have influenced the outcomes.

5 Conclusion

The CCR measured within the first 24 h of admission shows promise as a valuable biomarker for predicting the severity of AP. However, further multicenter prospective cohort studies are needed to confirm its clinical utility and investigate its role in improving treatment strategies and patient management.

Data availability statement

The data analyzed in this study is subject to the following licenses/restrictions: the datasets generated or analyzed during this study are available from the corresponding author upon reasonable request. Requests to access these datasets should be directed to Xinqi Chen, nydxc2010@163.com.

Ethics statement

The studies involving humans were approved by Ethics Committee of Quanzhou First Hospital. The studies were conducted in accordance with the local legislation and institutional requirements. The ethics committee/institutional review board waived the requirement of written informed consent for participation from the participants or the participants' legal guardians/next of kin because given its retrospective nature and

use of anonymized data, informed consent was waived. Written informed consent was not obtained from the individual(s) for the publication of any potentially identifiable images or data included in this article because given its retrospective nature and use of anonymized data, informed consent was waived.

Author contributions

XC: Conceptualization, Methodology, Writing – original draft. YH: Conceptualization, Formal analysis, Methodology, Software, Writing – review & editing. QX: Data curation, Writing – original draft. BZ: Data curation, Writing – original draft. YW: Writing – review & editing, Supervision. MH: Writing – review & editing, Supervision.

Funding

The author(s) declare that no financial support was received for the research, authorship, and/or publication of this article.

Acknowledgments

We thank Jie Liu, Ph.D. (Department of Vascular and Endovascular Surgery, Chinese PLA General Hospital), for his valuable input on the study design and manuscript.

Conflict of interest

The authors declare that the research was conducted in the absence of any commercial or financial relationships that could be construed as a potential conflict of interest.

Generative AI statement

The author(s) declare that no Gen AI was used in the creation of this manuscript.

Publisher's note

All claims expressed in this article are solely those of the authors and do not necessarily represent those of their affiliated organizations, or those of the publisher, the editors and the reviewers. Any product that may be evaluated in this article, or claim that may be made by its manufacturer, is not guaranteed or endorsed by the publisher.

Supplementary material

The Supplementary material for this article can be found online at: https://www.frontiersin.org/articles/10.3389/fmed.2025.1506543/full#supplementary-material

References

1. Liu Q, Zheng HL, Wu MM, Wang QZ, Yan SJ, Wang M, et al. Association between lactate-to-albumin ratio and 28-days all-cause mortality in patients with acute pancreatitis: a retrospective analysis of the MIMIC-IV database. *Front Immunol*. (2022) 13:1076121. doi: 10.3389/fimmu.2022.1076121

2. Zhou H, Mei X, He X, Lan T, Guo S. Severity stratification and prognostic prediction of patients with acute pancreatitis at early phase: a retrospective study. *Medicine*. (2019) 98:e15275. doi: 10.1097/MD.0000000000015275

3. Szatmary P, Grammatikopoulos T, Cai W, Huang W, Mukherjee R, Halloran C, et al. Acute pancreatitis: diagnosis and treatment. *Drugs*. (2022) 82:1251–76. doi: 10.1007/s40265-022-01766-4

4. Boxhoorn L, Voermans RP, Bouwense SA, Bruno MJ, Verdonk RC, Boermeester MA, et al. Acute pancreatitis. *Lancet (London, England)*. (2020) 396:726–34. doi: 10.1016/S0140-6736(20)31310-6

5. Saluja A, Dudeja V, Dawra R, Sah RP. Early intra-acinar events in pathogenesis of pancreatitis. *Gastroenterology*. (2019) 156:1979–93. doi: 10.1053/j.gastro.2019.01.268

6. Schepers NJ, Bakker OJ, Besselink MG, Ahmed Ali U, Bollen TL, Gooszen HG, et al. Impact of characteristics of organ failure and infected necrosis on mortality in necrotising pancreatitis. *Gut*. (2019) 68:1044–51. doi: 10.1136/gutjnl-2017-314657

7. Onnekink AM, Boxhoorn L, Timmerhuis HC, Bac ST, Besselink MG, Boermeester MA, et al. Endoscopic versus surgical step-up approach for infected necrotizing pancreatitis (ExTENSION): long-term follow-up of a randomized trial. *Gastroenterology*. (2022) 163:712–22.e14. doi: 10.1053/j.gastro.2022.05.015

8. Trikudanathan G, Wolbrink DRJ, van Santvoort HC, Mallery S, Freeman M, Besselink MG. Current concepts in severe acute and necrotizing pancreatitis: an evidence-based approach. *Gastroenterology*. (2019) 156:1994–2007.e3. doi: 10.1053/j.gastro.2019.01.269

9. Ranson JH, Rifkind KM, Roses DF, Fink SD, Eng K, Localio SA. Objective early identification of severe acute pancreatitis. *Am J Gastroenterol*. (1974) 61:443–51.

10. Wu BU, Johannes RS, Sun X, Tabak Y, Conwell DL, Banks PA. The early prediction of mortality in acute pancreatitis: a large population-based study. *Gut*. (2008) 57:1698–703. doi: 10.1136/gut.2008.152702

11. Balthazar EJ, Robinson DL, Megibow AJ, Ranson JH. Acute pancreatitis: value of CT in establishing prognosis. *Radiology*. (1990) 174:331–6. doi: 10.1148/radiology.174.2.2296641

12. Knaus WA, Draper EA, Wagner DP, Zimmerman JE. APACHE II: a severity of disease classification system. *Crit Care Med*. (1985) 13:818–29. doi: 10.1097/00003246-198510000-00009

13. Chen X, Lin Z, Chen Y, Lin C. C-reactive protein/lymphocyte ratio as a prognostic biomarker in acute pancreatitis: a cross-sectional study assessing disease severity. *Int J Surg (London, England)*. (2024) 110:3223–9. doi: 10.1097/JS9.0000000000001273

14. Huang L, Chen C, Yang L, Wan R, Hu G. Neutrophil-to-lymphocyte ratio can specifically predict the severity of hypertriglyceridemia-induced acute pancreatitis compared with white blood cell. *J Clin Lab Anal*. (2019) 33:e22839. doi: 10.1002/jcla.22839

15. Banks PA, Bollen TL, Dervenis C, Gooszen HG, Johnson CD, Sarr MG, et al. Classification of acute pancreatitis—2012: revision of the Atlanta classification and definitions by international consensus. *Gut*. (2013) 62:102–11. doi: 10.1136/gutjnl-2012-302779

16. Qu X, Yang H, Yu Z, Jia B, Qiao H, Zheng Y, et al. Serum zinc levels and multiple health outcomes: implications for zinc-based biomaterials. *Bioactive Mat*. (2020) 5:410–22. doi: 10.1016/j.bioactmat.2020.03.006

17. Han T, Cheng T, Liao Y, He Y, Liu B, Lai Q, et al. The ratio of red blood cell distribution width to serum calcium predicts severity of patients with acute pancreatitis. *Am J Emerg Med*. (2022) 53:190–5. doi: 10.1016/j.ajem.2022.01.024

18. Chen Y, Tang S, Wang Y. Prognostic value of glucose-to-lymphocyte ratio in critically ill patients with acute pancreatitis. *Int J Gen Med*. (2021) 14:5449–60. doi: 10.2147/IJGM.S327123

19. Kong W, He Y, Bao H, Zhang W, Wang X. Diagnostic value of neutrophil-lymphocyte ratio for predicting the severity of acute pancreatitis: a Meta-analysis. *Dis Markers*. (2020) 2020:1–9. doi: 10.1155/2020/9731854

20. Silva-Vaz P, Abrantes AM, Castelo-Branco M, Gouveia A, Botelho MF, Tralhão JG. Multifactorial scores and biomarkers of prognosis of acute pancreatitis: applications to research and practice. *Int J Mol Sci*. (2020) 21:338. doi: 10.3390/ijms21010338

21. Mikó A, Vigh É, Mátrai P, Soós A, Garami A, Balaskó M, et al. Computed tomography severity index vs. other indices in the prediction of severity and mortality in acute pancreatitis: a predictive accuracy Meta-analysis. *Front Physiol*. (2019) 10:1002. doi: 10.3389/fphys.2019.01002

22. Tian F, Li H, Wang L, Li B, Aibibula M, Zhao H, et al. The diagnostic value of serum C-reactive protein, procalcitonin, interleukin-6 and lactate dehydrogenase in patients with severe acute pancreatitis. *Int J Clin Chem*. (2020) 510:665–70. doi: 10.1016/j.cca.2020.08.029

23. Yu S, Wu D, Jin K, Yin L, Fu Y, Liu D, et al. Low serum ionized calcium, elevated high-sensitivity C-reactive protein, neutrophil-lymphocyte ratio, and body mass index (BMI) are risk factors for severe acute pancreatitis in patients with hypertriglyceridemia pancreatitis. *Med Sci Mon*. (2019) 25:6097–103. doi: 10.12659/MSM.915526

24. Peng T, Peng X, Huang M, Cui J, Zhang Y, Wu H, et al. Serum calcium as an indicator of persistent organ failure in acute pancreatitis. *Am J Emerg Med*. (2017) 35:978–82. doi: 10.1016/j.ajem.2017.02.006

25. Wu W, Zhang YP, Pan YM, He ZJ, Tan YP, Wang DD, et al. Predictive value of C-reactive protein/albumin ratio for acute kidney injury in patients with acute pancreatitis. *J Inflamm Res*. (2024) 17:5495–507. doi: 10.2147/JIR.S473466

26. Weir GC, Lesser PB, Drop LJ, Fischer JE, Warshaw AL. The hypocalcemia of acute pancreatitis. *Ann Intern Med*. (1975) 83:185–9. doi: 10.7326/0003-4819-83-2-185

frontiers | Frontiers in Immunology

TYPE Original Research
PUBLISHED 10 February 2025
DOI 10.3389/fimmu.2025.1544917

OPEN ACCESS

EDITED BY
Yi Wu,
Xi'an Jiaotong University, China

REVIEWED BY
Johannes Zeller,
Freiburg University Medical Center, Germany
Bin Cheng,
Lanzhou University, China

*CORRESPONDENCE
Fan Zhang
yifan52518@163.com
Wenjian Li
bolite@163.com

†These authors have contributed equally to this work

RECEIVED 13 December 2024
ACCEPTED 23 January 2025
PUBLISHED 10 February 2025

CITATION
Wu Y, Zheng G, Zhang F and Li W (2025) Association of high-sensitivity C-reactive protein with hepatic fibrosis in patients with metabolic dysfunction-associated steatotic liver disease. *Front. Immunol.* 16:1544917. doi: 10.3389/fimmu.2025.1544917

Association of high-sensitivity C-reactive protein with hepatic fibrosis in patients with metabolic dysfunction-associated steatotic liver disease

Yunfei Wu[1,2†], Guojun Zheng[2,3†], Fan Zhang[2,4,5*] and Wenjian Li[2,6*]

[1]Department of Pathology, Changzhou Third People's Hospital, Changzhou, China, [2]Changzhou Clinical College, Xuzhou Medical University, Changzhou, China, [3]Clinical Laboratory, Changzhou Third People's Hospital, Changzhou, China, [4]Department of Endocrinology, Changzhou Third People's Hospital, Changzhou, China, [5]Department of Clinical Nutrition, Changzhou Third People's Hospital, Changzhou, China, [6]Department of Urology, Changzhou Third People's Hospital, Changzhou, China

Objective: This study aimed to investigate the association between high-sensitivity C-reactive protein (hsCRP) levels and hepatic fibrosis in patients with metabolic dysfunction-associated steatotic liver disease (MASLD) and assess its predictive efficacy.

Methods: The study included 1,477 participants from the United States and 1,531 from China diagnosed with MASLD. Liver stiffness measurement (LSM) and controlled attenuation parameter (CAP) were assessed by vibration-controlled transient elastography (VCTE) to evaluate the presence and degree of hepatic fibrosis and steatosis. The relationship between hsCRP levels and hepatic fibrosis in MASLD patients was examined using multivariable-adjusted and restricted cubic spline (RCS) models. Additionally, subgroup analyses were conducted to investigate the potential heterogeneity among different characteristic subgroups.

Results: The results demonstrated a significant correlation between elevated hsCRP levels and an increased risk of significant fibrosis, advanced fibrosis, and cirrhosis in the US cohort of MASLD patients (OR 2.22, 1.69, and 2.85, respectively; all P <0.05). The results of the Chinese cohort were consistent with those of the US cohort, and there was a significant and positive correlation between hsCRP levels and the risk of hepatic fibrosis in patients with MASLD (OR 2.53, 3.85, and 3.78, respectively, all P <0.001). The RCS analysis revealed a significant non-linear relationship between hsCRP levels and the degree of hepatic fibrosis, with disparate inflection point values observed across different cohorts (approximately 9 mg/L in the US cohort and 4 mg/L in the Chinese cohort). The impact of hsCRP levels on the risk of hepatic fibrosis varied across different subgroups with distinct characteristics.

Conclusion: The present study demonstrated a significant correlation between hsCRP levels and the degree of hepatic fibrosis in patients with MASLD, with notable dose-response relationships and subgroup differences.

KEYWORDS

high-sensitivity C-reactive protein, metabolic dysfunction-associated steatotic liver disease, hepatic fibrosis, cross-regional study, dose-response relationship

1 Introduction

Metabolic dysfunction-associated steatotic liver disease (MASLD) is a modern lifestyle disease that has emerged as a significant public health concern, with a marked increase in prevalence across the globe in recent years (1–4). MASLD not only disrupts the normal physiological function of the liver but also frequently coexists with components of metabolic syndrome, including obesity, diabetes mellitus (DM), hypertension, and dyslipidemia. These comorbidities further elevate the risk of cardiovascular disease (1, 3, 5–8). In the pathological progression of MASLD, hepatic fibrosis represents a pivotal stage whereby the liver's repair response to chronic injury, specifically the aberrant proliferation of intrahepatic connective tissue and its gradual replacement of normal liver tissue, becomes evident. In the absence of timely and effective intervention, hepatic fibrosis will continue to deteriorate, potentially leading to the development of cirrhosis or even hepatocellular carcinoma (2, 5, 9, 10). This can have a significantly detrimental impact on the lives and health of patients.

The pathogenesis of hepatic fibrosis is a complex and intricate process involving many factors, such as inflammation, oxidative stress, and abnormalities in lipid metabolism. Among these, inflammation plays a pivotal role at the core of the disease (9, 11, 12). As a sensitive inflammatory marker, the high-sensitivity C-reactive protein (hsCRP) concentration in the blood can be a sensitive indicator of the body's low-grade inflammatory response (13, 14). A substantial body of evidence indicates that hsCRP levels are strongly linked to the onset of cardiovascular disease, diabetes, and its associated complications (15–17). In recent years, there has been a notable increase in research activity concerning the role of hsCRP in the study of non-alcoholic fatty liver disease (NAFLD) and its complications. Several studies have demonstrated that elevated hsCRP levels are positively correlated with the severity of NAFLD and the progression of hepatic fibrosis, indicating that inflammatory responses play a pivotal role in the pathological process of NAFLD (18–21). Nevertheless, research examining the correlation between hsCRP and hepatic fibrosis in patients with MASLD remains limited. In contrast to NAFLD, MASLD emphasizes the pivotal role of metabolic irregularities in the pathogenesis of the disease, encompassing a spectrum of metabolic abnormalities such as obesity, insulin resistance, dyslipidemia, and other metabolic disorders. Although there are numerous similarities between MASLD and NAFLD regarding the underlying pathophysiological mechanisms, there may be notable differences between the two regarding the clinical manifestations, rate of disease progression, and incidence of complications. It is, therefore, of great significance to explore the association between MASLD and hsCRP to deepen the understanding of MASLD and optimize its prevention and treatment strategies.

To address this research gap, this study examined the relationship between hsCRP levels and hepatic fibrosis in patients with MASLD. To this end, data from two distinct cohorts were integrated: the National Health and Nutrition Examination Survey (NHANES) cohort in the United States and the Third People's Hospital Cohort in Changzhou, China. The NHANES cohort, as one of the most representative national health surveys in the United States, provides a wealth of cross-sectional data, which can facilitate a comprehensive understanding of the prevalence of MASLD and its associated complications. The Changzhou Third People's Hospital cohort, on the other hand, provided pertinent data from the Chinese population, enabling this study to transcend geographical boundaries and enhance the representativeness and generalizability of the results.

This study aimed to verify whether hsCRP levels are associated with an increased risk of hepatic fibrosis in patients with MASLD and to elucidate the underlying mechanisms of this association, the dose-response relationship, and the differences in different population subgroups. The central inquiries of this study are as follows: (1) Is there a correlation between hsCRP levels and the degree of hepatic fibrosis in patients with MASLD? (2) Can hsCRP independently predict hepatic fibrosis in patients with MASLD? By constructing a multivariable adjustment model and a restricted cubic spline model, this study aimed to explore the possible independent association and dose-response relationship between the two to provide new insights and rationale for the clinical management of MASLD.

2 Materials and methods

2.1 Study population

The data for this study were derived from two distinct cohorts: the NHANES cohort from 2017 to 2018 in the United States and the Changzhou Third People's Hospital cohort in China from 2018 to 2023. The NHANES database contains data from cross-sectional

surveys conducted every two years by the Centers for Disease Control and Prevention (CDC). The study protocol for the database was approved by the Ethics Review Committee of the National Center for Health Statistics (NCHS), and all participants provided informed consent. Following NIH regulations, the NHANES data, which were not collected through direct interaction with participants, could be utilized directly for data analysis without further review by the institutional ethics committee. Given the considerations above, the Ethics Committee of Changzhou Third People's Hospital concluded that no further ethical review was necessary for the NHANES data utilized in this study. Additionally, the study of the Chinese cohort was also approved by the Ethics Committee of Changzhou Third People's Hospital. This study was conducted by the principles outlined in the Declaration of Helsinki.

The study included 9,254 US participants and 10,477 Chinese participants. During the screening process, the following participants were excluded: those under the age of 20 or pregnant, those with no liver stiffness measurement (LSM) or controlled attenuation parameter (CAP) data or no hsCRP data, those with excessive alcohol consumption, and those with viral hepatitis B or C. Additionally, participants with any history of autoimmune hepatitis or hepatocellular carcinoma, those who had taken any medications that may cause fatty liver (e.g., amiodarone, methotrexate, and tamoxifen) within the three months before survey recruitment, and those with missing demographic data, chronic disease data, or critical biochemical markers were excluded. Non-MASLD participants were also excluded. After a comprehensive screening process, 1,477 US and 1,531 Chinese participants were ultimately included in the study for data analysis (Figure 1).

2.2 Assessment of MASLD and hepatic fibrosis

Vibration-controlled transient elastography (VCTE) was conducted to evaluate the degree of hepatic steatosis, with CAP measurements taken for this purpose. Each participant's CAP value of 269 dB/m or greater indicated hepatic steatosis (22). Furthermore, a diagnosis of MASLD was confirmed if any of the following five cardiometabolic criteria were met: (1) A body mass index (BMI) of 25 kg/m^2 or greater or a waist circumference (WC) of 94 cm or greater for males and 80 cm or greater for females; (2) a fasting plasma glucose

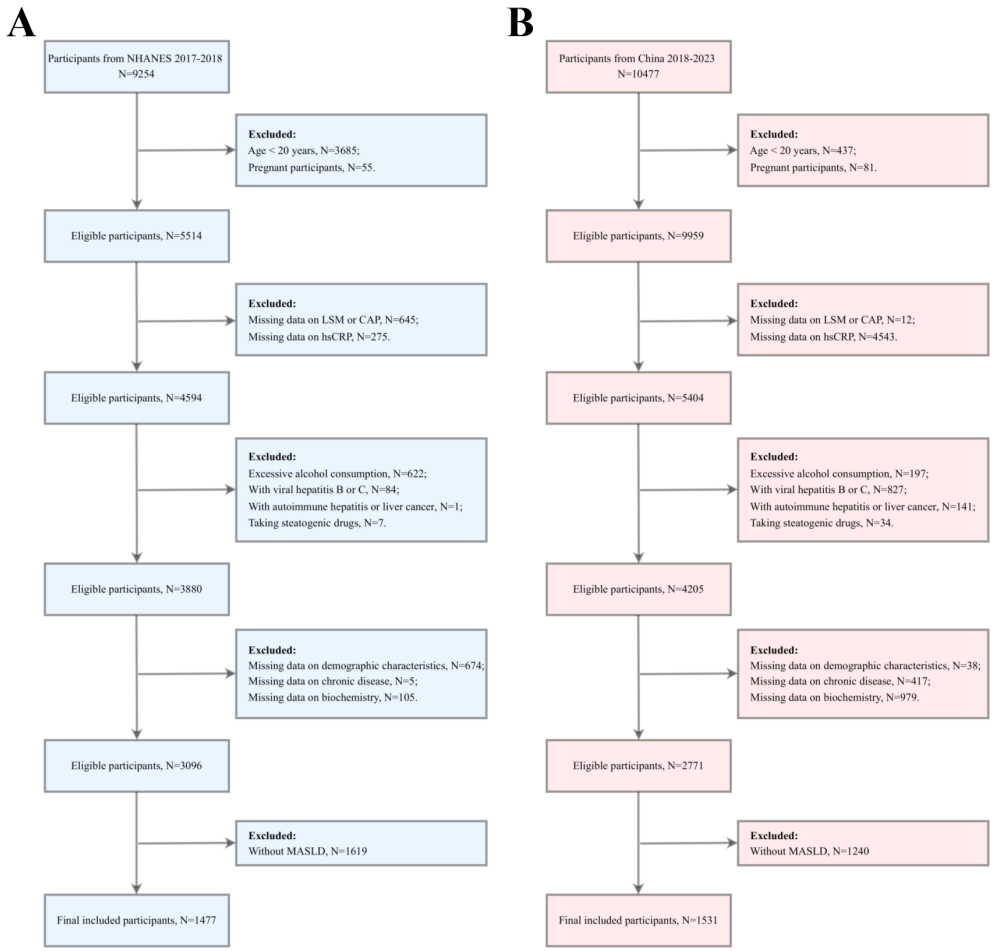

FIGURE 1
Participant screening flowchart. **(A)** the US cohort; **(B)** the Chinese cohort. LSM, Liver stiffness measurement; CAP, Controlled attenuation parameter; hsCRP, high-sensitivity C-reactive protein; MASLD, Metabolic dysfunction-associated steatotic liver disease.

(FPG) level of 100 mg/dL or greater, or a two-hour post-load blood glucose level of 140 mg/dL or greater, or a glycated hemoglobin (HbA1C) level of 5.7% or greater, or a diagnosis of DM or on glucose-lowering therapy for DM; (3) a blood pressure reading of ≥130/85 mmHg, or the use of antihypertensive medication; (4) a triglyceride (TG) level ≥150 mg/dL or the use of lipid-lowering therapy; (5) a high-density lipoprotein cholesterol (HDL-C) level <40 mg/dL in men or an HDL-C level <50 mg/dL in women or the use of lipid-lowering therapy (5).

Hepatic fibrosis was evaluated based on LSM values. An LSM of ≥7.6 was considered indicative of significant hepatic fibrosis (F2), while an LSM of ≥9.8 was indicative of advanced hepatic fibrosis (F3). An LSM of ≥12.9 was indicative of cirrhosis (F4) (22).

2.3 hsCRP assessment

In the United States cohort, the hsCRP assay during the 2017-2018 cycle was conducted using a near-infrared particle immunoassay rate method with a Roche Cobas 6000 chemistry analyzer (Cobas 6000), as detailed in the Laboratory Methods Documentation section of the NHANES. The hsCRP assay for the Chinese cohort was based on an immunoscattering turbidimetric method, with measurements taken using a Lifotronic Specific Protein Analyzer (PA-990Pro).

2.4 Assessment of covariates

In this study, the covariates included gender (male/female), age (years), smoking status (yes/no), drinking habits (yes/no), and history of chronic diseases such as DM, hypertension, and dyslipidemia. DM was determined based on the participant's professional doctor's diagnosis, FPG level of 126 mg/dl or more, HbA1c level of not less than 6.5%, and treatment with diabetes medication or insulin. Hypertension was identified based on the participant's self-reported medical history or current prescription for hypertension medication. Dyslipidemia was defined as the presence of one or more of the following in participants: total cholesterol (TC) ≥200 mg/dL, TG ≥150 mg/dL, HDL-C <50 mg/dL (in women) or <40 mg/dL (in men), and low-density lipoprotein cholesterol (LDL-C) ≥130 mg/dL.

2.5 Statistical analysis

This study assessed normality for continuous variables using the Kolmogorov-Smirnov test. Variables that exhibited a normal distribution were expressed as mean ± standard deviation, whereas those that did not conform to a normal distribution were described using the median (and 25th to 75th percentile). To compare the differences between these variables, one-way ANOVA or Kruskal-Wallis tests were selected for statistical analysis based on the distributional characteristics of the data. Categorical variables were presented as frequencies and percentages, and the chi-square test was employed to compare differences between groups.

We constructed a logistic regression model to investigate the potential association between hsCRP and hepatic fibrosis in patients with MASLD. We calculated the odds ratio (OR) and its 95% confidence interval (CI). We constructed multivariable-adjusted models to assess this relationship more accurately and control for potential confounding variables. Specifically, Model 1 was the unadjusted base model; Model 2 incorporated gender and age as adjustment variables based on Model 1; and Model 3 further adjusted for smoking, alcohol consumption, diabetes, hypertension, and dyslipidemia based on Model 2. Furthermore, we employed the restricted cubic spline (RCS) model to investigate the potential dose-response relationship between hsCRP and hepatic fibrosis in MASLD patients. Based on the inflection point values obtained from the RCS analysis, the data were divided into two intervals and subjected to further analysis using segmented logistic regression. This allowed for a more detailed examination of the associations between the predictor variables and the results of each segment.

To investigate the relationship between hsCRP and the risk of hepatic fibrosis in MASLD patients across different subgroups, we conducted a subgroup analysis according to gender (male/female), smoking status (yes/no), alcohol consumption (yes/no), presence of DM (yes/no), hypertension (yes/no), and dyslipidemia (yes/no), and performed an interaction analysis. To assess the efficacy of hsCRP in predicting the degree of hepatic fibrosis in patients with MASLD, we employed receiver operating characteristic (ROC) curve analysis.

All statistical analyses employed a two-sided test, and a P-value of less than 0.05 was used as the threshold for determining statistical significance. All statistical analyses were conducted using R 4.4.0 (R Foundation, http://www.R-project.org) and SPSS 23.0 (IBM Corporation, Armonk, NY, USA) software. GraphPad Prism version 9.0 (GraphPad Software, Inc., USA) facilitated the generation of graphical representations.

3 Results

3.1 Baseline characteristics of patients with MASLD based on hsCRP quartiles in the US cohort

The results demonstrated a statistically significant reduction in the proportion of male patients (from 62.30% to 35.04%, P < 0.001) with increasing hsCRP levels. The median age decreased (57.00 to 52.00 years, P < 0.001). The proportions of alcohol consumption, hypertension, DM, and dyslipidemia differed significantly among the different hsCRP quartiles (P values of 0.004, 0.029, <0.001, and <0.001, respectively). Furthermore, BMI, WC, HbA1c, TC, white blood cells (WBC), neutrophils, lymphocytes, monocytes, platelets, gamma-glutamyltransferase (GGT), LSM, and CAP increased with elevated hsCRP levels (all P <0.05). Conversely, HDL-C levels exhibited a decline. Regarding hepatic fibrosis, the prevalence of significant fibrosis, advanced fibrosis, and cirrhosis demonstrated a notable increase with elevated hsCRP levels (P values of <0.001, 0.005, and <0.001, respectively) (Table 1).

10.3389/fimmu.2025.1544917

TABLE 1 Baseline characteristics of MASLD patients based on hsCRP quartiles in the US cohort.

Variables	hsCRP				
	Quartile 1 (n = 366)	Quartile 2 (n = 372)	Quartile 3 (n = 368)	Quartile 4 (n = 371)	*P*
Gender, n (%)					<0.001
Male	228 (62.30)	222 (59.68)	183 (49.73)	130 (35.04)	
Female	138 (37.70)	150 (40.32)	185 (50.27)	241 (64.96)	
Age (years)	57.00 (43.00,68.00)	56.00 (42.00,68.00)	52.00 (41.00,64.00)	52.00 (39.00,62.00)	<0.001
Smoke, n (%)					0.276
Yes	156 (42.62)	145 (38.98)	155 (42.12)	171 (46.09)	
No	210 (57.38)	227 (61.02)	213 (57.88)	200 (53.91)	
Alcohol, n (%)					0.004
Yes	193 (52.73)	179 (48.12)	173 (47.01)	147 (39.62)	
No	173 (47.27)	193 (51.88)	195 (52.99)	224 (60.38)	
Hypertension, n (%)					0.029
Yes	147 (40.16)	176 (47.31)	186 (50.54)	180 (48.52)	
No	219 (59.84)	196 (52.69)	182 (49.46)	191 (51.48)	
Diabetes, n (%)					<0.001
Yes	89 (24.32)	112 (30.11)	103 (27.99)	150 (40.43)	
No	277 (75.68)	260 (69.89)	265 (72.01)	221 (59.57)	
Dyslipidemia, n (%)					<0.001
Yes	250 (68.31)	277 (74.46)	296 (80.43)	292 (78.71)	
No	116 (31.69)	95 (25.54)	72 (19.57)	79 (21.29)	
BMI (kg/m^2)	28.60 (26.30,32.10)	30.55 (28.00,34.20)	33.45 (29.10,37.70)	36.90 (31.75,42.80)	<0.001
WC (cm)	99.70 (94.53,108.80)	105.60 (98.55,114.82)	110.55 (101.25,120.90)	117.50 (106.20,128.40)	<0.001
FPG (mg/dL)	96.00 (89.00,106.75)	96.00 (89.00,110.25)	97.00 (89.75,110.00)	99.00 (90.00,118.50)	0.064
HbA1c (%)	5.70 (5.40,6.00)	5.70 (5.40,6.20)	5.80 (5.40,6.20)	5.90 (5.50,6.70)	<0.001
TC (mg/dL)	185.50 (160.00,219.75)	190.00 (161.00,218.00)	195.50 (169.00,221.00)	187.00 (161.00,213.00)	0.036
TG (mg/dL)	133.00 (95.00,196.00)	150.00 (101.00,212.25)	150.00 (106.00,214.25)	139.00 (105.00,189.50)	0.052
HDL-c (mg/dL)	49.00 (41.00,61.00)	46.00 (39.00,55.00)	45.00 (39.00,52.00)	46.00 (38.00,55.00)	<0.001
WBC (10^3 cells/μL)	6.60 (5.60,8.07)	7.10 (6.10,8.40)	7.50 (6.30,8.90)	8.30 (6.80,10.00)	<0.001
Neutrophils (10^3 cells/μL)	3.50 (2.90,4.60)	4.10 (3.20,5.10)	4.30 (3.48,5.30)	5.00 (3.80,6.27)	<0.001
Lymphocyte (10^3 cells/μL)	2.10 (1.70,2.60)	2.20 (1.80,2.70)	2.30 (1.80,2.70)	2.35 (1.80,2.90)	0.001
Monocyte (10^3 cells/μL)	0.50 (0.40,0.70)	0.60 (0.50,0.70)	0.60 (0.50,0.70)	0.60 (0.50,0.70)	<0.001
Platelet (10^3 cells/μL)	226.50 (197.00,264.75)	233.00 (193.75,271.00)	242.50 (207.75,281.00)	267.00 (228.00,311.00)	<0.001
AST (U/L)	20.00 (17.00,24.75)	21.00 (17.00,25.00)	20.00 (17.00,26.25)	18.00 (14.00,24.00)	<0.001
ALT (U/L)	21.00 (15.00,29.00)	22.00 (16.00,32.00)	22.00 (16.00,31.25)	19.00 (14.00,29.00)	0.003
GGT (IU/L)	22.50 (17.00,33.00)	26.00 (18.00,41.00)	26.00 (19.00,42.00)	27.00 (19.00,43.00)	<0.001
LSM (kpa)	5.15 (4.20,6.30)	5.40 (4.40,6.80)	5.60 (4.60,7.20)	5.80 (4.80,7.70)	<0.001
CAP (dB/m)	301.00 (283.25,330.00)	309.00 (287.00,338.00)	316.00 (291.00,352.00)	326.00 (299.50,359.00)	<0.001

(Continued)

TABLE 1 Continued

Variables	hsCRP				
	Quartile 1 (n = 366)	Quartile 2 (n = 372)	Quartile 3 (n = 368)	Quartile 4 (n = 371)	*P*
Significant fibrosis, n (%)					<0.001
Yes	53 (14.48)	66 (17.74)	83 (22.55)	103 (27.76)	
No	313 (85.52)	306 (82.26)	285 (77.45)	268 (72.24)	
Advanced fibrosis, n (%)					0.005
Yes	31 (8.47)	31 (8.33)	54 (14.67)	52 (14.02)	
No	335 (91.53)	341 (91.67)	314 (85.33)	319 (85.98)	
Cirrhosis, n (%)					<0.001
Yes	9 (2.46)	15 (4.03)	32 (8.70)	27 (7.28)	
No	357 (97.54)	357 (95.97)	336 (91.30)	344 (92.72)	

Data are shown as median (25th, 75th percentiles) or percentages, p <0.05 considered statistically significant.
MASLD, Metabolic dysfunction-associated steatotic liver disease; hsCRP, high-sensitivity C-reactive protein; BMI, Body mass index; WC, Waist circumference; FPG, Fasting plasma-glucose; HbA1c, Hemoglobin A1c; TC, Total cholesterol; TG, Triglyceride; HDL-C, High density lipoprotein cholesterol; WBC, White blood cell; AST, Aspartate aminotransferase; ALT, Alanine transaminase; GGT, Gamma-glutamyl transferase; LSM, Liver stiffness measurement; CAP, Controlled attenuation parameter.

3.2 Baseline characteristics of MASLD patients based on hsCRP quartiles in the Chinese cohort

In the Chinese cohort, the results demonstrated no statistically significant difference in the proportion of male and female patients between different hsCRP quartiles (P = 0.071). The median age was similar between the groups (P = 0.667). The proportions of patients who smoke, consume alcohol, hypertension, and dyslipidemia did not differ significantly between hsCRP quartiles (P values of 0.604, 0.407, 0.481, and 0.116, respectively). However, the proportion of DM increased with hsCRP levels (P = 0.019). Additionally, there was a significant positive correlation between hsCRP levels and the following variables: BMI, WC, HbA1c, TG, GGT, and LSM (all P < 0.05). Conversely, there was a significant negative correlation between hsCRP levels and HDL-C levels (P < 0.05). The prevalence of significant fibrosis, advanced fibrosis, and cirrhosis exhibited a notable increase with elevated hsCRP levels (all P < 0.001) (Table 2).

3.3 Association of hsCRP with hepatic fibrosis in MASLD patients in the US cohort

The relationship between hsCRP and hepatic fibrosis in patients with MASLD was investigated using multivariable model logistic regression in the US cohort. The results demonstrated that patients in the highest quartile of hsCRP exhibited a markedly elevated risk of significant fibrosis (OR = 2.27, P < 0.001), advanced fibrosis (OR = 1.76, P = 0.018), and cirrhosis (OR = 3.11, P = 0.004) in comparison to those in the lowest quartile of hsCRP. These associations remained significant after adjustment for potential confounding factors, including gender, age, smoking, alcohol consumption, DM, hypertension, and dyslipidemia (OR = 2.22, P < 0.001; OR = 1.69, P = 0.041; OR = 2.85, P = 0.011). These findings suggest that hsCRP may be a valuable predictor of hepatic fibrosis progression in patients with MASLD (Table 3).

3.4 Association of hsCRP with hepatic fibrosis in MASLD patients in the Chinese cohort

A similar investigation was conducted into the relationship between hsCRP levels and hepatic fibrosis in the Chinese cohort. The findings indicated that hsCRP levels were significantly correlated with the risk of significant fibrosis, advanced fibrosis, and cirrhosis after adjustment for various factors. Patients in the higher quartiles exhibited progressively elevated risks of significant fibrosis (OR = 2.53, P < 0.001), advanced fibrosis (OR = 3.85, P < 0.001), and cirrhosis (OR = 3.78, P < 0.001) relative to those in the lowest hsCRP quartile. These results are consistent with those observed in the US cohort, providing further support for the potential of hsCRP as a predictor of hepatic fibrosis in patients with MASLD (Table 4).

3.5 RCS analysis

In the context of RCS analyses, an investigation was conducted to elucidate the correlation between serum hsCRP levels and the degree of hepatic fibrosis in patients diagnosed with MASLD. All analyses were adjusted for potential confounding factors, including gender, age, smoking status, alcohol consumption, diabetes, hypertension, and dyslipidemia. In the US cohort, significant nonlinear associations were identified between hsCRP levels and significant fibrosis (Figure 2A), advanced fibrosis (Figure 2B), and cirrhosis (Figure 2C) (P < 0.001, P-Nonlinear < 0.001; P = 0.004, P-

10.3389/fimmu.2025.1544917

TABLE 2 Baseline characteristics of MASLD patients based on hsCRP quartiles in the Chinese cohort.

Variables	hsCRP				
	Quartile 1 (n = 383)	Quartile 2 (n = 381)	Quartile 3 (n = 384)	Quartile 4 (n = 383)	*P*
Gender, n (%)					0.071
Male	231 (60.31)	217 (56.96)	254 (66.15)	231 (60.31)	
Female	152 (39.69)	164 (43.04)	130 (33.85)	152 (39.69)	
Age (years)	42.00 (32.00,53.00)	44.00 (33.00,53.00)	41.00 (33.00,54.00)	42.00 (34.00,53.00)	0.667
Smoke, n (%)					0.604
Yes	128 (33.42)	126 (33.07)	136 (35.42)	118 (30.81)	
No	255 (66.58)	255 (66.93)	248 (64.58)	265 (69.19)	
Alcohol, n (%)					0.407
Yes	93 (24.28)	75 (19.69)	87 (22.66)	92 (24.02)	
No	290 (75.72)	306 (80.31)	297 (77.34)	291 (75.98)	
Hypertension, n (%)					0.481
Yes	102 (26.63)	99 (25.98)	117 (30.47)	111 (28.98)	
No	281 (73.37)	282 (74.02)	267 (69.53)	272 (71.02)	
Diabetes, n (%)					0.019
Yes	86 (22.45)	98 (25.72)	119 (30.99)	118 (30.81)	
No	297 (77.55)	283 (74.28)	265 (69.01)	265 (69.19)	
Dyslipidemia, n (%)					0.116
Yes	292 (76.24)	304 (79.79)	307 (79.95)	319 (83.29)	
No	91 (23.76)	77 (20.21)	77 (20.05)	64 (16.71)	
BMI (kg/m^2)	27.20 (24.90,29.70)	27.50 (25.50,30.00)	27.70 (25.58,30.20)	27.70 (25.70,30.60)	0.014
WC (cm)	94.90 (89.65,101.95)	95.50 (89.10,102.50)	96.70 (90.70,105.75)	96.80 (90.25,103.15)	0.008
FPG (mg/dL)	97.20 (90.00,109.80)	97.20 (90.00,113.40)	97.20 (90.00,112.05)	99.00 (90.00,116.37)	0.247
HbA1c (%)	5.88 (5.60,6.35)	5.94 (5.62,6.40)	5.98 (5.66,6.56)	6.02 (5.70,6.57)	0.010
TC (mg/dL)	177.54 (155.69,201.52)	180.64 (155.88,207.71)	180.25 (155.49,206.26)	184.12 (162.26,207.71)	0.199
TG (mg/dL)	138.22 (91.26,202.01)	141.76 (92.14,191.38)	145.30 (105.21,221.72)	168.34 (116.95,241.88)	<0.001
HDL-C (mg/dL)	42.13 (36.72,48.70)	42.13 (35.94,53.72)	41.16 (34.30,49.09)	40.58 (35.17,49.28)	0.023
WBC (10^3 cells/μL)	6.26 (5.38,7.20)	6.29 (5.31,7.27)	6.19 (5.30,7.20)	6.41 (5.51,7.34)	0.724
Neutrophils (10^3 cells/μL)	3.55 (3.02,4.26)	3.61 (2.86,4.30)	3.50 (2.83,4.16)	3.66 (2.90,4.21)	0.538
Lymphocyte (10^3 cells/μL)	2.08 (1.69,2.46)	2.02 (1.66,2.35)	2.05 (1.73,2.46)	2.04 (1.71,2.47)	0.367
Monocyte (10^3 cells/μL)	0.44 (0.36,0.53)	0.44 (0.37,0.53)	0.43 (0.36,0.51)	0.44 (0.37,0.53)	0.669
Platelet (10^3 cells/μL)	224.00 (193.00,256.38)	216.00 (180.00,253.00)	221.00 (187.53,261.00)	225.00 (184.00,262.93)	0.277
AST (U/L)	25.00 (19.00,37.00)	26.00 (19.00,40.00)	25.00 (19.00,37.25)	25.00 (18.00,37.50)	0.926
ALT (U/L)	39.00 (22.55,63.99)	36.00 (21.00,63.87)	38.00 (22.00,66.17)	36.80 (23.00,65.50)	0.865
GGT (IU/L)	38.00 (22.40,59.40)	35.90 (23.00,69.50)	41.65 (25.15,75.20)	40.30 (25.00,72.95)	0.043
LSM (kpa)	6.00 (5.00,7.00)	6.30 (5.10,8.40)	6.70 (5.20,9.20)	6.50 (5.20,9.30)	<0.001
CAP (dB/m)	323.00 (298.00,345.00)	324.00 (301.00,352.00)	330.50 (303.00,355.25)	329.00 (300.50,355.00)	0.108

(Continued)

TABLE 2 Continued

Variables	hsCRP				
	Quartile 1 (n = 383)	Quartile 2 (n = 381)	Quartile 3 (n = 384)	Quartile 4 (n = 383)	*P*
Significant fibrosis, n (%)					<0.001
Yes	68 (17.75)	132 (34.65)	157 (40.89)	135 (35.25)	
No	315 (82.25)	249 (65.35)	227 (59.11)	248 (64.75)	
Advanced fibrosis, n (%)					<0.001
Yes	28 (7.31)	63 (16.54)	78 (20.31)	90 (23.50)	
No	355 (92.69)	318 (83.46)	306 (79.69)	293 (76.50)	
Cirrhosis, n (%)					<0.001
Yes	13 (3.39)	27 (7.09)	26 (6.77)	46 (12.01)	
No	370 (96.61)	354 (92.91)	358 (93.23)	337 (87.99)	

Data are shown as median (25th, 75th percentiles) or percentages, p <0.05 considered statistically significant.
MASLD, Metabolic dysfunction-associated steatotic liver disease; hsCRP, high-sensitivity C-reactive protein; BMI, Body mass index; WC, Waist circumference; FPG, Fasting plasma-glucose; HbA1c, Hemoglobin A1c; TC, Total cholesterol; TG, Triglyceride; HDL-C, High density lipoprotein cholesterol; WBC, White blood cell; AST, Aspartate aminotransferase; ALT, Alanine transaminase; GGT, Gamma-glutamyl transferase; LSM, Liver stiffness measurement; CAP, Controlled attenuation parameter.

TABLE 3 Relationship between hsCRP and hepatic fibrosis in patients with MASLD in the US cohort.

Variables	Model 1		Model 2		Model 3	
	OR (95%CI)	*P*	OR (95%CI)	*P*	OR (95%CI)	*P*
Significant fibrosis						
hsCRP						
Quartile 1	1.00 (Reference)		1.00 (Reference)		1.00 (Reference)	
Quartile 2	1.27 (0.86 ~ 1.89)	0.229	1.30 (0.87 ~ 1.93)	0.198	1.20 (0.80 ~ 1.79)	0.374
Quartile 3	1.72 (1.18 ~ 2.52)	0.005	1.90 (1.29 ~ 2.80)	0.001	1.73 (1.17 ~ 2.56)	0.006
Quartile 4	2.27 (1.57 ~ 3.28)	<0.001	2.73 (1.86 ~ 4.01)	<0.001	2.22 (1.49 ~ 3.29)	<0.001
Advanced fibrosis						
hsCRP						
Quartile 1	1.00 (Reference)		1.00 (Reference)		1.00 (Reference)	
Quartile 2	0.98 (0.58 ~ 1.65)	0.947	1.00 (0.59 ~ 1.69)	0.995	0.91 (0.54 ~ 1.54)	0.720
Quartile 3	1.86 (1.16 ~ 2.97)	0.009	2.08 (1.30 ~ 3.35)	0.002	1.84 (1.14 ~ 2.98)	0.013
Quartile 4	1.76 (1.10 ~ 2.82)	0.018	2.17 (1.34 ~ 3.53)	0.002	1.69 (1.02 ~ 2.79)	0.041
Cirrhosis						
hsCRP						
Quartile 1	1.00 (Reference)		1.00 (Reference)		1.00 (Reference)	
Quartile 2	1.67 (0.72 ~ 3.86)	0.233	1.70 (0.73 ~ 3.95)	0.214	1.48 (0.63 ~ 3.45)	0.366
Quartile 3	3.78 (1.78 ~ 8.03)	<0.001	4.24 (1.98 ~ 9.06)	<0.001	3.64 (1.69 ~ 7.85)	<0.001
Quartile 4	3.11 (1.44 ~ 6.72)	0.004	3.86 (1.76 ~ 8.44)	<0.001	2.85 (1.28 ~ 6.37)	0.011

Model 1: crude.
Model 2: adjusted for Gender and Age.
Model 3: adjusted for Gender, Age, Smoke, Alcohol, Diabetes, Hypertension, and Dyslipidemia.
hsCRP, high-sensitivity C-reactive protein; MASLD, Metabolic dysfunction-associated steatotic liver disease; OR, Odds ratio; CI, Confidence interval.

TABLE 4 Relationship between hsCRP and hepatic fibrosis in patients with MASLD in the Chinese cohort.

Variables	Model 1		Model 2		Model 3	
	OR (95%CI)	*P*	OR (95%CI)	*P*	OR (95%CI)	*P*
Significant fibrosis						
hsCRP						
Quartile 1	1.00 (Reference)		1.00 (Reference)		1.00 (Reference)	
Quartile 2	2.46 (1.75 ~ 3.44)	<0.001	2.45 (1.75 ~ 3.42)	<0.001	2.48 (1.77 ~ 3.49)	<0.001
Quartile 3	3.20 (2.30 ~ 4.46)	<0.001	3.22 (2.31 ~ 4.49)	<0.001	3.22 (2.31 ~ 4.51)	<0.001
Quartile 4	2.52 (1.80 ~ 3.53)	<0.001	2.52 (1.80 ~ 3.52)	<0.001	2.53 (1.80 ~ 3.55)	<0.001
Advanced fibrosis						
hsCRP						
Quartile 1	1.00 (Reference)		1.00 (Reference)		1.00 (Reference)	
Quartile 2	2.51 (1.57 ~ 4.02)	<0.001	2.49 (1.56 ~ 3.99)	<0.001	2.49 (1.55 ~ 3.99)	<0.001
Quartile 3	3.23 (2.04 ~ 5.11)	<0.001	3.26 (2.06 ~ 5.16)	<0.001	3.19 (2.01 ~ 5.07)	<0.001
Quartile 4	3.89 (2.48 ~ 6.12)	<0.001	3.87 (2.46 ~ 6.09)	<0.001	3.85 (2.44 ~ 6.07)	<0.001
Cirrhosis						
hsCRP						
Quartile 1	1.00 (Reference)		1.00 (Reference)		1.00 (Reference)	
Quartile 2	2.17 (1.10 ~ 4.27)	0.025	2.17 (1.10 ~ 4.29)	0.026	2.16 (1.09 ~ 4.28)	0.028
Quartile 3	2.07 (1.05 ~ 4.09)	0.037	2.06 (1.04 ~ 4.10)	0.039	1.97 (0.99 ~ 3.93)	0.055
Quartile 4	3.88 (2.06 ~ 7.32)	<0.001	3.85 (2.03 ~ 7.29)	<0.001	3.78 (1.99 ~ 7.19)	<0.001

Model 1: crude.
Model 2: adjusted for Gender and Age.
Model 3: adjusted for Gender, Age, Smoke, Alcohol, Diabetes, Hypertension, and Dyslipidemia.
hsCRP, high-sensitivity C-reactive protein; MASLD, Metabolic dysfunction-associated steatotic liver disease; OR, Odds ratio; CI, Confidence interval.

Nonlinear = 0.002; P = 0.002, P-Nonlinear = 0.001). For significant fibrosis, advanced fibrosis, and cirrhosis, the inflection point occurred at an hsCRP level of approximately 9 mg/L. At levels of hsCRP below 9 mg/L, the OR values for each type of hepatic fibrosis increased significantly with increasing hsCRP levels. When hsCRP levels reached or exceeded 9 mg/L, the OR values tended to flatness or decrease.

In the Chinese cohort, significant nonlinear relationships were also observed between hsCRP levels and significant fibrosis (Figure 2D), advanced fibrosis (Figure 2E), and cirrhosis (Figure 2F) (P < 0.001, P-Nonlinear < 0.001; P < 0.001, P-Nonlinear < 0.001; P < 0.001, P-Nonlinear = 0.047). The inflection point was observed at hsCRP levels of 4 mg/L. At levels of hsCRP less than 4 mg/L, the ORs for each type of hepatic fibrosis increased significantly with increasing hsCRP levels. At hsCRP levels of 4 mg/L or above, the upward trajectory of the ORs for advanced fibrosis and cirrhosis leveled off, while the ORs for significant fibrosis began to decline.

3.6 Segmented logistic regression analysis of the effect of hsCRP levels on hepatic fibrosis in patients with MASLD

A segmented logistic regression analysis was conducted to investigate the effect of hsCRP levels on hepatic fibrosis based on the inflection point values identified through RCS analysis. In the US cohort, the results demonstrated that the risk of significant fibrosis (OR = 1.10, P = 0.005), advanced fibrosis (OR = 1.10, P = 0.037), and cirrhosis (OR = 1.12, P = 0.042) was markedly elevated when hsCRP levels <9 mg/L were adjusted for relevant confounding variables. However, these associations were no longer significant when hsCRP levels were ≥9 mg/L (P values of 0.310, 0.960, and 0.730, respectively) (Table 5). This indicates the potential existence of a threshold effect of hsCRP levels on hepatic fibrosis.

In the Chinese cohort, the results demonstrated that after adjusting for potential confounding variables, patients with hsCRP levels below 4 mg/L exhibited a notable increase in the

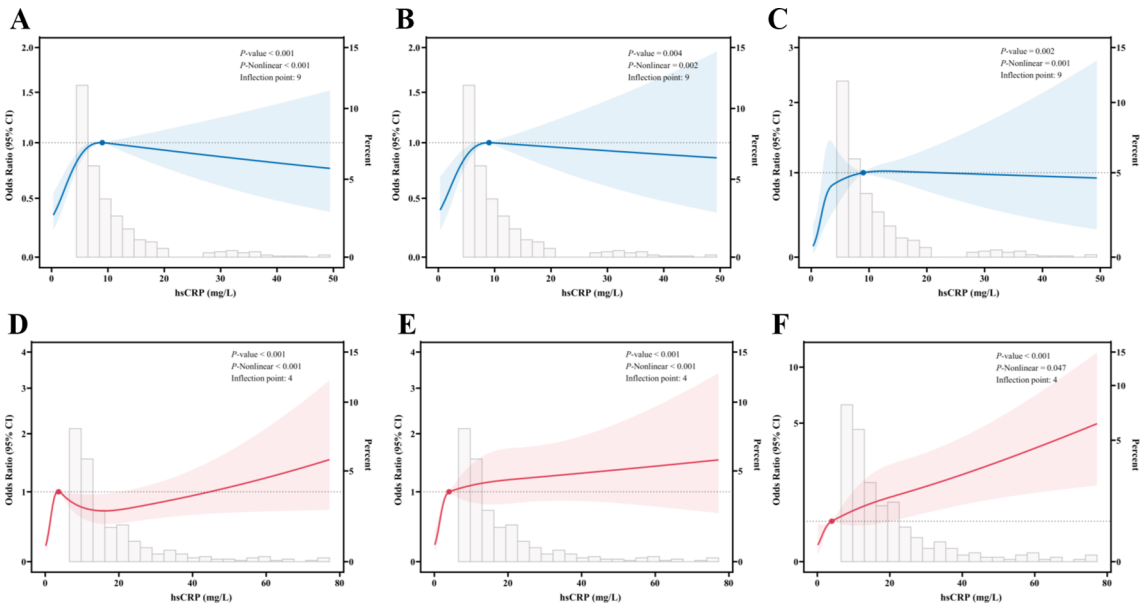

FIGURE 2
Restricted cubic spline fitting for the association between hsCRP and hepatic fibrosis in patients with MASLD. **(A)** association between hsCRP and significant fibrosis in the US cohort; **(B)** association between hsCRP and advanced fibrosis in the US cohort; **(C)** association between hsCRP and cirrhosis in the US cohort; **(D)** association between hsCRP and significant fibrosis in the Chinese cohort; **(E)** association between hsCRP and advanced fibrosis in the Chinese cohort; **(F)** association between hsCRP and cirrhosis in the Chinese cohort. The solid line displays the odds ratio, with the 95% CI represented by shading. They were adjusted for gender, age, smoke, alcohol, diabetes, hypertension, and dyslipidemia. hsCRP, high-sensitivity C-reactive protein; MASLD, Metabolic dysfunction-associated steatotic liver disease; CI, Confidence interval.

risk of significant fibrosis (OR = 1.41, P< 0.001), advanced fibrosis (OR = 1.32, P = 0.002), and cirrhosis (OR = 1.15, P = 0.037) as hsCRP levels increased. However, when hsCRP levels reached or exceeded 4 mg/L, the increased risk of significant fibrosis and advanced fibrosis was no longer significant (P values of 0.440 and 0.660, respectively), although the risk of cirrhosis remained increased (OR = 1.02, P = 0.016) (Table 6). These results further confirm the potential for differences in the predictive value of hsCRP levels at varying thresholds for hepatic fibrosis in patients with MASLD.

3.7 Subgroup analysis

In the US cohort, we conducted a subgroup analysis to investigate the relationship between hsCRP levels and hepatic fibrosis in patients with MASLD. We adjusted for potential confounding variables, including gender, age, smoking status, alcohol consumption, diabetes, hypertension, and dyslipidemia. The results are presented in Figure 3. For significant fibrosis (Figure 3A), a significant association was observed between hsCRP levels and the risk of fibrosis. In general, patients with

TABLE 5 Segmented logistic regression analysis of the effect of hsCRP level on hepatic fibrosis in the US cohort.

Variables	OR (95% CI)	*P*	OR per SD (95%CI)	*P*
Significant fibrosis				
hsCRP (< 9 mg/L)	1.10 (1.03 ~ 1.17)	0.005	1.21 (1.06 ~ 1.38)	0.005
hsCRP (≥ 9 mg/L)	0.99 (0.97 ~ 1.01)	0.310	0.83 (0.59 ~ 1.18)	0.310
Advanced fibrosis				
hsCRP (< 9 mg/L)	1.10 (1.01 ~ 1.21)	0.037	1.20 (1.01 ~ 1.43)	0.037
hsCRP (≥ 9 mg/L)	0.99 (0.98 ~ 1.02)	0.960	0.99 (0.69 ~ 1.42)	0.960
Cirrhosis				
hsCRP (< 9 mg/L)	1.12 (1.00 ~ 1.25)	0.042	1.27 (1.01 ~ 1.60)	0.042
hsCRP (≥ 9 mg/L)	0.99 (0.96 ~ 1.03)	0.730	0.91 (0.55 ~ 1.53)	0.730

ORs were adjusted for Gender, Age, Smoke, Alcohol, Diabetes, Hypertension, and Dyslipidemia.
hsCRP, high-sensitivity C-reactive protein; OR, Odds ratio; SD, Standardized; CI, Confidence interval.

TABLE 6 Segmented logistic regression analysis of the effect of hsCRP level on hepatic fibrosis in the Chinese cohort.

Variables	OR (95% CI)	P	OR per SD (95%CI)	P
Significant fibrosis				
hsCRP (< 4 mg/L)	1.41 (1.23 ~ 1.62)	<0.001	1.44 (1.25 ~ 1.66)	<0.001
hsCRP (≥ 4 mg/L)	1.00 (0.99 ~ 1.01)	0.440	1.07 (0.91 ~ 1.26)	0.440
Advanced fibrosis				
hsCRP (< 4 mg/L)	1.32 (1.11 ~ 1.58)	0.002	1.34 (1.11 ~ 1.62)	0.002
hsCRP (≥ 4 mg/L)	1.00 (0.99 ~ 1.01)	0.660	1.04 (0.87 ~ 1.25)	0.660
Cirrhosis				
hsCRP (< 4 mg/L)	1.15 (1.01 ~ 1.32)	0.037	1.28 (1.02 ~ 1.61)	0.037
hsCRP (≥ 4 mg/L)	1.02 (1.00 ~ 1.03)	0.016	1.35 (1.06 ~ 1.73)	0.016

ORs were adjusted for Gender, Age, Smoke, Alcohol, Diabetes, Hypertension, and Dyslipidemia.
hsCRP, high-sensitivity C-reactive protein; OR, Odds ratio; SD, Standardized; CI, Confidence interval.

hsCRP levels of 9 mg/L or greater exhibited an adjusted OR of 2.00 (95% CI: 1.39, 2.87) with a P-value of less than 0.001 compared to patients with hsCRP levels below 9 mg/L. In all but the male and smokers subgroups, there was a significant association between hsCRP levels and the risk of fibrosis ($P < 0.05$). Furthermore, no significant interaction was observed in any subgroup, except for the smokers subgroup. In the analysis of advanced fibrosis (Figure 3B), patients with hsCRP levels ≥9 mg/L exhibited an adjusted OR of 1.84 (95% CI: 1.18, 2.87) in comparison to patients with hsCRP levels <9 mg/L, with a P-value of 0.007. In the subgroups of females, non-smokers, non-drinkers, diabetic patients, and patients with dyslipidemia, a significant association was observed between hsCRP levels and the risk of fibrosis ($P < 0.05$). Nevertheless, no significant interaction was observed in any subgroups except the smoking subgroup. The results of the analyses also supported a significant association between hsCRP levels and the risk of cirrhosis (Figure 3C). The adjusted OR was 2.27 (95% CI: 1.29, 4.00), with a P-value of 0.005. The correlation between hsCRP levels and the likelihood of cirrhosis was statistically significant in the following subgroups: females, non-smokers, non-drinkers, and patients with diabetics, hypertension, and dyslipidemia ($P < 0.05$). No significant interaction was identified in any of the subgroups.

The results of the subgroup analysis for the Chinese cohort are presented in Figure 4. In the study of significant fibrosis (Figure 4A), patients with hsCRP levels of 4 mg/L or greater exhibited an adjusted OR of 1.59 (95% CI: 1.27, 1.98) in comparison to patients with hsCRP levels below 4 mg/L, with a P-value of less than 0.001. In all but the drinkers subgroup, there was a significant association between hsCRP levels and the risk of fibrosis ($P < 0.05$). Furthermore, no significant interaction was observed in any subgroup (P for interaction > 0.05). About advanced fibrosis (Figure 4B), patients with hsCRP levels of 4 mg/L or above exhibited an adjusted OR of 2.14 (95% CI: 1.63, 2.81) in comparison to patients with hsCRP levels below 4 mg/L, with a P-value of less than 0.001. Similarly, in all but the drinkers subgroup, there was a significant association between hsCRP levels and the risk of fibrosis ($P < 0.05$). Nevertheless, no significant interaction was observed in any subgroups except the alcohol subgroup (P for interaction = 0.012). In the analysis of cirrhosis (Figure 4C), patients with hsCRP levels ≥4 mg/L exhibited an adjusted OR of 1.95 (95% CI: 1.32, 2.90) in comparison to patients with hsCRP levels <4 mg/L, with a P-value of 0.001. Similarly, in the alcohol subgroup, the correlation between hsCRP levels and the risk of cirrhosis in non-drinkers was statistically significant ($P < 0.001$), with a notable between-group interaction (P for interaction = 0.030). No significant interaction was identified in the remaining subgroups (P for interaction > 0.05).

3.8 ROC curves of hsCRP in predicting hepatic fibrosis in MASLD patients

In the US cohort (Figure 5A), the area under the curve (AUC) values of hsCRP for predicting significant fibrosis, advanced fibrosis, and cirrhosis were 0.593 (95% CI: 0.557-0.628), 0.584 (95% CI: 0.539-0.629), and 0.636 (95% CI: 0.581-0.692), respectively. These AUC values indicate that hsCRP has some degree of discriminatory power in predicting the degree of hepatic fibrosis in US patients with MASLD, particularly in the prediction of cirrhosis. In the Chinese cohort (Figure 5B), the AUC values of hsCRP for predicting significant fibrosis, advanced fibrosis, and cirrhosis were 0.592 (95% CI: 0.563-0.621), 0.654 (95% CI: 0.619-0.688), and 0.652 (95% CI: 0.599-0.706), respectively. As with the US cohort, these findings illustrate the effectiveness of hsCRP in forecasting the degree of hepatic fibrosis in Chinese patients with MASLD. However, the comparatively low AUC values suggest that its predictive accuracy is constrained.

4 Discussion

In this study, we comprehensively analyzed data from both the US and the Chinese cohorts to investigate the potential association between hsCRP and hepatic fibrosis in patients with MASLD. The study's findings indicated a notable nonlinear correlation between hsCRP levels and the degree of hepatic fibrosis in patients with MASLD, as observed in both the US and Chinese cohorts.

10.3389/fimmu.2025.1544917

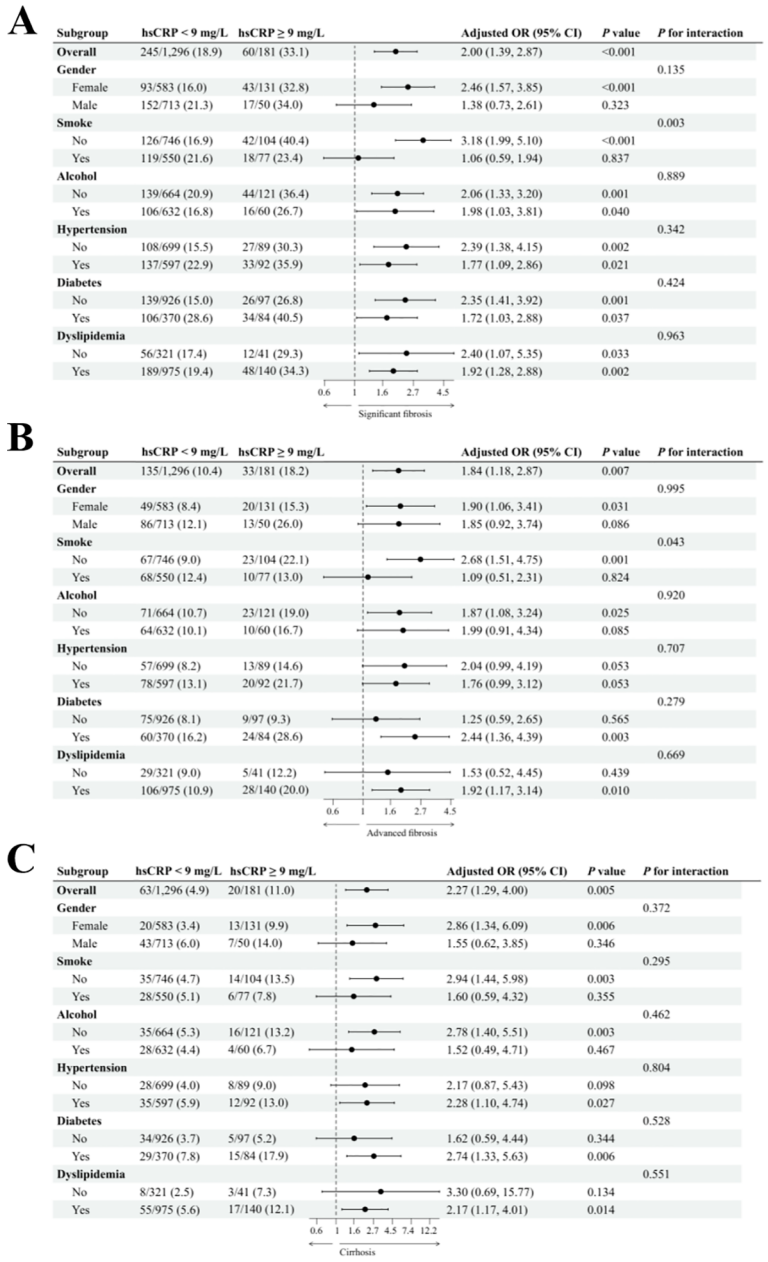

FIGURE 3
Subgroup analysis of the association between hsCRP and hepatic fibrosis in patients with MASLD in the US cohort. **(A)** association between hsCRP and significant fibrosis; **(B)** association between hsCRP and advanced fibrosis; **(C)** association between hsCRP and cirrhosis. Adjusted variables: gender, age, smoke, alcohol, diabetes, hypertension, and dyslipidemia. The model was not adjusted for the stratification variables themselves in the corresponding stratification analysis. hsCRP, high-sensitivity C-reactive protein; MASLD, Metabolic dysfunction-associated steatotic liver disease; OR, odds ratio; CI, confidence interval.

Additionally, the study identified specific inflection point values. Specifically, the risk of significant fibrosis, advanced fibrosis, and cirrhosis in patients with MASLD was significantly elevated with increasing hsCRP levels within a specific range, and this association remained significant after adjusting for multiple confounding variables. These findings further substantiate the utility of hsCRP as a potential predictor of hepatic fibrosis in patients with MASLD.

CRP, a pivotal pro-inflammatory factor, plays a pivotal role in various pathological conditions. It has been demonstrated that the pentameric form of CRP (pCRP) can dissociate into a pro-inflammatory monomeric form (mCRP) under specific shear or inflammatory conditions, thereby further activating the inflammatory response (23–25). For instance, in aortic stenosis (AS), shear force-induced dissociation of pCRP activates endothelial cells and platelets, leading to inflammation and thrombosis (24). Similarly, mCRP exacerbates localized tissue damage in atherosclerosis and myocardial infarction by binding to cell membrane phospholipids, inducing leukocyte adhesion and inflammatory cell activation (25).

10.3389/fimmu.2025.1544917

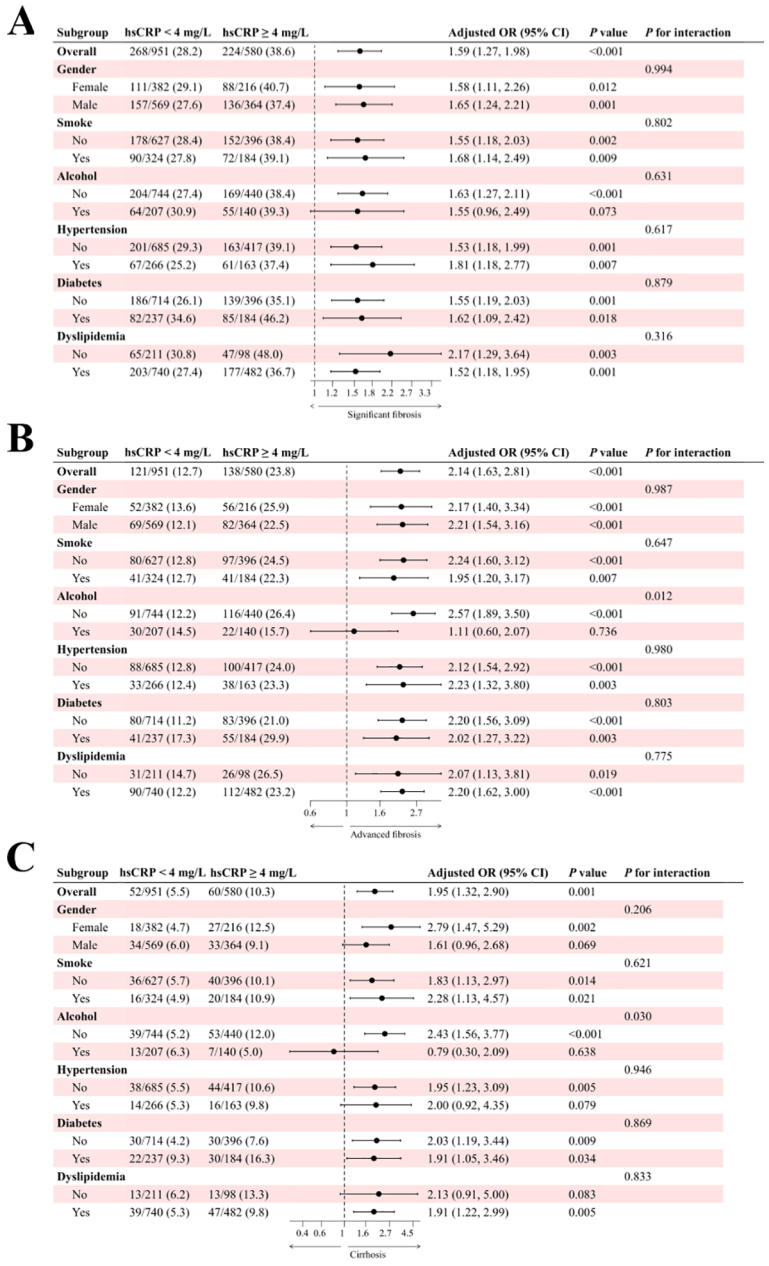

FIGURE 4
Subgroup analysis of the association between hsCRP and hepatic fibrosis in patients with MASLD in the Chinese cohort. **(A)** association between hsCRP and significant fibrosis; **(B)** association between hsCRP and advanced fibrosis; **(C)** association between hsCRP and cirrhosis. Adjusted variables: gender, age, smoke, alcohol, diabetes, hypertension, and dyslipidemia. The model was not adjusted for the stratification variables themselves in the corresponding stratification analysis. hsCRP, high-sensitivity C-reactive protein; MASLD, Metabolic dysfunction-associated steatotic liver disease; OR, odds ratio; CI, confidence interval.

Additionally, mCRP interacts with lipid rafts in endothelial cell membranes to regulate cytokine release and endothelial dysfunction, further promoting inflammatory responses (26).

Some studies have indicated a positive correlation between elevated hsCRP levels, a sensitive marker of the inflammatory response, and the degree of hepatic fibrosis in patients with NAFLD (18, 20, 21). The present study not only corroborates previous findings but also underscores the significance of hsCRP in the context of MASLD. These findings further reinforce the notion that chronic low-grade inflammation plays a pivotal role in the progression of MASLD to hepatic fibrosis. Furthermore, the results of the present study align with a series of observational studies that have identified an association between hsCRP levels and cardiometabolic risk factors, including hypertension, diabetes, and dyslipidemia. These risk factors are also strongly associated with the progression of hepatic fibrosis in MASLD (15–17).

Some biological mechanisms may mediate the relationship between hsCRP and hepatic fibrosis in patients with MASLD. Firstly,

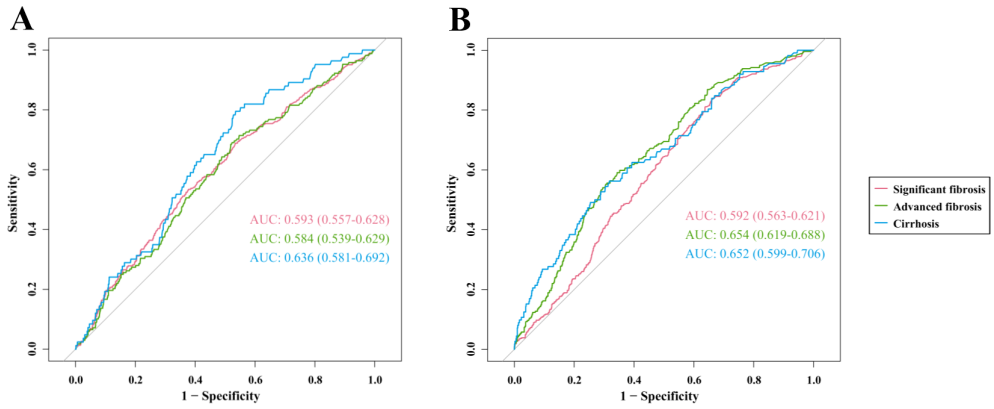

FIGURE 5
ROC curves of hsCRP for predicting hepatic fibrosis in patients with MASLD. **(A)** ROC curves for predicting significant fibrosis, advanced fibrosis, and cirrhosis in the US cohort; **(B)** ROC curves for predicting significant fibrosis, advanced fibrosis, and cirrhosis in the Chinese cohort. ROC, Receiver operating characteristics; hsCRP, high-sensitivity C-reactive protein; MASLD, Metabolic dysfunction-associated steatotic liver disease; AUC, Area under receiver operating characteristics curve.

elevated levels of hsCRP, a nonspecific inflammatory marker, typically indicate the presence of a low-grade inflammatory response within the body (13, 14). In patients with MASLD, persistent hepatic inflammation represents a pivotal factor in the progression of hepatic fibrosis (11). The infiltration and activation of inflammatory cells release a variety of pro-inflammatory cytokines and chemokines that activate hepatic stellate cells (HSCs), prompting their transformation into myofibroblasts and secretion of large quantities of extracellular matrix (ECM), which in turn drive the onset and progression of hepatic fibrosis (9, 11). Secondly, insulin resistance, a core feature of MASLD, is closely associated with elevated hsCRP levels (27). Insulin resistance may result in aberrant hepatic lipid and glucose metabolism, exacerbating hepatic inflammation and fibrosis (28). Additionally, insulin resistance may directly promote the activation and proliferation of HSCs through the activation of signaling pathways such as c-Jun N-terminal kinase and mechanistic target of rapamycin, thereby further accelerating the process of hepatic fibrosis (29–31). Moreover, patients with MASLD frequently present with dyslipidemia, which can result in the accumulation of lipids within the liver. The accumulation of lipids is susceptible to peroxidation in the presence of oxidative stress, generating many oxidation products and free radicals. These oxidation products and free radicals not only directly damage hepatocyte membranes, mitochondria, and other cellular organelles but also activate inflammatory signaling pathways, thus exacerbating hepatic inflammation and fibrosis (28, 32). hsCRP, as a component of the inflammatory response, and its elevated level may reflect the state of this oxidative stress and lipid peroxidation. Furthermore, alterations in the intestinal microbiota are strongly linked to the onset of MASLD and may impact hsCRP levels. Metabolites produced by the intestinal flora, including short-chain fatty acids and bile acids, have the potential to influence the metabolic and inflammatory state of the liver, which in turn affects hepatic fibrosis (33–35).

The present study also identified findings that differed from those observed in existing studies. Specifically, the application of RCS analysis identified a potential inflection point value for the dose-response relationship between hsCRP levels and hepatic fibrosis. This inflection point value may vary across geographic and ethnic populations. In the US cohort, the inflection point was approximately 9 mg/L, whereas in the Chinese cohort, it was 4 mg/L. This finding suggests that the effect of hsCRP on hepatic fibrosis may exhibit a threshold effect in different populations. That is to say; when the hsCRP level is lower than the inflection point, its elevation will significantly increase the risk of hepatic fibrosis. Conversely, when it exceeds the inflection point, its contributing effect on the risk of hepatic fibrosis may diminish or no longer be significant. These findings have important theoretical and practical implications for developing screening and monitoring strategies for hepatic fibrosis based on hsCRP levels.

Furthermore, this study investigated the impact of hsCRP levels on the likelihood of hepatic fibrosis in patients with varying characteristics of MASLD through subgroup analysis. The results demonstrated notable discrepancies in the correlation between hsCRP levels and the possibility of hepatic fibrosis across subgroups with disparate characteristics. For instance, the impact of hsCRP levels on the risk of hepatic fibrosis was more pronounced in the subgroups of non-smoking and non-drinking patients, and there was a significant between-group interaction. This phenomenon may be attributed to the fact that there were fewer potential confounding factors in participants who were non-smokers and non-drinkers compared to individuals who smoked or drank. This may have resulted in a clearer and stronger association between hsCRP levels and hepatic fibrosis risk. These findings offer novel insights into the personalized assessment of hepatic fibrosis risk in patients with MASLD, which can assist clinicians in formulating more precise and efficacious therapeutic regimens tailored to individual patient profiles.

Moreover, this study assessed the effectiveness of hsCRP in predicting the degree of hepatic fibrosis in patients with MASLD.

Specifically, the AUC values of hs-CRP in predicting significant fibrosis, advanced fibrosis, and cirrhosis in patients with MASLD were all approximately 0.6. These findings indicate that hsCRP, when used as a single predictor, exhibits some discriminatory efficacy in differentiating between the various stages of hepatic fibrosis in patients with MASLD. However, its overall predictive accuracy remains limited. In light of these findings, we propose that hsCRP should be employed in conjunction with other predictors of hepatic fibrosis in clinical practice. Furthermore, we recommend that the accuracy and specificity of prediction be enhanced by comprehensively considering a range of biomarkers.

A substantial body of research has demonstrated the considerable therapeutic potential of CRP in the treatment of inflammation-related diseases. The suppression of the pro-inflammatory effects of CRP through diverse mechanisms has been identified as a highly effective anti-inflammatory strategy (23). For instance, the development of specific small-molecule inhibitors (e.g., 1,6-bis(phosphocholine)-hexane) has been shown to impede CRP function and mitigate tissue damage in myocardial infarction and stroke (36). In addition, selective CRP-scavenging therapies, which expeditiously reduce circulating CRP levels through blood purification techniques, have significantly improved clinical symptoms and reduced mortality among patients with severe pneumonia caused by COVID-19 (37–39). Furthermore, low molecular weight CRP inhibitors offer novel insights for anti-inflammatory therapy by mimicking the structure of phospholipids, specifically binding to the phosphorylcholine-binding pocket of CRP and inhibiting its conversion to pro-inflammatory isoforms (40). These studies validate the feasibility of CRP as a therapeutic target and demonstrate its promising broad application in various inflammatory diseases, providing strong support for the development of novel anti-inflammatory therapies.

While the findings of this study are consistent across two large cohorts, it is important to acknowledge the limitations of the study design. First, due to the cross-sectional study design, it was impossible to establish a definitive causal relationship between hsCRP and hepatic fibrosis. Accordingly, future studies must adopt a longitudinal design to validate this association further. Secondly, although the study included two geographically diverse cohorts, the sample size was still insufficient. It may have been affected by selection bias and unmeasured confounders, which may have impacted the study results. Furthermore, there were discrepancies in hsCRP measurements between the two cohorts, which may have negatively impacted the direct comparison of results. It is recommended that future studies employ a prospective cohort design to not only validate the relationship between hsCRP and hepatic fibrosis in patients with MASLD in greater depth but also to explore the applicability of hsCRP in populations of different races and regions. Ultimately, as this study concentrated on hsCRP as a singular inflammatory marker, future research could be expanded to investigate the correlation between other inflammatory markers and hepatic fibrosis and the potential utility of combining multiple inflammatory markers for hepatic fibrosis risk assessment.

5 Conclusion

In conclusion, the present study employed cross-regional and large-scale data analysis to investigate the correlation between hsCRP levels and hepatic fibrosis in MASLD patients. The findings revealed a potential dose-response relationship and variability in different subgroups. These findings underscore the pivotal role of inflammation in the progression of MASLD and offer a novel perspective and empirical basis for risk assessment of hepatic fibrosis in patients with MASLD. They also provide a valuable reference for future research directions. Further research is required to elucidate the mechanisms by which hsCRP may contribute to hepatic fibrosis. Additionally, more extensive longitudinal studies encompassing diverse geographical and ethnic groups must confirm these findings. This study aims to validate the findings and elucidate the underlying pathophysiological mechanisms, providing more effective preventive and therapeutic strategies for MASLD patients.

Data availability statement

The US cohort data presented in this study can be found in online repositories. The names of the repository/repositories and accession number(s) can be found below: https://www.cdc.gov/nchs/nhanes/index.htm. The Chinese cohort data utilized and analyzed in the present study are accessible from the corresponding author/s without undue reservation.

Ethics statement

The studies involving humans were approved by National Center for Health Statistics Ethics Review Board and Ethics Committee of Changzhou Third People's Hospital. The studies were conducted in accordance with the local legislation and institutional requirements. The participants provided their written informed consent to participate in this study.

Author contributions

YW: Data curation, Investigation, Project administration, Writing – original draft. GZ: Data curation, Investigation, Project administration, Writing – original draft. FZ: Conceptualization, Data curation, Formal analysis, Funding acquisition, Investigation, Methodology, Project administration, Writing – review & editing. WL: Conceptualization, Formal analysis, Methodology, Supervision, Visualization, Writing – review & editing.

Funding

The author(s) declare financial support was received for the research, authorship, and/or publication of this article. This work

was supported by the Key Talents Project of Changzhou Third People's Hospital.

Acknowledgments

We thank all the study participants and staff for their contributions.

Conflict of interest

The authors declare that the research was conducted in the absence of any commercial or financial relationships that could be construed as a potential conflict of interest.

Generative AI statement

The author(s) declare that no Generative AI was used in the creation of this manuscript.

Publisher's note

All claims expressed in this article are solely those of the authors and do not necessarily represent those of their affiliated organizations, or those of the publisher, the editors and the reviewers. Any product that may be evaluated in this article, or claim that may be made by its manufacturer, is not guaranteed or endorsed by the publisher.

References

1. Younossi ZM, Kalligeros M, Henry L. Epidemiology of metabolic dysfunction-associated steatotic liver disease. *Clin Mol Hepatol.* (2024). doi: 10.3350/cmh.2024.0431

2. Chan WK, Chuah KH, Rajaram RB, Lim LL, Ratnasingam J, Vethakkan SR. Metabolic dysfunction-associated steatotic liver disease (MASLD): A state-of-the-art review. *J Obes Metab Syndr.* (2023) 32:197–213. doi: 10.7570/jomes23052

3. Fan W, Bradford TM, Török NJ. Metabolic dysfunction-associated liver disease and diabetes: Matrix remodeling, fibrosis, and therapeutic implications. *Ann N Y Acad Sci.* (2024) 1538:21–33. doi: 10.1111/nyas.v1538.1

4. Israelsen M, Francque S, Tsochatzis EA, Krag A. Steatotic liver disease. *Lancet.* (2024) 404:1761–78. doi: 10.1016/S0140-6736(24)01811-7

5. Rinella ME, Lazarus JV, Ratziu V, Francque SM, Sanyal AJ, Kanwal F, et al. A multisociety Delphi consensus statement on new fatty liver disease nomenclature. *J Hepatol.* (2023) 79:1542–56. doi: 10.1016/j.jhep.2023.06.003

6. Riley DR, Hydes T, Hernadez G, Zhao SS, Alam U, Cuthbertson DJ. The synergistic impact of type 2 diabetes and MASLD on cardiovascular, liver, diabetes-related and cancer outcomes. *Liver Int.* (2024) 44:2538–50. doi: 10.1111/liv.v44.10

7. Choe HJ, Moon JH, Kim W, Koo BK, Cho NH. Steatotic liver disease predicts cardiovascular disease and advanced liver fibrosis: A community-dwelling cohort study with 20-year follow-up. *Metabolism.* (2024) 153:155800. doi: 10.1016/j.metabol.2024.155800

8. Zheng H, Sechi LA, Navarese EP, Casu G, Vidili G. Metabolic dysfunction-associated steatotic liver disease and cardiovascular risk: a comprehensive review. *Cardiovasc Diabetol.* (2024) 23:346. doi: 10.1186/s12933-024-02434-5

9. Loomba R, Friedman SL, Shulman GI. Mechanisms and disease consequences of nonalcoholic fatty liver disease. *Cell.* (2021) 184:2537–64. doi: 10.1016/j.cell.2021.04.015

10. Hagström H, Shang Y, Hegmar H, Nasr P. Natural history and progression of metabolic dysfunction-associated steatotic liver disease. *Lancet Gastroenterol Hepatol.* (2024) 9:944–56. doi: 10.1016/S2468-1253(24)00193-6

11. Wang M, Li L, Xu Y, Du J, Ling C. Roles of hepatic stellate cells in NAFLD: From the perspective of inflammation and fibrosis. *Front Pharmacol.* (2022) 13:958428. doi: 10.3389/fphar.2022.958428

12. Alkhouri N, Noureddin M. Management strategies for metabolic dysfunction-associated steatotic liver disease (MASLD). *Am J Manag Care.* (2024) 30:S159–s74. doi: 10.37765/ajmc.2024.89635

13. Moutachakkir M, Lamrani Hanchi A, Baraou A, Boukhira A, Chellak S. Immunoanalytical characteristics of C-reactive protein and high sensitivity C-reactive protein. *Ann Biol Clin (Paris).* (2017) 75:225–9. doi: 10.1684/abc.2017.1232

14. Pathak A, Agrawal A. Evolution of C-reactive protein. *Front Immunol.* (2019) 10:943. doi: 10.3389/fimmu.2019.00943

15. Yang X, Tao S, Peng J, Zhao J, Li S, Wu N, et al. High-sensitivity C-reactive protein and risk of type 2 diabetes: A nationwide cohort study and updated meta-analysis. *Diabetes Metab Res Rev.* (2021) 37:e3446. doi: 10.1002/dmrr.v37.8

16. Xue Q, Yang X, Huang Y, Zhu D, Wang Y, Wen Y, et al. Association between baseline and changes in high-sensitive C-reactive protein and metabolic syndrome: a nationwide cohort study and meta-analysis. *Nutr Metab (Lond).* (2022) 19:2. doi: 10.1186/s12986-021-00632-6

17. Liu Y, He W, Ji Y, Wang Q, Li X. A linear positive association between high-sensitivity C-reactive protein and the prevalence of cardiovascular disease among individuals with diabetes. *BMC Cardiovasc Disord.* (2024) 24:411. doi: 10.1186/s12872-024-04091-8

18. Yoneda M, Mawatari H, Fujita K, Iida H, Yonemitsu K, Kato S, et al. High-sensitivity C-reactive protein is an independent clinical feature of nonalcoholic steatohepatitis (NASH) and also of the severity of fibrosis in NASH. *J Gastroenterol.* (2007) 42:573–82. doi: 10.1007/s00535-007-2060-x

19. Okekunle AP, Youn J, Song S, Chung GE, Yang SY, Kim YS, et al. Predicted pro-inflammatory hs-CRP score and non-alcoholic fatty liver disease. *Gastroenterol Rep (Oxf).* (2023) 11:goad059. doi: 10.1093/gastro/goad059

20. Jamialahmadi T, Bo S, Abbasifard M, Sathyapalan T, Jangjoo A, Moallem SA, et al. Association of C-reactive protein with histological, elastographic, and sonographic indices of non-alcoholic fatty liver disease in individuals with severe obesity. *J Health Popul Nutr.* (2023) 42:30. doi: 10.1186/s41043-023-00372-8

21. Zhu C, Huang D, Ma H, Qian C, You H, Bu L, et al. High-sensitive CRP correlates with the severity of liver steatosis and fibrosis in obese patients with metabolic dysfunction associated fatty liver disease. *Front Endocrinol (Lausanne).* (2022) 13:848937. doi: 10.3389/fendo.2022.848937

22. Cao YT, Xiang LL, Qi F, Zhang YJ, Chen Y, Zhou XQ. Accuracy of controlled attenuation parameter (CAP) and liver stiffness measurement (LSM) for assessing steatosis and fibrosis in non-alcoholic fatty liver disease: A systematic review and meta-analysis. *EClinicalMedicine.* (2022) 51:101547. doi: 10.1016/j.eclinm.2022.101547

23. Zeller J, Bogner B, McFadyen JD, Kiefer J, Braig D, Pietersz G, et al. Transitional changes in the structure of C-reactive protein create highly pro-inflammatory molecules: Therapeutic implications for cardiovascular diseases. *Pharmacol Ther.* (2022) 235:108165. doi: 10.1016/j.pharmthera.2022.108165

24. Zeller J, Loseff-Silver J, Khoshmanesh K, Baratchi S, Lai A, Nero TL, et al. Shear-sensing by C-reactive protein: linking aortic stenosis and inflammation. *Circ Res.* (2024) 135:1033–47. doi: 10.1161/CIRCRESAHA.124.324248

25. Thiele JR, Habersberger J, Braig D, Schmidt Y, Goerendt K, Maurer V, et al. Dissociation of pentameric to monomeric C-reactive protein localizes and aggravates inflammation: *in vivo* proof of a powerful proinflammatory mechanism and a new anti-inflammatory strategy. *Circulation.* (2014) 130:35–50. doi: 10.1161/CIRCULATIONAHA.113.007124

26. Ji SR, Ma L, Bai CJ, Shi JM, Li HY, Potempa LA, et al. Monomeric C-reactive protein activates endothelial cells via interaction with lipid raft microdomains. *FASEB J.* (2009) 23:1806–16. doi: 10.1096/fj.08-116962

27. Alissa EM, Algarni SA, Khaffji AJ, Al Mansouri NM. Role of inflammatory markers in polycystic ovaries syndrome: In relation to insulin resistance. *J Obstet Gynaecol Res.* (2021) 47:1409–15. doi: 10.1111/jog.14684

28. Bansal SK, Bansal MB. Pathogenesis of MASLD and MASH - role of insulin resistance and lipotoxicity. *Aliment Pharmacol Ther.* (2024) 59 Suppl 1:S10–s22. doi: 10.1111/apt.v59.s1

29. Seki E, Brenner DA, Karin M. A liver full of JNK: signaling in regulation of cell function and disease pathogenesis, and clinical approaches. *Gastroenterology.* (2012) 143:307–20. doi: 10.1053/j.gastro.2012.06.004

30. Marcondes-de-Castro IA, Reis-Barbosa PH, Marinho TS, Aguila MB, Mandarim-de-Lacerda CA. AMPK/mTOR pathway significance in healthy liver and

non-alcoholic fatty liver disease and its progression. *J Gastroenterol Hepatol*. (2023) 38:1868–76. doi: 10.1111/jgh.16272

31. Parlati L, Régnier M, Guillou H, Postic C. New targets for NAFLD. *JHEP Rep*. (2021) 3:100346. doi: 10.1016/j.jhepr.2021.100346

32. Clare K, Dillon JF, Brennan PN. Reactive oxygen species and oxidative stress in the pathogenesis of MAFLD. *J Clin Transl Hepatol*. (2022) 10:939–46. doi: 10.14218/JCTH.2022.00067

33. Bashiardes S, Shapiro H, Rozin S, Shibolet O, Elinav E. Non-alcoholic fatty liver and the gut microbiota. *Mol Metab*. (2016) 5:782–94. doi: 10.1016/j.molmet.2016.06.003

34. Bahitham W, Alghamdi S, Omer I, Alsudais A, Hakeem I, Alghamdi A, et al. Double trouble: how microbiome dysbiosis and mitochondrial dysfunction drive non-alcoholic fatty liver disease and non-alcoholic steatohepatitis. *Biomedicines*. (2024) 12:550. doi: 10.3390/biomedicines12030550

35. Benedé-Ubieto R, Cubero FJ, Nevzorova YA. Breaking the barriers: the role of gut homeostasis in Metabolic-Associated Steatotic Liver Disease (MASLD). *Gut Microbes*. (2024) 16:2331460. doi: 10.1080/19490976.2024.2331460

36. Pepys MB, Hirschfield GM, Tennent GA, Gallimore JR, Kahan MC, Bellotti V, et al. Targeting C-reactive protein for the treatment of cardiovascular disease. *Nature*. (2006) 440:1217–21. doi: 10.1038/nature04672

37. Ringel J, Ramlow A, Bock C, Sheriff A. Case report: C-reactive protein apheresis in a patient with COVID-19 and fulminant CRP increase. *Front Immunol*. (2021) 12:708101. doi: 10.3389/fimmu.2021.708101

38. Schumann C, Heigl F, Rohrbach IJ, Sheriff A, Wagner L, Wagner F, et al. A report on the first 7 sequential patients treated within the C-reactive protein apheresis in COVID (CACOV) registry. *Am J Case Rep*. (2022) 23:e935263. doi: 10.12659/AJCR.935263

39. Esposito F, Matthes H, SChad F. Seven COVID-19 patients treated with C-reactive protein (CRP) apheresis. *J Clin Med*. (2022) 11:1956. doi: 10.3390/jcm11071956

40. Zeller J, Cheung Tung Shing KS, Nero TL, McFadyen JD, Krippner G, Bogner B, et al. A novel phosphocholine-mimetic inhibits a pro-inflammatory conformational change in C-reactive protein. *EMBO Mol Med*. (2023) 15:e16236. doi: 10.15252/emmm.202216236

frontiers | Frontiers in Immunology

TYPE Review
PUBLISHED 28 February 2025
DOI 10.3389/fimmu.2025.1564607

OPEN ACCESS

EDITED BY
Yi Wu,
Xi'an Jiaotong University, China

REVIEWED BY
Ivan Melnikov,
Ministry of Health of the Russian Federation, Russia
Toh Gang,
St. Jude Children's Research Hospital, United States

*CORRESPONDENCE
Lawrence A. Potempa
lpotempa01@roosevelt.edu

†PRESENT ADDRESS
Ibraheem M. Rajab,
Tabuk Pharmaceuticals Manufacturing Company, Amman, Jordan-

RECEIVED 21 January 2025
ACCEPTED 13 February 2025
PUBLISHED 28 February 2025

CITATION
Potempa M, Hart PC, Rajab IM and Potempa LA (2025) Redefining CRP in tissue injury and repair: more than an acute pro-inflammatory mediator. *Front. Immunol.* 16:1564607. doi: 10.3389/fimmu.2025.1564607

Redefining CRP in tissue injury and repair: more than an acute pro-inflammatory mediator

Marc Potempa[1], Peter C. Hart[2], Ibraheem M. Rajab[2†] and Lawrence A. Potempa[1,2*]

[1]Acphazin Inc., Deerfield, IL, United States, [2]College of Science, Health, and Pharmacy, Roosevelt University, Schaumburg, IL, United States

Most early studies investigating the role of C-reactive protein (CRP) in tissue damage determined it supported pro-hemostatic and pro-inflammatory activities. However, these findings were not universal, as other data suggested CRP inhibited these same processes. A potential explanation for these disparate observations finally emerged with the recognition that CRP undergoes context-dependent conformational changes *in vivo*, and each of its three isoforms – pentameric CRP (pCRP), modified pentameric CRP (pCRP*), and monomeric CRP (mCRP) – have different effects. In this review, we consider this new paradigm and re-evaluate the role of CRP and its isoforms in the tissue repair process. Indeed, a growing body of evidence points toward the involvement of CRP not just in hemostasis and inflammation, but also in the resolution of inflammation and in tissue regeneration. Additionally, we briefly discuss the shortcomings of the currently available diagnostic tests for CRP and highlight the need for change in how CRP is currently utilized in clinical practice.

KEYWORDS

pCRP, pCRP*, mCRP, hemostasis, inflammation resolution, tissue regeneration, therapeutic use

Introduction

The tissue repair process begins immediately after tissue damage and lasts for several weeks (1, 2). During this time, a series of biological processes occur that collectively staunch the injury (hemostasis) (3), stymie any invading pathogens (inflammation), (4), limit further damage (inflammation resolution and debris removal), (4, 5), and regenerate the tissue (angiogenesis, cellular proliferation, and tissue remodeling), (1, 4). While they overlap in practice, the various phases of the recovery process occur at roughly the following time frames: hemostasis, the first minutes to hours; inflammation, the first 72 hours; inflammation resolution, from 72 hours to ~1 week; and tissue regeneration and remodeling, ~1 week to ~1 month (1, 2).

For many years, C-Reactive Protein (CRP) was considered an important effector for only the earliest portions of the tissue repair response. This conclusion was driven by most biochemical and functional investigations of CRP determining that it potently supported pro-hemostatic and pro-inflammatory activities (6, 7). There was also a temporal logic to that argument, as plasma CRP concentrations increase up to 1000-fold during the pro-inflammatory phase and begin decreasing in tandem with the overall switch to inflammation resolution (8, 9). However, not all data were consistent with that interpretation. Some studies reported results in which CRP exhibited anti-inflammatory properties (10–15). Moreover, the 19-hour half-life of CRP means its levels are elevated above baseline even during the early tissue regeneration phase – a perplexing observation for something with strong pro-inflammatory potential (16). For a long time, these findings were difficult to reconcile and, to some extent, have limited the usefulness of CRP as a clinical tool and target.

Progress toward resolving these conflicting observations finally arrived with the recognition that CRP, in serum a very stable homo-pentameric macromolecule, undergoes conformational changes and dissociation at sites of inflammation *in vivo* (17). There had been *in vitro* observations to suggest a modified, monomeric version of CRP (mCRP) was the primary pro-inflammatory form of CRP (18–21), but evidence for the existence of mCRP *in vivo* had been difficult to obtain. The reasons for its delayed identification *in vivo* were multi-fold: for example, dissociation *in vitro* requires non-physiological amounts of heat, urea, or acidic environments (22–25); the exceptional insolubility of mCRP means it is only membrane-associated and/or -embedded *in vivo* (26–29); and, is inconsistently detectable on microvesicles in the serum of individuals without ongoing inflammatory disorders (27, 30–34). Nevertheless, improvements in techniques and reagents finally led to observations of pCRP dissociation *in vivo* in a rat model of myocardial infarction (17), its presence on circulating microvesicles in humans with inflammatory disorders (26, 27, 32–37), and its presence in human myocardial tissue and burn wounds (17, 38). A transitory intermediate form of CRP called pCRP* (pCRP star; also known as mCRPm) was identified shortly thereafter in which pCRP has undergone some conformational changes and exhibits some pro-inflammatory effector functions but has nevertheless not yet dissociated (39–42).

In this review, we distinguish between the three CRP isoforms and re-evaluate each of their potential roles in the tissue repair process. Specific isoforms of CRP will be described where possible, though many studies took place at a time where the need to differentiate the contributions of each isoform was not known or the ability to differentiate the isoforms was not readily possible. For these studies, the concentrations of CRP (low [i.e., non-saturating concentrations], pCRP*/mCRP; high, pCRP) and the time frame (≥0.5-2 hours, pCRP*/mCRP) in which results were observed provide potential ways to differentiate whether the reported effects were due to pCRP or pCRP*/mCRP (11, 39, 43). Nevertheless, there are inherent limitations to the discussion. Lastly, we briefly discuss the need for how CRP is used clinically to evolve in the wake of this new understanding of CRP bioactivity.

CRP isoforms and their bioavailability

Structure and general functions

Pentameric CRP is a compact, non-glycosylated, homo-polymeric molecule with a central void and radial symmetry (44). Each of the five monomers contains 206 amino acids and a single intramolecular disulfide bond, whereas the intermolecular interactions holding the pentamer together are non-covalent (44, 45). All monomers are oriented in the same direction, allowing pCRP to be conceptualized as two-sided (46). On one side is the binding face (or B-face), whose primary role is to bind phosphocholine (PC) (46–48). Though ubiquitously present, PC is normally buried within membranes and inaccessible to CRP. However, changes in membrane architecture due to lipid modification by enzymes (e.g., phospholipase A2) or reactive oxygen species (ROS) causes PC to 'pop up' and expose itself for CRP recognition (49–51). Upon exposure, it becomes a damage-associated molecular pattern (DAMP), an endogenous molecule containing a conserved motif the immune system utilizes to recognize abnormal situations and initiate an inflammatory response (52). Phosphocholine may also be found on Gram-positive bacterial cell walls (53), making it both a DAMP and pathogen-associated molecular pattern (PAMP; i.e., a conserved motif present on non-self organisms) (52). Interactions between CRP and PC are calcium-dependent and rely on CRP residues Phe-66 and Glu-81 (46). Notably, other DAMPs (e.g., oxidized low-density lipoprotein, histones, and fibronectin) and PAMPs (e.g., phosphoethanolamine [found on Gram-negative bacteria]) have also been identified as ligands for the CRP binding face (54–58).

On the reverse side of pCRP is the effector face, (also called the activating face or A-face), (46, 59). The most well-recognized binding partners for this half are the globular head of complement protein C1q and various Fc receptors (e.g., FcγRI [CD64], FcγRIIa [CD32a], FcγRIII [CD16], FcαRI [CD89]), (60, 61). Several other receptor binding partners have been suggested, including toll-like receptor 4 (TLR4), GPIbα, GPIIb/IIIa, CD31, CD36, integrin αvβ3, lectin-like oxidized low-density lipoprotein receptor-1 (LOX-1), and receptor activator of NF-κB ligand (62–70). While the binding site for C1q and the Fc receptors all overlap, the individual amino acids in CRP that facilitate binding to each ligand are distinct, even among the Fcγ receptors (FcγRs) (71). Importantly, three-dimensional models of the interaction between CRP and C1q suggest part of the interaction domain is inaccessible in the pentameric conformation (amino acids 199-206) (59). This implies pCRP is not inherently pro-inflammatory, instead requiring a conformational change into an alternative isoform for those activities to manifest. This is supported by the results of a clinical trial in which pCRP injected into healthy individuals did not elicit an inflammatory response (72). By extension, these results suggest environmental cues associated with ongoing inflammation are necessary to trigger conformational changes in pCRP, and the pro-inflammatory versions of CRP are amplifiers of inflammation rather than instigators. Unmodified pCRP may even have regulatory or anti-inflammatory activities, given *in vitro* observations of inhibitory effects on platelet, neutrophil,

macrophage, dendritic cell (DC), and fibroblast activities in a dose-dependent manner (10–14, 73–78).

The pCRP* isoform is presumed to be an intermediate step between pCRP and its dissociation into mCRP (6, 39). Structurally, the pentameric assembly remains, but it has 'relaxed' sufficiently that the pro-inflammatory neoepitope (the aforementioned residues 199-206) is fully exposed (40, 41). At present, circumstances *in vivo* in which pCRP converts to pCRP* include ligand binding at regions of high membrane curvature and mildly acidic microenvironments such as those present at sites of inflammation (40, 79–82). Curved surfaces make PC more available, make hydrophobic regions of membrane lipids accessible, and expose binding sites on membrane-anchored proteins (81–83). Ultimately, the intermolecular interactions that hold pCRP subunits together undergo rearrangement resulting in exposure of the neoepitope (41). Alternatively (or additionally), acidic conditions can cause the protonation of histidine residues nearby the disulfide bonds within each CRP molecule (84). This alters the intramolecular hydrogen bonding network, causing structural changes in pCRP that again result in the exposure of the neoepitope.

Functionally, pCRP* stimulates the immune response by activating the classical complement pathway (39, 41). Interactions between CRP and C1q are primarily electrostatic in nature and demonstrate high avidity, making pCRP* the most potent CRP isoform at activating complement (41, 85). Of note, CRP-induced activation of the complement cascade biases it toward opsonization/phagocytosis as opposed to activation of the membrane attack complex (MAC)/cellular lysis (86, 87), thereby preventing excessive inflammation (87). Investigation of pCRP* activities beyond complement activation are limited due to its recent identification and the current limitations in experimentally distinguishing it from other isoforms. However, microvesicle-associated pCRP* can increase adhesion molecule expression on endothelial cells (41), and the overlap of the complement and FcγR binding sites implies pCRP* likely also stimulates FcγRs (71).

The terminal form of CRP is its monomeric form, mCRP. Dissolution of the pentamer occurs after newly exposed hydrophobic residues in pCRP* form interactions with the hydrophobic tails of lipids in membranes or with insoluble extracellular plaques in tissues (17, 22, 88). Thus, mCRP is found *in vivo* embedded within cellular membranes, associated with circulating microvesicles, or sequestered with insoluble components of the extracellular matrix (ECM) (17, 26–28, 38, 88, 89). The amino acids key to membrane-entry (residues 35-47, VCLHFYTELSSTR) preferentially interact with cholesterol, biasing mCRP membrane localization to lipid raft domains (28). Exposure of the cholesterol binding site is supported by reactive oxygen species (ROS) generated at sites of inflammation, presumably because the oxidative modifications to pCRP/pCRP* loosen its pentameric structure (79, 90). However, optimal exposure requires reduction of the intrachain disulfide bond, something it is primed to do in acidic conditions (79, 84, 89–91).

Pro-inflammatory activities have been described for mCRP in numerous settings and are discussed in detail in several recent reviews (6, 7, 92–99). In brief, mCRP promotes cellular chemotaxis and adhesion (14, 17, 18, 21, 68, 89, 100–105), augments platelet activation and aggregation (65, 70, 90, 106–108), and stimulates cytokine, ROS, and nitric oxide (NO) production (28, 38, 73, 79, 89, 102, 109–112). These effects are partially mediated through interactions with FcγRs, but not completely, as blockade of FcγRs does not completely abrogate the effects of mCRP (19–21, 113). Notably, mCRP potency is greater when the intramolecular disulfide bond in mCRP has been reduced (110). Monomeric CRP also retains the ability to interact with C1q and additionally interacts with negative regulators of complement activity (Factor H and C4-binding protein) (61, 114).

In summary, the long-appreciated role of CRP as an immune stimulant is now known to be attributable to pCRP* and mCRP, whereas pCRP is non- or anti-inflammatory. However, the bioactivities of CRP are not limited to impacting the inflammatory response. As we will shortly discuss, evidence has been accumulating to suggest CRP augments each additional phase of the tissue repair response: hemostasis, immune resolution, and tissue regeneration (Figure 1; Table 1).

CRP bioavailability

In the absence of ongoing inflammation, the steady-state concentration of pCRP in blood is <1 to 3 mg/L (115–117). Circulating pCRP is produced by hepatocytes, though extrahepatic macrophages, lymphocytes, endothelial cells, adipocytes, and smooth muscle cells can express CRP (98, 118). It is unknown if non-hepatic CRP is secreted as pCRP or acts as an autocrine factor. Information on the steady-state levels of pCRP* and mCRP in the blood is limited. The pro-inflammatory CRP isoforms have been detected on microvesicles, but most efforts to quantify pCRP*/mCRP concentrations in the serum of individuals without inflammatory disorders place its concentration from undetectable (<1) to 25 ng/mL (26, 27, 33–36, 119–123). Outside of the blood, immunohistochemical staining finds pCRP*/mCRP to be present in arterial plaques and areas surrounding recently damaged vascular tissue (89, 99, 103, 124–126).

During the early stages of an inflammatory response, hepatocytes respond to elevated levels of interleukin (IL-6) and IL-1β by releasing pre-existing stores of pCRP and dramatically increasing production of new pCRP (127–129). Serum concentrations of pCRP can rise to over 500 mg/L within the first 72 hours of the response (9, 130). Similarly, microvesicle-associated CRP levels significantly increase during acute inflammatory events (34, 120, 123). Both pCRP and mCRP levels remain elevated in chronic conditions (27, 31–33, 35–37, 119, 121), with multiple reports finding a direct correlation between mCRP levels and disease severity (31, 32, 35–37, 131). This was in contrast to pCRP concentrations, which were not consistently predictive. Relatedly, there is disagreement about whether a correlation exists between mCRP and pCRP concentrations. Among 12 studies reporting correlations included in this review, nine found a lack of significant correlation (27, 30–34, 36, 37, 120–122, 131, 132).

Once secreted, the half-life of pCRP is ~19 hours (16, 117). Its rate of disappearance is independent of its plasma concentration (16), making the measured pCRP concentrations a reflection of recent synthesis rates and not changes in consumption/excretion.

10.3389/fimmu.2025.1564607

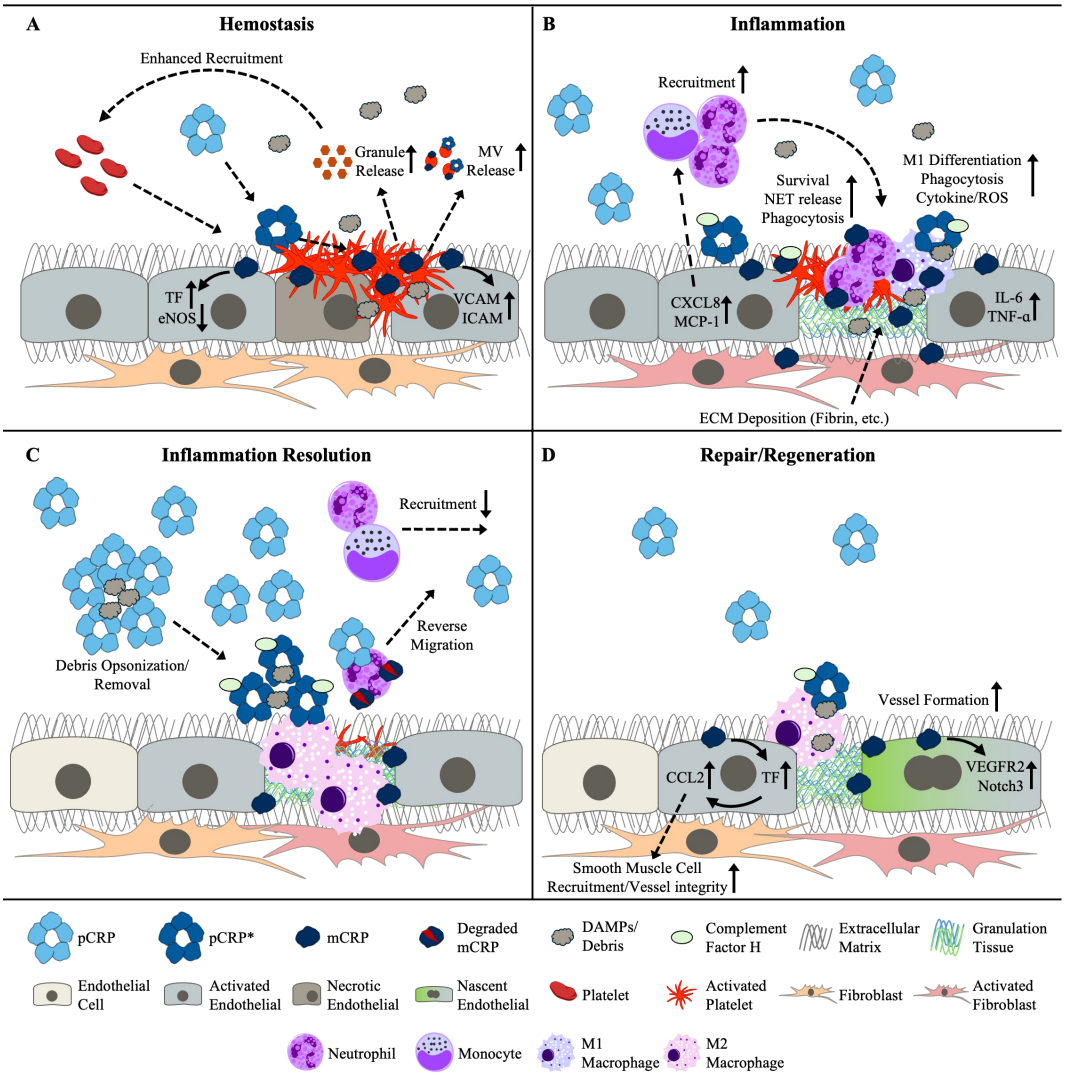

FIGURE 1
Reported and putative roles for the CRP isoforms on activities associated with **(A)** hemostasis, **(B)** inflammation, **(C)** the resolution of inflammation, and **(D)** tissue repair and regeneration. CRP, C-reactive protein; DAMPs, damage-associated molecular patterns ECM, extracellular matrix; eNOS, endothelial nitric oxide synthase; ICAM, intercellular adhesion molecule; IL-6, interleukin-6; MCP-1, monocyte chemoattractant protein-1; mCRP, monomeric CRP; MV, microvesicle; NET, neutrophil extracellular trap; pCRP, pentameric CRP; pCRP*, pCRP star; ROS, reactive oxygen species; TF, tissue factor; TNF-α; tumor necrosis-factor-alpha; VCAM, vascular cell adhesion molecule; VEGFR2, vascular endothelial growth factor receptor 2.

Due to the large amount produced and its relatively slow half-life, it is common to see elevated concentrations of circulating pCRP for more than a week after an inciting inflammatory event (133). The rate at which pCRP converts to pCRP* *in vivo* and the length of time before pCRP* dissociates into mCRP are unknown. *In vitro* observations found the neoepitope could be detected 30 minutes after treating cells with pCRP and that evidence of pentamer dissociation appeared approximately 90 minutes later (39). This timeframe roughly agrees with a second study that reported the appearance of mCRP at approximately 2 hours post application of pCRP (43). Information on the half-life of mCRP in humans is unavailable, both in the circulation and in tissues. However, data from mouse models revealed mCRP could be detected in tissues for three times longer than pCRP in the blood (134).

CRP in tissue damage and repair

Hemostasis

When bleeding occurs, multiple intertwined processes are initiated to close the wounded blood vessel (3, 135, 136). One process begins when platelets adhere to collagen in the exposed ECM. Binding activates the platelets, which recruit additional platelets that together coalesce into a primary plug. Secretions from activated platelets also provide a means for the activation a second clotting process, the intrinsic coagulation cascade. Platelet-derived polyphosphates provide a binding surface for coagulation Factor XII. Binding activates Factor XII and, after several additional steps, culminates in the activation of Factor X. In a third process, the

extrinsic coagulation pathway, circulating coagulation Factor VII complexes with Tissue Factor (TF) expressed on the surface of smooth muscle cells and fibroblasts and this complex also activates Factor X. Activated Factor X combines with and activates Factor V, forming prothrombinase; prothrombinase converts prothrombin into thrombin; thrombin converts fibrinogen into fibrin; and Factor XIII, also activated by thrombin, covalently crosslinks fibrin molecules together. This fibrin mesh combines with the platelet plug to form a stable patch over the wound and prevent further blood loss (3, 135).

TABLE 1 Reported pro-inflammatory and pro-resolution activities of CRP by cell type.

Cell Type	Reported effects of CRP
Platelets	
Pro-inflammatory	• Promotes adhesion and aggregation (65, 70, 90, 112, 138) • Enhances signaling through major platelet adhesion receptor GPIIb/IIIa and boosts responsiveness to other stimuli (65, 106) • Stimulates release of Factor V, vWF, Fibronectin, and high mobility group box 1 (65, 107, 108)
Pro-resolution	• Stimulates release of VEGF and PDGF (65, 108) • Inhibits aggregation (78)
Endothelial cells	
Pro-inflammatory	• Upregulates VCAM-1 and ICAM-1 expression (21, 28, 101, 105, 108, 141, 142, 152) • Promotes IL-6, CXCL8, and MCP-1 production and release (21, 28, 156, 159) • Increases surface expression of Tissue Factor (43, 145–148) • Inhibits endothelial nitric oxide synthase (143, 144) • Disrupts endothelial barrier integrity (105, 182, 193)
Pro-resolution	• Induces proliferation and tube formation (124, 145, 183, 194) • Upregulates VEGF receptor 2 and Notch3 expression (183, 187) • Regulates VE-cadherin and N-cadherin expression (187) • Upregulates thrombomodulin and downregulates vWF (142)
Smooth muscle cells	
Pro-inflammatory	• Increases surface expression of Tissue Factor (145, 149) • Stimulates expression of IL-6, MCP-1, and TNF-α (63, 167, 195) • Upregulates matrix metalloproteinase expression (196, 197)
Pro-resolution	• Promotes migration and proliferation (145, 198)
Neutrophils	
Pro-inflammatory	• Upregulates CD11b/CD18 expression and promotes infiltration (18, 104) • Increases nitric oxide and reactive oxygen species production (20, 102) • Enhances phagocytosis of debris (11, 113) • Promotes NET formation (107, 152, 162) • Delays apoptosis (19)
Pro-resolution	• Inhibits neutrophil chemotaxis and adhesion (11, 12)
Monocytes/Macrophages	
Pro-inflammatory	• Promotes differentiation into M1 macrophages and foam cells (111, 125, 169) • Augments expression of TNF-α, IL-1β, IL-6, and CXCL8 (15, 112, 152, 168) • Upregulates CD11b/CD18 expression and promotes recruitment (14, 68, 89, 101, 112, 147) • Increases nitric oxide and reactive oxygen species production (38, 73, 109, 152) • Enhances clearance of necrotic and apoptotic cells (38)
Pro-resolution	• Upregulates expression of LXRα (15) • Induces VEGF and IL-10 expression (176, 188) • Suppresses nitric oxide production (73) • Prevents conversion to foam cells and facilitates M2 polarization (77, 170)
Conventional dendritic cells	
Pro-inflammatory	• Promotes maturation of immature dendritic cells (199, 200) • Increases production of TNF-α and IL-12 (199)
Pro-resolution	• Suppresses stimulation of T cells (75, 201, 202) • Inhibits IFNα production in response to TLR ligands (13) • Drives formation of myeloid-derived suppressor cells (74)

(Continued)

TABLE 1 Continued

Cell Type	Reported effects of CRP
Plasmacytoid dendritic cells	
Pro-resolution	• Suppresses IFNα production to autoantigens (203)
Mast cells	
Pro-inflammatory	• Promotes histamine release (204)
Fibroblasts	
Pro-inflammatory	• Increases IL-6, CXCL8, and VCAM-1 production (205, 206)
Pro-resolution	• Inhibits migration (76)

CRP, C-reactive protein; CXCL8, C-X-C motif ligand 8; HMGB1, high mobility group box 1; ICAM-1, intercellular adhesion molecule-1; IFNα, interferon alpha; LXRα, liver X receptor alpha; MCP-1, monocyte chemoattractant protein-1; NET, neutrophil extracellular trap; PDGF, platelet-derived growth factor; TLR, toll-like receptor; TNF-α, tumor necrosis factor alpha; VCAM-1, vascular cell adhesion molecule-1; VEGF, vascular endothelial growth factor; vWF, von Willebrand Factor.

Foremost among the ways CRP boosts hemostatic processes is by enhancing platelet activation and aggregation (65, 70, 90, 106–108, 112, 137, 138). Platelets provide optimal conditions for the conversion of pCRP into pCRP* and mCRP. More specifically, the membranes of activated platelets contain an abundance of oxidized phospholipids and undergo membrane 'ruffling,' thus providing both exposed PC and regions of increased membrane curvature (89, 136). Indeed, half of all platelet-derived microvesicles have neoepitope-expressing CRP associated with them in people with an acute inflammatory condition (34), suggesting a close relationship between the two effectors *in vivo*. Functionally, mCRP enhances signaling through the major platelet adhesion receptor GPIIb/IIIa and boosts the responsiveness of platelets to other stimuli, such as adenosine diphosphate, epinephrine, and thrombin (65, 70, 90, 106). Platelets stimulated with mCRP release more of their granules (65, 108), which contain a variety of pro-coagulation factors (e.g., Factor V, von Willebrand Factor, fibronectin) and pro-repair factors (e.g., platelet-derived growth factor [PDGF], insulin-like growth factor-1, transforming growth factor [TGF]-β) (136). Increased secretion of High Mobility Group Box 1 (HMGB1) by platelets stimulated with mCRP has also been reported, which has downstream effects on neutrophils (107). The platelet scavenger receptor CD36 and adhesion receptor GPIIb/IIIa have been implicated in mediating some of the effects mCRP exerts on platelets (65, 70). Additionally, we note that platelets express ample amounts of FcγRIIa and TLR4, and there is substantial overlap between the effects observed with mCRP and those with FcγRIIa and TLR4 stimulation (139, 140).

Platelet activities are also affected by interactions between CRP and endothelial cells. Like with platelets, CRP can bind and dissociate on the membranes of endothelial cells at sites of inflammation (21). Stimulation of endothelial cells with mCRP leads to the upregulation of vascular cell adhesion molecule (VCAM)-1 and intercellular adhesion molecule (ICAM-1) (21, 28, 105, 108, 141, 142), the latter of which is a ligand for platelet GPIIb/IIIa (136). Thus, mCRP reinforces a major GPIIb/IIIa adhesion and signaling axis for platelets from both ends. CRP also supports platelet adhesion by inhibiting the expression and activity of endothelial nitric oxide synthase (eNOS) in endothelial cells (143, 144). Under normal conditions, endothelial cells produce nitric oxide to prevent unnecessary platelet aggregation and degranulation (3). By inhibiting eNOS, mCRP facilitates platelet adhesion and aggregation.

While its effects are less direct, CRP also impacts the extrinsic and intrinsic coagulation cascades. Endothelial cells and smooth muscle cells exposed to CRP upregulate TF (43, 145–149), thereby boosting the extrinsic coagulation pathway. Support for the intrinsic pathway stems from CRP-mediated activation of neutrophils. Neutrophils that swarm to the injury site generate structures called Neutrophil Extracellular Traps (NETs) (150). While the primary role of NETs is the capture of pathogenic organisms and cellular debris, they include polyanions that can also activate Factor XII (151). Among its numerous effects on neutrophils, mCRP has recently been suggested to promote NET formation, though this may be through an indirect mechanism in which neutrophils increase NETs in response to the HMGB1 secreted by platelets (107, 152, 162).

Inflammation

The local immune response to tissue injury begins with the release of pro-inflammatory cytokines and DAMPs from damaged and dead cells (153–155). Nearby epithelial cells, endothelial cells, fibroblasts, mast cells, and tissue-resident macrophages respond to and amplify these signals to recruit nearby and circulating immune cells. For example, endothelial cells release IL-1β, IL-6, CXCL8 (i.e., IL-8), tumor necrosis factor (TNF)-α, and monocyte chemotactic protein (MCP)-1 to activate and attract immune cells and upregulate integrins like ICAM-1 and VCAM-1 to facilitate leukocyte adhesion to the site of damage (105, 108, 153–156). Aspects of the hemostasis response also contribute, with molecules such as thrombin stimulating cytokine secretion from local cells and platelets releasing pro-inflammatory chemokines and cytokines (136, 157).

A variety of innate immune cells, including neutrophils, monocytes, invariant NKT cells, mast cells, and plasmacytoid dendritic cells, respond to those pro-inflammatory cues and populate the wound site (154). Among them, neutrophils are the major effector for the first 24-48 hours post-injury, representing

more than 50% of infiltrating leukocytes (4, 154). In general, their major activities are the secretion of antimicrobial substances (e.g., ROS) and the formation of NETs to capture and kill any potential pathogens. They also have a role as phagocytes, albeit only for smaller pieces of debris (150). After neutrophils, monocytes are the other major immune cell during the early response, peaking in number with a slight delay relative to neutrophils at approximately 72 hours post-injury (4). Responding monocytes initially differentiate into pro-inflammatory (i.e., M1) macrophages, release various pro-inflammatory cytokines and antimicrobial substances, and phagocytose pathogens, tissue debris, and apoptotic cells (4, 158). The specific contributions of the other cell types have been investigated more sparsely, though they are no less important to the timely repair of tissue damage (1).

The role of CRP in augmenting the acute inflammatory response is extensive and has been discussed at length by multiple other recent reviews (6, 7, 92–99). For brevity, we will briefly describe only a few key connections between CRP and neutrophils or monocytes/macrophages, and direct readers to the other reviews for more detailed information.

There is ample evidence linking CRP to enhanced neutrophil responses. First, CRP promotes neutrophil recruitment through its effects on endothelial cells and platelets. As described above, pCRP dissociates into mCRP on the surface of endothelial cells and promotes their activation. In doing so, mCRP boosts endothelial cell release of CXCL8 and upregulation of ICAM-1 (21, 28, 141, 159), a potent neutrophil chemoattractant and key ligand for neutrophil adhesion processes, respectively (4, 160). Similarly, CRP increases P-selection expression on platelets (65, 78, 138), which has a key role in neutrophil localization (21, 161). Neutrophils reciprocally upregulate CD11b/CD18 (Mac-1) after stimulation with mCRP (18, 162). In addition to its effects on neutrophil recruitment, stimulation of neutrophils with mCRP increases NO production, enhances phagocytosis of debris, delays their apoptosis, and has recently been demonstrated to be a potent inducer of NET formation (11, 19, 20, 107, 113, 152, 162). Some effects are downstream of interactions between mCRP and FcγRIIIb (19, 21), which is amply expressed on the neutrophil surface (163), whereas other effects may be downstream of FcαRI (164).

Monocyte and macrophage recruitment is similarly enhanced by CRP through the upregulation of MCP-1 expression in endothelial cells, and through the stimulation of receptors with which CRP is known to engage (21, 159, 165, 166), such as FcγRI, FcγRIIa, and toll-like receptor TLR4 (62, 63, 71, 167). Interactions between mCRP and monocyte (FcγRs) promote monocyte differentiation into M1 macrophages and contribute to the cellular metabolic reprogramming necessary for macrophages to perform their effector functions (17, 27, 111, 168–170). Cytokines released by monocytes/macrophages whose secretion has been augmented by mCRP include at least TNF-α, IL-1β, IL-6, and CXCL8 (63, 111, 112, 167, 169). Other effects of stimulating monocytes with mCRP include the upregulation of CD11b/CD18, increased NO and ROS production, and enhanced clearance of necrotic and apoptotic cells (14, 17, 73, 109, 111).

Inflammation resolution

While inflammation is necessary for the elimination of pathogens and clearance of cellular debris, prolonged inflammation will stymie reparative activities (4). To prevent this, there are numerous 'built-in' mechanisms to ensure a timely resolution to inflammatory processes. For example, NETs catch cytokines and chemokines produced during the initial response, which results in their degradation by NET-associated proteases and a reduction in further effector cell recruitment (171). Activated neutrophils recruit monocytes and macrophages (172), and those macrophages subsequently contribute to suppressing neutrophil responses through efferocytosis and promoting neutrophil reverse migration (173, 174). Efferocytosis simultaneously promotes the conversion of M1 macrophages to the pro-resolution M2 phenotype that produce anti-inflammatory factors such as TGF-β and IL-10 (175). Overall, by approximately 72 hours post-injury, the inflammatory response to tissue injury should be ending and a pro-repair microenvironment forming.

There is evidence to suggest CRP has its own negative feedback mechanism. As noted, circulating pCRP concentrations may increase up to 1000-fold in the first 72 hours of an inflammatory response (9, 130). Interestingly, several *in vitro* observations have found high concentrations of pCRP to cause the opposite effects of pCRP*/mCRP or outright suppressive activities (10–13, 73–75, 78, 170). For instance, elevated pCRP concentration may help abate inflammation by suppressing the differentiation of pro-inflammatory DCs and driving the formation of myeloid-derived suppressor cells and M2-type macrophages (13, 74, 75, 170, 176). Moreover, whereas lower concentrations of CRP promote neutrophil chemotaxis and adhesion, higher amounts inhibit those activities (11, 12, 78, 177). At least for neutrophils, mCRP and pCRP may bind different receptors (178), ostensibly providing a mechanistic basis for these opposing effects. Notably, whereas pCRP is generally resistant to proteolysis, mCRP is susceptible to degradation by neutrophil-associated proteases and those peptides demonstrate dominant negative-like activities *in vitro* (177, 179, 180). Thus, mCRP binding sites may not be re-exposed after degradation of mCRP, which would also shift the balance of CRP activities toward those mediated by pCRP. Such mechanisms may contribute to the enigmatic process of neutrophil reverse migration (173).

Elevated CRP concentrations may also help limit inflammation by reducing and/or obscuring DAMPs. For example, CRP neutralizes extracellular histones from inducing endothelial cell cytotoxicity by outcompeting cell-associated binding partners that facilitate histone uptake (54). Furthermore, CRP prevents the activation of endothelial cells and macrophages by modified lipids if allowed to complex with those lipids prior to being added to cell cultures, suggesting a potential competitive inhibitory effect when in excess (14, 77). Thus, we propose that upregulation of CRP may serve as a mechanism by which an inflammatory response is curtailed through use of CRP as an "antigen sink." The role of CRP as an opsonin of cellular debris is arguably also an anti-inflammatory mechanism of action, given the interaction of CRP

with inhibitors of the MAC results in the clearance of inflammatory materials without inciting an inflammatory response (86). Higher concentrations ostensibly facilitate greater clearance, especially as the peak of CRP concentrations coincide with the peak of monocyte/macrophage infiltration.

Altogether, these findings suggest the up to 1000-fold increase in CRP concentration seen during the first 72 hours of a response may constitute an anti-inflammatory process rather than one meant to amplify inflammation. These anti-inflammatory effects may be achieved through at least two mechanisms: saturation of mCRP binding followed by the initiation of alternative anti-inflammatory interactions, and hiding/eliminating DAMPs/PAMPs by acting as an antigen sink. Further research into the anti-inflammatory properties of CRP are needed, especially as there is some evidence suggesting additional feedback mechanisms. For example, stimulation of macrophages through FcγRI by CRP upregulates expression of the inhibitory liver X receptor (LXR) alpha and specific ligands may lead to differing pro- or anti-inflammatory effects (15, 170, 176).

Tissue regeneration and remodeling

The tissue regeneration and remodeling phase includes its own set of interdependent processes, which together account for the growth of new blood vessels (i.e., angiogenesis), the deposition of granulation tissue, the proliferation of parenchymal cells, and the remodeling of the tissue into a stable long-term structure (1, 4). Though conceptually these processes occur after hemostasis, inflammation, and inflammation resolution, considerable groundwork for them takes place during those earlier stages (4). For example, platelets secrete many pro-angiogenic factors (e.g., PDGF, vascular endothelial growth factor [VEGF], and TGF-β), stirring endothelial cells to proliferate and begin the formation of new capillaries (181). Proteases released by neutrophils free VEGF sequestered within the ECM and facilitate endothelial cell expansion into the wound (160). Histamine and trypase released by mast cells enhance fibroblast proliferation and the deposition of collagen (1, 4). Macrophages consume dead vasculature and secrete wound healing factors like arginase, TGF-β, VEGF, PDGF, and insulin-like growth factor (158). Indeed, there is an ever-growing list of interactions between the immune response to tissue damage and tissue regrowth.

Several observations now point toward mCRP being among the list of immune mediators to enhance tissue regeneration. Most of that evidence revolves around the effect of mCRP on neovascularization. For one, mCRP colocalizes with a marker of angiogenesis (i.e., endoglin [CD105]) in stroke patients (124, 182), suggesting a potential relationship *in vivo*. Results from *in vitro* wound healing assays support this, as aortic endothelial cells treated with mCRP exhibited greater vessel formation (124, 183). The upregulation of two critical receptors for vessel development, VEGF receptor 2 and Notch3, by endothelial cells after mCRP exposure offers a potential mechanism for this observation (183–185). Moreover, angiopoietins are upregulated downstream of Notch receptors and its production enhanced by hypoxia-inducible factor (HIF)-1α (184). CRP has also been shown to stimulate HIF-1α in a pro-angiogenic capacity (186), implying CRP both promotes Notch receptor expression and enhances signaling downstream of those receptors. There is also evidence to suggest mCRP contributes to both the formation and stability of neo-vessels by variably promoting or downregulating the expression of VE-cadherin and N-cadherin depending on co-stimulatory signals (187). The enhanced expression of TF by endothelial cells in the presence of mCRP adds another layer (43, 145–149), as TF activation increases endothelial cells secretion of CCL2, which recruits vascular smooth muscle cells that strengthen vessel integrity (43). Lastly, there are also indirect effects stemming from mCRP-mediated release of pro-angiogenic factors such as VEGF and PDGF (183, 186, 188).

The effect of CRP on other aspects of tissue regeneration and remodeling process has been investigated much more sparsely. There are likely effects on granulation tissue formation, since CRP has been reported to enhance the epithelial-to-mesenchymal transition (91). Conversely, other work has shown CRP can inhibit fibroblast migration (76), though this was again dose-dependent and so may represent another concentration-dependent negative feedback mechanism.

In the clinic

At present, the only diagnostic tests for CRP measures plasma concentrations of the pCRP isoform (27). Clinicians have traditionally used results of those tests to report the presence of inflammation if the levels are above 10 mg/L (roughly 3- to 10-fold above baseline). However, such individual measurements cannot discern whether the inflammation is due to a chronic ongoing inflammatory event or a recent acute inflammatory event that has concluded. And because the amount of pCRP made varies from event to event and person to person (189, 190), single measurements are also unable to discern how long ago or how severe such an acute event might have been. Therefore, given the currently available diagnostic tests, we encourage physicians to measure pCRP levels multiple times with the understanding that its concentration should halve approximately every 19 hours (16, 117, 189, 191), excluding any potential effects of changes in treatment regimen. This minor change could at least assist clinicians in diagnosing the nature of a condition as acute or chronic.

Regardless, the more significant benefit to clinical practice would be the development of a routine clinical method for determining the abundance of the pro-inflammatory CRP isoforms (i.e., pCRP* and mCRP), as advances in the CRP field over the previous decade have confirmed these to be the potentially immunopathogenic forms of CRP (6, 96, 99, 192). Unfortunately, both the standard and high-sensitivity tests for pCRP are unable to detect pCRP*/mCRP and, critically, most findings have found there is no definitive correlation between serum concentrations of pCRP and pCRP*/mCRP (27, 30–34, 36, 37, 120–122, 132). This means there is no concrete means of discerning the amount of potentially immunopathogenic CRP from current standard practices. Of note,

this potential absence of a relationship between the different isoforms may also explain the lack of agreement among studies investigating whether baseline pCRP levels predict the incidence of various cardiovascular conditions (6). There are putative correlations between CRP-positive microparticles (which ostensibly represents ligand-bound, neoepitope-exposed CRP) and C1q-positive microparticles, suggesting there may yet be surrogate methodologies in the absence of direct mechanisms; but even these relationships may be condition-specific (119, 120). Ultimately, it is imperative that routine, standardized assays are developed for the specific detection of pCRP*/mCRP. Only then can the relationship between CRP and underlying inflammatory diseases be clearly elucidated.

Conclusion

The recognition that CRP undergoes context-dependent conformational changes *in vivo* has helped resolve long-standing contradictions in CRP research. Moreover, the distinct activities of pCRP, pCRP*, and mCRP have revealed the existence of a much more complex role for CRP in the biological response to tissue damage. Not only does CRP promote early hemostatic and inflammatory processes, but it also contributes to the resolution of inflammation and to angiogenesis. Moving forward, more efforts should be put toward defining the specific conditions in which each isoform is abundant, including considerations for factors such as the specific ligands available and cell receptor density. Toward that end, the development of standardized assays capable of detecting the pCRP* and mCRP isoforms is of paramount importance, as neither the general nor high-sensitivity CRP assays currently available have that ability. Such advances could also transform CRP from a general inflammatory marker into a more precise diagnostic tool, potentially enabling better monitoring of disease progression and therapeutic responses across a range of inflammatory conditions.

Author contributions

MP: Conceptualization, Visualization, Writing – original draft, Writing – review & editing. PH: Resources, Supervision, Visualization, Writing – review & editing. IR: Resources, Supervision, Writing – review & editing. LP: Conceptualization, Funding acquisition, Supervision, Writing – review & editing.

Funding

The author(s) declare that financial support was received for the research, authorship, and/or publication of this article. This submission was partially supported by a subcontract of an NIH RO1 grant awarded to Boston University Medical School Titled: Identification and characterization of the CD31-ApoE-mCRP pathway for Alzheimer's disease in humans. Award Number: 1RF1AG075832-01A1.

Conflict of interest

LP is founder and shareholder of Acphazin, Inc. MP is an employee and shareholder of Acphazin, Inc. IR is an employee of Tabuk Pharmaceuticals.

The remaining authors declare that the research was conducted in the absence of any commercial or financial relationships that could be construed as a potential conflict of interest.

The author(s) declared that they were an editorial board member of Frontiers, at the time of submission. This had no impact on the peer review process and the final decision.

Generative AI statement

The author(s) declare that no Generative AI was used in the creation of this manuscript.

Publisher's note

References

1. Rodrigues M, Kosaric N, Bonham CA, Gurtner GC. Wound healing: A cellular perspective. *Physiol Rev.* (2019) 99:665–706. doi: 10.1152/physrev.00067.2017

2. Almadani YH, Vorstenbosch J, Davison PG, Murphy AM. Wound healing: A comprehensive review. *Semin Plast Surg.* (2021) 35:141–4. doi: 10.1055/s-0041-1731791

3. Versteeg HH, Heemskerk JW, Levi M, Reitsma PH. New fundamentals in hemostasis. *Physiol Rev.* (2013) 93:327–58. doi: 10.1152/physrev.00016.2011

4. Soliman AM, Barreda DR. Acute inflammation in tissue healing. *Int J Mol Sci.* (2022) 24:641. doi: 10.3390/ijms24010641

5. Sugimoto MA, Sousa LP, Pinho V, Perretti M, Teixeira MM. Resolution of inflammation: what controls its onset? *Front Immunol.* (2016) 7:160. doi: 10.3389/fimmu.2016.00160

6. Dix C, Zeller J, Stevens H, Eisenhardt SU, Shing K, Nero TL, et al. C-reactive protein, immunothrombosis and venous thromboembolism. *Front Immunol.* (2022) 13:1002652. doi: 10.3389/fimmu.2022.1002652

7. Olson ME, Hornick MG, Stefanski A, Albanna HR, Gjoni A, Hall GD, et al. A biofunctional review of C-reactive protein (CRP) as a mediator of inflammatory and immune responses: differentiating pentameric and modified CRP isoform effects. *Front Immunol.* (2023) 14:1264383. doi: 10.3389/fimmu.2023.1264383

8. Muire PJ, Mangum LH, Wenke JC. Time course of immune response and immunomodulation during normal and delayed healing of musculoskeletal wounds. *Front Immunol*. (2020) 11:1056. doi: 10.3389/fimmu.2020.01056

9. Mantovani A, Garlanda C. Humoral innate immunity and acute-phase proteins. *N Engl J Med*. (2023) 388:439–52. doi: 10.1056/NEJMra2206346

10. Vigo C. Effect of C-reactive protein on platelet-activating factor-induced platelet aggregation and membrane stabilization. *J Biol Chem*. (1985) 260:3418–22. doi: 10.1016/S0021-9258(19)83638-4

11. Buchta R, Fridkin M, Pontet M, Contessi E, Scaggiante B, Romeo D. Modulation of human neutrophil function by C-reactive protein. *Eur J Biochem*. (1987) 163:141–6. doi: 10.1111/j.1432-1033.1987.tb10747.x

12. Tatsumi N, Hashimoto K, Okuda K, Kyougoku T. Neutrophil chemiluminescence induced by platelet activating factor and suppressed by C-reactive protein. *Clin Chim Acta*. (1988) 172:85–92. doi: 10.1016/0009-8981(88)90123-4

13. Svanberg C, Enocsson H, Govender M, Martinsson K, Potempa LA, Rajab IM, et al. Conformational state of C-reactive protein is critical for reducing immune complex-triggered type I interferon response: Implications for pathogenic mechanisms in autoimmune diseases imprinted by type I interferon gene dysregulation. *J Autoimmun*. (2023) 135:102998. doi: 10.1016/j.jaut.2023.102998

14. Eisenhardt SU, Starke J, Thiele JR, Murphy A, Bjorn Stark G, Bassler N, et al. Pentameric CRP attenuates inflammatory effects of mmLDL by inhibiting mmLDL–monocyte interactions. *Atherosclerosis*. (2012) 224:384–93. doi: 10.1016/j.atherosclerosis.2012.07.039

15. Hanriot D, Bello G, Ropars A, Seguin-Devaux C, Poitevin G, Grosjean S, et al. C-reactive protein induces pro- and anti-inflammatory effects, including activation of the liver X receptor alpha, on human monocytes. *Thromb Haemost*. (2008) 99:558–69. doi: 10.1160/TH07-06-0410

16. Vigushin DM, Pepys MB, Hawkins PN. Metabolic and scintigraphic studies of radioiodinated human C-reactive protein in health and disease. *J Clin Invest*. (1993) 91:1351–7. doi: 10.1172/JCI116336

17. Thiele JR, Habersberger J, Braig D, Schmidt Y, Goerendt K, Maurer V, et al. Dissociation of pentameric to monomeric C-reactive protein localizes and aggravates inflammation: *in vivo* proof of a powerful proinflammatory mechanism and a new anti-inflammatory strategy. *Circulation*. (2014) 130:35–50. doi: 10.1161/CIRCULATIONAHA.113.007124

18. Zouki C, Haas B, Chan JS, Potempa LA, Filep JG. Loss of pentameric symmetry of C-reactive protein is associated with promotion of neutrophil-endothelial cell adhesion. *J Immunol*. (2001) 167:5355–61. doi: 10.4049/jimmunol.167.9.5355

19. Khreiss T, Jozsef L, Hossain S, Chan JS, Potempa LA, Filep JG. Loss of pentameric symmetry of C-reactive protein is associated with delayed apoptosis of human neutrophils. *J Biol Chem*. (2002) 277:40775–81. doi: 10.1074/jbc.M205378200

20. Khreiss T, Jozsef L, Potempa LA, Filep JG. Loss of pentameric symmetry in C-reactive protein induces interleukin-8 secretion through peroxynitrite signaling in human neutrophils. *Circ Res*. (2005) 97:690–7. doi: 10.1161/01.RES.0000183881.11739.CB

21. Khreiss T, Jozsef L, Potempa LA, Filep JG. Conformational rearrangement in C-reactive protein is required for proinflammatory actions on human endothelial cells. *Circulation*. (2004) 109:2016–22. doi: 10.1161/01.CIR.0000125527.41598.68

22. Wu Y, Ji SR, Wang HW, Sui SF. Study of the spontaneous dissociation of rabbit C-reactive protein. *Biochem (Mosc)*. (2002) 67:1377–82. doi: 10.1023/A:1021862027061

23. Taylor KE, van den Berg CW. Structural and functional comparison of native pentameric, denatured monomeric and biotinylated C-reactive protein. *Immunology*. (2007) 120:404–11. doi: 10.1111/j.1365-2567.2006.02516.x

24. Kresl JJ, Potempa LA, Anderson BE. Conversion of native oligomeric to a modified monomeric form of human C-reactive protein. *Int J Biochem Cell Biol*. (1998) 30:1415–26. doi: 10.1016/S1357-2725(98)00078-8

25. Potempa LA, Maldonado BA, Laurent P, Zemel ES, Gewurz H. Antigenic, electrophoretic and binding alterations of human C-reactive protein modified selectively in the absence of calcium. *Mol Immunol*. (1983) 20:1165–75. doi: 10.1016/0161-5890(83)90140-2

26. Habersberger J, Strang F, Scheichl A, Htun N, Bassler N, Merivirta RM, et al. Circulating microparticles generate and transport monomeric C-reactive protein in patients with myocardial infarction. *Cardiovasc Res*. (2012) 96:64–72. doi: 10.1093/cvr/cvs237

27. Crawford JR, Trial J, Nambi V, Hoogeveen RC, Taffet GE, Entman ML. Plasma levels of endothelial microparticles bearing monomeric C-reactive protein are increased in peripheral artery disease. *J Cardiovasc Transl Res*. (2016) 9:184–93. doi: 10.1007/s12265-016-9678-0

28. Ji SR, Ma L, Bai CJ, Shi JM, Li HY, Potempa LA, et al. Monomeric C-reactive protein activates endothelial cells via interaction with lipid raft microdomains. *FASEB J*. (2009) 23:1806–16. doi: 10.1096/fj.08-116962

29. Ji SR, Wu Y, Potempa LA, Qiu Q, Zhao J. Interactions of C-reactive protein with low-density lipoproteins: implications for an active role of modified C-reactive protein in atherosclerosis. *Int J Biochem Cell Biol*. (2006) 38:648–61. doi: 10.1016/j.biocel.2005.11.004

30. Melnikov I, Kozlov S, Saburova O, Zubkova E, Guseva O, Domogatsky S, et al. CRP is transported by monocytes and monocyte-derived exosomes in the blood of patients with coronary artery disease. *Biomedicines*. (2020) 8:435. doi: 10.3390/biomedicines8100435

31. Karlsson J, Wettero J, Potempa LA, Fernandez-Botran R, O'Neill Y, Wirestam L, et al. Extracellular vesicles opsonized by monomeric C-reactive protein (CRP) are accessible as autoantigens in patients with systemic lupus erythematosus and associate with autoantibodies against CRP. *J Autoimmun*. (2023) 139:103073. doi: 10.1016/j.jaut.2023.103073

32. Liang Y, Xu K, Liu W, Liu X, Yuan P, Xu P, et al. Monomeric C-reactive protein level is associated with osteoarthritis. *Exp Ther Med*. (2022) 23:277. doi: 10.3892/etm.2022.11206

33. Fujita C, Sakurai Y, Yasuda Y, Homma R, Huang CL, Fujita M. mCRP as a biomarker of adult-onset still's disease: quantification of mCRP by ELISA. *Front Immunol*. (2022) 13:938173. doi: 10.3389/fimmu.2022.938173

34. Fendl B, Weiss R, Eichhorn T, Linsberger I, Afonyushkin T, Puhm F, et al. Extracellular vesicles are associated with C-reactive protein in sepsis. *Sci Rep*. (2021) 11:6996. doi: 10.1038/s41598-021-86489-4

35. Zhang L, Li HY, Li W, Shen ZY, Wang YD, Ji SR, et al. An ELISA assay for quantifying monomeric C-reactive protein in plasma. *Front Immunol*. (2018) 9:511. doi: 10.3389/fimmu.2018.00511

36. Giralt L, Figueras-Roca M, Eguileor BL, Romero B, Zarranz-Ventura J, Alforja S, et al. C-reactive protein-complement factor H axis as a biomarker of activity in early and intermediate age-related macular degeneration. *Front Immunol*. (2024) 15:1330913. doi: 10.3389/fimmu.2024.1330913

37. Munuswamy R, De Brandt J, Burtin C, Derave W, Aumann J, Spruit MA, et al. Monomeric CRP is elevated in patients with COPD compared to non-COPD control persons. *J Inflammation Res*. (2021) 14:4503–7. doi: 10.2147/JIR.S320659

38. Braig D, Kaiser B, Thiele JR, Bannasch H, Peter K, Stark GB, et al. A conformational change of C-reactive protein in burn wounds unmasks its proinflammatory properties. *Int Immunol*. (2014) 26:467–78. doi: 10.1093/intimm/dxu056

39. Ji SR, Wu Y, Zhu L, Potempa LA, Sheng FL, Lu W, et al. Cell membranes and liposomes dissociate C-reactive protein (CRP) to form a new, biologically active structural intermediate: mCRP(m). *FASEB J*. (2007) 21:284–94. doi: 10.1096/fj.06-6722com

40. Hammond DJ Jr., Singh SK, Thompson JA, Beeler BW, Rusinol AE, Pangburn MK, et al. Identification of acidic pH-dependent ligands of pentameric C-reactive protein. *J Biol Chem*. (2010) 285:36235–44. doi: 10.1074/jbc.M110.142026

41. Braig D, Nero TL, Koch HG, Kaiser B, Wang X, Thiele JR, et al. Transitional changes in the CRP structure lead to the exposure of proinflammatory binding sites. *Nat Commun*. (2017) 8:14188. doi: 10.1038/ncomms14188

42. Lv JM, Wang MY. *In vitro* generation and bioactivity evaluation of C-reactive protein intermediate. *PloS One*. (2018) 13:e0198375. doi: 10.1371/journal.pone.0198375

43. Pena E, de la Torre R, Arderiu G, Slevin M, Badimon L. mCRP triggers angiogenesis by inducing F3 transcription and TF signalling in microvascular endothelial cells. *Thromb Haemost*. (2017) 117:357–70. doi: 10.1160/TH16-07-0524

44. Shrive AK, Cheetham GM, Holden D, Myles DA, Turnell WG, Volanakis JE, et al. Three dimensional structure of human C-reactive protein. *Nat Struct Biol*. (1996) 3:346–54. doi: 10.1038/nsb0496-346

45. Lv JM, Lu SQ, Liu ZP, Zhang J, Gao BX, Yao ZY, et al. Conformational folding and disulfide bonding drive distinct stages of protein structure formation. *Sci Rep*. (2018) 8:1494. doi: 10.1038/s41598-018-20014-y

46. Thompson D, Pepys MB, Wood SP. The physiological structure of human C-reactive protein and its complex with phosphocholine. *Structure*. (1999) 7:169–77. doi: 10.1016/S0969-2126(99)80023-9

47. Agrawal A, Xu Y, Ansardi D, Macon KJ, Volanakis JE. Probing the phosphocholine-binding site of human C-reactive protein by site-directed mutagenesis. *J Biol Chem*. (1992) 267:25353–8. doi: 10.1016/S0021-9258(19)74047-2

48. Lee RT, Takagahara I, Lee YC. Mapping the binding areas of human C-reactive protein for phosphorylcholine and polycationic compounds. Relationship between the two types of binding sites. *J Biol Chem*. (2002) 277:225–32. doi: 10.1074/jbc.M106039200

49. Khan SA, Ilies MA. The phospholipase A2 superfamily: structure, isozymes, catalysis, physiologic and pathologic roles. *Int J Mol Sci*. (2023) 24:1353. doi: 10.3390/ijms24021353

50. Endale HT, Tesfaye W, Mengstie TA. ROS induced lipid peroxidation and their role in ferroptosis. *Front Cell Dev Biol*. (2023) 11:1226044. doi: 10.3389/fcell.2023.1226044

51. Rajab IM, Majerczyk D, Olson ME, Addams JMB, Choe ML, Nelson MS, et al. C-reactive protein in gallbladder diseases: diagnostic and therapeutic insights. *Biophysics Rep*. (2020) 6:49–67. doi: 10.1007/s41048-020-00108-9

52. Cicchinelli S, Pignataro G, Gemma S, Piccioni A, Picozzi D, Ojetti V, et al. PAMPs and DAMPs in sepsis: A review of their molecular features and potential clinical implications. *Int J Mol Sci*. (2024) 25:962. doi: 10.3390/ijms25020962

53. Zhang Y, Jen FE, Fox KL, Edwards JL, Jennings MP. The biosynthesis and role of phosphorylcholine in pathogenic and nonpathogenic bacteria. *Trends Microbiol.* (2023) 31:692–706. doi: 10.1016/j.tim.2023.01.006

54. Abrams ST, Zhang N, Dart C, Wang SS, Thachil J, Guan Y, et al. Human CRP defends against the toxicity of circulating histones. *J Immunol.* (2013) 191:2495–502. doi: 10.4049/jimmunol.1203181

55. Suresh MV, Singh SK, Agrawal A. Interaction of calcium-bound C-reactive protein with fibronectin is controlled by pH: *in vivo* implications. *J Biol Chem*. (2004) 279:52552–7. doi: 10.1074/jbc.M409054200

56. Chang MK, Binder CJ, Torzewski M, Witztum JL. C-reactive protein binds to both oxidized LDL and apoptotic cells through recognition of a common ligand: Phosphorylcholine of oxidized phospholipids. *Proc Natl Acad Sci U S A*. (2002) 99:13043–8. doi: 10.1073/pnas.192399699

57. Schwalbe RA, Dahlback B, Coe JE, Nelsestuen GL. Pentraxin family of proteins interact specifically with phosphorylcholine and/or phosphorylethanolamine. *Biochemistry*. (1992) 31:4907–15. doi: 10.1021/bi00135a023

58. Salonen EM, Vartio T, Hedman K, Vaheri A. Binding of fibronectin by the acute phase reactant C-reactive protein. *J Biol Chem*. (1984) 259:1496–501. doi: 10.1016/S0021-9258(17)43435-1

59. Agrawal A, Shrive AK, Greenhough TJ, Volanakis JE. Topology and structure of the C1q-binding site on C-reactive protein. *J Immunol*. (2001) 166:3998–4004. doi: 10.4049/jimmunol.166.6.3998

60. Lu J, Mold C, Du Clos TW, Sun PD. Pentraxins and fc receptor-mediated immune responses. *Front Immunol.* (2018) 9:2607. doi: 10.3389/fimmu.2018.02607

61. Biro A, Rovo Z, Papp D, Cervenak L, Varga L, Fust G, et al. Studies on the interactions between C-reactive protein and complement proteins. *Immunology*. (2007) 121:40–50. doi: 10.1111/j.1365-2567.2007.02535.x

62. Liu N, Liu J, Ji Y, Lu P. Toll-like receptor 4 signaling mediates inflammatory activation induced by C-reactive protein in vascular smooth muscle cells. *Cell Physiol Biochem*. (2010) 25:467–76. doi: 10.1159/000303052

63. Liu N, Liu JT, Ji YY, Lu PP. C-reactive protein triggers inflammatory responses partly via TLR4/IRF3/NF-kappaB signaling pathway in rat vascular smooth muscle cells. *Life Sci*. (2010) 87:367–74. doi: 10.1016/j.lfs.2010.07.012

64. Boncler M, Rywaniak J, Szymanski J, Potempa LA, Rychlik B, Watala C. Modified C-reactive protein interacts with platelet glycoprotein Ibalpha. *Pharmacol Rep*. (2011) 63:464–75. doi: 10.1016/S1734-1140(11)70513-8

65. Molins B, Pena E, de la Torre R, Badimon L. Monomeric C-reactive protein is prothrombotic and dissociates from circulating pentameric C-reactive protein on adhered activated platelets under flow. *Cardiovasc Res*. (2011) 92:328–37. doi: 10.1093/cvr/cvr226

66. Jia ZK, Li HY, Liang YL, Potempa LA, Ji SR, Wu Y. Monomeric C-reactive protein binds and neutralizes receptor activator of NF-kappaB ligand-induced osteoclast differentiation. *Front Immunol*. (2018) 9:234. doi: 10.3389/fimmu.2018.00234

67. Zhang Z, Na H, Gan Q, Tao Q, Alekseyev Y, Hu J, et al. Monomeric C-reactive protein via endothelial CD31 for neurovascular inflammation in an ApoE genotype-dependent pattern: A risk factor for Alzheimer's disease? *Aging Cell.* (2021) 20:e13501. doi: 10.1111/acel.v20.11

68. Fujita M, Takada YK, Izumiya Y, Takada Y. The binding of monomeric C-reactive protein (mCRP) to Integrins alphavbeta3 and alpha4beta1 is related to its pro-inflammatory action. *PLoS One*. (2014) 9:e93738. doi: 10.1371/journal.pone.0093738

69. Fujita Y, Kakino A, Nishimichi N, Yamaguchi S, Sato Y, Machida S, et al. Oxidized LDL receptor LOX-1 binds to C-reactive protein and mediates its vascular effects. *Clin Chem*. (2009) 55:285–94. doi: 10.1373/clinchem.2008.119750

70. de la Torre R, Pena E, Vilahur G, Slevin M, Badimon L. Monomerization of C-reactive protein requires glycoprotein IIb-IIIa activation: pentraxins and platelet deposition. *J Thromb Haemost*. (2013) 11:2048–58. doi: 10.1111/jth.12415

71. Bang R, Marnell L, Mold C, Stein MP, Clos KT, Chivington-Buck C, et al. Analysis of binding sites in human C-reactive protein for FcgammaRI, FcgammaRIIA, and C1q by site-directed mutagenesis. *J Biol Chem*. (2005) 280:25095–102. doi: 10.1074/jbc.M504782200

72. Lane T, Wassef N, Poole S, Mistry Y, Lachmann HJ, Gillmore JD, et al. Infusion of pharmaceutical-grade natural human C-reactive protein is not proinflammatory in healthy adult human volunteers. *Circ Res*. (2014) 114:672–6. doi: 10.1161/CIRCRESAHA.114.302770

73. Sproston NR, El Mohtadi M, Slevin M, Gilmore W, Ashworth JJ. The effect of C-reactive protein isoforms on nitric oxide production by U937 monocytes/macrophages. *Front Immunol.* (2018) 9:1500. doi: 10.3389/fimmu.2018.01500

74. Jimenez RV, Kuznetsova V, Connelly AN, Hel Z, Szalai AJ. C-reactive protein promotes the expansion of myeloid derived cells with suppressor functions. *Front Immunol.* (2019) 10:2183. doi: 10.3389/fimmu.2019.02183

75. Jimenez RV, Wright TT, Jones NR, Wu J, Gibson AW, Szalai AJ. C-reactive protein impairs dendritic cell development, maturation, and function: implications for peripheral tolerance. *Front Immunol.* (2018) 9:372. doi: 10.3389/fimmu.2018.00372

76. Kikuchi K, Kohyama T, Yamauchi Y, Kato J, Takami K, Okazaki H, et al. C-reactive protein modulates human lung fibroblast migration. *Exp Lung Res*. (2009) 35:48–58. doi: 10.1080/01902140802404138

77. Singh SK, Suresh MV, Prayther DC, Moorman JP, Rusinol AE, Agrawal A. C-reactive protein-bound enzymatically modified low-density lipoprotein does not transform macrophages into foam cells. *J Immunol*. (2008) 180:4316–22. doi: 10.4049/jimmunol.180.6.4316

78. Khreiss T, Jozsef L, Potempa LA, Filep JG. Opposing effects of C-reactive protein isoforms on shear-induced neutrophil-platelet adhesion and neutrophil aggregation in whole blood. *Circulation*. (2004) 110:2713–20. doi: 10.1161/01.CIR.0000146846.00816.DD

79. Li SL, Feng JR, Zhou HH, Zhang CM, Lv GB, Tan YB, et al. Acidic pH promotes oxidation-induced dissociation of C-reactive protein. *Mol Immunol*. (2018) 104:47–53. doi: 10.1016/j.molimm.2018.09.021

80. Erra Diaz F, Dantas E, Geffner J. Unravelling the interplay between extracellular acidosis and immune cells. *Mediators Inflamm*. (2018) 2018:1218297. doi: 10.1155/2018/1218297

81. Wang MS, Messersmith RE, Reed SM. Membrane curvature recognition by C-reactive protein using lipoprotein mimics. *Soft Matter*. (2012) 8:7909–18. doi: 10.1039/c2sm25779c

82. Alnaas AA, Moon CL, Alton M, Reed SM, Knowles MK. Conformational changes in C-reactive protein affect binding to curved membranes in a lipid bilayer model of the apoptotic cell surface. *J Phys Chem B*. (2017) 121:2631–9. doi: 10.1021/acs.jpcb.6b11505

83. Hatzakis NS, Bhatia VK, Larsen J, Madsen KL, Bolinger PY, Kunding AH, et al. How curved membranes recruit amphipathic helices and protein anchoring motifs. *Nat Chem Biol*. (2009) 5:835–41. doi: 10.1038/nchembio.213

84. Noone DP, van der Velden TT, Sharp TH. Cryo-electron microscopy and biochemical analysis offer insights into the effects of acidic pH, such as occur during acidosis, on the complement binding properties of C-reactive protein. *Front Immunol.* (2021) 12:757633. doi: 10.3389/fimmu.2021.757633

85. Noone DP, Isendoorn MME, Hamers S, Keizer ME, Wulffele J, van der Velden TT, et al. Structural basis for surface activation of the classical complement cascade by the short pentraxin C-reactive protein. *Proc Natl Acad Sci U.S.A*. (2024) 121:e2404542121. doi: 10.1073/pnas.2404542121

86. Gershov D, Kim S, Brot N, Elkon KB. C-Reactive protein binds to apoptotic cells, protects the cells from assembly of the terminal complement components, and sustains an antiinflammatory innate immune response: implications for systemic autoimmunity. *J Exp Med*. (2000) 192:1353–64. doi: 10.1084/jem.192.9.1353

87. Haapasalo K, Meri S. Regulation of the complement system by pentraxins. *Front Immunol.* (2019) 10:1750. doi: 10.3389/fimmu.2019.01750

88. Strang F, Scheichl A, Chen YC, Wang X, Htun NM, Bassler N, et al. Amyloid plaques dissociate pentameric to monomeric C-reactive protein: a novel pathomechanism driving cortical inflammation in Alzheimer's disease? *Brain Pathol*. (2012) 22:337–46. doi: 10.1111/j.1750-3639.2011.00539.x

89. Eisenhardt SU, Habersberger J, Murphy A, Chen YC, Woollard KJ, Bassler N, et al. Dissociation of pentameric to monomeric C-reactive protein on activated platelets localizes inflammation to atherosclerotic plaques. *Circ Res*. (2009) 105:128–37. doi: 10.1161/CIRCRESAHA.108.190611

90. Boncler M, Kehrel B, Szewczyk R, Stec-Martyna E, Bednarek R, Brodde M, et al. Oxidation of C-reactive protein by hypochlorous acid leads to the formation of potent platelet activator. *Int J Biol Macromol*. (2018) 107:2701–14. doi: 10.1016/j.ijbiomac.2017.10.159

91. Zhang L, Shen ZY, Wang K, Li W, Shi JM, Osoro EK, et al. C-reactive protein exacerbates epithelial-mesenchymal transition through Wnt/beta-catenin and ERK signaling in streptozocin-induced diabetic nephropathy. *FASEB J*. (2019) 33:6551–63. doi: 10.1096/fj.201801865RR

92. Luan YY, Yao YM. The clinical significance and potential role of C-reactive protein in chronic inflammatory and neurodegenerative diseases. *Front Immunol.* (2018) 9:1302. doi: 10.3389/fimmu.2018.01302

93. Sproston NR, Ashworth JJ. Role of C-reactive protein at sites of inflammation and infection. *Front Immunol.* (2018) 9:754. doi: 10.3389/fimmu.2018.00754

94. McFadyen JD, Kiefer J, Braig D, Loseff-Silver J, Potempa LA, Eisenhardt SU, et al. Dissociation of C-reactive protein localizes and amplifies inflammation: evidence for a direct biological role of C-reactive protein and its conformational changes. *Front Immunol.* (2018) 9:1351. doi: 10.3389/fimmu.2018.01351

95. Yao Z, Zhang Y, Wu H. Regulation of C-reactive protein conformation in inflammation. *Inflammation Res*. (2019) 68:815–23. doi: 10.1007/s00011-019-01269-1

96. Potempa LA, Rajab IM, Olson ME, Hart PC. C-reactive protein and cancer: interpreting the differential bioactivities of its pentameric and monomeric, modified isoforms. *Front Immunol.* (2021) 12:744129. doi: 10.3389/fimmu.2021.744129

97. Rizo-Tellez SA, Sekheri M, Filep JG. C-reactive protein: a target for therapy to reduce inflammation. *Front Immunol*. (2023) 14:1237729. doi: 10.3389/fimmu.2023.1237729

98. Ji SR, Zhang SH, Chang Y, Li HY, Wang MY, Lv JM, et al. C-reactive protein: the most familiar stranger. *J Immunol*. (2023) 210:699–707. doi: 10.4049/jimmunol.2200831

99. Pastorello Y, Carare RO, Banescu C, Potempa L, Di Napoli M, Slevin M. Monomeric C-reactive protein: A novel biomarker predicting neurodegenerative disease and vascular dysfunction. *Brain Pathol*. (2023) 33:e13164. doi: 10.1111/bpa.13164

100. Li HY, Wang J, Meng F, Jia ZK, Su Y, Bai QF, et al. An intrinsically disordered motif mediates diverse actions of monomeric C-reactive protein. *J Biol Chem*. (2016) 291:8795–804. doi: 10.1074/jbc.M115.695023

101. Ullah N, Ma FR, Han J, Liu XL, Fu Y, Liu YT, et al. Monomeric C-reactive protein regulates fibronectin mediated monocyte adhesion. *Mol Immunol*. (2020) 117:122–30. doi: 10.1016/j.molimm.2019.10.013

102. Thiele JR, Zeller J, Kiefer J, Braig D, Kreuzaler S, Lenz Y, et al. A conformational change in C-reactive protein enhances leukocyte recruitment and reactive oxygen species generation in ischemia/reperfusion injury. *Front Immunol*. (2018) 9:675. doi: 10.3389/fimmu.2018.00675

103. Torzewski M, Rist C, Mortensen RF, Zwaka TP, Bienek M, Waltenberger J, et al. C-reactive protein in the arterial intima: role of C-reactive protein receptor-dependent monocyte recruitment in atherogenesis. *Arterioscler Thromb Vasc Biol*. (2000) 20:2094–9. doi: 10.1161/01.ATV.20.9.2094

104. Fujita C, Sakurai Y, Yasuda Y, Takada Y, Huang CL, Fujita M. Anti-monomeric C-reactive protein antibody ameliorates arthritis and nephritis in mice. *J Immunol*. (2021) 207:1755–62. doi: 10.4049/jimmunol.2100349

105. Chirco KR, Whitmore SS, Wang K, Potempa LA, Halder JA, Stone EM, et al. Monomeric C-reactive protein and inflammation in age-related macular degeneration. *J Pathol*. (2016) 240:173–83. doi: 10.1002/path.4766

106. Miyazawa K, Kiyono S, Inoue K. Modulation of stimulus-dependent human platelet activation by C-reactive protein modified with active oxygen species. *J Immunol*. (1988) 141:570–4. doi: 10.4049/jimmunol.141.2.570

107. Xu PC, Lin S, Yang XW, Gu DM, Yan TK, Wei L, et al. C-reactive protein enhances activation of coagulation system and inflammatory response through dissociating into monomeric form in antineutrophil cytoplasmic antibody-associated vasculitis. *BMC Immunol*. (2015) 16:10. doi: 10.1186/s12865-015-0077-0

108. Zeller J, Loseff-Silver J, Khoshmanesh K, Baratchi S, Lai A, Nero TL, et al. Shear-sensing by C-reactive protein: linking aortic stenosis and inflammation. *Circ Res*. (2024) 135:1033–47. doi: 10.1161/CIRCRESAHA.124.324248

109. Zeller J, Bogner B, Kiefer J, Braig D, Winninger O, Fricke M, et al. CRP enhances the innate killing mechanisms phagocytosis and ROS formation in a conformation and complement-dependent manner. *Front Immunol*. (2021) 12:721887. doi: 10.3389/fimmu.2021.721887

110. Wang MY, Ji SR, Bai CJ, El Kebir D, Li HY, Shi JM, et al. A redox switch in C-reactive protein modulates activation of endothelial cells. *FASEB J*. (2011) 25:3186–96. doi: 10.1096/fj.11-182741

111. Pastorello Y, Manu D, Sawkulycz X, Caprio V, Banescu C, Dobreanu M, et al. mCRP-induced focal adhesion kinase-dependent monocyte aggregation and M1 polarization, which was partially blocked by the C10M inhibitor. *Int J Mol Sci*. (2024) 25:3097. doi: 10.3390/ijms25063097

112. Slevin M, Iemma RS, Zeinolabediny Y, Liu D, Ferris GR, Caprio V, et al. Acetylcholine inhibits monomeric C-reactive protein induced inflammation, endothelial cell adhesion, and platelet aggregation; A potential therapeutic? *Front Immunol*. (2018) 9:2124. doi: 10.3389/fimmu.2018.02124

113. Chi M, Tridandapani S, Zhong W, Coggeshall KM, Mortensen RF. C-reactive protein induces signaling through Fc gamma RIIa on HL-60 granulocytes. *J Immunol*. (2002) 168:1413–8. doi: 10.4049/jimmunol.168.3.1413

114. Mihlan M, Blom AM, Kupreishvili K, Lauer N, Stelzner K, Bergstrom F, et al. Monomeric C-reactive protein modulates classic complement activation on necrotic cells. *FASEB J*. (2011) 25:4198–210. doi: 10.1096/fj.11-186460

115. Carlson CS, Aldred SF, Lee PK, Tracy RP, Schwartz SM, Rieder M, et al. Polymorphisms within the C-reactive protein (CRP) promoter region are associated with plasma CRP levels. *Am J Hum Genet*. (2005) 77:64–77. doi: 10.1086/431366

116. Kardys I, de Maat MP, Uitterlinden AG, Hofman A, Witteman JC. C-reactive protein gene haplotypes and risk of coronary heart disease: the Rotterdam Study. *Eur Heart J*. (2006) 27:1331–7. doi: 10.1093/eurheartj/ehl018

117. Aziz N, Fahey JL, Detels R, Butch AW. Analytical performance of a highly sensitive C-reactive protein-based immunoassay and the effects of laboratory variables on levels of protein in blood. *Clin Diagn Lab Immunol*. (2003) 10:652–7. doi: 10.1128/CDLI.10.4.652-657.2003

118. Zeller J, Bogner B, McFadyen JD, Kiefer J, Braig D, Pietersz G, et al. Transitional changes in the structure of C-reactive protein create highly pro-inflammatory molecules: Therapeutic implications for cardiovascular diseases. *Pharmacol Ther*. (2022) 235:108165. doi: 10.1016/j.pharmthera.2022.108165

119. Biro E, Nieuwland R, Tak PP, Pronk LM, Schaap MC, Sturk A, et al. Activated complement components and complement activator molecules on the surface of cell-derived microparticles in patients with rheumatoid arthritis and healthy individuals. *Ann Rheum Dis*. (2007) 66:1085–92. doi: 10.1136/ard.2006.061309

120. van der Zee PM, Biro E, Trouw LA, Ko Y, de Winter RJ, Hack CE, et al. C-reactive protein in myocardial infarction binds to circulating microparticles but is not associated with complement activation. *Clin Immunol*. (2010) 135:490–5. doi: 10.1016/j.clim.2010.01.002

121. van Eijk IC, Tushuizen ME, Sturk A, Dijkmans BA, Boers M, Voskuyl AE, et al. Circulating microparticles remain associated with complement activation despite intensive anti-inflammatory therapy in early rheumatoid arthritis. *Ann Rheum Dis*. (2010) 69:1378–82. doi: 10.1136/ard.2009.118372

122. Karlsson J, Wettero J, Weiner M, Ronnelid J, Fernandez-Botran R, Sjowall C. Associations of C-reactive protein isoforms with systemic lupus erythematosus phenotypes and disease activity. *Arthritis Res Ther*. (2022) 24:139. doi: 10.1186/s13075-022-02831-9

123. Wang J, Tang B, Liu X, Wu X, Wang H, Xu D, et al. Increased monomeric CRP levels in acute myocardial infarction: a possible new and specific biomarker for diagnosis and severity assessment of disease. *Atherosclerosis*. (2015) 239:343–9. doi: 10.1016/j.atherosclerosis.2015.01.024

124. Slevin M, Matou-Nasri S, Turu M, Luque A, Rovira N, Badimon L, et al. Modified C-reactive protein is expressed by stroke neovessels and is a potent activator of angiogenesis *in vitro*. *Brain Pathol*. (2010) 20:151–65. doi: 10.1111/j.1750-3639.2008.00256.x

125. Torzewski J, Torzewski M, Bowyer DE, Frohlich M, Koenig W, Waltenberger J, et al. C-reactive protein frequently colocalizes with the terminal complement complex in the intima of early atherosclerotic lesions of human coronary arteries. *Arterioscler Thromb Vasc Biol*. (1998) 18:1386–92. doi: 10.1161/01.ATV.18.9.1386

126. Al-Baradie RS, Pu S, Liu D, Zeinolabediny Y, Ferris G, Sanfeli C, et al. Monomeric C-reactive protein localized in the cerebral tissue of damaged vascular brain regions is associated with neuro-inflammation and neurodegeneration-an immunohistochemical study. *Front Immunol*. (2021) 12:644213. doi: 10.3389/fimmu.2021.644213

127. Ngwa DN, Pathak A, Agrawal A. IL-6 regulates induction of C-reactive protein gene expression by activating STAT3 isoforms. *Mol Immunol*. (2022) 146:50–6. doi: 10.1016/j.molimm.2022.04.003

128. Kramer F, Torzewski J, Kamenz J, Veit K, Hombach V, Dedio J, et al. Interleukin-1beta stimulates acute phase response and C-reactive protein synthesis by inducing an NFkappaB- and C/EBPbeta-dependent autocrine interleukin-6 loop. *Mol Immunol*. (2008) 45:2678–89. doi: 10.1016/j.molimm.2007.12.017

129. Macintyre S, Samols D, Dailey P. Two carboxylesterases bind C-reactive protein within the endoplasmic reticulum and regulate its secretion during the acute phase response. *J Biol Chem*. (1994) 269:24496–503. doi: 10.1016/S0021-9258(19)51111-5

130. Vanderschueren S, Deeren D, Knockaert DC, Bobbaers H, Bossuyt X, Peetermans W. Extremely elevated C-reactive protein. *Eur J Intern Med*. (2006) 17:430–3. doi: 10.1016/j.ejim.2006.02.025

131. Molins B, Figueras-Roca M, Valero O, Llorenc V, Romero-Vazquez S, Sibila O, et al. C-reactive protein isoforms as prognostic markers of COVID-19 severity. *Front Immunol*. (2022) 13:1105343. doi: 10.3389/fimmu.2022.1105343

132. Williams RD, Moran JA, Fryer AA, Littlejohn JR, Williams HM, Greenhough TJ, et al. Monomeric C-reactive protein in serum with markedly elevated CRP levels shares common calcium-dependent ligand binding properties with an *in vitro* dissociated form of C-reactive protein. *Front Immunol*. (2020) 11:115. doi: 10.3389/fimmu.2020.00115

133. Santonocito C, De Loecker I, Donadello K, Moussa MD, Markowicz S, Gullo A, et al. C-reactive protein kinetics after major surgery. *Anesth Analg*. (2014) 119:624–9. doi: 10.1213/ANE.0000000000000263

134. Motie M, Schaul KW, Potempa LA. Biodistribution and clearance of 125I-labeled C-reactive protein and 125I-labeled modified C-reactive protein in CD-1 mice. *Drug Metab Dispos*. (1998) 26:977–81.

135. LaPelusa A, Dave HD. *Physiology, Hemostasis*. Treasure Island (FL: StatPearls (2024).

136. Scridon A. Platelets and their role in hemostasis and thrombosis-from physiology to pathophysiology and therapeutic implications. *Int J Mol Sci*. (2022) 23:12772. doi: 10.3390/ijms232112772

137. Potempa LA, Zeller JM, Fiedel BA, Kinoshita CM, Gewurz H. Stimulation of human neutrophils, monocytes, and platelets by modified C-reactive protein (CRP) expressing a neoantigenic specificity. *Inflammation*. (1988) 12:391–405. doi: 10.1007/BF00915774

138. Molins B, Pena E, Vilahur G, Mendieta C, Slevin M, Badimon L. C-reactive protein isoforms differ in their effects on thrombus growth. *Arterioscler Thromb Vasc Biol*. (2008) 28:2239–46. doi: 10.1161/ATVBAHA.108.174359

139. Qiao J, Al-Tamimi M, Baker RI, Andrews RK, Gardiner EE. The platelet Fc receptor, FcgammaRIIa. *Immunol Rev*. (2015) 268:241–52. doi: 10.1111/imr.2015.268.issue-1

140. Clark SR, Ma AC, Tavener SA, McDonald B, Goodarzi Z, Kelly MM, et al. Platelet TLR4 activates neutrophil extracellular traps to ensnare bacteria in septic blood. *Nat Med*. (2007) 13:463–9. doi: 10.1038/nm1565

141. Pasceri V, Willerson JT, Yeh ET. Direct proinflammatory effect of C-reactive protein on human endothelial cells. *Circulation*. (2000) 102:2165–8. doi: 10.1161/01.CIR.102.18.2165

142. Blann AD, Lip GY. Effects of C-reactive protein on the release of von Willebrand factor, E-selectin, thrombomodulin and intercellular adhesion molecule-1 from human umbilical vein endothelial cells. *Blood Coagul Fibrinolysis*. (2003) 14:335–40. doi: 10.1097/00001721-200306000-00003

143. Venugopal SK, Devaraj S, Yuhanna I, Shaul P, Jialal I. Demonstration that C-reactive protein decreases eNOS expression and bioactivity in human aortic endothelial cells. *Circulation*. (2002) 106:1439–41. doi: 10.1161/01.CIR.0000033116.22237.F9

144. Singh U, Devaraj S, Vasquez-Vivar J, Jialal I. C-reactive protein decreases endothelial nitric oxide synthase activity via uncoupling. *J Mol Cell Cardiol*. (2007) 43:780–91. doi: 10.1016/j.yjmcc.2007.08.015

145. Cirillo P, Golino P, Calabro P, Cali G, Ragni M, De Rosa S, et al. C-reactive protein induces tissue factor expression and promotes smooth muscle and endothelial cell proliferation. *Cardiovasc Res*. (2005) 68:47–55. doi: 10.1016/j.cardiores.2005.05.010

146. Chen Y, Wang J, Yao Y, Yuan W, Kong M, Lin Y, et al. CRP regulates the expression and activity of tissue factor as well as tissue factor pathway inhibitor via NF-kappaB and ERK 1/2 MAPK pathway. *FEBS Lett*. (2009) 583:2811–8. doi: 10.1016/j.febslet.2009.07.037

147. Ji Y, Fish PM, Strawn TL, Lohman AW, Wu J, Szalai AJ, et al. C-reactive protein induces expression of tissue factor and plasminogen activator inhibitor-1 and promotes fibrin accumulation in vein grafts. *J Thromb Haemost*. (2014) 12:1667–77. doi: 10.1111/jth.12680

148. Li R, Ren M, Luo M, Chen N, Zhang Z, Luo B, et al. Monomeric C-reactive protein alters fibrin clot properties on endothelial cells. *Thromb Res*. (2012) 129:e251–6. doi: 10.1016/j.thromres.2012.03.014

149. Wu J, Stevenson MJ, Brown JM, Grunz EA, Strawn TL, Fay WP. C-reactive protein enhances tissue factor expression by vascular smooth muscle cells: mechanisms and *in vivo* significance. *Arterioscler Thromb Vasc Biol*. (2008) 28:698–704. doi: 10.1161/ATVBAHA.107.160903

150. Burn GL, Foti A, Marsman G, Patel DF, Zychlinsky A. The neutrophil. *Immunity*. (2021) 54:1377–91. doi: 10.1016/j.immuni.2021.06.006

151. von Bruhl ML, Stark K, Steinhart A, Chandraratne S, Konrad I, Lorenz M, et al. Monocytes, neutrophils, and platelets cooperate to initiate and propagate venous thrombosis in mice *in vivo*. *J Exp Med*. (2012) 209:819–35. doi: 10.1084/jem.20112322

152. Zeller J, Cheung Tung Shing KS, Nero TL, McFadyen JD, Krippner G, Bogner B, et al. A novel phosphocholine-mimetic inhibits a pro-inflammatory conformational change in C-reactive protein. *EMBO Mol Med*. (2023) 15:e16236. doi: 10.15252/emmm.202216236

153. Huber-Lang M, Lambris JD, Ward PA. Innate immune responses to trauma. *Nat Immunol*. (2018) 19:327–41. doi: 10.1038/s41590-018-0064-8

154. Wang Z, Qi F, Luo H, Xu G, Wang D. Inflammatory microenvironment of skin wounds. *Front Immunol*. (2022) 13:789274. doi: 10.3389/fimmu.2022.789274

155. Johnson BZ, Stevenson AW, Prele CM, Fear MW, Wood FM. The role of IL-6 in skin fibrosis and cutaneous wound healing. *Biomedicines*. (2020) 8:101. doi: 10.3390/biomedicines8050101

156. Li HY, Wang J, Wu YX, Zhang L, Liu ZP, Filep JG, et al. Topological localization of monomeric C-reactive protein determines proinflammatory endothelial cell responses. *J Biol Chem*. (2014) 289:14283–90. doi: 10.1074/jbc.M114.555318

157. Foley JH, Conway EM. Cross talk pathways between coagulation and inflammation. *Circ Res*. (2016) 118:1392–408. doi: 10.1161/CIRCRESAHA.116.306853

158. Wynn TA, Vannella KM. Macrophages in tissue repair, regeneration, and fibrosis. *Immunity*. (2016) 44:450–62. doi: 10.1016/j.immuni.2016.02.015

159. Wang Q, Zhu X, Xu Q, Ding X, Chen YE, Song Q. Effect of C-reactive protein on gene expression in vascular endothelial cells. *Am J Physiol Heart Circ Physiol*. (2005) 288:H1539–45. doi: 10.1152/ajpheart.00963.2004

160. Wang J. Neutrophils in tissue injury and repair. *Cell Tissue Res*. (2018) 371:531–9. doi: 10.1007/s00441-017-2785-7

161. Pitchford S, Pan D, Welch HC. Platelets in neutrophil recruitment to sites of inflammation. *Curr Opin Hematol*. (2017) 24:23–31. doi: 10.1097/MOH.0000000000000297

162. Karasu E, Halbgebauer R, Schutte L, Greven J, Blasius FM, Zeller J, et al. A conformational change of C-reactive protein drives neutrophil extracellular trap formation in inflammation. *BMC Biol*. (2025) 23:4. doi: 10.1186/s12915-024-02093-8

163. Wang Y, Jonsson F. Expression, role, and regulation of neutrophil fcgamma receptors. *Front Immunol*. (2019) 10:1958. doi: 10.3389/fimmu.2019.01958

164. Lu J, Marjon KD, Marnell LL, Wang R, Mold C, Du Clos TW, et al. Recognition and functional activation of the human IgA receptor (FcalphaRI) by C-reactive protein. *Proc Natl Acad Sci U S A*. (2011) 108:4974–9. doi: 10.1073/pnas.1018369108

165. Guilliams M, Bruhns P, Saeys Y, Hammad H, Lambrecht BN. The function of Fcgamma receptors in dendritic cells and macrophages. *Nat Rev Immunol*. (2014) 14:94–108. doi: 10.1038/nri3582

166. Wei J, Zhang Y, Li H, Wang F, Yao S. Toll-like receptor 4: A potential therapeutic target for multiple human diseases. *BioMed Pharmacother*. (2023) 166:115338. doi: 10.1016/j.biopha.2023.115338

167. Liu N, Liu J, Ji Y, Lu P, Wang C, Guo F. C-reactive protein induces TNF-alpha secretion by p38 MAPK-TLR4 signal pathway in rat vascular smooth muscle cells. *Inflammation*. (2011) 34:283–90. doi: 10.1007/s10753-010-9234-z

168. Newling M, Sritharan L, van der Ham AJ, Hoepel W, Fiechter RH, de Boer L, et al. C-reactive protein promotes inflammation through fcgammaR-induced glycolytic reprogramming of human macrophages. *J Immunol*. (2019) 203:225–35. doi: 10.4049/jimmunol.1900172

169. Zha Z, Cheng Y, Cao L, Qian Y, Liu X, Guo Y, et al. Monomeric CRP aggravates myocardial injury after myocardial infarction by polarizing the macrophage to pro-inflammatory phenotype through JNK signaling pathway. *J Inflammation Res*. (2021) 14:7053–64. doi: 10.2147/JIR.S316816

170. Trial J, Cieslik KA, Entman ML. Phosphocholine-containing ligands direct CRP induction of M2 macrophage polarization independent of T cell polarization: Implication for chronic inflammatory states. *Immun Inflammation Dis*. (2016) 4:274–88. doi: 10.1002/iid3.2016.4.issue-3

171. Schauer C, Janko C, Munoz LE, Zhao Y, Kienhofer D, Frey B, et al. Aggregated neutrophil extracellular traps limit inflammation by degrading cytokines and chemokines. *Nat Med*. (2014) 20:511–7. doi: 10.1038/nm.3547

172. Prame Kumar K, Nicholls AJ, Wong CHY. Partners in crime: neutrophils and monocytes/macrophages in inflammation and disease. *Cell Tissue Res*. (2018) 371:551–65. doi: 10.1007/s00441-017-2753-2

173. Xu Q, Zhao W, Yan M, Mei H. Neutrophil reverse migration. *J Inflammation (Lond)*. (2022) 19:22. doi: 10.1186/s12950-022-00320-z

174. Bratton DL, Henson PM. Neutrophil clearance: when the party is over, clean-up begins. *Trends Immunol*. (2011) 32:350–7. doi: 10.1016/j.it.2011.04.009

175. Elliott MR, Koster KM, Murphy PS. Efferocytosis signaling in the regulation of macrophage inflammatory responses. *J Immunol*. (2017) 198:1387–94. doi: 10.4049/jimmunol.1601520

176. Rodriguez W, Mold C, Kataranovski M, Hutt JA, Marnell LL, Verbeek JS, et al. C-reactive protein-mediated suppression of nephrotoxic nephritis: role of macrophages, complement, and Fcgamma receptors. *J Immunol*. (2007) 178:530–8. doi: 10.4049/jimmunol.178.1.530

177. Zouki C, Beauchamp M, Baron C, Filep JG. Prevention of *in vitro* neutrophil adhesion to endothelial cells through shedding of L-selectin by C-reactive protein and peptides derived from C-reactive protein. *J Clin Invest*. (1997) 100:522–9. doi: 10.1172/JCI119561

178. Heuertz RM, Schneider GP, Potempa LA, Webster RO. Native and modified C-reactive protein bind different receptors on human neutrophils. *Int J Biochem Cell Biol*. (2005) 37:320–35. doi: 10.1016/j.biocel.2004.07.002

179. Ying SC, Shephard E, de Beer FC, Siegel JN, Harris D, Gewurz BE, et al. Localization of sequence-determined neoepitopes and neutrophil digestion fragments of C-reactive protein utilizing monoclonal antibodies and synthetic peptides. *Mol Immunol*. (1992) 29:677–87. doi: 10.1016/0161-5890(92)90205-C

180. El Kebir D, Zhang Y, Potempa LA, Wu Y, Fournier A, Filep JG. C-reactive protein-derived peptide 201-206 inhibits neutrophil adhesion to endothelial cells and platelets through CD32. *J Leukoc Biol*. (2011) 90:1167–75. doi: 10.1189/jlb.0111032

181. Everts PA, Lana JF, Onishi K, Buford D, Peng J, Mahmood A, et al. Angiogenesis and tissue repair depend on platelet dosing and bioformulation strategies following orthobiological platelet-rich plasma procedures: A narrative review. *Biomedicines*. (2023) 11:1922. doi: 10.3390/biomedicines11071922

182. Slevin M, Matou S, Zeinolabediny Y, Corpas R, Weston R, Liu D, et al. Monomeric C-reactive protein–a key molecule driving development of Alzheimer's disease associated with brain ischaemia? *Sci Rep*. (2015) 5:13281. doi: 10.1038/srep13281

183. Turu MM, Slevin M, Matou S, West D, Rodriguez C, Luque A, et al. C-reactive protein exerts angiogenic effects on vascular endothelial cells and modulates associated signalling pathways and gene expression. *BMC Cell Biol*. (2008) 9:47. doi: 10.1186/1471-2121-9-47

184. Guo M, Niu Y, Xie M, Liu X, Li X. Notch signaling, hypoxia, and cancer. *Front Oncol*. (2023) 13:1078768. doi: 10.3389/fonc.2023.1078768

185. Wang X, Bove AM, Simone G, Ma B. Molecular bases of VEGFR-2-mediated physiological function and pathological role. *Front Cell Dev Biol*. (2020) 8:599281. doi: 10.3389/fcell.2020.599281

186. Chen J, Gu Z, Wu M, Yang Y, Zhang J, Ou J, et al. C-reactive protein can upregulate VEGF expression to promote ADSC-induced angiogenesis by activating HIF-1alpha via CD64/PI3k/Akt and MAPK/ERK signaling pathways. *Stem Cell Res Ther*. (2016) 7:114. doi: 10.1186/s13287-016-0377-1

187. Boras E, Slevin M, Alexander MY, Aljohi A, Gilmore W, Ashworth J, et al. Monomeric C-reactive protein and Notch-3 co-operatively increase angiogenesis through PI3K signalling pathway. *Cytokine*. (2014) 69:165–79. doi: 10.1016/j.cyto.2014.05.027

188. Bello G, Cailotto F, Hanriot D, Kolopp-Sarda MN, Latger-Cannard V, Hess K, et al. C-reactive protein (CRP) increases VEGF-A expression in monocytic cells via a PI3-kinase and ERK 1/2 signaling dependent pathway. *Atherosclerosis*. (2008) 200:286–93. doi: 10.1016/j.atherosclerosis.2007.12.046

189. Cherny SS, Brzezinski RY, Wasserman A, Adler A, Berliner S, Nevo D, et al. Characterizing CRP dynamics during acute infections. *Infection*. (2024). doi: 10.1007/s15010-024-02422-7

190. Hage FG, Szalai AJ. C-reactive protein gene polymorphisms, C-reactive protein blood levels, and cardiovascular disease risk. *J Am Coll Cardiol*. (2007) 50:1115–22. doi: 10.1016/j.jacc.2007.06.012

191. Levinson T, Wasserman A. C-reactive protein velocity (CRPv) as a new biomarker for the early detection of acute infection/inflammation. *Int J Mol Sci*. (2022) 23:8100. doi: 10.3390/ijms23158100

192. Badimon L, Pena E, Arderiu G, Padro T, Slevin M, Vilahur G, et al. C-reactive protein in atherothrombosis and angiogenesis. *Front Immunol*. (2018) 9:430. doi: 10.3389/fimmu.2018.00430

193. Zhang Z, Lin W, Gan Q, Lei M, Gong B, Zhang C, et al. The influences of ApoE isoforms on endothelial adherens junctions and actin cytoskeleton responding to mCRP. *Angiogenesis*. (2024) 27:861–81. doi: 10.1007/s10456-024-09946-4

194. Verma S, Wang CH, Li SH, Dumont AS, Fedak PW, Badiwala MV, et al. A self-fulfilling prophecy: C-reactive protein attenuates nitric oxide production and inhibits angiogenesis. *Circulation*. (2002) 106:913–9. doi: 10.1161/01.CIR.0000029802.88087.5E

195. Hattori Y, Matsumura M, Kasai K. Vascular smooth muscle cell activation by C-reactive protein. *Cardiovasc Res*. (2003) 58:186–95. doi: 10.1016/S0008-6363(02)00855-6

196. Cimmino G, Ragni M, Cirillo P, Petrillo G, Loffredo F, Chiariello M, et al. C-reactive protein induces expression of matrix metalloproteinase-9: a possible link between inflammation and plaque rupture. *Int J Cardiol*. (2013) 168:981–6. doi: 10.1016/j.ijcard.2012.10.040

197. Doronzo G, Russo I, Mattiello L, Trovati M, Anfossi G. C-reactive protein increases matrix metalloproteinase-2 expression and activity in cultured human vascular smooth muscle cells. *J Lab Clin Med*. (2005) 146:287–98. doi: 10.1016/j.lab.2005.07.010

198. Ho KJ, Owens CD, Longo T, Sui XX, Ifantides C, Conte MS. C-reactive protein and vein graft disease: evidence for a direct effect on smooth muscle cell phenotype via modulation of PDGF receptor-beta. *Am J Physiol Heart Circ Physiol*. (2008) 295:H1132–H40. doi: 10.1152/ajpheart.00079.2008

199. He W, Ren Y, Wang X, Chen Q, Ding S. C reactive protein and enzymatically modified LDL cooperatively promote dendritic cell-mediated T cell activation. *Cardiovasc Pathol*. (2017) 29:1–6. doi: 10.1016/j.carpath.2017.03.009

200. Van Vre EA, Bult H, Hoymans VY, Van Tendeloo VF, Vrints CJ, Bosmans JM. Human C-reactive protein activates monocyte-derived dendritic cells and induces dendritic cell-mediated T-cell activation. *Arterioscler Thromb Vasc Biol*. (2008) 28:511–8. doi: 10.1161/ATVBAHA.107.157016

201. Yoshida T, Ichikawa J, Giuroiu I, Laino AS, Hao Y, Krogsgaard M, et al. C reactive protein impairs adaptive immunity in immune cells of patients with melanoma. *J Immunother Cancer*. (2020) 8:e000234. doi: 10.1136/jitc-2019-000234

202. Tobiasova-Czetoova Z, Palmborg A, Lundqvist A, Karlsson G, Adamson L, Bartunkova J, et al. Effects of human plasma proteins on maturation of monocyte-derived dendritic cells. *Immunol Lett*. (2005) 100:113–9. doi: 10.1016/j.imlet.2005.03.009

203. Mold C, Clos TW. C-reactive protein inhibits plasmacytoid dendritic cell interferon responses to autoantibody immune complexes. *Arthritis Rheumatol*. (2013) 65:1891–901. doi: 10.1002/art.37968

204. Nazarov PG, Pronina AP. The influence of cholinergic agents on histamine release from HMC-1 human mast cell line stimulated with IgG, C-reactive protein and compound 48/80. *Life Sci*. (2012) 91:1053–7. doi: 10.1016/j.lfs.2012.08.004

205. Ruiz-Fernandez C, Ait Eldjoudi D, Gonzalez-Rodriguez M, Cordero Barreal A, Farrag Y, Garcia-Caballero L, et al. Monomeric CRP regulates inflammatory responses in human intervertebral disc cells. *Bone Joint Res*. (2023) 12:189–98. doi: 10.1302/2046-3758.123.BJR-2022-0223.R1

206. Ruiz-Fernandez C, Gonzalez-Rodriguez M, Francisco V, Rajab IM, Gomez R, Conde J, et al. Monomeric C reactive protein (mCRP) regulates inflammatory responses in human and mouse chondrocytes. *Lab Invest*. (2021) 101:1550–60. doi: 10.1038/s41374-021-00584-8

frontiers | Frontiers in Pediatrics

TYPE Systematic Review
PUBLISHED 09 May 2025
DOI 10.3389/fped.2025.1555671

OPEN ACCESS

EDITED BY
Yi Wu,
Xi'an Jiaotong University, China

REVIEWED BY
Yue Chang,
Lanzhou University, China
Bin Cheng,
Lanzhou University of Technology, China

*CORRESPONDENCE
Jun Luo
✉ luojun-78@163.com

RECEIVED 05 January 2025
ACCEPTED 25 April 2025
PUBLISHED 09 May 2025

CITATION
Xu F, Luo J and Li W (2025) Comparison of the diagnostic accuracy of resistin and CRP levels for sepsis in neonates and children: a systematic review and meta-analysis.
Front. Pediatr. 13:1555671.
doi: 10.3389/fped.2025.1555671

Comparison of the diagnostic accuracy of resistin and CRP levels for sepsis in neonates and children: a systematic review and meta-analysis

Fen Xu[1], Jun Luo[1*] and Wenbin Li[2]

[1]Department of Neonatology, Shenzhen Baoan Women's and Children's Hospital, Guangdong, China, [2]Department of Pediatrics, Tongji Hospital, Tongji Medical College, Huazhong University of Science and Technology, Wuhan, China

Background: Resistin (RETN) levels are potential diagnostic markers for sepsis in neonates and children. However, studies have yielded inconsistent results. This study aimed to compare the diagnostic accuracy of RETN levels with that of C-reactive protein (CRP) levels in the diagnosis of paediatric and neonatal sepsis through a comprehensive review of recent literature.
Methods: A standard methodology for systematic reviews and meta-analyses was followed. The PubMed, Embase and Cochrane databases were searched from January 1996 to October 2024 (PROSPERO CRD42024621872). Eligible studies were selected and analysed using Review Manager 5.4 and STATA 17. Meta-DiSc version 1.4 was used to describe and calculate the sensitivity, specificity, summary receiver operating characteristic (SROC) curves and areas under the curves (AUCs). SROC curve analysis was used to summarize the overall performance.
Results: A total of 437 neonates and children were included in six identified studies, all of which demonstrated reasonable methodological quality. The pooled sensitivity for the RETN level was 0.88 [95% confidence interval (CI), 0.83–0.92], which surpassed that of the CRP level at 0.85 (95% CI, 0.79–0.90). However, the pooled specificity for the RETN level was 0.78 (95% CI, 0.71–0.83), which was lower than that of the CRP level at 0.84 (95% CI, 0.77–0.90). Furthermore, the SROC curves for RETN and CRP in predicting sepsis in neonates and children indicated high predictive abilities, with AUC values of 0.925 and 0.945, respectively.
Conclusions: The current evidence suggests that the RETN level is a valuable biomarker for detecting paediatric and neonatal sepsis.

Systematic Review Registration: https://www.crd.york.ac.uk/PROSPERO/, identifier [CRD42024621872].

KEYWORDS

resistin, CRP, paediatric sepsis, neonatal sepsis, meta-analysis

1 Introduction

Despite recent advancements in neonatal intensive care units (NICUs) and paediatric intensive care units (PICUs), sepsis continues to be a significant contributor to morbidity and mortality, particularly in preterm infants (1, 2). More than half of fatalities in children under five years of age are attributed to infectious diseases, such as pneumonia and

diarrhoea, which can precipitate sepsis (3). The prevalence of sepsis-related morbidity and mortality in children ranges from 6.2% to 23.1% and from 9% to 20.0%, respectively (4). Clinicians are actively seeking clinical indicators or biomarkers to facilitate early diagnosis and treatment of paediatric and neonatal sepsis. However, early diagnosis remains challenging because of the nonspecific clinical signs and symptoms of sepsis in neonates and children. Therefore, timely and precise diagnosis of sepsis is crucial for implementing appropriate antibiotic therapy to mitigate the risk of adverse outcomes.

Resistin (RETN) was first identified and named for its involvement in insulin resistance in 2001 (5). In humans, RETN appears to be predominantly secreted by macrophages rather than adipocytes (6, 7). The proinflammatory adipokine RETN has subsequently been found to be elevated during sepsis in an intensive care unit (ICU) (8). RETN enhances inflammatory responses by activating nuclear factor kappa-B (NF-κB) signaling through toll-like receptor 4 (TLR4), triggering interleukin-6 (IL-6) and tumor necrosis factor-alpha (TNF-α) production (9). C-reactive protein (CRP), a classic acute-phase protein, increases from ∼1 μg/ml to potentially 1,000-fold higher levels during inflammation. This rapid response begins within 6–8 h, peaks at 24–48 h, and makes CRP valuable for clinical monitoring (10–12). Khttab et al. reported that RETN was a valuable biomarker for diagnosing neonatal sepsis, and its levels were correlated with indicators of disease severity. At a cut-off level of 22.8 ng/ml, RETN demonstrated a sensitivity of 98.3% and a specificity of 99.97% (13). However, Aliefendioglu et al. reported moderate diagnostic performance for RETN, with a sensitivity of approximately 73.7% and a specificity of approximately 45.8%, yielding positive and negative predictive values of 68.3% and 52.4%, respectively. The findings also indicated that the diagnostic utility of RETN was limited compared with that of other inflammatory markers, including CRP, procalcitonin, and interleukin-6 (IL-6) (14, 15). In view of this controversy, a more thorough review encompassing the latest literature is warranted to compare the diagnostic accuracy of RETN levels with that of CRP levels in diagnosing paediatric and neonatal sepsis.

Consequently, we conducted a systematic review and meta-analysis to examine the correlation between elevated RETN levels and the risk of sepsis in neonates and children. Our primary objective was to systematically and quantitatively assess all published studies regarding the diagnostic application of RETN and CRP levels for sepsis in these populations.

2 Methods

2.1 Retrieval and selection of studies

The common approach to a computer-aided literature search was used to search PubMed, EMBASE (http://www.embase.com/) and the Cochrane Library (http://www.the-cochranelibrary.com/view/0/index.html) for relevant citations from January 1996 to October 2024. The search strings are included in the Supplementary Material. We also examined the references of known articles. A prospective registration was made in PROSPERO (ID CRD42024621872; available at https://www.crd.york.ac.uk/PROSPERO/).

The following criteria were used to select studies for inclusion in our meta-analysis: (1) observational or interventional studies; (2) studies measuring RETN and/or CRP levels; (3) neonatal and paediatric patients with sepsis were classified as the experimental group, while participants suspected of having sepsis but not confirmed were classified into the control group; (4) sufficient data to calculate the outcome metrics (true positive [TP], false positive [FP], true negative [TN], and false negative [FN]); (5) blood measurements of RETN must have been conducted at the time of clinical presentation with suspected sepsis, prior to the initiation of antimicrobial therapy, or in asymptomatic neonates or children at the time of the inclusion in the study; and (6) sepsis must have been defined as the outcome. Neonatal sepsis was defined as a positive microbial blood culture in the studies reviewed. Paediatric sepsis was defined on the basis of the criteria established by the American College of Chest Physicians/Society of Critical Care Medicine. The exclusion criteria included the following: (1) abstracts, reviews, and animal studies; (2) diagnostic methods for sepsis did not involve the measurement of RETN levels; (3) inadequate data to derive outcome metrics (TP, FP, TN, and FN); (4) bioinformatics analyses and duplicate publications; and (5) studies published in a language other than English. Article selection was conducted independently by two investigators to ensure a high level of accuracy.

2.2 Data extraction

This investigation identified 258 original articles through searches in the three medical databases, from which 205 duplicate articles and bioinformatic analyses were excluded. Following title and abstract screening, 25 irrelevant articles were excluded. After eliminating non-English language publications, animal studies, and those lacking a direct link to RETN levels and sepsis, six studies ultimately met our inclusion criteria (13, 14, 16–19). Figure 1 illustrates the selection process. The detailed characteristics and data for each included study are presented in Table 1.

Two reviewers independently extracted relevant information from all the articles concerning the key study design and characteristics of the study population, including the study name, year, design, region, assay method, testing time, cut-off values, sepsis onset, patient characteristics and numbers, and outcome data (TP, FP, FN, and TN). Any disagreements were resolved through a consensus or, if necessary, by consulting a third reviewer.

2.3 Quality assessment

The quality of the studies was evaluated independently by two reviewers using the QUADAS-2 tool, following the recommended methodologies outlined in the Cochrane Handbook for Diagnostic Test Accuracy Reviews, with each item rated as a low

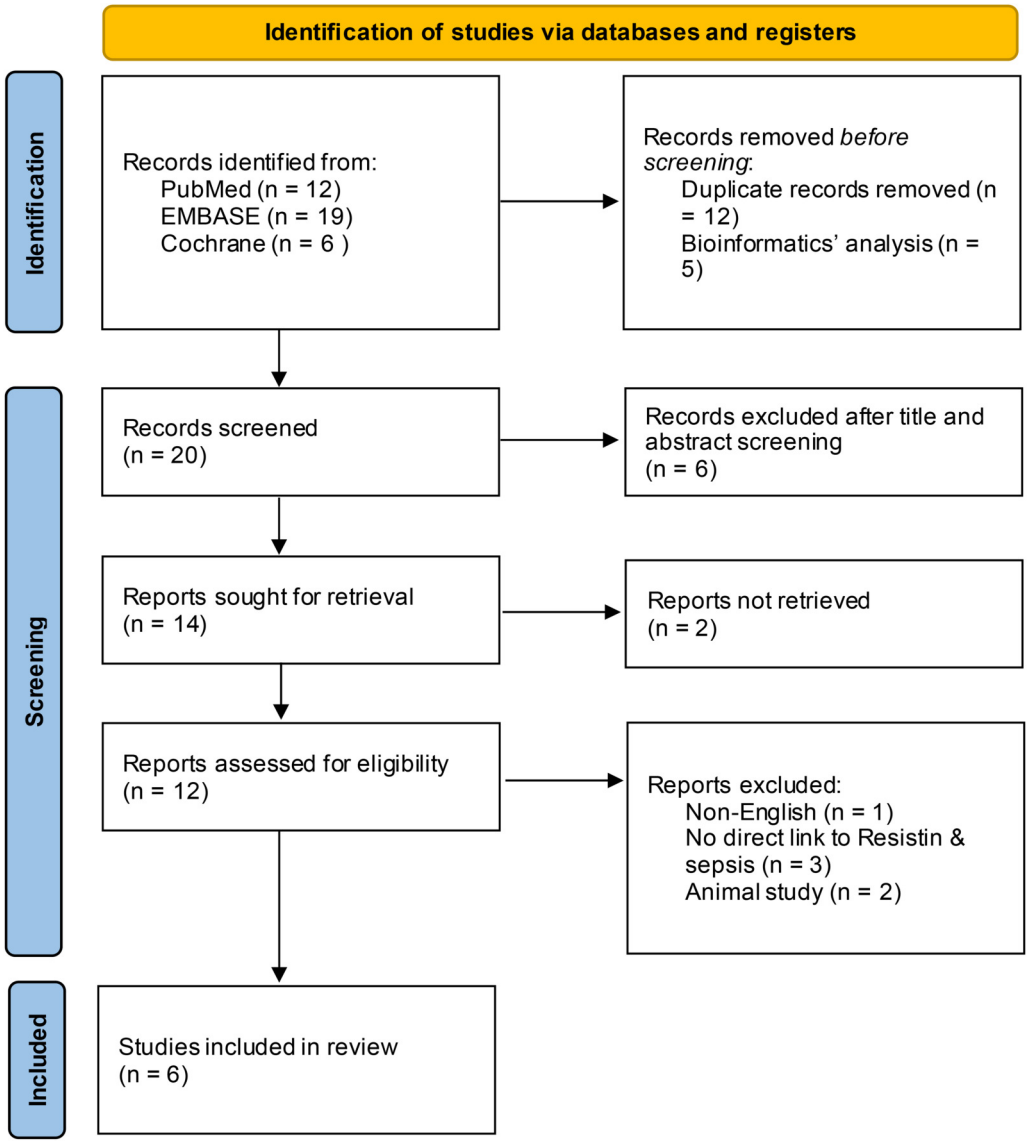

FIGURE 1
Flowchart of the article screening and selection process. After screening, 25 irrelevant articles were excluded, and six studies met the inclusion criteria after non-English language, animal and unrelated studies were removed.

risk of bias, a high risk of bias, or an unclear bias (20). The results of the bias risk assessment conducted using the QUADAS-2 tool are illustrated in Figure 2. High-risk assessments are indicated by red circles, low-risk assessments are indicated by green circles, and unclear risk assessments are indicated by yellow circles. Uncertainties and unclear risks denote insufficient clarity and a lack of definitive judgement associated with the limited details of the studies.

In terms of patient selection, two studies were classified as having an unclear risk of bias regarding the consecutive or random sampling of the enrolled patients (14, 18). For the reference standard, the articles by Aliefendioglu et al. and Saboktakin et al. were assessed as having high and unclear risks of bias, respectively (14, 16). Regarding flow and timing, one study was deemed to have an unclear risk of bias, whereas three studies were classified as having a high risk of bias (13, 14, 17, 18).

2.4 Statistical analysis

The quality assessment results of the included studies were generated using the RevMan 5.4 software. Statistical analyses were conducted with the Meta-DiSc 1.4 and STATA 17.0 software. The overall diagnostic performances of RETN and CRP levels in diagnosing neonatal and paediatric sepsis were evaluated using the summary receiver operating characteristic (SROC) curves. Heterogeneity among the included studies was assessed using the Cochran Q statistic and quantified with the I^2 statistic,

10.3389/fped.2025.1555671

TABLE 1 Characteristics of the 6 studies included in this meta-analysis.

Reference	Region	Study design	Outcome	Sample size (Cases/Controls)	Age	Biomarker	Cut-off *	Measurement	Sensitivity (%)	Specificity (%)	AUC
Saboktakin et al., 2019 (16)	Iran	Prospective	Paediatric sepsis	36 (24/12)	Under 12 years of age	Resistin	5.2	ELISA	82.4	72	0.864
Khattab et al., 2018 (13)	Egypt	Prospective	Culture-proven LOS	90 (60/30)	Neonate (term or late preterm)	Resistin	21.5	ELISA	100	96.7	0.999
						CRP	5	immunoturbidometry	100	100	1
Cekmez et al., 2011 (18)	Turkey	Prospective	Culture-proven LOS	105 (62/43)	am	Resistin	8	ELISA	93	95	0.912
						CRP	0.82	immunoturbidometry	82	79	0.845
Aliefendioglu et al., 2014 (14)	Turkey	Prospective	Culture-proven EOS	86 (43/43)	Neonate (preterm infants)	Resistin	50	ELISA	73.7	45.8	0.74
Gokmen et al., 2013 (17)	Turkey	Prospective	Culture-proven EOS and LOS	58 (20/38)	Neonate (<32 weeks preterm infants)	Resistin	28.1	ELISA	90	90.1	0.94
						CRP	1	immunoturbidometry	50	97.7	0.827
Ozdemir and Elgormus, 2017 (19)	Turkey	Prospective	Culture-proven EOS	62 (29/33)	Neonate (term or near term)	Resistin	36.8	ELISA	76	67	0.72
						CRP	4.15	immunoturbidometry	83	61	0.84

*Resistin, ng/ml; CRP, mg/dl.
EOS, early-onset sepsis; LOS, late-onset sepsis.

which ranges from 0% to 100% (21). A P value of the Q test < 0.05 and an I^2 index ≥50% indicated moderate heterogeneity, necessitating a discussion of its sources. Deek's funnel plot asymmetry test was used to assess publication bias in the included literature (22). If the result of the Deek's symmetry test yielded $P < 0.05$, the presence of publication bias was suggested.

3 Results

3.1 Diagnostic accuracy

Among the six articles that met our inclusion criteria, we examined the correlation between RETN levels and neonatal and paediatric sepsis. The meta-analysis results revealed that RETN testing had a greater sensitivity than specificity, whereas CRP testing had a greater specificity than sensitivity for diagnosing sepsis in neonates and children. The pooled sensitivity and specificity estimates for RETN levels were 0.88 (95% CI, 0.83–0.92) and 0.78 (95% CI, 0.71–0.83), respectively (Figure 3A). The positive likelihood ratio (LR+) of 5.13 (95% CI, 1.82–14.47) for the RETN test was sufficiently elevated to be used as a rule-in test, whereas the high negative likelihood ratio (LR−) of 0.17 (95% CI, 0.06–0.43) was inadequate to lower the pretest probability to a level that would allow for the safe exclusion of sepsis (Figure 3A). We constructed SROC curves for both RETN and CRP. The area under the curve (AUC) for RETN was 0.925 ± 0.074 (Figure 4A).

CRP had an AUC of 0.945 ± 0.067 (Figure 4B). The pooled sensitivity and specificity estimates for CRP were 0.85 (95% CI, 0.79–0.90) and 0.84 (95% CI, 0.77–0.90), respectively (Figure 3B). The LR+ of 6.00 (95% CI, 1.78–20.21) for the CRP test was sufficiently high to serve as a rule-in test, whereas the elevated LR− at 0.23 (95% CI, 0.09–0.61) could not diminish the pretest probability to a level that would allow for the safe exclusion of sepsis.

The diagnostic odds ratio (OR) for RETN was 36.20 (95% CI, 6.16–212.68), whereas that for CRP was 33.34 (95% CI, 6.16–180.43), as illustrated in Figure 3.

3.2 Heterogeneity assessment

The heterogeneity observed in sensitivity ($I^2 = 81.6\%$), specificity ($I^2 = 88.8\%$), positive LR ($I^2 = 91.3\%$), negative LR ($I^2 = 82.5\%$), and diagnostic odds ratio ($I^2 = 87.8\%$) was substantial according to forest plot results (see Supplementary Figures). There was notable variability in the ages of the patients (from newborns to children) and a broad range of cut-off values (5.2–50.0 ng/ml). A subgroup analysis was conducted on the basis of the timing of sepsis [early-onset sepsis [EOS] vs. late-onset sepsis [LOS]], population (term or near-term infants vs. others), geographical location (Turkey), and sample size (≤80 vs. >80) to explore the heterogeneity in diagnostic accuracy (I^2 sensitivity) (Table 2).

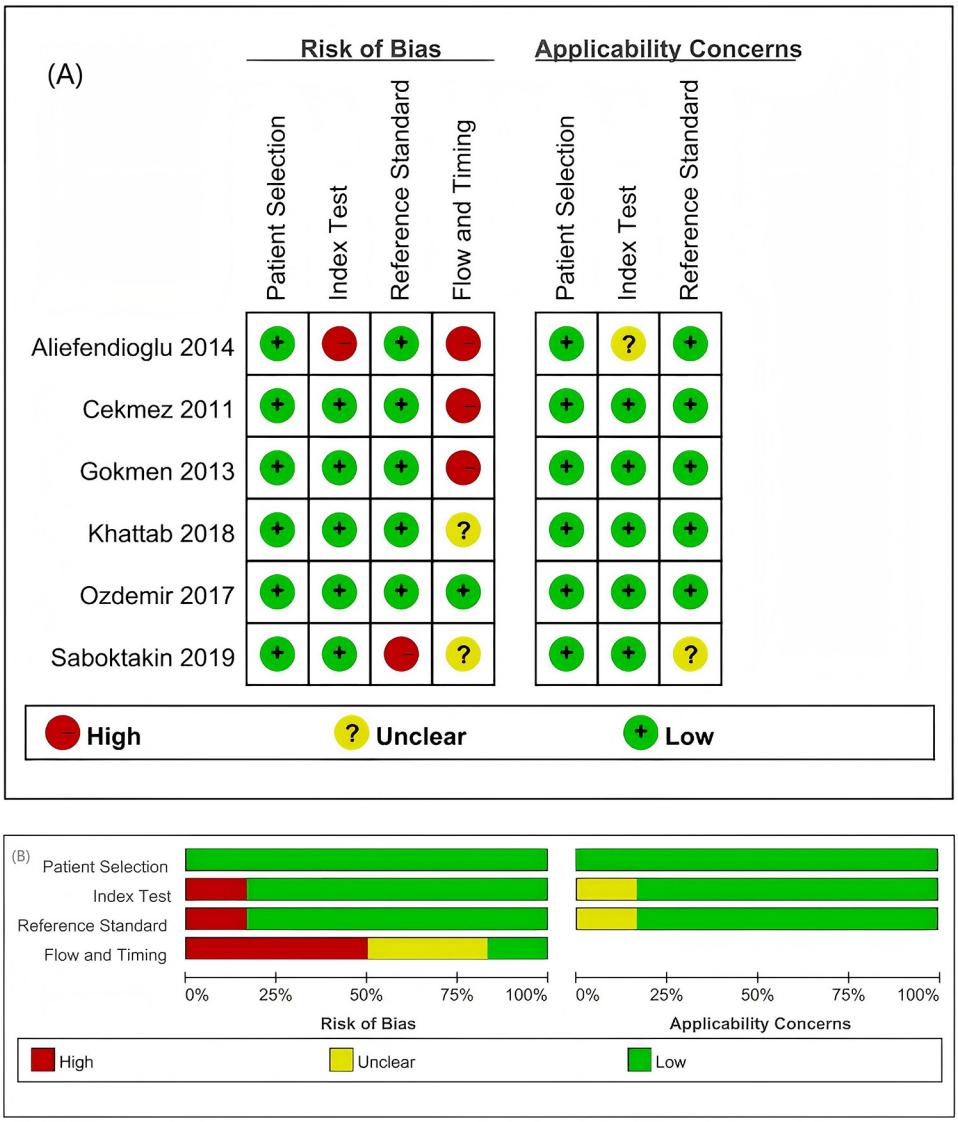

FIGURE 2
Summary of the risk of bias and applicability concerns based on the judgement of the review authors regarding each domain for each included study. **(A)** Risk of bias in the included studies. **(B)** Evaluation of the risk of bias in the included studies on patients with sepsis. Two studies exhibited an unclear risk (marked yellow) in the patient selection domain; one study demonstrated a high risk (red) in the reference standards, with another showing an unclear risk, whereas flow and timing assessments identified three studies with a high risk and one with an unclear risk.

The pooled sensitivity was greater in studies with 80 or more participants than in those with fewer than 80 participants, at 91% (95% CI, 85–95) vs. 82% (95% CI, 71–90), respectively. However, the specificity remained consistent at 78% (95% CI, 69–85) for both groups, with diagnostic odds ratios of 101.44 (95% CI, 1.38–7,432) and 17 (95% CI, 4.02–71.80), respectively. The pooled sensitivity was also greater in studies involving a population of term or near-term infants than in those involving other populations, at 93% (95% CI, 87–96) vs. 80% (95% CI, 71–88), whereas the specificity was significantly greater at 87% (95% CI, 79–93) vs. 68% (95% CI, 57–77), with diagnostic odds ratios of 131.8 (95% CI, 3.97–4,374) and 12.78 (95% CI, 1.61–101.59), respectively. The pooled sensitivity and specificity for the timing of sepsis (EOS) were 78% (95% CI, 68–86) and 67% (95% CI, 57–75), respectively, with a diagnostic odds ratio of 9.06 (95% CI, 1.71–48.05) and an I^2 of 16%, respectively (Table 2).

3.3 Publication bias

In the evaluation of publication bias, the results of the regression line test indicated that there was no publication bias (bias = −9.55; 95% CI, −24.31–5.22; $P = 0.15$). The findings from the Deek's funnel plot are illustrated in Figure 5.

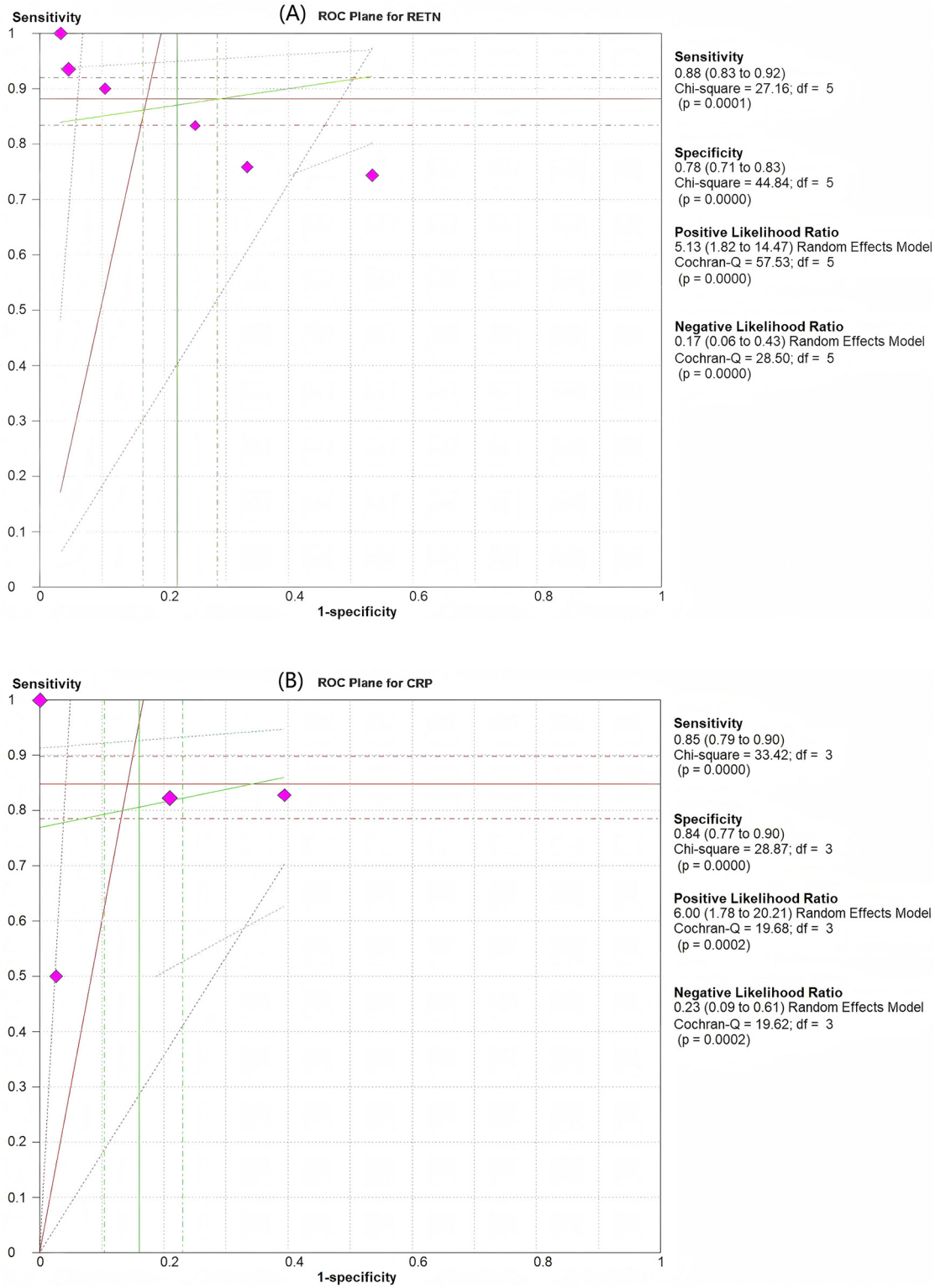

FIGURE 3
Pooled results of the studies assessing the diagnostic accuracy of resistin and CRP levels for the prediction of sepsis in infants and children. **(A)** ROC plane for resistin. **(B)** ROC plane for CRP. The diamond-shaped symbol marked in purplish red represents one study.

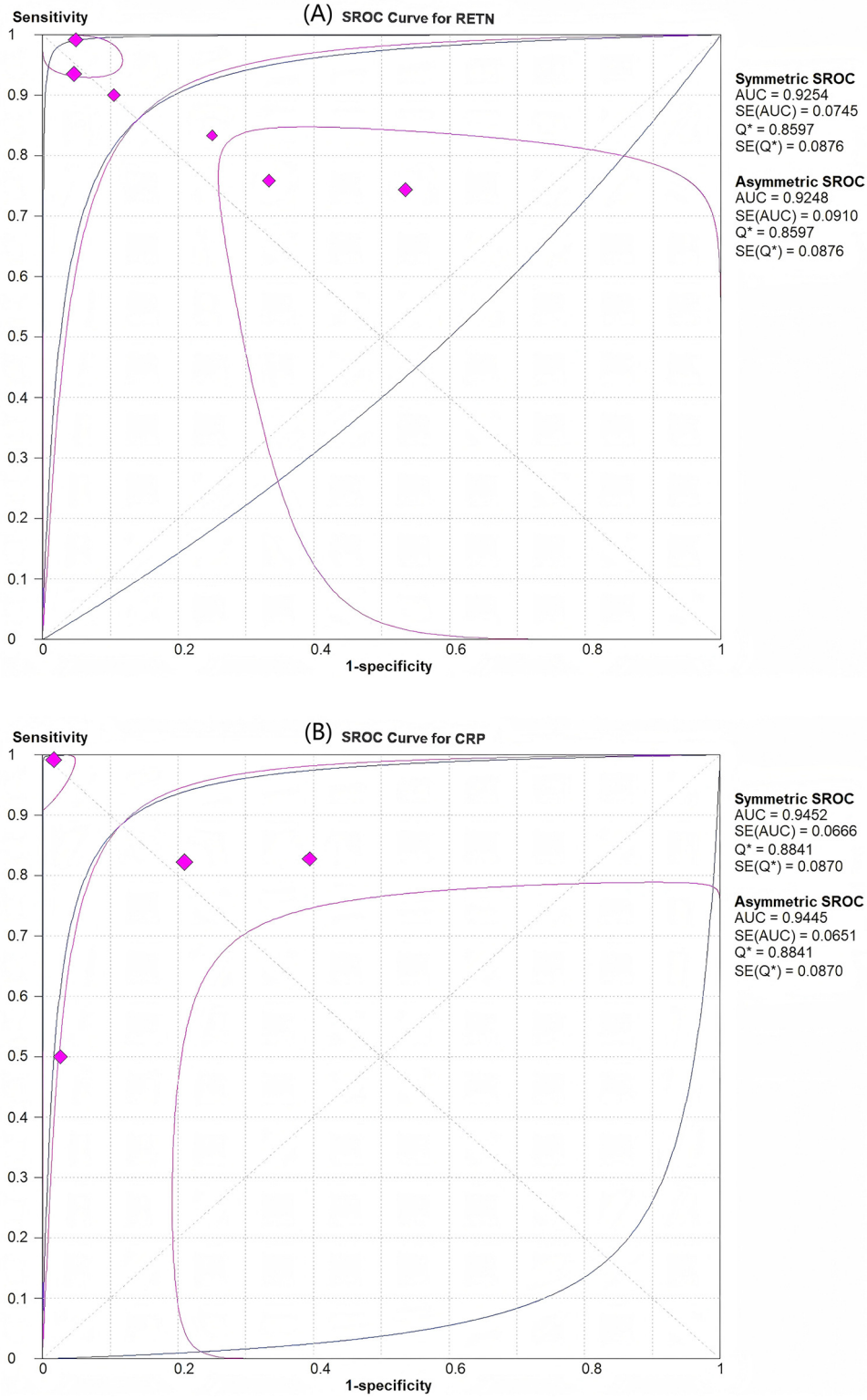

FIGURE 4
SROC curves for assessment of the diagnostic accuracy of resistin and CRP levels for predicting sepsis in infants and children. **(A)** Resistin had an area under the curve (AUC) of 0.925. **(B)** CRP had an AUC of 0.945.

TABLE 2 Subgroup analysis for assessing the diagnostic accuracy of resistin levels in predicting sepsis in infants and children.

Subgroup	No. of studies	Pooled sensitivity (%) (95% CI)	Pooled specificity (%) (95% CI)	Pooled LR+ (95% CI)*	Pooled LR− (95% CI)†	Pooled DOR 95% CI	I^2 sensitivity %
Sample size (≥80)	3	91 (85–95)	78 (69–85)	7.99 (0.31–204.91)	0.09 (0.01–0.91)	101.44 (1.38–7,432)	90.9
Sample size (<80)	3	82 (71–90)	78 (68–87)	3.78 (1.67–8.54)	0.25 (0.13–0.47)	17 (4.02–71.80)	0
Population (term or near term)	3	93 (87–96)	87 (79–93)	9.2 (0.98–86.65)	0.08 (0.01–0.57)	131.8 (3.97–4,374)	88.3
Population (others)	3	80 (71–88)	68 (57–77)	3.24 (0.92–11.39)	0.27 (0.10–0.71)	12.78 (1.61–101.59)	17.2
Region (Turkey)	4	84 (78–90)	75 (67–81)	4.28 (1.34–13.67)	0.21 (0.08–0.59)	21.87 (2.83–169.26)	68.9
Timing of sepsis (EOS)	3	78 (68–86)	67 (57–75)	2.72 (1.13–6.56)	0.34 (0.16–0.73)	9.06 (1.71–48.05)	16

*LR+, positive likelihood ratio.
†LR−, negative likelihood ratio.
EOS, early-onset sepsis.

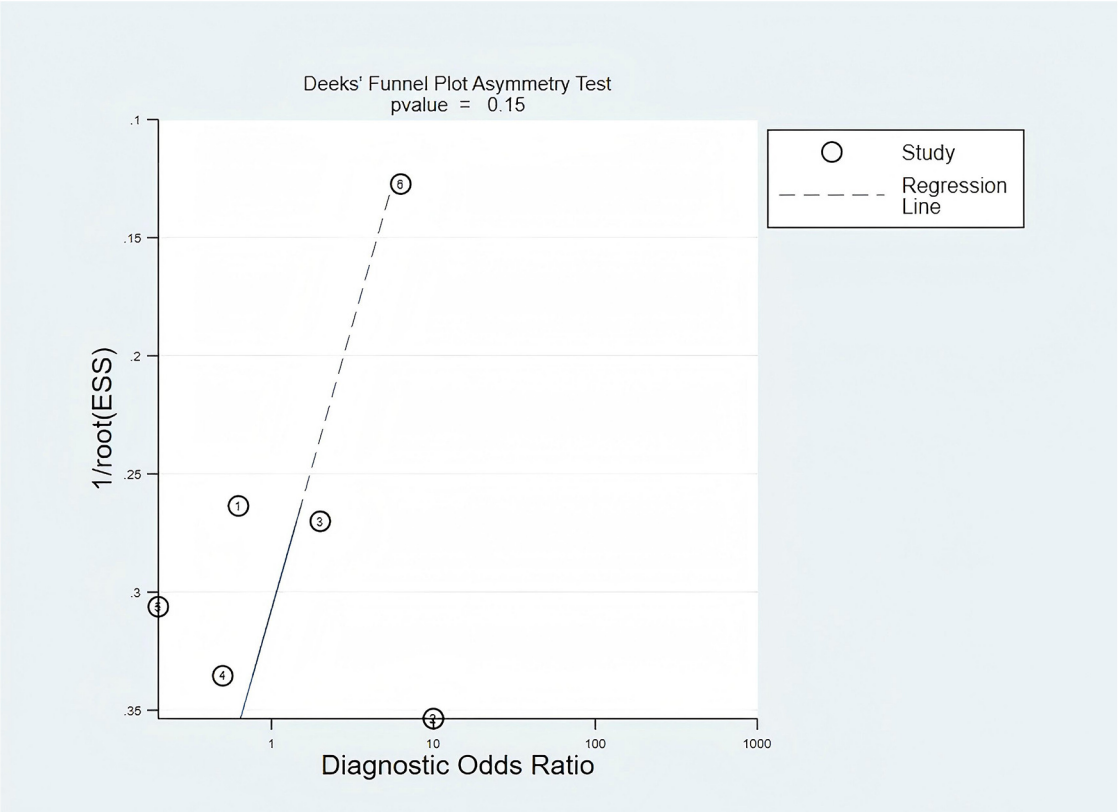

FIGURE 5
Publication bias was assessed using Deek's funnel plot. The value of $P = 0.15$ indicated that there was no significant publication bias among the included studies.

4 Discussion

This meta-analysis demonstrated that the diagnostic accuracy of RETN levels for sepsis in neonates and children was not inferior to that of CRP levels. The SROC curve for RETN levels in the prediction of sepsis revealed a robust predictive ability. The overall pooled estimates for the sensitivity and specificity of elevated RETN concentrations in detecting sepsis were 0.88 (95% CI, 0.83–0.92) and 0.78 (95% CI, 0.71–0.83), respectively, with an AUC of 0.93. To our knowledge, this meta-analysis is the first to evaluate the relationship between RETN levels and sepsis and to compare the diagnostic accuracy of RETN levels with that of CRP levels.

RETN, identified as an adipokine in 2001, is minimally expressed in healthy individuals, but its level significantly

increases upon activation of inflammatory mediators following infection or injury (5, 23). RETN promotes inflammatory cell activation, disrupts the immune balance, and damages vascular endothelial cells, thereby contributing to the pathogenesis of sepsis (24, 25). Research has indicated that RETN activates various cell types, leading to the production of proinflammatory cytokines, such as IL-6, IL-1β and tumour necrosis factor-alpha (TNF-α) through the Toll-like receptor 4 (TLR4)- or cyclase-associated protein 1 (CAP1)-mediated signalling pathways (26–29). The presence of RETN may also lead to an aberrant immune response in specific contexts and diseases, suggesting its role as a bidirectional immunomodulatory molecule (26). Additionally, RETN can induce endoplasmic reticulum stress, inhibit insulin-stimulated endothelial nitric oxide production, impair insulin signalling in vascular endothelial cells, and increase the production of reactive oxygen species, along with the increase of the mRNA expression of proinflammatory cytokines, ultimately resulting in endothelial cell dysfunction (30). However, RETN has been shown to increase autophagy in bovine alveolar macrophages by activating the adenosine monophosphate-activated protein kinase (AMPK) and mammalian target of rapamycin (mTOR) signalling pathways, potentially alleviating lipopolysaccharide (LPS)-induced inflammation (31). Consequently, the precise clinical significance of this molecule remains uncertain.

Several studies have shown that the RETN level may be a specific marker for the early identification of patients at increased risk of sepsis (32, 33). A study by Aliefendioglu established a RETN concentration cut-off of 50 ng/ml, yielding a sensitivity of 73.7% and a specificity of 45.8% for the early detection of neonatal sepsis (14). A study conducted by Saboktakin demonstrated that RETN levels could be used as indicators of sepsis in children admitted to the PICU, with a sensitivity of 0.824 and a specificity of 0.72 on the first day (16). And the diagnostic value of RETN was found to be limited compared with that of other inflammatory markers, including C-reactive protein, procalcitonin, and IL-6 (13, 14, 16). However, Lan et al. reported that the specificity of the RETN level as a diagnostic marker for sepsis was 91.7%, indicating high accuracy (31). Cekmez et al. reported a notable diagnostic accuracy for RETN levels, with 93% sensitivity and 95% specificity for neonatal sepsis (18). Our findings support the RETN level as a reliable sepsis marker in infants and children.

Typically, there exists a trade-off between sensitivity and specificity in diagnostic accuracy tests, with an increase in sensitivity (true positive rate) often accompanied by a decrease in specificity (true negative rate). Therefore, relying solely on sensitivity and specificity may not provide the most accurate estimation of diagnostic accuracy. Alternatively, the area under the SROC curve, or AUC, may serve as a more reliable metric. The AUC ranges from 0.50 to 1.00 and correlates with overall diagnostic accuracy. The current study revealed that the AUC for the SROC curve of RETN was 0.93, indicating that the RETN level is a valuable diagnostic marker for sepsis in neonates and children.

Given the high mortality and morbidity associated with neonatal and paediatric sepsis, diagnostic tests with high sensitivity and a high negative predictive value are highly important. CRP, a well-established biomarker for the early diagnosis of sepsis, has extensively been used in clinical settings (34–36). Our meta-analysis revealed that the sensitivity of RETN surpassed that of CRP, although its specificity was lower. Our study revealed high AUCs for both RETN and CRP, indicating that these two biomarkers exhibit enhanced diagnostic accuracy for sepsis. Compared with CRP levels, RETN levels were found to be equally effective in diagnosing sepsis in neonates and children. Furthermore, RETN levels provide critical diagnostic gains by improving early sepsis detection when traditional markers remain equivocal. The 3% higher pooled sensitivity of RETN than that of CRP (88% vs. 85%) in our meta-analyses enhances the rule-out capability, potentially reducing the number of missed cases during the initial triage. The biomarker's rapid elevation within 2–4 h of infection offers a temporal advantage over CRP (typically rising after 6–8 h), enabling earlier antibiotic decisions in time-sensitive scenarios like paediatric and neonatal sepsis (37).

The cut-off values for RETN levels in the diagnosis of sepsis have not been consistently reported across studies, even when the same assay is used, which significantly impedes the clinical application of this biomarker. Macdonald et al. reported that sustained elevations of RETN levels were linked to severe sepsis or septic shock, with the levels ranging from 36.5 to 50.8 ng/ml within 30 h after sepsis onset in adults (38). In our investigation, the reported cut-off values varied from 5.2 to 50 ng/ml for RETN and from 0.82 to 5 mg/ml for CRP. The variability in cut-off values may be attributed to differences in sepsis severity, study designs, clinical environments, and sample types (33). Therefore, future investigations should aim to eliminate the influence of these confounding factors on RETN levels to establish clinically relevant cut-off values.

This meta-analysis has several limitations. First, some results exhibited high heterogeneity. While we identified certain sources of heterogeneity through various methods, some remain unclear. Second, only six studies that assessed the diagnostic value of RETN were included because of the limited data availability. Finally, most of the studies were conducted on European populations, and the findings may not be generalizable to other ethnic groups (13, 14, 17–19). These factors may introduce a risk of bias in the results of the current study.

In conclusion, on the basis of the currently available evidence, RETN levels are highly valuable for early detection of neonatal and paediatric sepsis. Further prospective controlled studies with adequate sample sizes that encompass all predisposing factors for sepsis are necessary to elucidate the relationship between RETN levels and sepsis.

Data availability statement

The original contributions presented in the study are included in the article/Supplementary Material, further inquiries can be directed to the corresponding author.

Author contributions

FX: Conceptualization, Investigation, Software, Validation, Writing – original draft. JL: Data curation, Formal analysis, Investigation, Methodology, Project administration, Supervision, Writing – original draft, Writing – review & editing. WL: Data curation, Formal analysis, Supervision, Writing – review & editing.

Funding

The author(s) declare that no financial support was received for the research and/or publication of this article.

Conflict of interest

The authors declare that the research was conducted in the absence of any commercial or financial relationships that could be construed as a potential conflict of interest.

Generative AI statement

The author(s) declare that no Generative AI was used in the creation of this manuscript.

Publisher's note

Supplementary material

The Supplementary Material for this article can be found online at: https://www.frontiersin.org/articles/10.3389/fped.2025.1555671/full#supplementary-material

References

1. Reddy AR, Stinson HR, Alcamo AM, Pinto NP, Fitzgerald JC. Pediatric sepsis requiring intensive care admission: potential structured follow-up protocols to identify and manage new or exacerbated medical conditions. *Risk Manag Healthc Policy*. (2023) 16:1881–91. doi: 10.2147/RMHP.S394458

2. Strunk T, Molloy EJ, Mishra A, Bhutta ZA. Neonatal bacterial sepsis. *Lancet*. (2024) 404(10449):277–93. doi: 10.1016/S0140-6736(24)00495-1

3. Liu L, Oza S, Hogan D, Perin J, Rudan I, Lawn JE, et al. Global, regional, and national causes of child mortality in 2000-13, with projections to inform post-2015 priorities: an updated systematic analysis. *Lancet*. (2015) 385(9966):430–40. doi: 10.1016/S0140-6736(14)61698-6

4. Kannikeswaran N, Mahajan P. Pediatric sepsis: new strategies for reducing sepsis related mortality. *Indian Pediatr*. (2023) 60(12):981–4. doi: 10.1007/s13312-023-3059-y

5. Shuldiner AR, Yang R, Gong DW. Resistin, obesity, and insulin resistance–the emerging role of the adipocyte as an endocrine organ. *N Engl J Med*. (2001) 345(18):1345–6. doi: 10.1056/NEJM200111013451814

6. Fedoce AG, Veras FP, Rosa MH, Schneider AH, Paiva IM, Machado MR, et al. Macrophage-derived human resistin promotes perivascular adipose tissue dysfunction in experimental inflammatory arthritis. *Biochem Pharmacol*. (2024) 224:116245. doi: 10.1016/j.bcp.2024.116245

7. Yang HM, Kim J, Kim BK, Seo HJ, Kim JY, Lee JE, et al. Resistin regulates inflammation and insulin resistance in humans via the endocannabinoid system. *Research (Wash D C)*. (2024) 7:0326. doi: 10.34133/research.0326

8. Chen H, Luo H, Tian T, Li S, Jiang Y. Integrated analyses of single-cell transcriptome and mendelian randomization reveal the protective role of resistin in sepsis survival in intensive care unit. *Int J Mol Sci*. (2023) 24(19):14982. doi: 10.3390/ijms241914982

9. Jang JC, Li J, Gambini L, Batugedara HM, Sati S, Lazar MA, et al. Human resistin protects against endotoxic shock by blocking LPS-TLR4 interaction. *Proc Natl Acad Sci U S A*. (2017) 114:E10399–408. doi: 10.1073/pnas.1716015114

10. Zhou HH, Tang YL, Xu TH, Cheng B. C-reactive protein: structure, function, regulation, and role in clinical diseases. *Front Immunol*. (2024) 15:1425168. doi: 10.3389/fimmu.2024.1425168

11. Cheng B, Lv JM, Liang YL, Zhu L, Huang XP, Li HY, et al. Secretory quality control constrains functional selection-associated protein structure innovation. *Commun Biol*. (2022) 5:268. doi: 10.1038/s42003-022-03220-3

12. Wu Y, Potempa LA, El Kebir D, Filep JG. C-reactive protein and inflammation: conformational changes affect function. *Biol Chem*. (2015) 396:1181–97. doi: 10.1515/hsz-2015-0149

13. Khattab AA, El-Mekkawy MS, Helwa MA, Omar ES. Utility of serum resistin in the diagnosis of neonatal sepsis and prediction of disease severity in term and late preterm infants. *J Perinat Med*. (2018) 46(8):919–25. doi: 10.1515/jpm-2018-0018

14. Aliefendioglu D, Gürsoy T, Çağlayan O, Aktaş A, Ovalı F. Can resistin be a new indicator of neonatal sepsis? *Pediatr Neonatol*. (2014) 55(1):53–7. doi: 10.1016/j.pedneo.2013.04.012

15. Bengnér J, Quttineh M, Gäddlin PO, Salomonsson K, Faresjö M. Serum amyloid A-A prime candidate for identification of neonatal sepsis. *Clin Immunol*. (2021) 229:108787. doi: 10.1016/j.clim.2021.108787

16. Saboktakin L, Bilan N, Ghalehgolab Behbahan A, Poorebrahim S. Relationship between resistin levels and sepsis among children under 12 years of age: a case control study. *Front Pediatr*. (2019) 7:355. doi: 10.3389/fped.2019.00355

17. Gokmen Z, Ozkiraz S, Kulaksizoglu S, Kilicdag H, Ozel D, Ecevit A, et al. Resistin–a novel feature in the diagnosis of sepsis in premature neonates. *Am J Perinatol*. (2013) 30(6):513–7. doi: 10.1055/s-0032-1329182

18. Cekmez F, Canpolat FE, Cetinkaya M, Aydinöz S, Aydemir G, Karademir F, et al. Diagnostic value of resistin and visfatin, in comparison with C-reactive protein, procalcitonin and interleukin-6 in neonatal sepsis. *Eur Cytokine Netw*. (2011) 22(2):113–7. doi: 10.1684/ecn.2011.0283

19. Ozdemir AA, Elgormus Y. Value of resistin in early onset neonatal sepsis. *J Child Sci*. (2017) 7:e146–50. doi: 10.1055/s-0037-1608713

20. Whiting P, Rutjes AW, Reitsma JB, Bossuyt PM, Kleijnen J. The development of QUADAS: a tool for the quality assessment of studies of diagnostic accuracy included in systematic reviews. *BMC Med Res Methodol*. (2003) 3:25. doi: 10.1186/1471-2288-3-25

21. Higgins JPT, Thompson SG, Deeks JJ, Altman DG. Measuring inconsistency in meta-analyses. *Br Med J*. (2003) 327(7414):557–60. doi: 10.1136/bmj.327.7414.557

22. Deeks JJ, Macaskill P, Irwig L. The performance of tests of publication bias and other sample size effects in systematic reviews of diagnostic test accuracy was assessed. *J Clin Epidemiol*. (2005) 58:882–93. doi: 10.1016/j.jclinepi.2005.01.016

23. Alhamdan F, Koutsogiannaki S, Yuki K. The landscape of immune dysregulation in pediatric sepsis at a single-cell resolution. *Clin Immunol*. (2024) 262:110175. doi: 10.1016/j.clim.2024.110175

24. Bonenfant J, Li J, Nasouf L, Miller J, Lowe T, Jaroszewski L, et al. Resistin concentration in early sepsis and all-cause mortality at a safety-net hospital in riverside county. *J Inflamm Res*. (2022) 15:3925–40. doi: 10.2147/JIR.S370788

25. Li G, Yang Z, Yang C, Xie Y, Gong S, Lv S, et al. Single-cell RNA sequencing reveals cell-cell communication and potential biomarker in sepsis and septic shock patients. *Int Immunopharmacol*. (2024) 132:111938. doi: 10.1016/j.intimp.2024.111938

26. Li Y, Yang Q, Cai D, Guo H, Fang J, Cui H, et al. Resistin, a novel host defense peptide of innate immunity. *Front Immunol*. (2021) 12:699807. doi: 10.3389/fimmu.2021.699807

27. Tarkowski A, Bjersing J, Shestakov A, Bokarewa MI. Resistin competes with lipopolysaccharide for binding to toll-like receptor 4. *J Cell Mol Med*. (2010) 14(6B):1419–31. doi: 10.1111/j.1582-4934.2009.00899.x

28. Silswal N, Singh AK, Aruna B, Mukhopadhyay S, Ghosh S, Ehtesham NZ. Human resistin stimulates the pro-inflammatory cytokines TNF-alpha and IL-12 in macrophages by NF-kappaB-dependent pathway. *Biochem Biophys Res Commun*. (2005) 334(4):1092–101. doi: 10.1016/j.bbrc.2005.06.202

29. Li B, Fang J, Zuo Z, Yin S, He T, Yang M, et al. Activation of the porcine alveolar macrophages via toll-like receptor 4/NF-κB mediated pathway provides a mechanism of resistin leading to inflammation. *Cytokine*. (2018) 110:357–66. doi: 10.1016/j.cyto.2018.04.002

30. Luo J, Huang L, Wang A, Liu Y, Cai R, Li W, et al. Resistin-induced endoplasmic reticulum stress contributes to the impairment of insulin signaling in endothelium. *Front Pharmacol*. (2018) 9:1226. doi: 10.3389/fphar.2018.01226

31. Ma X, Yang A, Fan X, Liu H, Gu Y, Wang Z, et al. Resistin alleviates lipopolysaccharide-induced inflammation in bovine alveolar macrophages by activating the AMPK/mTOR signaling pathway and autophagy. *Heliyon*. (2024) 10(19):e38026. doi: 10.1016/j.heliyon.2024.e38026

32. Lan Y, Guo W, Chen W, Chen M, Li S. Resistin as a potential diagnostic biomarker for sepsis: insights from DIA and ELISA analyses. *Clin Proteomics*. (2024) 21(1):46. doi: 10.1186/s12014-024-09498-1

33. Jiang Z, Luo Y, Wei L, Gu R, Zhang X, Zhou Y, et al. Bioinformatic analysis and machine learning methods in neonatal sepsis: identification of biomarkers and immune infiltration. *Biomedicines*. (2023) 11(7):1853. doi: 10.3390/biomedicines11071853

34. Goyal M, Mascarenhas D, Rr P, Haribalakrishna A. Diagnostic accuracy of point-of-care testing of C-reactive protein, interleukin-6, and procalcitonin in neonates with clinically suspected sepsis: a prospective observational study. *Med Princ Pract*. (2024) 33(3):291–98. doi: 10.1159/000536678

35. Cui N, Zhang YY, Sun T, Lv XW, Dong XM, Chen N. Utilizing procalcitonin, C-reactive protein, and serum amyloid A in combination for diagnosing sepsis due to urinary tract infection. *Int Urol Nephrol*. (2024) 56(7):2141–6. doi: 10.1007/s11255-024-03959-0

36. Binny R, Kotsanas D, Buttery J, Korman T, Tan K. Is neutrophil to lymphocyte ratio an accurate predictor of neonatal sepsis in premature infants? *Early Hum Dev*. (2025) 200:106147. doi: 10.1016/j.earlhumdev.2024.106147

37. Sundén-Cullberg J, Nyström T, Lee ML, Mullins GE, Tokics L, Andersson J, et al. Pronounced elevation of resistin correlates with severity of disease in severe sepsis and septic shock. *Crit Care Med*. (2007) 35:1536–42. doi: 10.1097/01.CCM.0000266536.14736.03

38. Macdonald SP, Stone SF, Neil CL, van Eeden PE, Fatovich DM, Arendts G, et al. Sustained elevation of resistin, NGAL and IL-8 are associated with severe sepsis/septic shock in the emergency department. *PLoS One*. (2014) 9:e110678. doi: 10.1371/journal.pone.0110678

frontiers | Frontiers in Immunology

TYPE Original Research
PUBLISHED 19 May 2025
DOI 10.3389/fimmu.2025.1598605

OPEN ACCESS

EDITED BY
Alok Agrawal,
Retired, Johnson City, TN, United States

REVIEWED BY
Li Haiyun,
Xi'an Jiaotong University, China
Bin Cheng,
Lanzhou University of Technology, China

*CORRESPONDENCE
Katja Hoffmann
katja.hoffmann@uniklinik-freiburg.de
Hartmut Hengel
hartmut.hengel@uniklinik-freiburg.de

†PRESENT ADDRESS
Anna Henning,
Clinic for Nephrology and Intensive Care Medicine at Charité - Universitätsmedizin Berlin, Germany
Haizhang Chen,
Department of Hematology, Oncology and Rheumatology, Heidelberg University Hospital, Heidelberg, Germany

RECEIVED 23 March 2025
ACCEPTED 22 April 2025
PUBLISHED 19 May 2025

CITATION
Henning A, Seer J, Zeller J, Peter K, Chen H, Thomé J, Kolb P, Eisenhardt SU, Hoffmann K and Hengel H (2025) Human Fcγ-receptors selectively respond to C-reactive protein isoforms.
Front. Immunol. 16:1598605.
doi: 10.3389/fimmu.2025.1598605

Human Fcγ-receptors selectively respond to C-reactive protein isoforms

Anna Henning[1†], Johanna Seer[1], Johannes Zeller[2], Karlheinz Peter[3,4], Haizhang Chen[1†], Julia Thomé[2], Philipp Kolb[1], Steffen U. Eisenhardt[2], Katja Hoffmann[1*] and Hartmut Hengel[1*]

[1]Institute of Virology, University Medical Center, Faculty of Medicine, University of Freiburg, Freiburg, Germany, [2]Department of Plastic and Hand Surgery, University of Freiburg Medical Centre, Medical Faculty of the University of Freiburg, Freiburg, Germany, [3]Baker Department of Cardiometabolic Health, University of Melbourne, Parkville, VIC, Australia, [4]Atherothrombosis and Vascular Biology Laboratory, Baker Heart and Diabetes Institute, Melbourne, VIC, Australia

Introduction: The pentameric C-reactive protein (pCRP), an acute-phase protein, binds to lysophosphatidylcholine (LPC) displayed on the surface of dying cells and microorganisms to activate the complement system and to opsonize immune cells via Fcγ-receptors (FcγRs). Members of the FcγR family are characterized by the recognition of the Fc part of IgG antibodies.

Methods: We utilized a mouse thymoma BW5147 reporter cell panel stably expressing chimeric human FcγR-CD3ζ-chain receptors to define the molecular requirements for FcγR crosslinking by C-reactive protein (CRP).

Results: Applying this approach, we show a robust activation of CD64/FcγRI and CD32a/FcγRIIa by immobilized CRP isoforms as well as triggering of inhibitory CD32b/FcγRIIb. Of note, activation of FcγRIIa was restricted to the 131R allelic variant but not observed with 131H. In contrast, FcγRIII isoforms CD16aF, CD16aV and CD16b were not activated by pCRP, although binding of CRP isoforms to FcγRIII was detectable. Activation of FcγRs by free pCRP in solution phase was considerably lower than with immobilized pCRP on hydrophilic plastic surfaces and readily abolished by IgG at serum level concentrations, whereas it was enhanced by the addition of streptococci. The types of FcγRs mainly responding to pCRP in solution phase (CD64/FcγRI and CD32aR/FcγRIIaR) clearly differed from FcγRs responding to soluble multimeric IgG complexes (i.e., CD16aV/FcγRIIIaV and CD32aH/FcγRIIaH). Compared to pCRP, monomeric CRP (mCRP) showed lower levels of activation in those selective FcγRs. FcγR activation was linked to recognition by conformation-dependent CRP antibodies. Unmasking of the mAb 9C9-defined neoepitope in pCRP* correlated with the triggering of FcγRs, indicating that pCRP* is the major FcγR-activating CRP conformation.

Discussion: The assay provides a novel, scalable approach to determine the molecular properties of CRP as a physiological ligand of FcγR-mediated bioactivities.

KEYWORDS

C-reactive protein, CRP isoforms, Fcγ receptor, immunoglobulin, immune complex

1 Introduction

C-reactive protein (CRP) is a pattern recognition molecule and prototypical acute-phase protein. It is widely used as a marker of acute inflammation in patients. CRP is a member of the pentraxin family and synthesized mainly by hepatocytes (1–3). The secreted CRP molecule consists of five identical non-covalently linked non-glycosylated protomers of ~23 kDa each. These protomers are aligned in planar symmetry to form a donut-shaped ring (4). This ring comprises two faces, i.e., the complement C1q or Fcγ-receptor (FcγR) binding 'effector' A-face and the ligand binding B-face. Phosphocholine (PC) head groups expressed on bacterial cell walls and damaged host cell membranes (5, 6) are the prototypic ligands for CRP. PC is bound in a calcium-dependent manner via the phosphocholine binding pockets expressed on the B-face. The opposite A-face of the pentamer contains overlapping binding sites for C1q and FcγRs, so that the two interaction domains are considered to be mutually exclusive (7).

Traditionally, a distinction is made between at least two main conformational isoforms of CRP: The circulating native, pentameric CRP (pCRP) and the monomeric isoform (mCRP), which is ultimately formed by dissociation of the pentameric molecule. Under experimental conditions, this process can be initiated by exposure to heat, acid or urea and leads to the exposure of neoepitopes on the CRP molecule that are inaccessible in the native pentameric form (8–10). *In vivo*, the dissociation process is observed on PC-rich membranes of activated platelets, monocytes or endothelial cells, by interaction with misfolded proteins and by mechanical stress in stenosed vessels (10–14). In contrast to pCRP, mCRP is insoluble and considered a pro-inflammatory, tissue- or cell-bound isoform of CRP found deposited to local inflammation. A third intermediate isoform of CRP, pCRP*, has only recently been described (10). Binding of pCRP to microparticles containing PC head groups released by activated cells leads to a conformational change in the structure of pCRP: the neoepitopes responsible for C1q and FcγR binding that are accessible in mCRP are also exposed in pCRP*, but unlike mCRP, the overall pentameric symmetry is preserved. Exposure of the neoepitopes facilitates C1q binding and complement activation, with the result that pCRP* can increase tissue inflammation (10).

FcRs form a vital link between humoral and cellular immunity: They recognize the Fc region of antibodies bound to antigens via their Fab region. IgG-binding FcγRs belong to the immunoglobulin superfamily expressed on most immune effector cells. They can be divided into activating and inhibitory FcγRs. Both FcγR types are often expressed on the same cell and form a binary system integrating activating and inhibitory signals (15). FcγRI (CD64), FcγRIIa (CD32aH/R), FcγRIIc (CD32c), FcγRIIIa (CD16aF/V) and FcγRIIIb (CD16b) are activating FcγRs and (except for FcγRIIIb) signal via immunoreceptor tyrosine based activating motifs (ITAMs) in their cytoplasmic regions (16, 17). FcγRIIb (CD32b), the only inhibitory FcγR, signals via an immunoreceptor tyrosine based inhibitory motif (ITIM) (18). FcγRI (CD64) is the high affinity receptor for IgG, whereas all other FcγRs have low to medium affinity to monomeric IgG (19). Binding of either immobilized or multimeric soluble immune complexes (ICs) to FcγRs leads to various effector functions that depend on the FcγRs expressed and the type of immune effector cell affected and include antibody-dependent cellular cytotoxicity (ADCC), antibody-dependent cellular phagocytosis (ADCP), cytokine release, oxidative burst and apoptosis (18, 20).

Recognition of pCRP by FcγRI (CD64) and FcγRIIa (CD32a) was first demonstrated by flow cytometry using transfected COS-cells and monoclonal antibodies (21, 22). Later studies characterized the binding of pCRP to FcγRs in antibody- and label-free setups. FcγRIIa was found to dock diagonally to two of the five pentraxin subunits on the effector face with its D1 and D2 domains, ensuring a one-to-one binding stoichiometry with no significant conformational changes (23). Binding of pCRP was observed not only with FcγRI (CD64) and FcγRIIa/b (CD32), but also with FcγRIII (CD16) (23, 24). Binding affinities of pCRP to FcγRs are in a similar range (24) and comparable to IgG binding to low affinity FcγRs (25). Pentraxin binding sites partially overlap with IgG binding sites on FcγRs, suggesting competitive binding (23). Binding of pCRP to FcγRs leads to opsonization, cytokine production and enhancement of phagocytosis (23, 26, 27).

Many aspects of CRP-FcγR interaction remain controversial. Preferential binding of pCRP to the 131R allelic variant of FcγRIIa compared to 131H has been considered certain for decades and various clinical observations have been attributed to this difference (28, 29). However, recent contrary observations of a potential difference in pCRP binding to FcγRIIa-H/R131 have been made in antibody free setups (23, 24). Whilst several studies investigate the interaction of different conformational isoforms of CRP (pCRP/pCRP*/mCRP) and C1q, little is known regarding the impact of the CRP isoforms on FcγR activation (10–12, 30, 31). Neither a clearly pro- nor anti-inflammatory role can be attributed to the CRP–FcγR interaction, as both pro- and anti-inflammatory cytokine expression have been reported (23, 27, 32). The precise contribution of CRP to immune complex-mediated diseases and the intricate interplay between CRP, IgG and FcγRs remains to be elucidated (24, 33–35).

The BW5147-FcγRζ reporter assay panel is based on mouse BW5147 thymoma cells stably transduced with the extracellular domain of individual human, rhesus, or mouse FcγRs (e.g., human FcγRI/IIaH/IIaR/IIb/IIIaF/IIIaV/IIIb), allowing for convenient, quantifiable, and high-throughput analysis of FcγR activation by IgG (33–35). The assay has been established for immobilized IgG, multimeric immune complexes in solution phase (sICs) and recombinant Fc-fusion therapeutics mediating activation of FcγRs (20, 33, 36, 37). Unlike the variety of FcγRs found on primary immune cells, each setup contains only one FcγR, allowing clear attribution of the observed activation. FcγR ectodomains are coupled to the signaling CD3ζ chain of the TCR, leading to mouse IL-2 (mIL-2) production upon receptor cross-linking and activation of the reporter cell. Here, we modified the test system to detect activation mediated by distinct human CRP isoforms and to compare CRP-dependent with IgG-mediated activation. While binding of pCRP has been investigated for individual FcγRs, pCRP-dependent activation has solely been examined in complex

settings with several FcγRs and/or more than one cell type present. In this study, the reductionistic setup of the BW5147-FcγRζ reporter assay allowed for comparing specific FcγR binding to distinct CRP isoforms with subsequent FcγR crosslinking and activation, as well as interactions of CRP with IgG and soluble immune complexes which are independent ligands of FcγRs. The BW5147-FcγRζ test system distinguished CRP-responsive (CD64/FcγRI, CD32aR/FcγRIIaR, and CD32b/FcγRIIb) from non-responsive human FcγRs and revealed a clear allele-dependent activation pattern of CD32a/FcγRIIa by CRP (131R>>H). Triggering of FcγRs was achieved by either soluble or immobilized pCRP or mCRP ligand, with immobilized pCRP showing highest triggering efficacy. Interestingly, effective pCRP signaling via FcγRs was associated with conformational unmasking of the pCRP*/mCRP neoepitope as detected by mAb clone 9C9 and activation caused by pCRP was stronger than for mCRP, suggesting pCRP* as the major FcγR activator (10).

2 Materials and methods

2.1 CRP preparation and detection, IgG source and sICs preparation

Highly purified human CRP from pleural fluid/ascites and recombinant CRP produced in *E. coli* (C7907–26 and C7907-03C) was purchased from US Biological Life Sciences (Salem, Massachusetts, USA) mCRP was prepared from purified pCRP as described previously (38) and concentrations of pCRP and mCRP were measured using Qubit Fluorometric Quantitation (Thermo Fisher Scientific, Waltham, MA, USA). Streptococcus pneumoniae serotype 27 was kindly provided by Dr. Mark van der Linden, Head of the National Reference Center for streptococci, Department of Medical Microbiology, University Hospital (RWTH, Aachen, Germany). To form CRP- streptococci complexes, 10 µl of suspended streptococci were added to 20/10/5 µg of CRP (39, 40).

Synthetic sICs formed by 25 nM Infliximab (149.1 kDa) and 50 nM TNFα monomer (17.5 kDa) to ensure a 1:1 stoichiometry were produced as described previously (20). sICs and CRP-streptococci complexes were incubated for two hours at room temperature (RT) prior to being used in the experiment. Polyclonal goat anti-human CRP antibody (A80-125A) was purchased from Bethyl (Montgomery, Texas, USA), monoclonal conformation-specific antibodies binding pCRP and pCRP*/mCRP (clone 8D8 and 9C9, respectively) were kindly provided by Prof. Lawrence A. Potempa, College of Pharmacy, Roosevelt University, Schaumburg, IL, USA. LPS (LPS EB Standard, 5 mg, #tlrl-eblps, LPS *E. coli* O111:B4) was purchased from InvivoGen (San Diego, California, USA). Purified human IgG (cytotect®, Biotest, Dreieich, Germany), recombinant Rituximab IgG1 (humanized monoclonal; Roche, University Hospital Freiburg Pharmacy), and concentrated IgG1 (human IgG1 kappa, #I5154-1MG; Sigma-Aldrich, St. Louis, Missouri, USA) served as sources of IgG.

2.2 BW5147 cell culture

The murine T lymphoblast cell line BW5147 (TIB-47™; ATTC, Manassas, VA, USA) was maintained in RPMI 1640 medium ("RPMI BW medium", GlutaMAX™; Gibco Life Technologies, Carlsbad, California, USA) supplemented with 10% (v/v) heat-inactivated FCS (Biochrom, Berlin, Germany), 1% (v/v) Pen-Strep (Gibco Life Technologies), 1% (v/v) sodium pyruvate (100 mM, Gibco Life Technologies), and 0.1% (v/v) β-mercaptoethanol (Sigma-Aldrich). Cells were cultured at 37°C with 5% CO_2 and split based on their growth rate. Cells were maintained at a density of 2×10^5/ml to 1×10^6/ml. For the FcγR activation assay, cells were seeded at $2–3\times10^5$ cells/mL one day prior to the experiment, resulting in a density of $4–6\times10^5$ cells/mL at the time of the assay. Cells were tested regularly for mycoplasma contamination using PCR (sense (#1427): 5′-GGGAGCAAACAGGATTAGATACCCT-3′; antisense (#1428): 5′-TGCACCATCTGTCACTCTGTTAACCTC-3′) with Kapa Polymerase (Peqlab, Erlangen, Germany #KK3604).

2.3 Flow cytometry

BW5147 cells (100,000) were counted using a Countess® II automated cell counter and centrifuged at 1,000 rpm at RT for six minutes. Cells were washed twice in 100 µl FACS buffer (PBS (Dulbecco's PBS, Gibco Life Technologies) with 3% (v/v) heat-inactivated FCS (Sigma-Aldrich)) on ice and centrifuged at 1,400 rpm at 4°C for five minutes. Each sample (100,000 BW5147 cells in 300 µl) was incubated with v/v 1:100 mouse-anti-human-CD16 allophycocyanin (APC) (FcγRIII, clone B73.1), mouse-anti-human-CD32 APC (FcγRII, clone FUN2), mouse-anti-human-CD64 APC (FcγRI, clone S18012C), or mouse-anti-human-CD99 APC (MIC2, clone hec2)-APC (200 µg/ml, BioLegend, San Diego, California, USA; cat. #360705, #303207, #399509, #398203, respectively) antibodies on ice for one hour. Respective anti-FcγR antibodies on BWCD99 cells or unstained BW parental cells served as negative controls for background antibody binding. Cells were washed three times and transferred to FACS round-bottom polystyrene test tubes (Falcon®) containing 200 µl FACS buffer. Samples were kept on ice until analysis using a BD LSR Fortessa™ Cell Analyzer (BD biosciences, Franklin Lakes, New Yersey, USA). A total of 20,000 events were measured per sample. Results were analyzed using FlowJo software (FlowJo LLC, Ashland, OR, USA), with gating applied to the main population (FSC/SSC gating). APC-A fluorescence was compared using histograms normalized to mode.

2.4 BW5147-FcγRζ reporter assay

The BW5147-FcγRζ-cell reporter assay, i.e., mouse BW5147 hybridoma cells stably expressing chimeric FcγR-CD3ζ chain molecules consisting of an extracellular domain of human FcγRs fused to the transmembrane and intracellular domains of the mouse

CD3ζ chain (32), enables analysis of IgG-mediated activation of individual subclasses of human FcγRs. The general procedure of the BW5147-FcγRζ reporter assay was utilized as described before (33) and modified to analyze human CRP-mediated activation (20, 33, 37). In brief, BW5147 cells that are stably transduced with the extracellular domain of one of the human FcγRs (FcγRI, IIaH, IIaR, IIb, IIIaF, IIIaV, IIIb) or with human CD99 as a negative control were used. The human FcγRζ-receptor ectodomain is fused to the signaling CD3ζ-chain of the mouse T cell receptor (TCR), subsequently inducing mouse IL-2 (mIL-2) expression upon receptor crosslinking. In this assay, mIL-2 production is directly proportional to FcγR activation. mIL-2 levels were measured using a sandwich ELISA as described in detail below. For this project, the assay was modified to measure human CRP-dependent and IgG-mediated activation by FcγRζ-receptor crosslinking and as a positive control, respectively. BW5147 reporter cells were stably transduced via lentiviral transduction as described previously (20, 33, 34, 41). FcγR expression was ensured by puromycin selection and two consecutive cell-sorting steps by FACS. BW5147-FcγRζ reporter assays were performed in 96-well ELISA MaxiSorp plates (Thermo Fisher Scientific, Immuno Platte F96 Maxi Pinchbar). For the 'standard' crosslinking assay, MaxiSorp plates were coated with graded concentrations of either IgG1 (human IgG1 kappa, #I5154-1MG, Sigma-Aldrich) or CRP isoforms in 50 µl PBS for one hour at 37°C with 5% CO_2 or overnight at 4°C. The protocol for the 'in solution' BW5147-FcγRζ reporter assay was adapted for CRP from the protocol established for soluble immune complexes (sICs) in our laboratory (20). ELISA wells were blocked by adding 300 µl ELISA blocking buffer (PBS with 10% (v/v) heat-inactivated FCS (Biochrom)) and incubating overnight at 4°C. sICs and complexes formed with pCRP and streptococci were incubated for two hours at RT. Complexes were added to ELISA wells in 100 µl of RPMI BW medium, followed by the addition of 100,000 BW5147-FcγRζ cells in another 100 µl of medium.

2.5 Sandwich mIL-2 ELISA

The level of mIL-2 secreted upon activation of BW5147 reporter cells was measured in a sandwich mIL-2 ELISA. ELISA MaxiSorp plates (Thermo Fisher Scientific) were coated with 50 µl of rat anti-mouse-IL2 antibody (1:500; 0.5 mg/ml; BD Pharmingen, BD biosciences, clone A85-1, #554424) in PBS -/- and incubated overnight at 4°C. Plates were washed and blocked as described above. Supernatants from the BW5147-FcγRζ reporter assay were transferred to the mIL-2-ELISA plates. Supernatants were incubated for 4 hours at RT on the ELISA plate, and wells were subsequently washed five times. 50 µl of biotinylated rat anti-mouse-IL2 (1:500; 0.5 mg/ml; BD Pharmingen, clone A85-1, #554426) in ELISA blocking buffer were added and incubated for 90 minutes at RT. Plates were washed five times, and 50 µl of Streptavidin-Peroxidase (1:1000; 1 mg/ml, Jackson ImmunoResearch, Philadelphia, PA, USA, #016-030-084) in blocking buffer was added for 30 minutes at RT. Wells were washed five times, and 50 µl of ELISA TMB 1-Step™ Ultra substrate solution (Thermo Fisher Scientific) was added, followed by 50 µl of 1 M H_2SO_4 to stop the reaction. Absorbance was measured using a Tecan ELISA Reader Infinite® M Plex (Tecan, Männedorf, Switzerland) at a wavelength of 450 nm and a reference wavelength of 620 nm.

2.6 Binding ELISA

Binding of recombinant His-tagged FcγRs (Sino Biological, Bejing, China, recombinant, HEK293/ECD, C-terminal polyhistidine tag: 1038-H08H1/10374-H08H1/10374-H08H/10259-H08H/10256-H08H/10389-H08C) to immobilized pCRP (US Biological Life Sciences) or IgG (human IgG1 kappa, # I5154-1MG, Sigma-Aldrich) was investigated by ELISA. Ninety-six-well ELISA MaxiSorp plates (Thermo Fisher Scientific) were coated with either pCRP, mCRP, or IgG1 overnight at 4°C, washed (PBS with 0.05% (v/v) Tween 20), and blocked with 300 µl of ELISA blocking buffer for one hour at RT. Blocking buffer was removed, and His-tagged FcγRs were added in 50 µl PBS. Binding was allowed to proceed overnight at 4°C. Subsequently, wells were washed five times, and 100 µl of blocking buffer/rabbit anti-His-antibody (1:5,000; 1 mg/ml, Bethyl: A190-114A) was added for overnight incubation at 4°C. Wells were washed five times, and goat anti-rabbit-peroxidase (POD) conjugated antibody (1:3,000; 1 mg/ml; Sigma-Aldrich; A0545) was added in 50 µl ELISA blocking buffer for one hour at 37°C. The ELISA readout using a Tecan ELISA Reader Infinite® M Plex at a wavelength of 450 nm and a reference wavelength of 620 nm was performed as described above. Binding assays in the 'reverse' setup were conducted following the same general procedure as described above. However, for this assay His-tagged hFcγRs were coated to ELISA wells in 50 µl PBS. Following the same blocking and washing steps as described above, IgG1, pCRP, or mCRP were added in 50 µl ELISA blocking buffer, and binding was detected using goat anti-hCRP antibody (1:3,000; 1 mg/ml; Bethyl: A80-125A) and donkey anti-goat (DAG) POD-conjugated antibody (DAG-POD; 1:5,000; 2,5mg/ml; Invitrogen, Waltham, Massachusetts, USA: A16005) for CRP (pCRP and mCRP) and goat anti-human-IgG-POD (1:3,000, 1 mg/ml; Rockland Immunochemical, Philadelphia, Pennsylvania, USA, #109-035-003) for IgG1.

2.7 Semi-native PAGE and Coomassie

The structural integrity of pCRP as well as the monomeric form of mCRP was verified by semi-native gel electrophoresis as described previously (14). mCRP was generated by treating pCRP with 8 M urea in the presence of 10 mM EDTA for 2 hours at 37°C. mCRP was thoroughly dialyzed in low-salt phosphate buffer (10 mM Na_2HPO_4, 10 mM NaH_2PO_4, and 15 mM NaCl, pH 7.4).

To confirm the use of pCRP or mCRP in the following assay setups, a pseudo-native SDS-PAGE and subsequent Coomassie staining or Western blot analysis with confirmation-specific CRP mAb was applied. In brief, samples were mixed with 15 µl of 1x sample buffer (1/20 of SDS as described in Lämmli-buffer, no DTT,

no ß-ME), and pCRP or mCRP as indicated (10 µg, 5 µg or 3 µg). Samples were left without heating or boiling and loaded onto 10% PAA-Gel (all gel components and 1-Lämmli running buffer only with 1/20 of 20% SDS; final SDS concentration 1%). The gel was either directly stained with Coomassie brilliant blue solution and destained with water, or transferred onto a nitrocellulose membrane for Western blot analysis.

2.8 Statistical analyses and Graph modeling

Statistical analyses were performed using GraphPad Prism software (v9) and appropriate tests (Standard deviation; Ordinary One-way ANOVA for univariate comparison, and Two-way ANOVA for multivariate comparison followed by Tukey's or Dunnett's multiple comparisons test to assess significance; Area under the curve with standard error to compare activation patterns for multiple concentrations in titration setups). Generally, a significance level of $p < 0.05$ was applied. Higher p-values were considered not significant (ns) and are indicated as such on the graph, whereas p-values are plotted for selected significant differences in binding or activation. A Spider Web diagram was created using Microsoft Office Excel software. Figure design was adapted using Affinity Designer 2. Schematic images were created using BioRender software (BioRender.com; license holder: Katja Hoffmann).

3 Results

3.1 Establishment of the BW5147-FcγRζ reporter cell assay for CRP detection

The setup of the BW5147-FcγRζ reporter cell assay was adapted from our previously developed assays (20, 33) and modified to analyze CRP-mediated activation of FcγRs (Figure 1A). BW5147-FcγRζ reporter cells (20) expressing human FcγRI (CD64), FcγRIIaH (CD32aH), FcγRIIaR (CD32aR), FcγRIIb (CD32b), FcγRIIIaV (CD16aV), FcγRIIIaF (CD16aF), FcγRIIIb (CD16b),

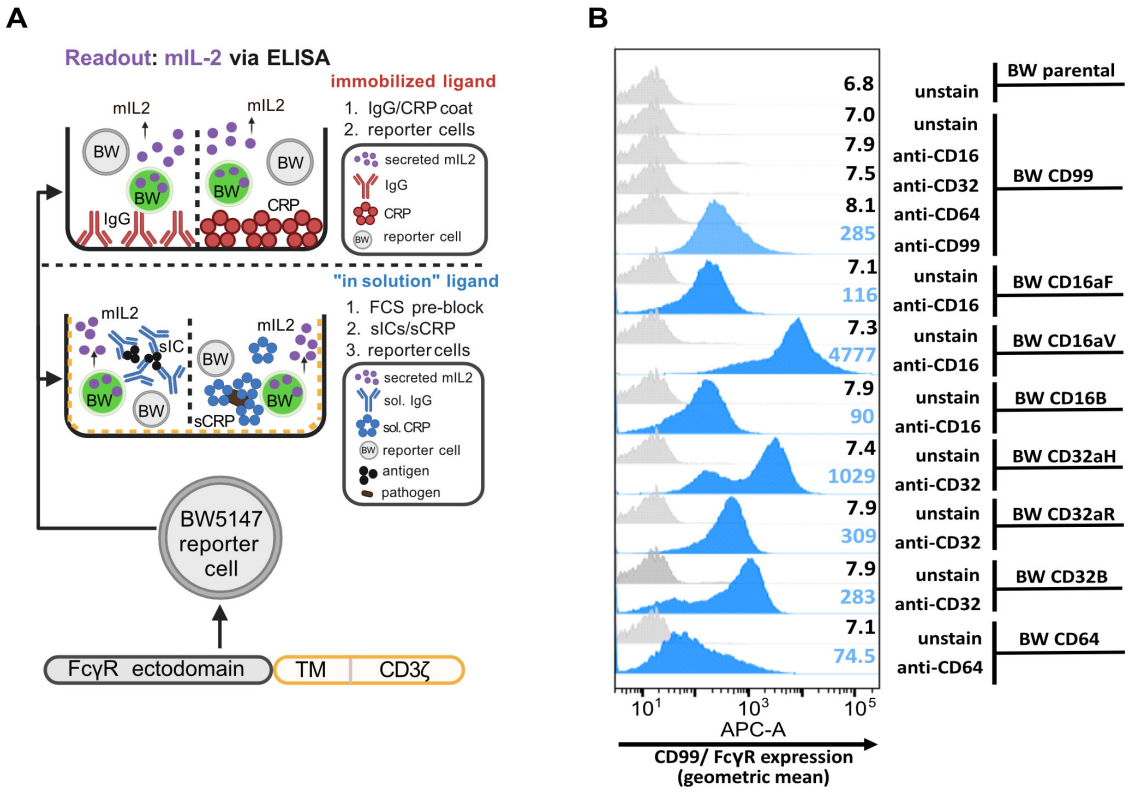

FIGURE 1
Setup of the BW5147-FcγRζ reporter cell assay and flow cytometry-based analysis of FcγR expression: **(A)** Schematic of the assay setup: BW5147 cells stably express chimeric FcγR-CD3ζ-chain receptors leading to secretion of mIL-2 upon FcγR-activation, which can be mediated by immobilized human IgG or CRP (upper schematic) as well as by soluble IgG-immune complexes (sol. ICs) or soluble CRP (alone or in complex with streptococci). The soluble assay setup requires pre-blocking of well plates with 10% FCS (lower schematic). mIL-2 levels in supernatant are measured by sandwich ELISA. **(B)** Characterization of BW reporter cells with anti-CD16/32/64- antibodies. A total of 100,000 BW5147 cells per sample were incubated with 100 µl flow cytometry buffer containing a 1:100 dilution of the respective anti-CD-APC antibody for one hour on ice. Unstained BWCD99 cells and BWCD99 cells incubated with respective anti-CD antibodies served as negative controls. Additionally, BWCD99 cells were stained with anti-CD99-APC as positive control. Cells were analyzed by flow cytometry using a FACS Fortessa instrument and FlowJo software, gating on the main population of living cells. Created in BioRender. Hoffmann, K. (2025): https://BioRender.com/bf8vz3b; https://BioRender.com/n08p187; https://BioRender.com/n6jkoc7; https://BioRender.com/lgmkfx9; https://BioRender.com/c5sm64s.

and human CD99 as a negative control, were characterized for FcγR expression by flow cytometry using APC-coupled antibodies. All BW5147 cell lines expressed the transduced extracellular domain of the respective human FcγR or human CD99 (Figure 1B). The density of FcγRs expressed on the cell surface was largely comparable, but not identical, between different cell lines. As observed before, high-affinity BW5147-FcγRI (CD64) cells expressed lower amounts of FcγRs than transfectants expressing low-affinity FcγRs, i.e., CD32 and CD16, potentially due to the additional Ig-like domain (20).

3.2 CRP-dependent crosslinking selectively activates BW5147 reporter cells expressing CD64 (*FcγRI*), BWCD32aR (*FcγRIIaR*) and BWCD32b (*FcγRIIb*), and pCRP* is the major mediator of FcγR triggering

FcγR activation occurs upon receptor crosslinking by specific ligands. This is achieved either by immobilized or by soluble multimeric FcγR ligands, e.g., IgG immune complexes (20, 33). Accordingly, immobilization of human IgG on MaxiSorp plates is the most basic BW5147-FcγRζ assay format (Figure 1A). This setup was transferred to pCRP by its immobilization on MaxiSorp wells at graded concentrations. As reported previously, all reporter cell lines became consistently activated when exposed to immobilized human IgG1 (Figure 2A, upper panel) (20, 33). In contrast, only BWCD32aR (FcγRIIaR), BWCD32b (FcγRIIb) and BWCD64 (FcγRI) responded to immobilized pCRP, whereas we saw broad unresponsiveness in BWCD16aF (FcγRIIIaF), BWCD16aV (FcγRIIIaV), BWCD16b (FcγRIIIb) and BWCD32aH (FcγRIIaH) reporter cells (Figure 2A, middle panel). When experiments were jointly analyzed (AUC of activation after normalization to mean OD of individual experiments) pCRP- mediated activation was significant for BWCD32aR (FcγRIIaR; $p<0.001$) and BWCD64 (FcγRI; $p<0.001$) cells, whereas activation of BWCD32b (FcγIIb) was clearly detectable and reproducible but did not reach significance in two-way ANOVA/Dunnett's multiple comparisons of all three ligands investigated ($p=0.212$) (Figure 2B). However, for individual analysis of pCRP as an activating ligand (one-way ANOVA/Dunnett's multiple comparisons) BWCD32b (FcγIIb) activation was significant compared to the negative control ($p=0.041$). The limit of detection for pCRP was in the nanomolar range. Activation was dose-dependent for both IgG and pCRP, respectively, but responses induced by pCRP tended to be lower than those to IgG, except for high-affinity BWCD64 cells where AUCs were similar for IgG1- and CRP- mediated activation (Figure 2B). AUCs were significantly higher for all BW cell lines for IgG compared to negative control ('no BWs'). AUCs for IgG1-mediated activation were significantly higher than for pCRP-mediated activation for all cell lines except BWCD32aR (FcγRIIaR) and BWCD64 (FcγRI) (two-way Anova/Tukey's multiple comparisons, significance levels not indicated within the graph due to space constraints). Responses caused by pCRP-mediated activation were 60-70% of maximal IgG-mediated activation for BWCD32aR and BWCD32b cell lines and about 95% for BWCD64 cells (Figure 2B). Levels of CRP-induced mIL-2 responses did not correlate with surface expression levels of FcγR on BW5147 reporter cells, i.e. comparatively low levels of FcγRI were sufficient for higher activation levels than seen with CD32aR (FcγRIIaR), and CD32b (FcγRIIb). Strikingly, activation of BWCD32a (FcγRIIa) cells strictly depended on the allelic variant, with robust CRP-mediated activation of BWCD32aR (FcγRIIaR) cells, but no response in BWCD32aH (FcγRIIaH). This binary functional difference is remarkable as the variants differ only in one amino acid at position 131. Longer titrations for selected reporter cell lines and inclusion of BWCD99 cells as a negative control are shown in Supplementary Figures 1A, B.

There is evidence that the native CRP pentamer undergoes conformational changes before its ultimate dissociation into monomeric CRP (10). CRP isoforms were found to differ in their interaction with C1q, but very little is known about the functional impact of distinct CRP isoforms on single FcγR family members interaction (10, 12, 31, 42, 43). We then explored how our assay could be used to generate insights and new hypotheses on this issue (10–12, 43). To find out more about conformational changes in the CRP pentamer induced by passive binding to MaxiSorp ELISA wells (designed for binding of medium to large sized hydrophilic biomolecules), an ELISA-based detection assay was performed using conformation-specific as well as polyclonal anti-CRP antibodies (Figure 2C). mCRP was generated as described previously (39) and concentrations of pCRP and mCRP preparations were matched using Qubit Fluorometric Quantitation. Conformation-specific monoclonal mouse anti-human CRP antibodies clone 8D8 (anti-pCRP) and clone 9C9 (anti-pCRP*/mCRP), and polyclonal goat anti-human CRP antibody (Figure 2C, upper schematic) were compared using graded concentrations of mCRP and pCRP preparations (12, 43, 44). All three CRP antibodies showed concentration-dependent binding to the coated pCRP (Figure 2C, middle panel), albeit with varying strength. mAb 8D8 recognized exclusively the inert pentamer exhibiting the weakest binding, particularly at low pCRP densities. As expected, 8D8 lost its capability to recognize CRP completely when tested with monomeric CRP (Figure 2C, lower panel). In contrast, mAb 9C9, which recognizes a neoepitope induced within the CRP pentamer and maintained after CRP fragmentation exhibited superior binding to mCRP, but also to pCRP. This finding indicates that the conformational change from pCRP to pCRP* has occurred to a relevant extent upon pCRP binding to the hydrophilic MaxiSorp surface. This observation is in line with the findings of Lv and Wang, who observed binding of both pCRP-specific and mCRP-specific antibodies upon immobilization on MaxiSorp plates and concluded that the dual antigenicity resulted from pCRP* expression rather than mixture of pCRP and mCRP (46).

As mCRP exposes the 9C9-defined neoepitope uncovered in pCRP* but has lost the 8D8-defined epitope characterizing native pCRP, we went on to investigate how activation is caused by coated mCRP compared to activation caused by coated pCRP in the BW5147-FcγRζ assay platform (Figure 2A, lower panel) Activation levels caused by mCRP were significantly diminished compared to pCRP for BWCD64 (FcγRI) cells ($p=0.001$, not

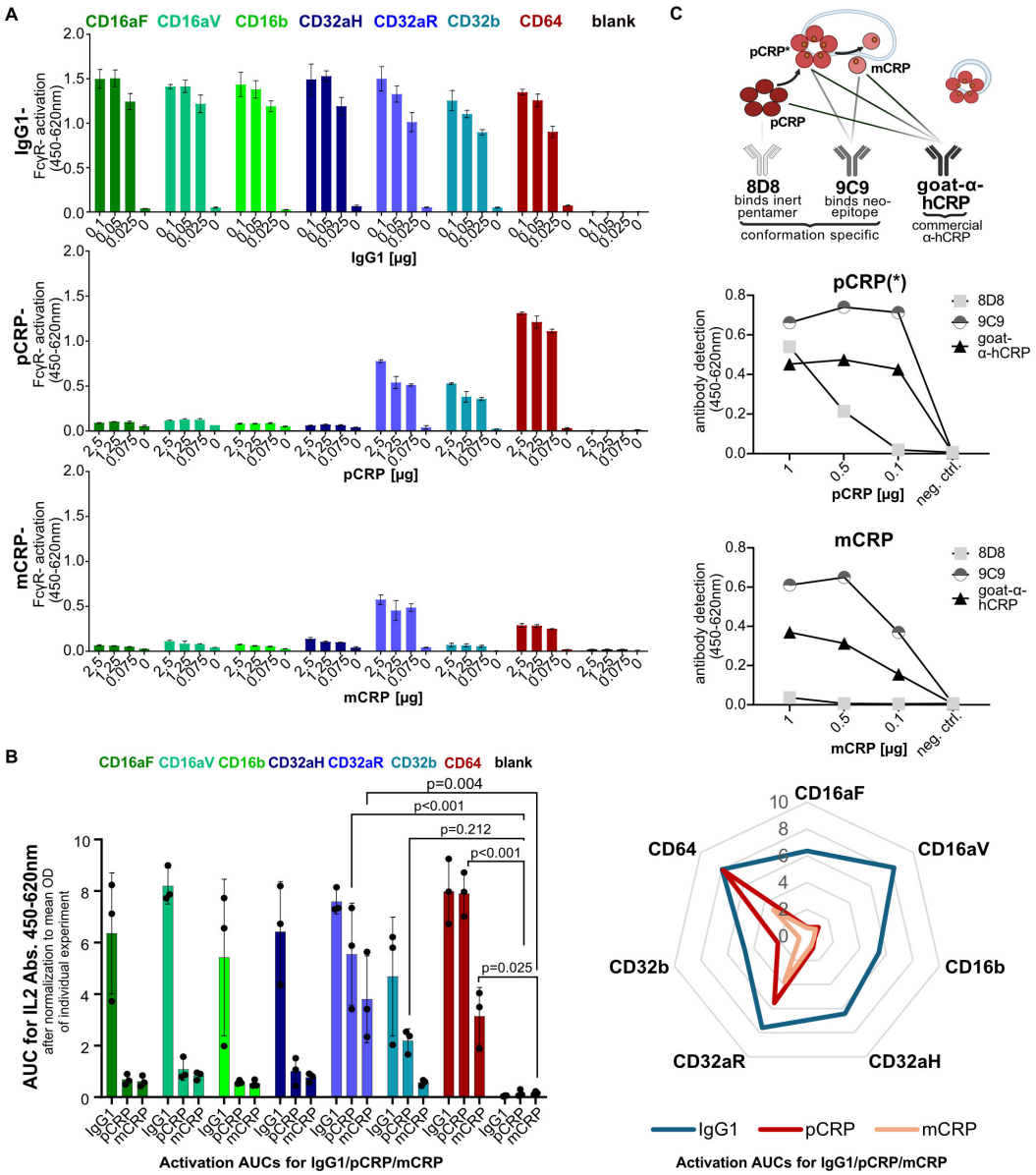

FIGURE 2
BW5147-FcγRζ reporter cell activation on immobilized IgG, pCRP and mCRP and binding of conformation specific antibodies to immobilized CRP isoforms: **(A)** Upper: mIL-2 levels produced by BW5147 cells on immobilized IgG1 (titrated from 0.1 to 0.025 µg in 50 µl medium). Each cell line was stably transduced with one FcγR only. Cell medium without BW cells ('blank') served as a negative control. Center/lower: mIL-2-levels produced by BW5147 reporter cells on immobilized pCRP (center) and mCRP (lower) (titrated from 2.5 to 0.63 µg in 50 µl medium, with concentrations matched using Qubit Fluorometric Quantitation). A total of 100,000 BW 5147 reporter cells were added to each well in 200 µl RPMI BW medium and incubated overnight at 37°C 5% CO_2. Data are shown in technical replicates (N=3) with standard deviation for one representative of at least three individual experiments for each cell line. Activation shown as OD in a sandwich mIL-2-ELISA. **(B)** Left: AUCs for activation of BW cells by immobilized IgG1, pCRP and mCRP after normalization of ODs to mean OD of individual experiment. AUCs were calculated and jointly analyzed for three independent experiments normalized to mean OD of individual experiment with three technical replicates each. Two-way ANOVA and Dunnett's multiple comparisons calculated using GraphPad Prism software. Right: Spider web plot of AUCs normalized to mean OD of individual experiment, created using Microsoft Excel Graph Software. **(C)** Upper: Schematic indicating recognition by conformation-specific monoclonal and polyclonal anti-CRP antibodies. Middle/lower: pCRP/mCRP was titrated from 1 µg to 0.1 µg/well and coated to MaxiSorp wells. Concentrations of pCRP and mCRP preparations were matched using Qubit Fluorometric Quantitation. CRP was detected using conformation specific 8D8 (anti-pCRP), 9C9 (anti-mCRP/pCRP*) and polyclonal goat anti-hCRP antibody. Created in BioRender. Hoffmann, K. (2025): https://BioRender.com/bf8vz3b; https://BioRender.com/n08p187; https://BioRender.com/n6jkoc7; https://BioRender.com/lgmkfx9; https://BioRender.com/c5sm64s.

depicted in the graph due to space constraints) and moderately diminished for BWCD32aR (FcγRIIaR) cells (p=0.357, not depicted). BWCD32b (FcγRIIb) cells showed minimal activation on coated mCRP. To exclude the possibility that mCRP preparations harmed the BW5147 reporter cells, the same amounts (20 + 20 µg; 10 + 10 µg; 5 + 5 µg) of mCRP and pCRP were coated together before testing BWCD64 reporter cells (Supplementary Figure 1C). mCRP did not appear to harm the

cells but had little effect on upregulating activation caused by pCRP. We concluded that pCRP*, as defined by mAb 9C9, represents the major conformation of CRP that triggers FcγRs, while mCRP still causes activation at clearly lower levels.

Figure 2B gives an overview of the activation profiles induced by IgG1, pCRP and mCRP comparing activation levels (AUCs) for three independent experiments after normalization to the mean OD of each experiment, shown as a bar graph (right) and a spider web plot to illustrate the patterns generated (left). Generally, activation levels caused by IgG1 were higher than for pCRP > mCRP. Activation levels varied for all ligands depending on the FcγR composition of each BW5147 reporter cell type. Consistently high activation levels were seen for IgG1-mediated activation throughout all cell lines, whereas pCRP only activated BWCD64 (FcγRI), BWCD32aR (FcγRIIaR) and BWCD32b (FcγRIIb) cell lines with higher activation levels than for mCRP, which activated BWCD32aR>BWCD64>BWCD32b cells at relatively low levels.

3.3 FcγR activation is caused by CRP itself- but detecting CRP binding in ELISA does not correlate with FcγR activation

To ensure that the observed reporter cell activation was solely caused by CRP itself and not by another potentially activating factor present in the CRP preparation used (US Biological Life Sciences), which is generated from patient ascites/pleural fluid, we compared the previously used CRP composition with recombinant CRP produced in *E. coli* (US Biological Life Sciences) with respect to their activation efficacy of BWCD64 and CD32b reporter cells. Patterns of activation for recombinant CRP precisely mirrored those of CRP purified from human ascites, indicating that CRP is necessary and sufficient to cause activation of FcγRs (Figure 3A). To exclude any effect of other components, e.g., sodium azide, the CRP preparation purified from ascites/pleural fluid was dialyzed against PBS with Ca^{2+}/Mg^{2+} through a dialysis membrane overnight as described previously (39). Dialysis had no significant effect on activation levels, confirming that CRP itself was the cause of the activation (Supplementary Figure 1D). As previous studies have shown that biological effects attributed to CRP are actually caused by LPS contamination of recombinant CRP preparations (47), we further excluded any effect of LPS on the BW5147 reporter cell assay system (Figure 3B). To this end, we added graded EU endotoxin units of LPS to our ascites/pleural fluid purified CRP preparation and additionally tested the potential effect of LPS alone on our cells by adding graded EU units/ml to the culture medium of the BWCD64 cells in this assay. LPS had no effect on FcγR-activation responses.

The BW5147-FcγRζ assay demonstrated activation of FcγRs CD32aR, CD32b and CD64, but not of CD16aF, CD16aV CD16b and CD32aH by pCRP. However, interaction of pCRP with CD16 as well as CD32aH has been previously reported (23, 24). Lu et al. observed binding to CD16, as did Temming et al., who additionally proposed a potential role in enhancement of IgG-mediated FcγR-activation through the interaction with pCRP. Nevertheless, CD64 and CD32a are proposed as the major CRP interactors, with a long-standing debate about the relevance of the CD32a allelic variants for both binding and activation (23, 24, 48–50). Since our assay system allows for unambiguously attributable responses of individual FcγRs and the available data on binding and activation were controversial, we set out to differentiate CRP-binding by and CRP-dependent activation of FcγRs as obtained in a comparable experimental setup.

To this end, the FcγR binding pattern to immobilized IgG1 (Figure 3C) was compared to immobilized pCRP (Figure 3D) and mCRP (Figure 3E) in a setup analogous to the activation setup, i.e. coated IgG1 and CRP and recombinant FcγRs added in solution for binding. AUCs for the individual binding curves were calculated (Figures 3C–E, lower panels). All recombinant his-tagged FcγR molecules showed binding to IgG1. Interestingly and in accordance with literature, the binding pattern observed for IgG1 (CD64>CD16aF/V>CD32aH>CD16b>CD32aR/CD32b) was different to the one of pCRP (CD64>CD16b>CD16aF>CD32aR >CD16aV/CD32aH/CD32b). The binding pattern for mCRP was similar to that of pCRP with slightly lower ODs. For IgG, in accordance with literature (51–53) binding for both allelic variants of CD32a was clearly detectable, with higher binding of the CD32aH allelic variant. The OD values measured in ELISA for IgG1-binding to the tested FcγRs were significantly higher than for pCRP. This observation correlates with the activation levels observed in the BW5147-FcγRζ activation assay and generally supports lower affinities of FcγR for pCRP. All human FcγRs bound to pCRP and mCRP with relatively lower strength as indicated by lower OD values. Binding of pCRP to CD64 showed the highest ODs/AUC, followed by CD16b>CD16aF>CD32aR> CD16aV/CD32aH/CD32b. At a generally low level, CRP binding to the CD32aR allelic variant was higher than to CD32aH, but this difference did not reach significance. Notably, ELISA binding in this very comparable setup did not correlate with FcγR triggering in the BW5147-FcγRζ reporter assay. E.g., pCRP-binding of CD16b was clearly stronger than binding of CD32b. However, BWCD16b (FcγRIIIb) cells were not activated by pCRP, whereas pCRP did readily activate BWCD32b (FcγRIIb) cells (Figure 2A). Thus, binding as detected by ELISA seems to be necessary but not sufficient for FcγR triggering.

3.4 Divergent FcγR activation profiles of solution-phase ICs and CRP, with pCRP* as the key activating isoform.

The preparation ("blocking") of hydrophilic MaxiSorp surfaces with saturating amounts of serum proteins allowed us to detect multimeric immune complexes in solution (sICs) as activating ligands of certain FcγRs (20, 37). To investigate whether unbound pCRP in solution phase is also capable of cross-linking FcγRs, the protocol established for sICs was adapted for use in a pCRP context. (i) Synthetic sICs, (ii) soluble pCRP and (iii) pCRP-*Streptococcus pneumoniae* complexes (39), respectively, were added to serum-blocked ELISA wells (Figure 4A). For the third approach, to allow ligand binding to the B-face of the molecule and promoting the

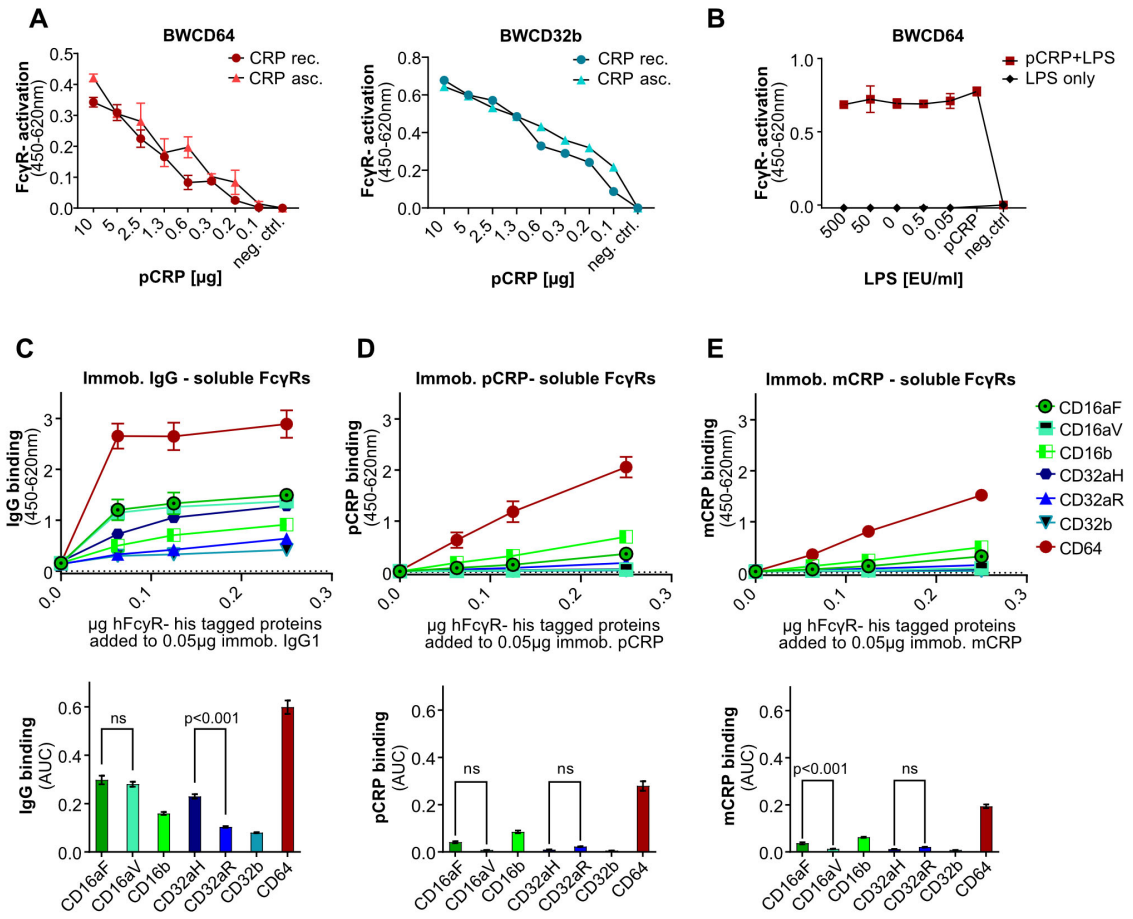

FIGURE 3
Effect of CRP source and addition of LPS on BW5147-FcγRζ activation and binding of epitope-tagged FcγRs to immobilized IgG, pCRP or mCRP: **(A)** BWCD64 and BWCD32b cell activation by recombinant human pCRP produced in *E coli* and pCRP purified from human ascites/pleural fluid. pCRP was coated in graded amounts in PBS. A total of 100,000 BW5147 reporter cells were added to each well and incubated overnight. **(B)** Addition of graded amounts of LPS to a pCRP (5 µg/well) preparation was compared with activation caused by LPS only using BWCD64 reporter cells. LPS was added at the concentrations stated. EU units as stated by supplier: 1 mg/ml=1x10^6 EU/ml. 100,000 BW5147 cells were added to each well and incubated overnight. FcγR-activation shown as OD in sandwich mIL-2-ELISA after subtraction of background. **(C–E)** Titration of recombinant His-tagged hFcγRs from 0.25 µg to 0 µg in 50 µl PBS; binding to 0.05 µg coated IgG1/pCRP or mCRP/well. ODs for 450–620 nm. Data shown with standard deviation for two individual experiments with three technical replicates each. Calculation of AUCs of the binding curves using GraphPad Prism software. AUC for N=6 with standard error. Ordinary one-way ANOVA and Tukey´s multiple comparisons test carried out using GraphPad Prism software and selected significances are indicated on the graph.

formation of pCRP*, pCRP was pre-incubated with *Streptococcus pneumoniae serotype 27* containing high amounts of 'C'-cell-wall-polysaccharide (CWPS). As observed before (20), soluble ICs formed by recombinant antigen and a recombinant monoclonal antibody, i.e., TNFα trimers and Infliximab, efficiently activated BWCD16aV (FcγRIIIaV) and BWCD32b (FcγRIIb) but neither BWCD32aR (FcγRIIaR) nor BWCD64 (FcγRI) reporter cells (Figure 4A, upper panel). In contrast, pCRP in solution phase and pCRP pre-bound to streptococci activated BWCD64> BWCD32aR>BWCD32b>BWCD16aV reporter cells, with BWCD16aV (FcγRIIIaV) and BWCD32b (FcγRIIb) only being slightly activated (Figure 4A, middle and lower panel). Therefore, the FcγRs that can be activated by pCRP and sICs in the solution phase are clearly distinct. Overall activation levels induced by sICs were higher than those caused by soluble CRP. Levels of BWCD64 (FcγRI) activation were substantially higher after pre-incubation with streptococci. This trend was less pronounced for BWCD32aR (FcγRIIaR) and BWCD32b (FcγRIIb) (Figure 4A, lower panel). Subsequently, activation levels induced by immobilized pCRP were compared with those induced by pCRP in solution or in solution pre-incubated with streptococci for recognition by BWCD64 (FcγRI) reporter cells (Figure 4B). As observed before, pre-incubation of pCRP with streptococci upregulated activation levels as compared to soluble pCRP only. This effect reached significance for 5 µg pCRP (p=0.044), but not 10 µg and 20 µg of pCRP (p=0.102 and p=0.204, respectively, Two-way ANOVA and Tukey`s multiple comparisons test). However, the activation induced by immobilized pCRP on MaxiSorp surfaces was significantly higher than both solution-phase approaches (with and without pre-incubation with streptococci) for all pCRP

10.3389/fimmu.2025.1598605

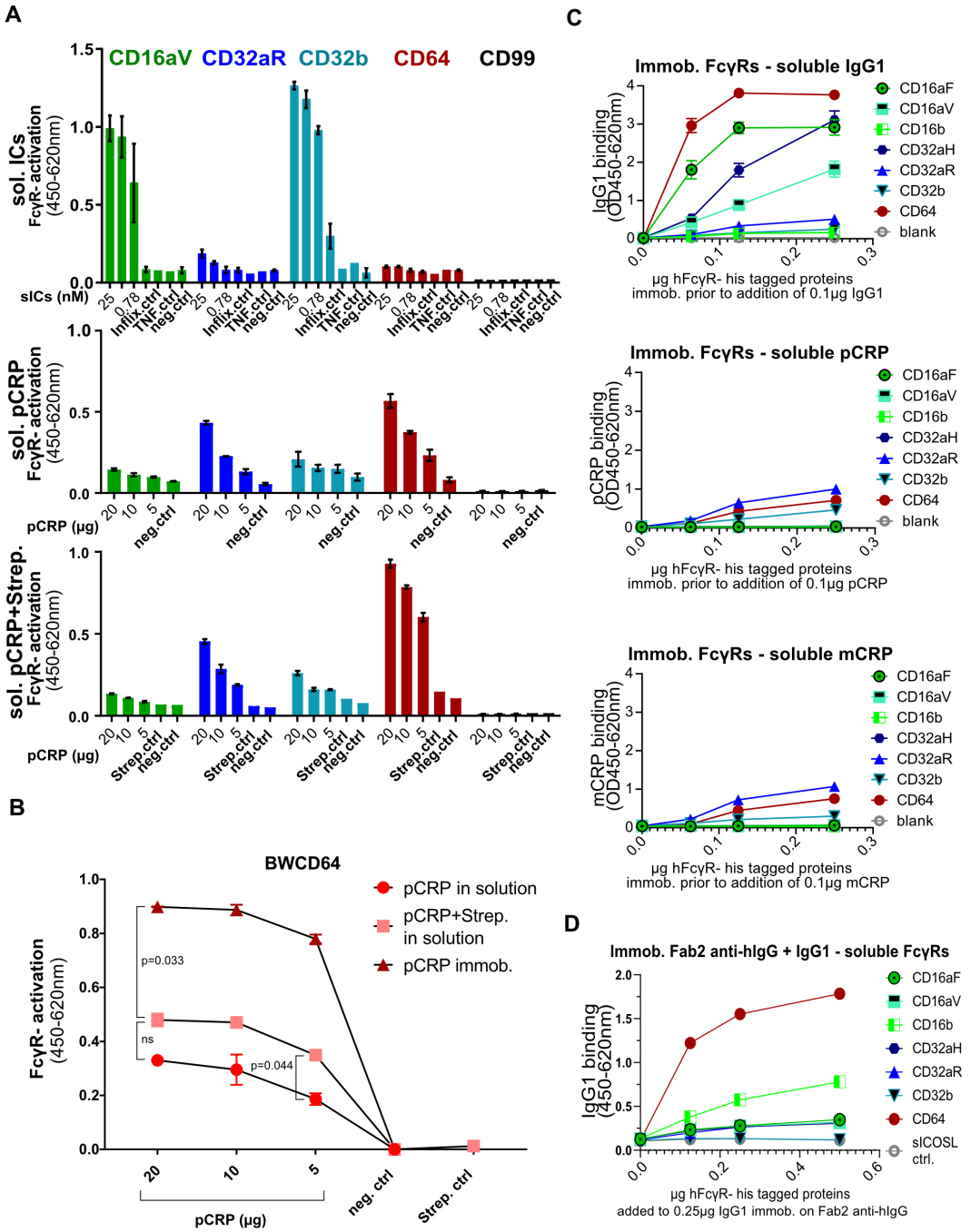

FIGURE 4
In solution phase BW5147-FcγRζ reporter assay for sol. ICs, sol. pCRP and sol. pCRP-streptococci complexes and binding of soluble IgG, pCRP and mCRP to coated His-tagged FcγRs: **(A)** MaxiSorp ELISA plates were saturated with 10% FCS. sICs as well as soluble CRP-streptococci complexes (with *S. pneumoniae* serotype 27) were allowed to incubate for two hours at RT prior to adding them to the experiment. Upper: sICs were added in 100 µl/well medium and consisted of 25 nM Infliximab (149.1 kDa) and 50 nM TNFα monomer (17.5 kDa) to ensure 1:1 stoichiometry (per ml stock of 25 nM ICs: 0.875 µg TNFα + 2.66 µg Infliximab). Selected values of log2 titration depicted in this graph. Central: pCRP in solution assay without pre-incubation with streptococci. CRP was added in 100 µl medium. Lower: 10 µl of streptococci were added to 20/10/5 µg of CRP. Complexes were added to wells in 100 µl medium. 100,000 BW5147 reporter cells were added to each well in another 100 µl of medium. Activation shown as OD in sandwich mIL-2-ELISA. Data are shown with standard deviation (N=2; N=3 for ICs). **(B)** BWCD64 activation assay comparing coated pCRP and soluble pCRP/soluble pCRP-streptococci complexes (N=2). Ordinary one-way ANOVA and Tukey´s multiple comparisons test carried out using GraphPad Prism software and selected significances are indicated on the graph. **(C)** Titration of His-tagged hFcγRs from 0.25 µg to 0 µg and coating to ELISA wells. Addition of 0.1 µg IgG1 (upper), pCRP (central) or mCRP (lower) and detection via goat-anti-hCRP antibody and DAG-POD for CRP and anti-human-IgG-POD for IgG1. ODs for 450–620 nm. Data shown with standard deviation for two individual experiments with three technical replicates each. **(D)** Coating of goat $F(ab)_2$ anti-human IgG (Fab-specific) (0.1 µg in 50 µl/well) was followed by blocking and addition of hIgG1 (0.25 µg in 50 µl/well) before addition of soluble human FcγR-His-proteins titrated as stated in the graph. Detection with rabbit anti-His antibody and GAR-POD was performed. Data shown in technical triplicates for two individual experiments.

concentrations investigated (not all p-values are indicated on the graph for space constraints, p-values for 20 µg pCRP: p=0.005 and p=0.033 for comparison of immobilized pCRP- mediated activation to soluble pCRP only and soluble pCRP pre-incubated with streptococci, respectively). As pre-incubation with streptococci as well as immobilization on well surface both favor pCRP* conformation these results support pCRP* likely being the FcγR activating CRP conformation.

To investigate, whether the 'in solution' activation could be correlated with an 'in solution' binding approach of CRP to FcγRs, we reversed the setup of our binding assay established before (Figures 3C–E). After coating MaxiSorb wells with recombinant His-tagged human FcγR proteins, IgG1 (Figure 4C, upper), pCRP (Figure 4C, center) or mCRP (Figure 4C, lower) were added and binding was investigated through goat anti-hCRP/DAG-POD or anti-human-IgG-POD for CRP and IgG, respectively. AUCs are compared in Supplementary Figure 2. For IgG1, the pattern observed in this 'reversed setup' was widely comparable to the pattern in the initial binding assay (CD64>CD16aF>CD32aH>CD16aV>CD32aR>CD16b>CD32b). Binding of the CD32aH allelic variant was significantly higher than for the CD32aR allelic variant ($p<0.001$; One-way ANOVA and Tukey´s multiple comparisons for AUCs; Supplementary Figure 2), as observed previously, whereas – in contrast to published literature (51) - a stronger binding to the CD16aF than to the CD16aV allelic variant ($p<0.001$) was seen in this setup, suggesting that the experimental conditions of the chosen assay setup could influence the extent of binding. To compare the effect of presentation of binding partners, human IgG1 was immobilized using goat $F(ab)_2$ anti-human IgG (Fab-specific) followed by the addition of soluble human FcγR-His-proteins (Figure 4D). Now CD16aV binding matched CD16aF binding. This confirms the impact of the presentation of the binding partners in these test formats and the need to compare different setups. Notably, for both pCRP and mCRP, the binding pattern obtained in this 'reversed setup' largely mirrored the activation pattern, with CD32aR, CD64 and CD32b showing the highest binding affinities (Figure 4C). Thus, although FcγR activation is generally strongest upon ligand immobilization, binding of soluble ligands to immobilized FcγR confirms the receptor crosslinking potential of ligands.

3.5 CRP ligand-ligand interactions in FcγR activation

Since pCRP, monomeric IgG, and soluble ICs represent distinct ligands that share the same immunological compartments, they may be recognized simultaneously by FcγRs. We applied the BW5147 reporter cell assay system to explore interactions between these ligands. First, the effect of pCRP in solution on activation caused by soluble ICs was investigated. As sICs were shown to efficiently activate BWCD16aV (FcγRIIIaV) and BWCD32b (FcγRIIb) cells (20), these reporter cell lines were chosen to investigate a possible inhibitory effect of pCRP. Two different concentrations of sICs (3 nM and 0.5 nM) were chosen to ensure that the effect of the addition of pCRP was analyzed under conditions of both high and low sIC-mediated activation. sICs were generated prior to addition of different concentrations of pCRP before adding BWCD16aV (FcγRIIIaV) or BWCD32b (FcγRIIb) reporter cells. pCRP in solution did not show any impact on sIC-mediated activation of both FcγRs tested, even when high concentrations of pCRP were added (Figure 5A).

Next, we investigated the impact of soluble, monomeric IgG on activation caused by (i) immobilized pCRP or (ii) unbound pCRP in solution phase. For this pCRP was coated (Figure 5B) or added to FCS-pretreated MaxiSorp plates keeping pCRP in solution (Figure 5C) before graded amounts of purified polyclonal human IgG (cytotect®), monoclonal Rituximab IgG1 (Rtx) or monoclonal Rtx IgA as control were added. None of these immunoglobulins caused a decrease in BWCD64 (FcγRI) activation levels mediated by immobilized pCRP (Figure 5B). A slight, non-significant increase in activation, especially seen with Rtx IgG1 ($p=0.066$), is likely attributable to residual Rtx binding after blocking of CRP-coated ELISA wells. However, when testing the activation caused by pCRP in solution, cytotect® caused a significant ($p=0.011$ for 5µg), dose-dependent decrease in BWCD64 (FcγRI) activation (Figure 5C). The addition of Rtx IgG1 also caused a significant decrease in activation levels ($p=0.047$), though this effect was less pronounced than for polyclonal IgG in cytotect®. Activation levels caused by solution-phase pCRP supplemented with Rtx IgA as a control remained unaffected (Figure 5C).

4 Discussion

The role of CRP as an activating ligand of FcγRs has been a matter of debate for decades (21–27, 48). Unraveling the bimolecular interactions between FcγRs and CRP is complicated by a number of intricate details. The confusion stems from complex experimental settings with different readouts, but also from the variety of existing FcγRs, different types of immune cells expressing different ranges of FcγRs, the influence of FcγR ligands other than CRP, the variability of CRP preparations, and finally CRP itself, which acquires intermediate conformations and isoforms, including pCRP, pCRP*, and mCRP, with different biophysical properties and functional consequences. Experimental setups using antibody-based detection systems are delicate because they may affect the Fc-binding capacity of human FcγRs, and there is potential for antibody-species cross-reactivity [e.g., binding of mouse IgG (54)]. Furthermore, the binding of CRP to human FcγRs is low-affinity and, as an opsonin with less binding specificity than immunoglobulins (5, 55), CRP interacts with many pathogen- or damage-associated patterns [e.g. apoptotic cells, oxLDL, phosphocholine groups (55, 56)] that may be present in the reagents used, making low affine binding of FcγRs to CRP even more difficult to detect. Moreover, CRP and CRP-bound molecules interact with multiple cellular receptors, such as different FcγRs. In

10.3389/fimmu.2025.1598605

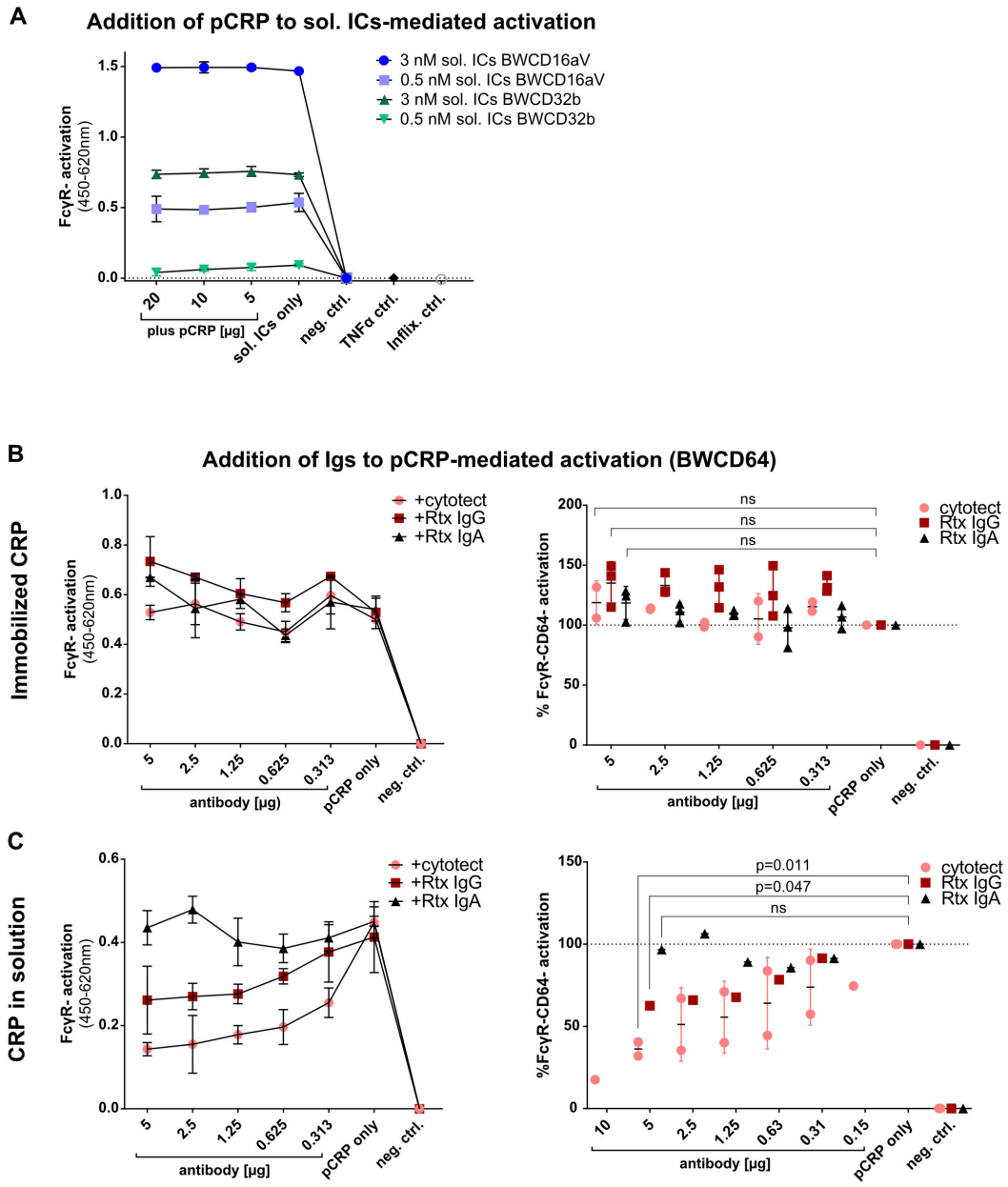

FIGURE 5
Competitive binding assays for distinct FcγR-ligands: **(A)** BW5147-FcγRζ reporter assay "in solution" with sol. ICs and added pCRP: ELISA wells were blocked with 10% FCS. Sol. ICs were allowed to incubate for one hour at RT in 100 µl BW medium prior to adding pCRP for 30 minutes. Both were added to 100 µl BW medium with 100,000 BWCD16aV or BWCD32b cells. sICs consisted of 3/0.5 nM Infliximab (149.1 kDa) and 6/1 nM TNFα monomer (17.5 kDa) to ensure 1:1 stoichiometry. Data are shown with standard deviation (N=2). Activation shown as OD in sandwich mIL-2-ELISA minus background control. **(B, C)** pCRP was immobilized **(B)** or added 'in solution' in 50 µl BW medium to pre-blocked wells **(C)**. 5 to 0 µg immunoglobulins cytotect®, Rtx IgG or Rtx IgA were added in 100 µl **(B)** /50 µl **(C)** BW medium 15 minutes prior to addition of 100,000 BWCD64 cells in 100 µl medium. Representative individual experiments in technical replicates (N=2) are shown on the left. The right side summarizes three/two independent experiments for activation caused by immobilized pCRP [setup **(B)**] or soluble pCRP [setup **(C)**] after normalization to "CRP only". Activation is caused by 10 µg coated or 15 µg soluble pCRP per well, respectively. Ordinary one-way ANOVA and Tukey´s multiple comparisons test carried out using GraphPad Prism software for 5 µg antibody results compared to "CRP only" control.

addition, CRP-mediated amplification of TLR signaling (27) complicates the attribution of the resulting signaling cascades in cells. In this situation, a highly reductionist assay approach, as explored here, is essential to analyze and quantify CRP-mediated molecularly defined interactions with individual FcγRs leading to receptor cross-linking.

4.1 Future applications of the BW5147-FcγRζ reporter cell assay

The BW5147-FcγRζ reporter cell panel allows rapid screening of FcγR types and isoforms and their discrimination into CRP-receptive, CRP-unresponsive and decoy FcγRs (Table 1; Figure 6).

TABLE 1 FcγR activation profiles induced by distinct ligands.

FcγR	CD16aF (*FcγRIIIaF*)	CD16aV (*FcγRIIIaV*)	CD16b (*FcγRIIIb*)	CD32aH (*FcγRIIaH*)	CD32aR (*FcγRIIaR*)	CD32b (*FcγRIIb*)	CD64 (*FcγRI*)
Immob. IgG	+	+	+	+	+	+	+
Immob. p/mCRP	-	-	-	-	+	+	+
Sol. ICs	**NA**	+	**NA**	+	(+)	+	-
Sol. pCRP	**NA**	-	**NA**	**NA**	+	(+)	+

FcγR-activation observed in BW5147-FcγRζ reporter assay for coating ('crosslinking') of IgG or p/mCRP, as well as soluble ICs (TNFα+Infliximab) and soluble pCRP (+/- pre-incubation with *S. pneumoniae* serotype 27). Activation "+" is defined as OD (Λ=450–620 nm) 0.3-2.0 higher than background level OD, threshold activation "(+)" is defined as OD=0.15-0.3 higher than background level, no activation "-" as OD<0.15 higher than background. NA, no data available.

Key advances of this reporter system include high accuracy and hierarchical resolution of FcγR type-specific activation compared to traditional indirect assessments such as CRP binding, and a scalable and quantifiable methodology that provides flexible high-throughput readouts such as mouse IL-2 detection in cell culture supernatants or CD69 plasma membrane densities (20). FcγR profiling and classification have important implications for a better understanding of pCRP in immune defense, inflammation, and autoimmune disorders. The incorporation of Fc-less Fab fragments from conformation-dependent CRP-specific monoclonal antibodies (12, 44, 45) in the BW5147-FcγRζ assay may allow more precise conclusions to be drawn about the intramolecular steps that ultimately lead to FcγR cross-linking. This approach may provide further insight into the molecular sequence of events leading from native pCRP to pCRP* to its degradation and finally to mCRP, which was found to be less efficient in activating FcγRs. Likewise, pharmaceutical CRP inhibitors such as phosphocholine mimetics (40), and physiological modulators like Ca^{2+} and C1q (23, 57) can be analyzed and screening for new drugs with superior efficacy will be possible. Although it has unique advantages, the reduction of an experimental set-up to a certain "necessary minimum" raises the question of the relevance of factors not taken into account. The relevance of this fact can be seen in cases where CRP does not exert a function alone, but rather affects the interplay of different ligands and receptors, e.g., enhancing the activation caused via TLRs (27) or in the interaction of FcγRs and C5a-receptor (58). This might be relevant for CRP- mediated activation of non-classical, CD16-positive monocytes and interaction of CRP isoforms with NK cells. The lack of CRP-mediated activation of CD16 isoforms in our reductionistic setup raises the question of potential co-receptors, like CD88/C5aR1 needed for activation or dependency on lipid rafts (59, 60). While not all scenarios can be addressed in our setup, in cases where CRP co-engages with receptors, co-expression of such immune receptors by BW5147-FcγRζ reporter cells may be feasible in the future.

4.2 CRP profiles of individual FcγRs as revealed by the BW5147-FcγRζ reporter cell assay

The BW5147-FcγRζ reporter assay allows for individual exploration of CRP-FcγR interaction resulting in effective receptor crosslinking rather than simple CRP binding. In agreement with the literature (21–24, 27), we observed a readily induced activation of CD64 (*FcγRI)* and FcγRs CD32a and CD32b (*FcγRII*) but not CD16aF, CD16aV, and CD16b (*FcγRIII)* (Table 1; Figure 6). Pronounced

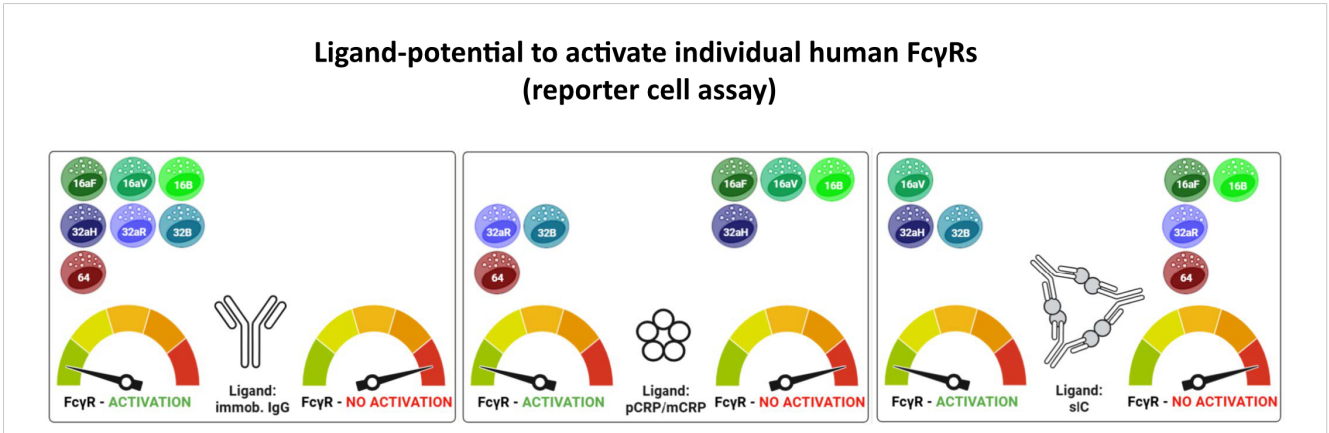

FIGURE 6
Graphical abstract summarizing FcγR- activation patterns for IgG, p/mCRP and soluble ICs. Created in BioRender. Hoffmann, K. (2025): https://BioRender.com/bf8vz3b; https://BioRender.com/n08p187; https://BioRender.com/n6jkoc7; https://BioRender.com/lgmkfx9; https://BioRender.com/c5sm64s.

differences were noted concerning FcγRII/CD32. The inhibitory FcγR CD32b as well as the activating allelic variant CD32aR responded to pCRP, but CD32aH did not. Again, this finding confirms earlier reports (23, 24, 26, 27). This allelic restriction was also observed in the 'reverse' ELISA binding assay, where CD32aR binding to coated CRP was in clear contrast to the very slight binding to CD32aH (Figure 4, less pronounced in the 'non-reversed' setup of Figure 3). Even though CRP binding to CD16aF or CD16b appeared stronger than CD32b in the 'standard' ELISA binding assay, no receptor crosslinking could be detected in this setting, whereas the FcγRs showing the highest binding affinity to CRP in the 'reverse' setup - CD32aR, CD64 and CD32b - were readily activated in the BW5147-FcγRζ reporter cell assay. Thus, the 'in solution' binding potential might be indicative of subsequent FcγR activation in this setting.

4.3 Insights into CRP conformation causing FcγR activation

While binding to and activation of FcγRs by CRP has been reported, little is known about the conformational isoforms of CRP that are capable of triggering FcγRs. Binding studies have analyzed the interaction of non-ligand-bound pCRP (23, 24), whereas experimental systems of CRP-mediated FcγR activation have often used ligand-bound CRP after pre-incubation with CWPS (27), streptococci (26) or Zymosan (23). Although binding to these ligands favors the formation of pCRP* conformation, as has been described for binding to PC groups on activated cell membranes and microvesicles (10), the conformation of the CRP isoform(s) that cause activation of individual FcγRs remains elusive.

Here, we present several lines of observation pointing to pCRP* as the major FcγR-activating CRP isoform. First, compared to pCRP in the solution phase, FcγR activation was significantly higher for immobilized pCRP on hydrophilic MaxiSorp surfaces. Second, pre-incubation with streptococci, likely favoring pCRP* conformation, increased activation levels compared to soluble pCRP. Third, activation levels caused by immobilized pCRP were higher than for immobilized mCRP. Intriguingly, conformation-specific mAbs, i.e., anti-pCRP antibody clone 8D8 binding the inert pentamer and anti-pCRP*/mCRP ('*neoepitope*') antibody clone 9C9, revealed the simultaneous presence of both isoforms after coating of pCRP to MaxiSorp wells. The coating of MaxiSorp surfaces with mCRP confirmed exclusive recognition by mAb 9C9 at comparatively low levels of FcγR triggering (Figure 2C), supporting the notion that 9C9 reactive pCRP* is closely associated with FcγR activation. This notion is consistent with the findings of Lv and Wang, who compared binding pattern of pCRP- as well as mCRP/pCRP*-specific mAbs upon immobilization on hydrophilic MaxiSorp plates (46). Considering the plastic surface properties, the time course of the coating inducing conformational changes and the lack of binding of soluble pCRP by immobilized mCRP, they concluded that the dual mAb antigenicity of 9C9 and 8D8 is caused by pCRP* rather than mixture of pCRP and mCRP (46). Thus, surface immobilization on plastic surfaces is suggested as a simple way to generate pCRP* *in vitro*, mimicking the process that takes place on cell membranes *in vivo* (46). Contrary to mCRP, Lv and Wang found surface immobilized pCRP* to bind solution phase pCRP. As the amounts of CRP used in our studies were about ten times higher than those employed in binding studies by Lv and Wang, association of native pCRP molecules in solution phase to coated pCRP* could have occurred during our coating process, explaining why 8D8 reactive material is found upon immobilization of higher amounts of CRP to plates. This resembles *in vivo* scenarios on cell membranes or pathogen interfaces, with native pCRP molecules changing conformation towards the pCRP* isotype upon binding and subsequently facilitating the recruitment of further pCRP molecules. This fconcept reflects the coordination of both, the opsonic activity of pCRP* followed by effective crosslinking of FcγRs as essential mediators of phagocytosis.

Increasing evidence indicates that mCRP is initiating most pro-inflammatory actions of CRP as highlighted by its increased binding capacity to C1q and exposure of the cholesterol-binding sequence (7, 61). Accordingly, mCRP is considered the relevant isoform of CRP in the regulation of local inflammation. Our findings could extend this concept: the data suggest that pCRP/pCRP* is generally also capable of mediating relevant immune effector functions via FcγR-bearing cells, and that mCRP-mediated activation of FcγRs is even lower than for pCRP*. In conjunction with the known differences in half-life between pCRP and mCRP the results suggest that CRP isoforms might trigger separate effectors, leading to step-by-step cascades of activation and decline.

4.4 Ligand-ligand interactions of CRP

IgG, CRP and soluble ICs are independently generated FcγR-ligands present within the same immunological compartments. This could allow for competitive binding and ligand displacement. We investigated the impact of these three ligands on activation mediated by any other one of the three. Interestingly, pCRP in the solution phase could not reduce the dominant activating effect of sICs on FcγRIIb/IIIaV (Figure 5A). However, conversely, pCRP-dependent activation of FcγRI showed significant inhibition by monomeric IgG but not by IgA used as a control. Intriguingly, the IgG levels employed in our experiments were in the range of 2.5 mg/dl which is at least one order of magnitude lower than the normal range of IgG levels in human serum (407-2,170 mg/dl) (62). Consequently, IgG may inhibit native pCRP-mediated activation even more pronouncedly than was documented in our experimental setting. Immobilization on MaxiSorp ELISA plates, however, enabled pCRP to activate FcγRI even in the presence of high concentrations of monomeric IgG (Figure 5B). Again, this observation along with the fact that *Streptococcus pneumoniae* serotype 27 increased pCRP bioactivity in the solution phase supports the concept that the conformational change of pCRP into pCRP* strongly increases its potency to crosslink FcγRs.

Notably, in the presence of physiological IgG concentrations found in plasma soluble pCRP has only negligible FcγRI/CD64 activating capabilities, implying an important anti-inflammatory role of IgG on CRP-dependent FcγR activation. In contrast, locally

immobilized pCRP in a pCRP* conformation readily acquires FcγRI/CD64 activating capabilities, unaffected by the presence of monomeric IgG. The findings highlight the role of pCRP* for FcγR activation in localized inflammatory processes.

4.5 Limitations of the BW5147 FcγRζ reporter cell-based CRP detection

Limitations of the assay platform are evident when testing native human material, e.g., sera and other liquid specimens containing a variety of different proteins and immunoglobulins present. Additionally, for solution-phase examinations we only observed FcγR activation by pCRP when using relatively high concentrations of pCRP (>100 μg/ml), which are only present in patients under certain conditions, e.g., severe inflammation or sepsis. Competing, abundant FcγR ligands with higher affinities than pCRP, like IgG or sICs, are consistently present in patient's liquid biopsies. Favored by the fact that BW5147 cells are largely inert to human cytokines, the BW5147-FcγRζ reporter cell platform has been successfully applied and validated for the highly sensitive detection of virus-specific IgG in serum, sICs in patient and animal samples, and viral FcγR ligands (21, 34, 35, 37, 63, 64). The presence of such ligands with high FcγR affinity in native clinical materials could easily cause confounding effects on BW5147-FcγRζ reporter cells, making the attribution of measured bioactivities to pCRP difficult or even impossible. Nevertheless, it will be useful in the future to carefully explore possible applications of the new test system by combining it with quantitative, highly sensitive CRP assays in patient-derived material or for clinical research purposes.

4.6 Conclusions

Key advances of this reporter cell system include (i) its high accuracy and resolution of FcγR type-specific activation, (ii) a scalable and quantifiable assay with flexible high-throughput readouts in the nanomolar range, (iii) a reporter system sensitive to CRP isoforms, (iv) a comprehensive panel including all human FcγRs, and (v) a test system that allows easy integration of additional FcγR ligands and modifiers of CRP-mediated activation. In practice, the platform is suitable for implementation in small or large screening setups in research laboratories. This reporter cell approach allows for future adaptations, as the FcγR-bearing reporter cells can be engineered with additional CRP interactors and alternative reporter modules to optimize the methodology for specific applications.

Data availability statement

The raw data supporting the conclusions of this article will be made available by the authors, without undue reservation.

Ethics statement

Ethical approval was not required for the studies on animals in accordance with the local legislation and institutional requirements because only commercially available established cell lines were used.

Author contributions

AH: Writing – original draft, Writing – review & editing, Methodology, Investigation. JS: Writing – review & editing, Investigation. JZ: Methodology, Writing – review & editing. KP: Methodology, Writing – review & editing. JT: Writing – review & editing, Methodology. PK: Methodology, Writing – review & editing. SE: Writing – review & editing, Methodology, Supervision. KH: Writing – review & editing, Funding acquisition, Writing – original draft, Methodology, Supervision, Conceptualization, Investigation. HH: Funding acquisition, Writing – original draft, Methodology, Supervision, Conceptualization, Writing – review & editing. HC: Writing - review & editing, Investigation, Formal analysis.

Funding

The author(s) declare that financial support was received for the research and/or publication of this article. This work was supported by the German Research foundation (DFG) through FOR2830, HE 2526/9–2 and "NaFoUniMedCovid19" (FKZ: 01KX2021 - COVIM to H.H). Further support was received in personal grants to SUE from the German Research Foundation (DFG) DFG EI 866/9–1 and EI 866/10-1. AH was supported by a stipend of the Cusanuswerk. JS was supported by a stipend of the University of Freiburg according to the Landesgraduiertenförderungsgesetz.

Acknowledgments

We are grateful to Dr. Mark van der Linden, National Reference Center for streptococci, Department of Medical Microbiology, University Hospital (RWTH), Aachen, for providing *S. pneumoniae*. We thank Prof Lawrence A. Potempa, College of Pharmacy, Roosevelt University, Schaumburg, IL, USA for kindly providing monoclonal antibodies detecting specific CRP conformations (clone 8D8 and 9C9). We are grateful to Sheena Kreuzaler for technical assistance and support for mCRP generation. We thank Verena Horner for her support with mCRP purification. Mona Wolf for technical assistance with cell culture. We are grateful to Anne Halenius and Zsolt Ruzsics for profound project discussions. We acknowledge support by the Open Access Publication Fund of the University of Freiburg.

Conflict of interest

The authors declare that the research was conducted in the absence of any commercial or financial relationships that could be construed as a potential conflict of interest.

The author(s) declared that they were an editorial board member of Frontiers, at the time of submission. This had no impact on the peer review process and the final decision.

Generative AI statement

The author(s) declare that no Generative AI was used in the creation of this manuscript.

Publisher's note

Supplementary material

The Supplementary Material for this article can be found online at: https://www.frontiersin.org/articles/10.3389/fimmu.2025.1598605/full#supplementary-material

References

1. Zhang D, Sun M, Samols D, Kushner I. STAT3 participates in transcriptional activation of the C-reactive protein gene by interleukin-6 (∗). *J Biol Chem*. (1996) 271:9503–9. doi: 10.1074/jbc.271.16.9503

2. Agrawal A, Cha-Molstad H, Samols D, Kushner I. Transactivation of C-reactive protein by IL-6 requires synergistic interaction of CCAAT/enhancer binding protein β (C/EBPβ) and rel p50. *J Immunol*. (2001) 166:2378–84. doi: 10.4049/jimmunol.166.4.2378

3. Peisajovich A, Marnell L, Mold C, Du Clos TW. C-reactive protein at the interface between innate immunity and inflammation. *Expert Rev Clin Immunol*. (2008) 4:379–90. doi: 10.1586/1744666X.4.3.379

4. Thompson D, Pepys MB, Wood SP. The physiological structure of human C-reactive protein and its complex with phosphocholine. *Structure*. (1999) 7:169–77. doi: 10.1016/S0969-2126(99)80023-9

5. Narkates AJ, Volanakis JE. C-reactive protein binding specificities: artificial and natural phospholipid bilayers*. *Ann N Y Acad Sci*. (1982) 389:172–82. doi: 10.1111/j.1749-6632.1982.tb22135.x

6. Li YP, Mold C, Clos TWD. Sublytic complement attack exposes C-reactive protein binding sites on cell membranes. *J Immunol*. (1994) 152:2995–3005. doi: 10.4049/jimmunol.152.6.2995

7. Agrawal A, Shrive AK, Greenhough TJ, Volanakis JE. Topology and structure of the C1q-binding site on C-reactive protein. *J Immunol*. (2001) 166:3998–4004. doi: 10.4049/jimmunol.166.6.3998

8. Potempa LA, Maldonado BA, Laurent P, Zemel ES, Gewurz H. Antigenic, electrophoretic and binding alterations of human C-reactive protein modified selectively in the absence of calcium. *Mol Immunol*. (1983) 20:1165–75. doi: 10.1016/0161-5890(83)90140-2

9. Kresl JJ, Potempa LA, Anderson BE. Conversion of native oligomeric to a modified monomeric form of human C-reactive protein. *Int J Biochem Cell Biol*. (1998) 30:1415–26. doi: 10.1016/S1357-2725(98)00078-8

10. Braig D, Nero TL, Koch HG, Kaiser B, Wang X, Thiele JR, et al. Transitional changes in the CRP structure lead to the exposure of proinflammatory binding sites. *Nat Commun*. (2017) 8:14188. doi: 10.1038/ncomms14188

11. Eisenhardt SU, Habersberger J, Murphy A, Chen YC, Woollard KJ, Bassler N, et al. Dissociation of pentameric to monomeric C-reactive protein on activated platelets localizes inflammation to atherosclerotic plaques. *Circ Res*. (2009) 105:128–37. doi: 10.1161/CIRCRESAHA.108.190611

12. Thiele JR, Habersberger J, Braig D, Schmidt Y, Goerendt K, Maurer V, et al. Dissociation of pentameric to monomeric C-reactive protein localizes and aggravates inflammation. *Circulation*. (2014) 130:35–50. doi: 10.1161/CIRCULATIONAHA.113.007124

13. Strang F, Scheichl A, Chen YC, Wang X, Htun NM, Bassler N, et al. Amyloid plaques dissociate pentameric to monomeric C-reactive protein: A novel pathomechanism driving cortical inflammation in alzheimer's disease? *Brain Pathol*. (2012) 22:337–46. doi: 10.1111/j.1750-3639.2011.00539.x

14. Zeller J, Loseff-Silver J, Khoshmanesh K, Baratchi S, Lai A, Nero TL, et al. Shear-sensing by C-reactive protein: linking aortic stenosis and inflammation. *Circ Res*. (2024) 135:1033–47. doi: 10.1161/CIRCRESAHA.124.324248

15. Ravetch JV, Lanier LL. Immune inhibitory receptors. *Science*. (2000) 290:84–9. doi: 10.1126/science.290.5489.84

16. Lanier LL, Yu G, Phillips JH. Co-association of CD3 zeta with a receptor (CD16) for IgG Fc on human natural killer cells. *Nature*. (1989) 342:803–5. doi: 10.1038/342803a0

17. Ernst LK, Duchemin AM, Anderson CL. Association of the high-affinity receptor for IgG (Fc gamma RI) with the gamma subunit of the IgE receptor. *Proc Natl Acad Sci U S A*. (1993) 90:6023–7. doi: 10.1073/pnas.90.13.6023

18. Nimmerjahn F, Ravetch JV. Fcγ receptors as regulators of immune responses. *Nat Rev Immunol*. (2008) 8:34–47. doi: 10.1038/nri2206

19. Harrison PT, Allen JM. High affinity IgG binding by FcgammaRI (CD64) is modulated by two distinct IgSF domains and the transmembrane domain of the receptor. *Protein Eng*. (1998) 11:225–32. doi: 10.1093/protein/11.3.225

20. Chen H, Maul-Pavicic A, Holzer M, Huber M, Salzer U, Chevalier N, et al. Detection and functional resolution of soluble immune complexes by an FcγR reporter cell panel. *EMBO Mol Med*. (2022) 14:e14182. doi: 10.15252/emmm.202114182

21. Marnell LL, Mold C, Volzer MA, Burlingame RW, Clos TWD. C-reactive protein binds to Fc gamma RI in transfected COS cells. *J Immunol*. (1995) 155:2185–93. doi: 10.4049/jimmunol.155.4.2185

22. Bharadwaj D, Stein MP, Volzer M, Mold C, Clos TWD. The major receptor for C-reactive protein on leukocytes is fcγ Receptor II. *J Exp Med*. (1999) 190:585–90. doi: 10.1084/jem.190.4.585

23. Lu J, Marnell LL, Marjon KD, Mold C, Du Clos TW, Sun PD. Structural recognition and functional activation of FcγR by innate pentraxins. *Nature*. (2008) 456:989–92. doi: 10.1038/nature07468

24. Temming AR, Tammes Buirs M, Bentlage AEH, Treffers LW, Feringa H, de Taeye SW, et al. C-reactive protein enhances igG-mediated cellular destruction through igG-fc receptors *in vitro*. *Front Immunol*. (2021) 12:598. doi: 10.3389/fimmu.2021.594773

25. Lu J, Mold C, Du Clos TW, Sun PD. Pentraxins and fc receptor-mediated immune responses. *Front Immunol*. (2018) 9:2607. doi: 10.3389/fimmu.2018.02607

26. Mold C, Clos TWD. C-Reactive Protein Increases Cytokine Responses to Streptococcus pneumoniae through Interactions with Fcγ Receptors. *J Immunol*. (2006) 176:7598–604. doi: 10.4049/jimmunol.176.12.7598

27. Newling M, Sritharan L, van der Ham AJ, Hoepel W, Fiechter RH, de Boer L, et al. C-reactive protein promotes inflammation through fcγR-induced glycolytic reprogramming of human macrophages. *J Immunol Baltim Md 1950*. (2019) 203:225–35. doi: 10.4049/jimmunol.1900172

28. West SD, Ziegler A, Brooks T, Krencicki M, Myers O, Mold C. An fcγRIIa polymorphism with decreased C-reactive protein binding is associated with sepsis and decreased monocyte HLA-DR expression in trauma patients. *J Trauma Acute Care Surg*. (2015) 79:773–81. doi: 10.1097/TA.0000000000000837

29. Zuniga R, Markowitz GS, Arkachaisri T, Imperatore EA, D'Agati VD, Salmon JE. Identification of IgG subclasses and C-reactive protein in lupus nephritis: The relationship between the composition of immune deposits and FCγ receptor type IIA alleles. *Arthritis Rheumatol*. (2003) 48:460–70. doi: 10.1002/art.10930

30. McFadyen JD, Zeller J, Potempa LA, Pietersz GA, Eisenhardt SU, Peter K. C-reactive protein and its structural isoforms: an evolutionary conserved marker and central player in inflammatory diseases and beyond. In: Hoeger U, Harris JR, editors. *Vertebrate and invertebrate respiratory proteins, lipoproteins and other body fluid proteins*. Springer International Publishing, Cham (2020). p. 499–520. doi: 10.1007/978-3-030-41769-7_20

31. Zeller J, Bogner B, McFadyen JD, Kiefer J, Braig D, Pietersz G, et al. Transitional changes in the structure of C-reactive protein create highly pro-inflammatory molecules: Therapeutic implications for cardiovascular diseases. *Pharmacol Ther*. (2022) 235:108165. doi: 10.1016/j.pharmthera.2022.108165

32. Mold C, Rodriguez W, Rodic-Polic B, Clos TWD. C-reactive protein mediates protection from lipopolysaccharide through interactions with fcγR. *J Immunol*. (2002) 169:7019–25. doi: 10.4049/jimmunol.169.12.7019

33. Corrales-Aguilar E, Trilling M, Reinhard H, Mercé-Maldonado E, Widera M, Schaal H, et al. A novel assay for detecting virus-specific antibodies triggering activation of Fcγ receptors. *J Immunol Methods*. (2013) 387:21–35. doi: 10.1016/j.jim.2012.09.006

34. Van den Hoecke S, Ehrhardt K, Kolpe A, El Bakkouri K, Deng L, Grootaert H, et al. Hierarchical and redundant roles of activating fcγRs in protection against influenza disease by M2e-specific igG1 and igG2a antibodies. *J Virol*. (2017) 91: e02500–16. doi: 10.1128/JVI.02500-16

35. Kolb P, Sijmons S, McArdle MR, Taher H, Womack J, Hughes C, et al. Identification and functional characterization of a novel fc gamma-binding glycoprotein in rhesus cytomegalovirus. *J Virol*. (2019) 93:e02077–18. doi: 10.1128/JVI.02077-18

36. Lagassé HAD, Hengel H, Golding B, Sauna ZE. Fc-fusion drugs have fcγR/C1q binding and signaling properties that may affect their immunogenicity. *AAPS J*. (2019) 21:62. doi: 10.1208/s12248-019-0336-8

37. Ankerhold J, Giese S, Kolb P, Maul-Pavicic A, Voll RE, Göppert N, et al. Circulating multimeric immune complexes contribute to immunopathology in COVID-19. *Nat Commun*. (2022) 13:5654. doi: 10.1038/s41467-022-32867-z

38. Potempa LA, Siegel JN, Fedel BA, Potempa RT, Gewurz H. Expression, detection and assay of a neoantigen (Neo-CRP) associated with a free, human C-reactive protein subunit. *Mol Immunol*. (1987) 24:531–41. doi: 10.1016/0161-5890(87)90028-9

39. Zeller J, Bogner B, Kiefer J, Braig D, Winninger O, Fricke M, et al. CRP enhances the innate killing mechanisms phagocytosis and ROS formation in a conformation and complement-dependent manner. *Front Immunol*. (2021) 12:721887. doi: 10.3389/fimmu.2021.721887

40. Zeller J, Cheung Tung Shing KS, Nero TL, McFadyen JD, Krippner G, Bogner B, et al. A novel phosphocholine-mimetic inhibits a pro-inflammatory conformational change in C-reactive protein. *EMBO Mol Med*. (2023) 15:e16236. doi: 10.15252/emmm.202216236

41. Halenius A, Hauka S, Dölken L, Stindt J, Reinhard H, Wiek C, et al. Human cytomegalovirus disrupts the major histocompatibility complex class I peptide-loading complex and inhibits tapasin gene transcription. *J Virol*. (2011) 85:3473–85. doi: 10.1128/JVI.01923-10

42. Ji SR, Wu Y, Potempa LA, Liang YH, Zhao J. Effect of modified C-reactive protein on complement activation: a possible complement regulatory role of modified or monomeric C-reactive protein in atherosclerotic lesions. *Arterioscler Thromb Vasc Biol*. (2006) 26:935–41. doi: 10.1161/01.ATV.0000206211.21895.73

43. McFadyen JD, Kiefer J, Braig D, Loseff-Silver J, Potempa LA, Eisenhardt SU, et al. Dissociation of C-reactive protein localizes and amplifies inflammation: evidence for a direct biological role of C-reactive protein and its conformational changes. *Front Immunol*. (2018) 9:1351. doi: 10.3389/fimmu.2018.01351

44. Ying SC, Gewurz H, Kinoshita CM, Potempa LA, Siegel JN. Identification and partial characterization of multiple native and neoantigenic epitopes of human C-reactive protein by using monoclonal antibodies. *J Immunol*. (1989) 143:221–8. doi: 10.4049/jimmunol.143.1.221

45. Thiele JR, Zeller J, Kiefer J, Braig D, Kreuzaler S, Lenz Y, et al. A conformational change in C-reactive protein enhances leukocyte recruitment and reactive oxygen species generation in ischemia/reperfusion injury. *Front Immunol*. (2018) 9:675. doi: 10.3389/fimmu.2018.00675

46. Lv JM, Wang MY. *In vitro* generation and bioactivity evaluation of C-reactive protein intermediate. *PloS One*. (2018) 13:e0198375. doi: 10.1371/journal.pone.0198375

47. Pepys MB, Hawkins PN, Kahan MC, Tennent GA, Gallimore JR, Graham D, et al. Proinflammatory effects of bacterial recombinant human C-reactive protein are caused by contamination with bacterial products, not by C-reactive protein itself. *Circ Res*. (2005) 97:e97–103. doi: 10.1161/01.RES.0000193595.03608.08

48. Stein MP, Edberg JC, Kimberly RP, Mangan EK, Bharadwaj D, Mold C, et al. C-reactive protein binding to FcγRIIa on human monocytes and neutrophils is allele-specific. *J Clin Invest*. (2000) 105:369–76. doi: 10.1172/JCI7817

49. Saeland E, van Royen A, Hendriksen K, Vilé-Weekhout H, Rijkers GT, Sanders LAM, et al. Human C-reactive protein does not bind to fcγRIIa on phagocyti cells. *J Clin Invest*. (2001) 107:641–2. doi: 10.1172/JCI12418

50. Devaraj S, Du Clos TW, Jialal I. Binding and internalization of C-reactive protein by fcgamma receptors on human aortic endothelial cells mediates biological effects. *Arterioscler Thromb Vasc Biol*. (2005) 25:1359–63. doi: 10.1161/01.ATV.0000168573.10844.ae

51. Bruhns P, Iannascoli B, England P, Mancardi DA, Fernandez N, Jorieux S, et al. Specificity and affinity of human Fcγ receptors and their polymorphic variants for human IgG subclasses. *Blood*. (2009) 113:3716–25.

52. Stewart R, Hammond SA, Oberst M, Wilkinson RW. The role of Fc gamma receptors in the activity of immunomodulatory antibodies for cancer. *J Immunother Cancer*. (2014) 2:1–10. doi: 10.1186/s40425-014-0029-x

53. Vidarsson G, Dekkers G, Rispens T. IgG subclasses and allotypes: from structure to effector functions. *Front Immunol*. (2014) 5:520. doi: 10.3389/fimmu.2014.00520

54. Temming AR, Bentlage AEH, de Taeye SW, Bosman GP, Lissenberg-Thunnissen SN, Derksen NIL, et al. Cross-reactivity of mouse IgG subclasses to human Fc gamma receptors: Antibody deglycosylation only eliminates IgG2b binding. *Mol Immunol*. (2020) 127:79–86. doi: 10.1016/j.molimm.2020.08.015

55. Zhang M, Liu Y, Liu Z, Wang J, Gong M, Ge H, et al. Hyper-acidic fusion minipeptides escort the intrinsic antioxidative ability of the pattern recognition receptor CRP in non-animal organisms. *Sci Rep*. (2019) 9:3032. doi: 10.1038/s41598-019-39388-8

56. Potempa LA, Qiu WQ, Stefanski A, Rajab IM. Relevance of lipoproteins, membranes, and extracellular vesicles in understanding C-reactive protein biochemical structure and biological activities. *Front Cardiovasc Med*. (2022) 9:979461. doi: 10.3389/fcvm.2022.979461

57. Du Clos TW. Pentraxins: structure, function, and role in inflammation. *ISRN Inflamm*. (2013) 2013:e379040. doi: 10.1155/2013/379040

58. Baumann U, Köhl J, Tschernig T, Schwerter-Strumpf K, Verbeek JS, Schmidt RE, et al. A codominant role of Fc gamma RI/III and C5aR in the reverse Arthus reaction. *J Immunol Baltim Md 1950*. (2000) 164:1065–70. doi: 10.1182/blood-2008-09-179754

59. Kiefer J, Zeller J, Schneider L, Thomé J, McFadyen JD, Hoerbrand IA, et al. C-reactive protein orchestrates acute allograft rejection in vascularized composite allotransplantation via selective activation of monocyte subsets. *J Adv Res*. (2024) 9, S2090-1232(24)00291-1. doi: 10.1016/j.jare.2024.07.007

60. Heuertz RM, Schneider GP, Potempa LA, Webster RO. Native and modified C-reactive protein bind different receptors on human neutrophils. *Int J Biochem Cell Biol*. (2005) 37:320–. doi: 10.1016/j.biocel.2004.07.002

61. Ullah N, Wu Y. Regulation of conformational changes in C-reactive protein alters its bioactivity. *Cell Biochem Biophys*. (2022) 80:595–608. doi: 10.1007/s12013-022-01089-x

62. Gonzalez-Quintela A, Alende R, Gude F, Campos J, Rey J, Meijide LM, et al. Serum levels of immunoglobulins (IgG, IgA, IgM) in a general adult population and their relationship with alcohol consumption, smoking and common metabolic abnormalities. *Clin Exp Immunol*. (2008) 151:42–50. doi: 10.1111/j.1365-2249.2007.03545.x

63. Corrales-Aguilar E, Trilling M, Reinhard H, Falcone V, Zimmermann A, Adams O, et al. Highly individual patterns of virus-immune IgG effector responses in humans. *Med Microbiol Immunol (Berl)*. (2016) 205:409–24. doi: 10.1007/s00430-016-0457-y

64. Iyer RF, Edwards DM, Kolb P, Raué HP, Nelson CA, Epperson ML, et al. The secreted protein Cowpox Virus 14 contributes to viral virulence and immune evasion by engaging Fc-gamma-receptors. *PloS Pathog*. (2022) 18:e1010783. doi: 10.1371/journal.ppat.1010783

frontiers | Frontiers in Endocrinology

TYPE Original Research
PUBLISHED 27 June 2025
DOI 10.3389/fendo.2025.1619370

OPEN ACCESS

EDITED BY
Alok Agrawal,
Retired, Johnson City, TN, United States

REVIEWED BY
Toh Gang,
ST Jude Children's Research Hospital, United States
Sanjay K Singh,
East Tennessee State University, United States

*CORRESPONDENCE
Qi Pan
panqi621@126.com
Guogang Xu
gxu@301hospital.org
Lixin Guo
glxwork@163.com

†These authors have contributed equally to this work and share first authorship

RECEIVED 28 April 2025
ACCEPTED 09 June 2025
PUBLISHED 27 June 2025

CITATION
Huang D, Ma J, Zhao Y, Pan Q, Xu G and Guo L (2025) Higher C-reactive protein to high-density lipoprotein cholesterol ratio is associated with hyperuricemia in diabetes and prediabetes: a cross-sectional study. *Front. Endocrinol.* 16:1619370. doi: 10.3389/fendo.2025.1619370

Higher C-reactive protein to high-density lipoprotein cholesterol ratio is associated with hyperuricemia in diabetes and prediabetes: a cross-sectional study

Dongni Huang[1,2†], Jing Ma[3†], Yan Zhao[1,2†], Qi Pan[1*], Guogang Xu[3*] and Lixin Guo[1,2*]

[1]Department of Endocrinology, Beijing Hospital, National Center for Gerontology, Institute of Geriatric Medicine, Chinese Academy of Medical Sciences, Beijing, China, [2]Graduate School of Peking Union Medical College, Chinese Academy of Medical Sciences, Beijing, China, [3]Health Management Institute, The Second Medical Center & National Clinical Research Center for Geriatric Diseases, Chinese PLA General Hospital, Beijing, China

Background: The ratio of C-reactive protein to high-density lipoprotein cholesterol (CRP/HDL-c) reflects systemic inflammation and lipid status, both of which are implicated in uric acid metabolism. This study aimed to investigate the association between CRP/HDL-c and the prevalence of hyperuricemia (HUA) among adults with diabetes or prediabetes.

Methods: This cross-sectional study included 10915 adults with diabetes or prediabetes from the Health Management Institute of the PLA General Hospital. Hyperuricemia was defined as a serum uric acid concentration ≥7 mg/dL in men and ≥6 mg/dL in women. Participants were divided into quartiles according to the ratio. Multivariate logistic regression and restricted cubic spline analyses were used to assess associations. Subgroup analyses and interaction tests were performed.

Results: The prevalence of HUA increased across CRP/HDL-c quartiles (18.43%, 20.39%, 24.54%, and 29.82%; P < 0.001). Higher CRP/HDL-c levels were independently associated with increased HUA risk (odds ratio [OR] = 1.64, 95% confidence interval [CI]: 1.14–2.36; $P = 0.008$). Participants in the highest quartile had a significantly higher risk compared to those in the lowest quartile (OR = 1.33, 95% CI: 1.15–1.54; $P < 0.001$). The association was stronger in females (OR = 1.30) than in males (OR = 1.14), with a significant gender interaction (P for interaction = 0.031). Among females, the association was more pronounced in those aged <50 years (OR = 1.47). RCS analysis indicated a linear dose–response relationship.

Conclusions: An elevated C-reactive protein to high-density lipoprotein cholesterol ratio is significantly associated with a higher risk of hyperuricemia in adults with diabetes or prediabetes, particularly in younger females.

KEYWORDS

hyperuricemia, CRP/HDL-c ratio, diabetes, prediabetes, inflammation, lipid metabolism

1 Introduction

Hyperuricemia (HUA) is a metabolic disorder syndrome caused by abnormalities in purine metabolism. Uric acid, the end product of purine metabolism, is mainly produced in the liver. Under normal conditions, uric acid production and excretion are maintained in dynamic balance. When uric acid production increases excessively or excretion decreases, serum uric acid levels rise, leading to HUA. Epidemiological and clinical studies have linked HUA with the development of various diseases, including chronic kidney disease, fatty liver, metabolic syndrome, hypertension, insulin resistance, obesity, as well as cardiovascular and cerebrovascular diseases (1–3). It is also an independent predictor of premature death (4). Recent trends suggest an increase in the prevalence of HUA, which is attributed to changes in lifestyle, particularly in high- and middle-income countries (5). According to the National Health and Nutrition Examination Survey (NHANES) in the United States, approximately 21% of adults, or 43 million people, have been diagnosed with HUA (6). The prevalence of HUA in China and South Korea is 6.4% and 11.4%, respectively (7, 8). HUA prevalence among diabetic patients has been reported to be 21.24% in China (9) and 20.70% in North America (10).

HUA is closely associated with abnormal glucose metabolism (11). Individuals with elevated serum uric acid levels are significantly more likely to develop diabetes than those with normal levels, and conversely, people with diabetes have an increased risk of developing HUA (12, 13). This bidirectional relationship likely involves multiple mechanisms. HUA may disrupt glucose homeostasis by impairing insulin signaling and promoting insulin resistance (14). In parallel, diabetes is often accompanied by metabolic disturbances such as obesity and dyslipidemia, which can further exacerbate uric acid metabolism disorders (15). Therefore, managing serum uric acid levels in patients with diabetes or prediabetes is essential—not only to reduce the risk of gout, but also to improve overall metabolic health, lower the incidence of chronic complications, and enhance both quality of life and life expectancy.

HUA and abnormal glucose metabolism are both closely linked to inflammation (16, 17). Raised uric acid levels and chronic disturbances in glucose metabolism can activate intracellular signaling pathways and promote the expression of inflammatory cytokines, triggering systemic inflammation and contributing to organ damage. Inflammatory states, in turn, may increase the risk of HUA, diabetes, and diabetes-related complications, creating a self-reinforcing cycle. C-reactive protein (CRP) is a widely used inflammatory marker. It plays a key role in inflammatory responses, atherosclerosis, autoimmune conditions and cardiovascular disease (18–20). Dyslipidemia—characterized by elevated triglycerides, total cholesterol, low-density lipoprotein cholesterol, and reduced high-density lipoprotein cholesterol (HDL-c)—is associated with higher risks of diabetes and HUA (21). Low HDL-c, in particular, is a known risk factor for diabetes, cardiovascular disease, and other metabolic disorders (22, 23). The CRP/HDL-c has been proposed as a combined marker of inflammation and lipid status, and has shown associations with cardiovascular and metabolic disease risk (24, 25). One study found a significant association between CRP/HDL-c and HUA in US adults (26). However, no studies have yet examined this relationship in people with diabetes or prediabetes, highlighting a gap that warrants further investigation.

Using data sourced from the Health Management Institute of the Second Medical Centre, PLA General Hospital, the aim of this study was to investigate the relationship between the CRP/HDL-c ratio and the risk of developing HUA in this population. The hypothesis of this study was that there would be a strong correlation between the CRP/HDL-c ratio and the risk of HUA among individuals with diabetes or prediabetes.

2 Materials and methods

2.1 Study population

This study utilized data from the Health Management Research Institute of PLA General Hospital, collected between November 2009 and December 2016. A total of 10,915 individuals aged 18 to 80 years with either diabetes or prediabetes were retrospectively included. All participants provided written informed consent for the use of their clinical data at the time of their hospital visit, in line with institutional policies. The study was approved by the Research Ethics Committee of Beijing Hospital (2025BJYYEC-KY03901). Diabetes and prediabetes were defined according to the American Diabetes Association (ADA) criteria (27). Diabetes was diagnosed based on a self-reported history of physician-diagnosed diabetes, a fasting plasma glucose (FPG) level ≥126 mg/dL, a 2-hour plasma glucose level ≥200 mg/dL after a 75-g oral glucose tolerance test (OGTT), or a hemoglobin A1c (HbA1c) level ≥6.5%. Prediabetes was defined as the absence of a prior diabetes diagnosis combined with either impaired fasting glucose (FPG 100–125 mg/dL), impaired glucose tolerance (2-hour plasma glucose 140–199 mg/dL after OGTT), or an HbA1c level of 5.7–6.4%. FPG was measured after an overnight fast of at least 10 hours. Both FPG and 2-hour plasma glucose levels following the OGTT were assessed according to standardized procedures. HbA1c was measured in a central laboratory using high-performance liquid chromatography with the boronate affinity method (Bio-Rad D-10 Hemoglobin Analyzer) following established protocols. Exclusion criteria included: (1) missing CRP or HDL-c data; (2) age <18 years; (3) pregnancy; (4) acute inflammatory or infectious diseases at the time of data collection; (5) use of medications influencing CRP or HDL-c (e.g., corticosteroids, statins); and (6) diagnosed malignancies.

2.2 Exposure and outcome definitions

In this study, the CRP/HDL-c, which is the ratio of CRP to HDL-c, was used as the exposure variable. HUA was defined as SUA levels ≥ 7 mg/dL (420umol/l) in men and ≥ 6 mg/dL(360umol/l) in women (28).

2.3 Covariate definitions

The study accounted for multiple potential covariates, including age (years), gender, smoking status, diabetes mellitus status, hypertension status, blood pressure, body mass index (BMI, kg/m^2), waist-to-hip ratio (WHR), and a series of biochemical markers. These included glycated hemoglobin (HbA1c, %), alanine aminotransferase (ALT, U/L), aspartate aminotransferase (AST, U/L), triglycerides (TG, mmol/L), low-density lipoprotein cholesterol (LDL-C, mmol/L), creatinine (Cr, μmol/L), and estimated glomerular filtration rate (eGFR, mL/min/1.73 m^2). BMI was categorized as <25 kg/m^2 (normal), 25–29.9 kg/m^2 (overweight), or ≥30 kg/m^2 (obese). The eGFR was calculated using the Chronic Kidney Disease Epidemiology Collaboration (CKD-EPI) equation (29). Smoke was defined as the consumption of ≥10 cigarettes per day for ≥1 year, based on criteria from relevant literature (30). Alcohol consumption was classified as limited drinking (no alcohol or ≤25 g/day for men and ≤15 g/day for women) or excessive drinking (≥25 g/day for men and ≥15 g/day for women) (31). Hypertension status was determined based on self-reported history.

2.4 Data collection

Electronic medical records were retrospectively reviewed to obtain demographic and biochemical data. Information including age, systolic and diastolic blood pressure (SBP and DBP), smoking status, and alcohol consumption was collected using standardized methods. Fasting venous blood samples were drawn from all participants following an overnight fast and processed in accordance with the quality control standards of the Clinical Laboratory at PLA General Hospital (32). Serum concentrations of total cholesterol (TC), triglycerides (TG), high-density lipoprotein cholesterol (HDL-C), low-density lipoprotein cholesterol (LDL-C), fasting blood glucose (FBG), hemoglobin A1c (HbA1c), alanine aminotransferase (ALT), aspartate aminotransferase (AST), blood urea nitrogen (BUN), creatinine (Cr), and uric acid (UA) were measured using validated laboratory techniques. C-reactive protein (CRP) levels were determined by nephelometry. The CRP-to-HDL-C ratio was subsequently calculated.

2.5 Statistical analysis

All statistical analyses were performed using R software (version 4.4.3). Continuous variables with a normal distribution were expressed as mean ± standard deviation (SD), while those with a skewed distribution were presented as median (interquartile range). Group differences in continuous variables were assessed using the independent samples t-test or the Mann–Whitney U test, as appropriate. Categorical variables were compared using the chi-square test. Logistic and linear regression models were employed to evaluate the associations of CRP, HDL-C, and the CRP/HDL-C ratio with both the risk of HUA and SUA concentrations. Multicollinearity was assessed using the variance inflation factor (VIF). Decision curve analysis (DCA) and receiver operating characteristic (ROC) curve analysis were conducted to assess the predictive value of CRP, HDL-C, and the CRP/HDL-C ratio for identifying HUA risk. Subgroup analyses were also performed. Finally, restricted cubic spline (RCS) logistic regression with three knots was applied to explore potential nonlinear relationships between the CRP/HDL-C ratio and the risk of developing HUA. A two-sided P value < 0.05 was considered statistically significant.

3 Results

3.1 Baseline characteristics of study participants

Table 1 showed the baseline characteristics of the study participants (n = 10915) with diabetes or pre-diabetes stratified by without or with hyperuricemia. The average age of the participants was 51.63 years, and 72.23% of them were male. Compared with the non-HUA group, the HUA group was younger and had more males, drinkers, and individuals with diabetes (P < 0.05). Additionally, individuals in this group exhibited increased SBP, DBP, BMI, WHR, ALT concentrations, AST concentrations, BUN concentrations, Cr concentrations, and UA concentrations, FBG values, FCP concentrations, FINS concentrations, HOMA-IR, TG concentrations, TC concentrations, LDL-c concentrations, CRP (P < 0.001). Conversely, reduced eGFR and lower levels of HDL-c were significantly more common in the HUA group (P < 0.001). The HUA group exhibited notably greater CRP/HDL-c values than did the non-HUA group (P < 0.001).

3.2 Baseline characteristics based on the quantiles of the CRP/HDL-c

According to the CRP/HDL-c, the subjects were categorized into four groups based on quantiles (Table 2). The high-CRP/HDL-c quantile group exhibited greater proportions of males, individuals with diabetes and hypertension (P < 0.001). Furthermore, SBP, DBP, BMI, waist to hip ratio, ALT concentrations, AST concentrations, eGFR, FBG values, HbA1c values, FCP concentrations, FINS concentrations, HOMA-IR, TG concentrations, CRP were obviously increased (P < 0.001). In contrast, the proportions of individuals with high eGFRs, and high HDL-c levels decreased (P < 0.001). Compared to those in the lowest CRP/HDL-c quartile, individuals in the second, third and fourth quartile were younger (P < 0.001). Notably, a higher CRP/HDL-c was related to increased levels of SUA and a greater prevalence of HUA (18% vs.20% vs. 25% vs. 30%, P < 0.001).

3.3 Association between the CRP/HDL-c and the risk of developing HUA

Table 3A showed that CRP/HDL-c was positively correlated with the prevalence of HUA, a statistically significant relationship

10.3389/fendo.2025.1619370

TABLE 1 Characteristics of participants with diabetes or pre-diabetes stratified by without or with hyperuricemia.

Characteristic	Non-HUA group (N = 8,372)	HUA group (N = 2,543)	*p*-value
Age (years)	51 (47, 57)	50 (45, 55)	<0.001
Male gender, n (%)	5,694 (68%)	2,190 (86%)	<0.001
SBP (mmHg)	123 (112, 135)	127 (116, 138)	<0.001
DBP (mmHg)	79 (72, 87)	82 (76, 89)	<0.001
BMI (kg/m^2)	25.6 (23.7, 27.7)	27.0 (25.1, 29.0)	<0.001
WHR	0.93 (0.86, 0.97)	0.95 (0.92, 0.98)	<0.001
ALT (U/L)	21 (15, 30)	26 (18, 38)	<0.001
AST (U/L)	19 (16, 23)	20 (17, 26)	<0.001
BUN (mmol/l)	5.10 (4.40, 6.00)	5.30 (4.50, 6.20)	<0.001
Cr (umol/l)	67 (57, 76)	75 (65, 83)	<0.001
eGFR(mL/min/ 1.73 m2)	103 (96, 109)	101 (92, 108)	<0.001
SUA (umol/l)	325 (276, 367)	455 (432, 494)	<0.001
FBG (mmol/l)	5.76 (5.24, 6.77)	5.87 (5.37, 6.64)	<0.001
HbA1c (%)	6.00 (5.80, 6.50)	6.00 (5.80, 6.40)	0.084
FCP (ng/ml)	2.52 (1.97, 3.20)	3.11 (2.57, 3.82)	<0.001
FINS (mU/L)	10 (7, 15)	12 (9, 17)	<0.001
HOMA-IR	2.62(1.73-3.93)	3.27(2.29-4.77)	<0.001
TG (mmol/l)	1.55 (1.10, 2.23)	2.08 (1.48, 3.08)	<0.001
TC (mmol/l)	4.80 (4.16, 5.47)	4.99 (4.35, 5.69)	<0.001
LDL-c (mmol/l)	3.15 (2.56, 3.73)	3.23 (2.62, 3.84)	<0.001
HDL-c (mmol/l)	1.15 (0.96, 1.38)	1.05 (0.90, 1.24)	<0.001
CRP (mg/l)	0.12 (0.07, 0.22)	0.15 (0.08, 0.27)	<0.001
CRP/HDL-c	0.11 (0.06, 0.20)	0.14 (0.07, 0.26)	<0.001
Smokers, n (%)	2,083 (25%)	661 (26%)	0.300
Drinkers, n (%)	2,595 (31%)	839 (33%)	0.013
Hypertension, n (%)	660 (7.9%)	204 (8.0%)	0.911
Diabetes, n (%)	1842 (22%)	786 (27%)	<0.001

Data are number of subjects (percentage) or medians (interquartile range).
Mann–Whitney U test was used to compare the median values between participants with and without hyperuricemia. Chi-square test was used to compare the percentage between participants with and without hyperuricemia.
SBP, systolic blood pressure; DBP, diastolic blood pressure; BMI, body mass index; WHR, waist to hip ratio; ALT, alanine aminotransferase; AST, aspartate aminotransferase; BUN, blood urea nitrogen; eGFR, estimated glomerular filtration rate; SUA, serum uric acid; FBG fasting blood glucose; HbA1c, glycated hemoglobin A; FCP, fasting plasma C-peptide; FINS, fasting insulin; HOMA-IR, homeostatic model assessment of insulin resistance; TG, triglycerides; TC, total cholesterol; LDL-c, low-density lipoprotein cholesterol; HDL-c, high- -density lipoprotein cholesterol.

that persisted across unadjusted, partially adjusted, and fully adjusted logistic regression models. After full adjustment, each unit increase in the CRP/HDL-c ratio was associated with a 64% higher risk of HUA (OR=1.64, 95% CI: 1.14 to 2.36; P=0.008; Supplementary Tables 1, 2). When stratified by quartiles, participants in the highest quartile of CRP/HDL-c had a significantly greater risk compared with those in the lowest quartile (OR=1.33, 95% CI: 1.15 to 1.54; P<0.001).In a linear regression analysis using SUA as the dependent variable, CRP/HDL-c was positively and significantly associated with SUA levels (β=0.26, 95% CI: 0.10 to 0.43; P=0.002; Table 3B). Receiver operating characteristic (ROC) curve analysis showed that the areas under the curve (AUCs) for CRP/HDL-c, CRP, and HDL-c were 60.36%, 55.08%, and 59.55%, respectively. Decision curve analysis (DCA) further demonstrated that CRP/HDL-c provided a greater net benefit compared with CRP or HDL-c alone (Figures 1, 2).

3.4 Sensitivity analysis of individual CRP and HDL-c levels

To assess whether the observed association between the CRP/HDL-c ratio and HUA was driven primarily by changes in CRP or HDL-c alone, we conducted a sensitivity analysis evaluating the associations of CRP and HDL-c quartiles separately with HUA. As shown in Supplementary Table 3, compared with participants in the lowest CRP quartile, those in the third and fourth quartiles had significantly higher odds of hyperuricemia (Q3: OR=1.17, 95% CI: 1.01 to 1.34, P = 0.031; Q4: OR = 1.26, 95% CI: 1.10 to 1.45, P=0.009), indicating a positive association between systemic inflammation and uric acid levels. In contrast, higher HDL-c levels were inversely associated with hyperuricemia risk. Compared with the lowest HDL-c quartile, participants in the third and fourth quartiles exhibited significantly lower odds of HUA (Q3: OR=0.87, 95% CI: 0.73 to 0.98, P=0.045; Q4: OR=0.83, 95% CI: 0.68 to 0.95, P=0.032).These findings suggest that both elevated CRP and reduced HDL-c independently contribute to increased HUA risk, thereby supporting the use of CRP/HDL-c as an integrative biomarker reflecting combined inflammatory and lipid-related risk factors.

3.5 Subgroup analysis

Subgroup analyses were carried out considering factors such as age, gender, BMI, smoking status, drinking status, diabetes status, hypertension status, and eGFR to evaluate the robustness of the association between CRP/HDL-c and the risk of developing HUA across different populations with diabetes or pre-diabetes (Figure 3). The results indicated that the positive association remained consistent across most subgroups. Notably, the association was stronger in females (OR = 1.30, 95% CI: 1.14–1.49) than in males (OR = 1.14, 95% CI: 1.07–1.21), with a significant interaction by gender (P for interaction = 0.031). Further age-stratified analyses among females revealed that the OR for the <50 years group was 1.47, which was higher than the OR of 1.23 observed in the ≥50 years group (P for interaction = 0.008) (Supplementary Figure 1). This finding suggests that the CRP/HDL ratio may serve as a stronger predictor of hyperuricemia in younger women.

10.3389/fendo.2025.1619370

TABLE 2 Baseline characteristics of participants according to the quartiles of the CRP/HDL-c.

Characteristic	Q1(0.02, 0.05) N = 2,729	Q2(0.07, 0.10) N = 2,731	Q3(0.13, 0.18) N = 2,726	Q4(0.27, 0.41) N = 2,729	*p* value
Age (years)	52 (47, 57)	51 (46, 56)	51 (46, 56)	50 (45, 56)	<0.001
Male gender, n (%)	1,826 (67%)	1,915 (70%)	2,021 (74%)	2,122 (78%)	<0.001
SBP (mmHg)	123 (111, 135)	122 (111, 135)	125 (113, 136)	127 (115, 138)	<0.001
DBP (mmHg)	80 (73, 87)	79 (72, 86)	80 (73, 87)	81 (74, 89)	<0.001
BMI (kg/m^2)	24.9 (22.8, 26.8)	25.5 (23.6, 27.5)	26.3 (24.6, 28.4)	27.2 (25.2, 29.3)	<0.001
Waist to hip ratio	0.92 (0.84, 0.96)	0.93 (0.86, 0.96)	0.94 (0.89, 0.98)	0.95 (0.91, 0.99)	<0.001
ALT (U/L)	20 (15, 29)	21 (15, 30)	23 (17, 35)	24 (17, 36)	<0.001
AST (U/L)	19 (16, 23)	19 (16, 23)	19 (16, 24)	19 (16, 25)	<0.001
BUN (mmol/l)	5.20 (4.40, 6.09)	5.10 (4.40, 6.00)	5.20 (4.40, 6.10)	5.10 (4.40, 6.00)	0.200
Cr (umol/l)	69 (59, 79)	68 (58, 78)	68 (59, 78)	69 (59, 78)	0.400
eGFR (mL/min/1.73 m2)	104 (95, 110)	103 (96, 109)	102 (95, 109)	101 (94, 107)	<0.001
SUA (umol/l)	336 (278, 394)	341 (285, 399)	356 (301, 412)	367 (311, 425)	<0.001
FBG (mmol/l)	5.70 (5.21, 6.53)	5.68 (5.21, 6.57)	5.84 (5.32, 6.74)	5.94 (5.35, 7.13)	<0.001
HbA1c (%)	5.90 (5.80, 6.30)	6.00 (5.80, 6.40)	6.00 (5.80, 6.50)	6.10 (5.80, 6.80)	<0.001
FCP (ng/ml)	2.33 (1.81, 2.98)	2.51 (1.99, 3.13)	2.79 (2.23, 3.45)	3.03 (2.43, 3.76)	<0.001
FINS (mU/L)	9 (6, 13)	10 (7, 14)	11 (8, 16)	13 (9, 18)	<0.001
HOMA-IR	2.28 (1.52, 3.37)	2.53 (1.69, 3.71)	3.01 (2.05, 4.28)	3.38 (2.28, 5.15)	<0.001
TG (mmol/l)	1.49 (1.05, 2.23)	1.49 (1.06, 2.18)	1.72 (1.26, 2.41)	1.92 (1.38, 2.79)	<0.001
TC (mmol/l)	4.88 (4.19, 5.59)	4.83 (4.18, 5.47)	4.86 (4.24, 5.51)	4.81 (4.18, 5.50)	0.110
LDL-c (mmol/l)	3.18 (2.53, 3.82)	3.18 (2.59, 3.76)	3.20 (2.63, 3.75)	3.12 (2.56, 3.73)	0.072
HDL-c (mmol/l)	1.29 (1.07, 1.54)	1.19 (1.02, 1.39)	1.08 (0.92, 1.25)	0.98 (0.84, 1.14)	<0.001
CRP (mg/l)	0.04 (0.02, 0.06)	0.10 (0.08, 0.12)	0.17 (0.14, 0.20)	0.37 (0.27, 0.41)	<0.001
Smoke, n (%)	677 (25%)	708 (26%)	662 (24%)	697 (26%)	0.501
Drink, n (%)	881 (32%)	890 (33%)	899 (33%)	890 (33%)	0.988
Hypertension, n (%)	141 (5.2%)	232 (8.5%)	247 (9.1%)	253 (9.3%)	<0.001
Diabetes, n (%)	595 (22%)	604 (22%)	721 (26%)	900 (33%)	<0.001
HUA	503 (18.43%)	557 (20.39%)	669 (24.54%)	814 (29.82%)	<0.001

Data are number of subjects (percentage) or medians (interquartile ranges).
Kruskal-Wallis rank sum test was used to compare the median values between participants.
Chi-square test was used to compare the percentage between participants.

No significant interactions were observed for age, BMI, smoking status, drinking status, diabetes, hypertension, or eGFR (all P for interaction > 0.05). Furthermore, the RCS results showed a linear relationship between the CRP/HDL-c and the risk of developing HUA across the entire diabetes and prediabetes population (Supplementary Figure 2).

4 Discussion

This population-based study provides novel evidence for an association between the CRP/HDL-c ratio and the risk of HUA in patients with diabetes or prediabetes. Compared with traditional lipid and inflammatory markers, a higher CRP/HDL-c ratio was more strongly associated with an increased risk of HUA in patients with diabetes or prediabetes.

Currently, an estimated 537 million adults globally are affected by diabetes, with over 90% of cases classified as type 2 diabetes mellitus (T2DM). This number is projected to increase to 783 million by 2045 (33). HUA and T2DM commonly coexist, and individuals with HUA have a 1.5-fold higher risk of developing T2DM compared with the general population (13). A cross-sectional analysis involving 1,037 individuals with diabetes and 272 healthy controls reported a significantly higher prevalence of

10.3389/fendo.2025.1619370

TABLE 3 Regression analyses for the association between CRP/HDL-c and HUA risk or SUA concentration.

A						
HUA	Model 1		Model 2		Model 3	
	OR (95%CI)	*P* value	OR (95%CI)	*P* value	OR (95%CI)	*P* value
Continuous						
CRP	2.25(1.55,3.29)	<0.001	2.24(1.54,3.25)	<0.001	1.95(1.26,2.98)	<0.001
HDL-c	0.30(0.26,0.36)	<0.001	0.63(0.53,0.75)	<0.001	0.90(0.71,1.14)	0.384
CRP/HDL-c	2.64(1.65,3.73)	<0.001	2.25(1.57,3.14)	<0.001	1.64(1.14,2.36)	0.008
Categories						
Quantile 1	reference		reference		reference	
Quantile 2	1.13(0.99,1.30)	0.067	1.02(0.89,1.17)	0.746	1.11(0.96,1.29)	0.146
Quantile 3	1.44(1.26,1.64)	<0.001	1.14(1.00,1.31)	0.049	1.17(1.02,1.36)	0.028
Quantile 4	1.88(1.66, 2.14)	<0.001	1.34(1.17,1.53)	<0.001	1.33(1.15,1.54)	<0.001
P for trend	< 0.001		<0.001		<0.001	
B						
SUA	Model 1		Model 2		Model 3	
	β(95%CI)	*P* value	β(95%CI)	*P* value	β(95%CI)	*P* value
Continuous						
CRP	1.00(0.81, 1.20)	<0.001	0.47(0.28,0.66)	<0.001	0.48(0.30,0.65)	<0.001
HDL-c	-1.30(-1.40, -1.20)	<0.001	-0.25(-0.33, -0.17)	<0.001	0.01(-0.11,0.09)	0.828
CRP/HDL-c	1.30(1.10, 1.50)	<0.001	0.47(0.30,0.65)	<0.001	0.26(0.10,0.43)	0.002
Categories						
Quantile 1	reference		reference		reference	
Quantile 2	0.10(0.02, 0.17)	0.009	-0.02(-0.08,0.05)	0.643	0.03(-0.03,0.09)	0.323
Quantile 3	0.35(0.27, 0.42)	<0.001	0.09(0.03,0.16)	0.004	0.10(0.04,0.16)	0.001
Quantile 4	0.53(0.46, 0.61)	<0.001	0.16(0.09,0.22)	<0.001	0.14(0.08,0.20)	<0.001
P for trend	< 0.001		< 0.001		< 0.001	

(A) Logistic regression analysis results for the association between the CRP/HDL-c and the risk of developing HUA. (B) Linear regression analysis results for the association between the CRP/HDL-c and the SUA concentration.
OR: odds ratio;95% CI: 95% confidence interval.
Model 2: adjusted for age, gender, BMI; Model 3: adjusted for age, gender, SBP, DBP, BMI, Waist to hip ratio, ALT, AST, BUN, Cr, eGFR, FBG, FCP, FINS, TC, TG, LDL-c, HbA1c, Drinkers, Hypertension.

HUA among patients with diabetes than among controls (34). Other studies have similarly shown that the prevalence of HUA is highest among individuals with impaired glucose tolerance, exceeding that observed in patients with T2DM or prediabetes individuals (35). Elevated serum uric acid levels have also been linked to an increased risk of chronic kidney disease (36), cardiovascular disease, hypertension (37), T2DM, metabolic syndrome (38, 39), and cognitive decline (40). Although the causal relationship between HUA and diabetes-related complications remains uncertain, several studies have identified elevated UA levels as a risk factor for atherosclerosis in patients with T2DM (41, 42). Given these findings, greater attention should be paid to the management of serum UA levels in individuals with diabetes or prediabetes to prevent the development of HUA. The identification of novel predictive markers is also warranted to enable early detection and timely intervention.

CRP/HDL-c has been introduced into clinical practice as a potential marker for predicting metabolic syndrome (MetS) (43). Compared with single biomarkers, this ratio may better capture the interplay between lipid metabolism and systemic inflammation, particularly in individuals with diabetes or prediabetes, thereby improving the accuracy of clinical risk stratification. In our study, the CRP/HDL-C ratio was strongly associated with the risk of HUA in both diabetic and prediabetic populations. Insulin resistance (IR), a common feature of diabetes and prediabetes, contributes to hyperglycemia, which may increase hepatic gluconeogenesis, impair lipid metabolism, and promote oxidative stress and inflammation—mechanisms that are likely to underlie the

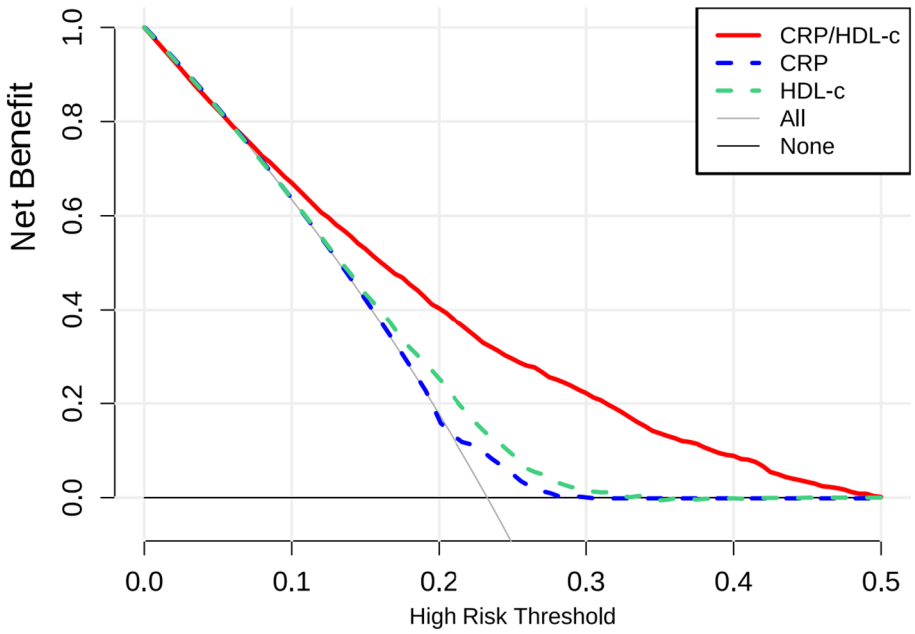

FIGURE 1
DCA results.

development of HUA (44). Previous animal studies have shown that small-molecule inhibitors targeting fatty acid synthase can improve hepatic function, reduce inflammation, and attenuate oxidative stress in obese mice fed a high-sugar diet (44).Our findings also showed that patients with diabetes or prediabetes and concurrent HUA had significantly higher HOMA-IR values, suggesting more severe insulin resistance in this group. Moreover, individuals in the highest quartile of CRP/HDL-C had both higher HOMA-IR levels and greater risk of HUA compared with those in the lowest quartile, consistent with previous research. Obesity was highly prevalent among participants with diabetes or prediabetes. Those with coexisting HUA had significantly higher BMI, indicating a

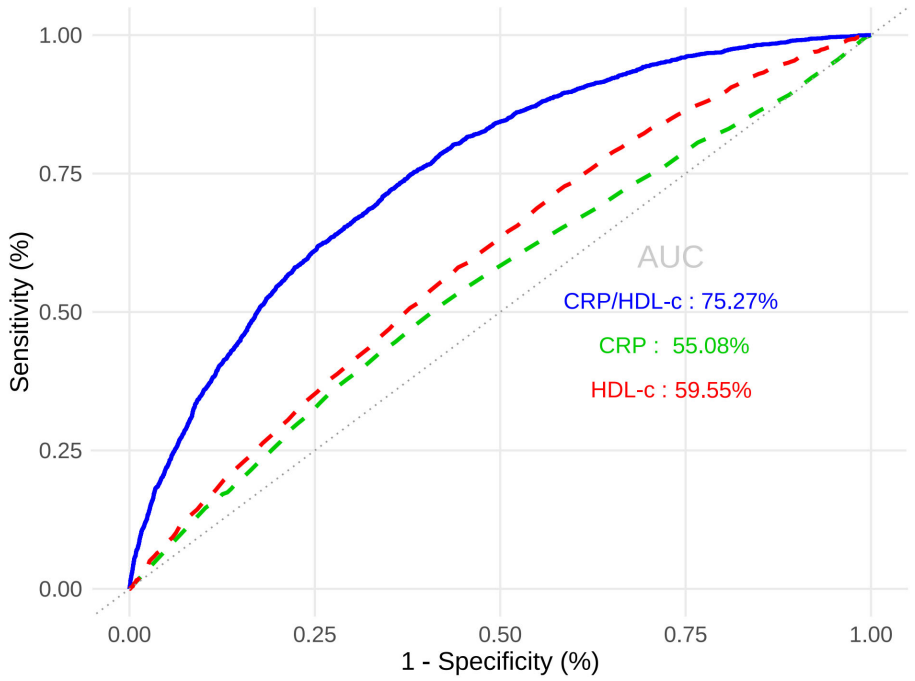

FIGURE 2
ROC results.

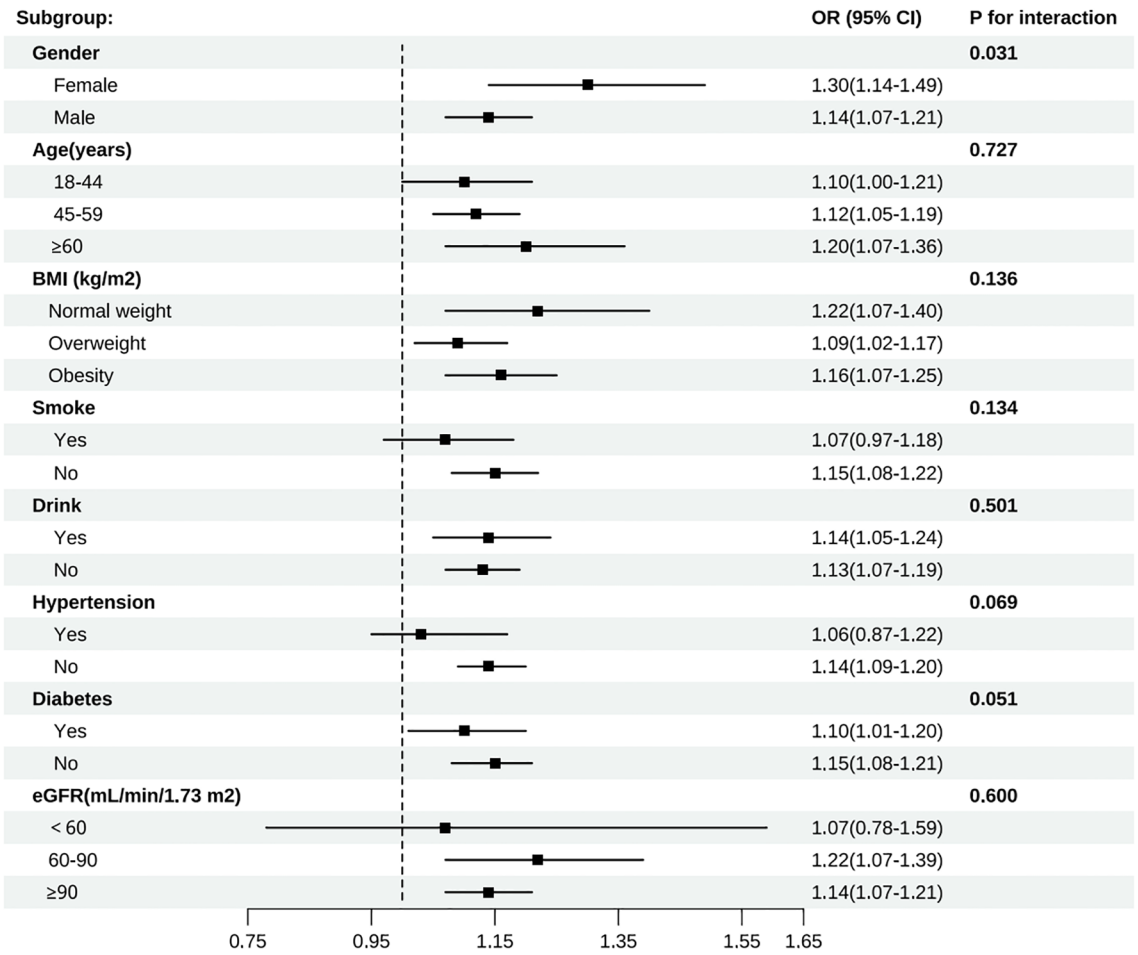

FIGURE 3
Subgroup analyses of all participants by gender, age, BMI, smoke, drink, hypertension, diabetes, and eGFR group.

possible link between obesity and elevated SUA through two main pathways. One relates to lifestyle factors such as diets high in purine-rich meat, fat, and alcohol. The other involves adipokine regulation. Low adiponectin levels have been associated with both microvascular and macrovascular complications of diabetes, while leptin has shown variable associations with coronary heart disease in patients with type 2 diabetes (45). Notably, previous studies have reported an inverse relationship between SUA and adiponectin levels in hypertensive patients with MetS (46). Interestingly, the association between CRP/HDL-c and hyperuricemia was stronger in females than in males, with a significant interaction by gender. Interestingly, our gender-stratified analyses revealed that the association between the CRP/HDL ratio and HUA was stronger in females than in males. Notably, this association was most pronounced among women aged <50 years. Several biological and hormonal mechanisms may underlie this observation. Estrogen is known to exert anti-inflammatory effects and to enhance HDL-C levels, potentially leading to a more dynamic balance between pro- and anti-inflammatory processes in premenopausal women (47, 48). As a result, fluctuations in the CRP/HDL ratio may better reflect early metabolic disturbances in this population. Moreover, estrogen has been shown to facilitate uric acid excretion via renal pathways, and declining estrogen levels with age may attenuate this protective effect. Prior studies have similarly demonstrated sex-specific differences in inflammation and lipid metabolism, highlighting the need for gender- and age-specific risk stratification in metabolic disease (49). These findings suggest that the CRP/HDL ratio may serve as a particularly sensitive marker of hyperuricemia risk in younger women.

This study possesses several important strengths. First, it utilised data from a large-scale and well-established health management database at the Second Medical Centre of the Chinese PLA General Hospital, ensuring a substantial sample size with strong representativeness and generalizability. Second, potential confounding factors were rigorously controlled for during both the design and analytical phases, thereby enhancing the internal validity and reliability of the results. Third, restricted cubic spline (RCS) modelling was employed to examine potential non-linear associations between CRP/HDL-C and hyperuricemia, and subgroup analyses were conducted to assess the robustness and consistency of the findings across different population subgroups. Fourth, to account for the possibility that an elevated CRP/HDL-c ratio may arise from distinct individual alterations in CRP or HDL-c, we examined their associations with hyperuricemia separately.

The consistent findings further supported the validity of CRP/HDL-c as a robust composite marker integrating inflammatory and lipid-related risk.

Nonetheless, several limitations should be acknowledged. First, the cross-sectional design of this study precludes causal inference, and the associations observed cannot establish temporal relationships. Longitudinal and interventional studies are warranted to elucidate underlying mechanisms. Second, although we adjusted for multiple covariates, residual confounding cannot be ruled out. For instance, we lacked data on the use of urate-lowering, lipid-lowering, and glucose-lowering medications, as well as key lifestyle factors such as alcohol consumption and dietary composition. Third, our study population exhibited relatively well-controlled glycemic levels, as indicated by low mean fasting glucose and HbA1c values. Future studies in populations with poorer glycemic control are needed to verify the generalizability of these findings. Fourth, although the CRP/HDL-c ratio functions as a composite marker integrating inflammation and lipid metabolism, it should be noted that a high ratio may result from elevated CRP, decreased HDL-c, or both. These scenarios may reflect different physiological mechanisms, and caution is warranted when interpreting the clinical implications of the ratio in isolation. Finally, although the CRP/HDL-c ratio was significantly associated with hyperuricemia in both males and females, we observed a stronger association in females (P for interaction = 0.031). Further subgroup analysis revealed that this association was particularly pronounced in females under 50 years old, with a significant interaction by age observed in women (P for interaction = 0.008). These findings underscore potential sex- and age-related heterogeneity, and suggest that this marker should be interpreted with consideration of demographic context and in conjunction with other clinical indicators.

5 Conclusion

We found a significant association between the CRP/HDL-c ratio and the risk of hyperuricemia in people with diabetes or prediabetes. Targeting inflammation and lipid metabolism to decrease this ratio may offer a potential strategy for risk assessment, prevention, and management of hyperuricemia in this population.

Data availability statement

The original contributions presented in the study are included in the article/Supplementary Material. Further inquiries can be directed to the corresponding authors.

Ethics statement

The studies involving humans were approved by Beijing hospital Research Ethics Committee(2025BJYYEC-KY039-01). The studies were conducted in accordance with the local legislation and institutional requirements. The participants provided their written informed consent to participate in this study.

Author contributions

DH: Writing – review & editing, Writing – original draft. JM: Writing – original draft. YZ: Writing – original draft. QP: Writing – review & editing. GX: Writing – review & editing. LG: Writing – review & editing.

Funding

The author(s) declare that financial support was received for the research and/or publication of this article. This study was supported by the National High-Level Hospital Clinical Research Funding (BJ-2021-200, BJ-2022-193, and BJ-2022-120), the National Natural Science Foundation of China (Grant No. 82170848), the Capital's Funds for Health Improvement and Research (Grant No. 2022-1-4051), and the Beijing Municipal Science and Technology Commission (Grant No. Z221100007422007).

Acknowledgments

This research has been conducted using the Health Management Institute, PLA General Hospital. The authors appreciate all the team members and participants involved in the study.

Conflict of interest

The authors declare that the research was conducted in the absence of any commercial or financial relationships that could be construed as a potential conflict of interest.

Generative AI statement

The author(s) declare that no Generative AI was used in the creation of this manuscript.

Publisher's note

Supplementary material

The Supplementary Material for this article can be found online at: https://www.frontiersin.org/articles/10.3389/fendo.2025.1619370/full#supplementary-material

References

1. Li L, Zhang Y, Zeng C. Update on the epidemiology, genetics, and therapeutic options of hyperuricemia. *Am J Trans Res*. (2020) 12:3167–81.

2. Sharma G, Dubey A, Nolkha N, Singh JA. Hyperuricemia, urate-lowering therapy, and kidney outcomes: a systematic review and meta-analysis. *Ther Adv In Musculoskeletal Disease*. (2021) 13:1759720X211016661. doi: 10.1177/1759720X211016661

3. Yu Y, Quan X, Wang H, Zhang B, Hou Y, Su C. Assessing the health risk of hyperuricemia in participants with persistent organic pollutants exposure - a systematic review and meta-analysis. *Ecotoxicol Environ Safety*. (2023) 251:114525. doi: 10.1016/j.ecoenv.2023.114525

4. Bardin T, Richette P. Impact of comorbidities on gout and hyperuricaemia: an update on prevalence and treatment options. *BMC Med*. (2017) 15:123. doi: 10.1186/s12916-017-0890-9

5. Lin D, Yao Z, Haorui L, Qiyue W, Lei X, Bo Y, et al. Hyperuricemia and its related diseases: mechanisms and advances in therapy. *Signal Transduction Targeted Ther*. (2024) 9:212. doi: 10.1038/s41392-024-01916-y

6. Zhu Y, Pandya BJ, Choi HK. Prevalence of gout and hyperuricemia in the US general population: the National Health and Nutrition Examination Survey 2007-2008. *Arthritis Rheumatism*. (2011) 63:3136–41. doi: 10.1002/art.30520

7. Kim Y, Kang J, Kim G-T. Prevalence of hyperuricemia and its associated factors in the general Korean population: an analysis of a population-based nationally representative sample. *Clin Rheumatol*. (2018) 37:2529–38. doi: 10.1007/s10067-018-4130-2

8. Rui L, Cheng H, Di W, Xinghai X, Jianqiu G, Haixia G, et al. Prevalence of hyperuricemia and gout in mainland China from 2000 to 2014: A systematic review and meta-analysis. *BioMed Res Int*. (2015) 2015:762820. doi: 10.1155/2015/762820

9. Shiyi S, Lihong C, Dawei C, Yan L, Guanjian L, Lin M, et al. Prevalence and associated factors of hyperuricemia among Chinese patients with diabetes: a cross-sectional study. *Ther Adv In Endocrinol Metab*. (2023) 14:20420188231198620. doi: 10.1177/20420188231198620

10. Jinguo J, Tingjing Z, Yashu L, Qing C, Yuhong Z, Chuanji G, et al. Prevalence of diabetes in patients with hyperuricemia and gout: A systematic review and meta-analysis. *Curr Diabetes Rep*. (2023) 23:103–17. doi: 10.1007/s11892-023-01506-2

11. Shuai Y, Ying C, Xu H, Donghua X, Kui C, Changgui L, et al. Serum uric acid levels and diabetic peripheral neuropathy in type 2 diabetes: a systematic review and meta-analysis. *Mol Neurobiol*. (2016) 53:1045–51. doi: 10.1007/s12035-014-9075-0

12. Bhole V, Choi JWJ, Kim SW, de Vera M, Choi H. Serum uric acid levels and the risk of type 2 diabetes: a prospective study. *Am J Med*. (2010) 123:957–61. doi: 10.1016/j.amjmed.2010.03.027

13. Ismail L, Materwala H, Al Kaabi J. Association of risk factors with type 2 diabetes: A systematic review. *Comput Struct Biotechnol J*. (2021) 19:1759–85. doi: 10.1016/j.csbj.2021.03.003

14. Yuzhang Z, Yaqiu H, Tianliang H, Yongneng Z, Zhi L, Chaohuan L, et al. High uric acid directly inhibits insulin signalling and induces insulin resistance. *Biochem Biophys Res Commun*. (2014) 447:707–14. doi: 10.1016/j.bbrc.2014.04.080

15. Lohsoonthorn V, Dhanamun B, Williams MA. Prevalence of hyperuricemia and its relationship with metabolic syndrome in Thai adults receiving annual health exams. *Arch Med Res*. (2006) 37:883–9. doi: 10.1016/j.arcmed.2006.03.008

16. Delun L, Siyu Y, Yiyao D, Xiaowan W, Shouhai W, Xuesheng C, et al. The dysregulation of immune cells induced by uric acid: mechanisms of inflammation associated with hyperuricemia and its complications. *Front In Immunol*. (2023) 14:1282890. doi: 10.3389/fimmu.2023.1282890

17. Lontchi-Yimagou E, Sobngwi E, Matsha TE, Kengne AP. Diabetes mellitus and inflammation. *Curr Diabetes Rep*. (2013) 13:435–44. doi: 10.1007/s11892-013-0375-y

18. Aeron MS, Ashley P, Giorgio EMM, Benjamin MS, Deepak LB, Itamar R, et al. Lipoprotein(a), C-reactive protein, and cardiovascular risk in primary and secondary prevention populations. *JAMA Cardiol*. (2024) 9:385–91. doi: 10.1001/jamacardio.2023.5605

19. Amirian A, Rahnemaei FA, Abdi F. Role of C-reactive Protein(CRP) or high-sensitivity CRP in predicting gestational diabetes Mellitus: Systematic review. *Diabetes Metab Syndrome*. (2020) 14:229–36. doi: 10.1016/j.dsx.2020.02.004

20. Koenig W. High-sensitivity C-reactive protein and atherosclerotic disease: from improved risk prediction to risk-guided therapy. *Int J Cardiol*. (2013) 168:5126–34. doi: 10.1016/j.ijcard.2013.07.113

21. Tao-Chun P, Chung-Ching W, Tung-Wei K, James Yi-Hsin C, Ya-Hui Y, Yaw-Wen C, et al. Relationship between hyperuricemia and lipid profiles in US adults. *BioMed Res Int*. (2015) 2015:127596. doi: 10.1155/2015/127596

22. Yanyu Z, Xiaoyi L, Deyun L, Bingli C, Chenyi L, Chenyu H, et al. Association of LDL-C/HDL-C ratio with hyperuricemia: A national cohort study. *Clin Trans Sci*. (2025) 18:e70122. doi: 10.1111/cts.70122

23. von Eckardstein A, Nordestgaard BG, Remaley AT, Catapano AL. High-density lipoprotein revisited: biological functions and clinical relevance. *Eur Heart J*. (2023) 44:1394–407. doi: 10.1093/eurheartj/ehac605

24. Yu G, Miyuan W, Ruiting W, Jinchi J, Yueyao H, Wei W, et al. The predictive value of the hs-CRP/HDL-C ratio, an inflammation-lipid composite marker, for cardiovascular disease in middle-aged and elderly people: evidence from a large national cohort study. *Lipids In Health Disease*. (2024) 23:66. doi: 10.1186/s12944-024-02055-7

25. Djesevic M, Hasic S, Lepara O, Jahic R, Kurtovic A, Fajkic A. CRP/HDL-C and monocyte/HDL-C ratios as predictors of metabolic syndrome in patients with type 2 diabetes mellitus. *Acta Informatica Med*. (2023) 31:254–9. doi: 10.5455/aim.2023.31.254-259

26. Jinfeng W, Jinhao G, Xianglin Y, Hongbin Q, Jiarui Z. Correlation of the lipid complex marker hs-CRP/HDL-C ratio with hyperuricaemia: a cross-sectional retrospective study from NHANES 2015-2018. *Sci Rep*. (2025) 15:8495. doi: 10.1038/s41598-024-83126-8

27. David BS, Mark A, George LB, David EB, Andrea RH, Åke L, et al. Guidelines and recommendations for laboratory analysis in the diagnosis and management of diabetes mellitus. *Diabetes Care*. (2023) 46:e151–99. doi: 10.2337/dci23-0036

28. Feig DI, Kang D-H, Johnson RJ. Uric acid and cardiovascular risk. *New Engl J Med*. (2008) 359:1811–21. doi: 10.1056/NEJMra0800885

29. Andrew SL, Lesley AS, Christopher HS, Yaping Lucy Z, Alejandro FC, Harold IF, et al. A new equation to estimate glomerular filtration rate. *Ann Internal Med*. (2009) 150:604–12. doi: 10.7326/0003-4819-150-9-200905050-00006

30. Zhenjie W, Christopher M, Shinichiro Y, Sanjeev B, Makiko M, Kengo T, et al. No effect modification of serum bilirubin or coffee consumption on the association of gamma-glutamyltransferase with glycated hemoglobin in a cross-sectional study of Japanese men and women. *BMC Endocrine Disord*. (2012) 12:24. doi: 10.1186/1472-6823-12-24

31. Wang S-S, Lay S, Yu H-N, Shen S-R. Dietary Guidelines for Chinese Residents (2016): comments and comparisons. *J Zhejiang University Sci B*. (2016) 17:649–56. doi: 10.1631/jzus.B1600341

32. Chen Z, Wang F, Zheng Y, Zeng Q, Liu H. H-type hypertension is an important risk factor of carotid atherosclerotic plaques. *Clin Exp Hypertension (New York N.Y: 1993)*. (2016) 38:424–8. doi: 10.3109/10641963.2015.1116547

33. Tönnies T, Rathmann W, Hoyer A, Brinks R, Kuss O. Quantifying the underestimation of projected global diabetes prevalence by the International Diabetes Federation (IDF) Diabetes Atlas. *BMJ Open Diabetes Res Care*. (2021) 9(1): e002122. doi: 10.1136/bmjdrc-2021-002122

34. Hiroyuki I, Mariko A, Mizuo M, Koshiro O, Shinichi A, Yuichiro T, et al. Hyperuricemia is independently associated with coronary heart disease and renal dysfunction in patients with type 2 diabetes mellitus. *PloS One*. (2011) 6:e27817. doi: 10.1371/journal.pone.0027817

35. Yuan H-J, Yang X-G, Shi X-Y, Tian R, Zhao Z-G. Association of serum uric acid with different levels of glucose and related factors. *Chin Med J*. (2011) 124:1443–8.

36. Mélanie G, Thomas B, Alain CS, François D, Jean-Pierre F, Régis G, et al. Hyperuricemia and hypertension, coronary artery disease, kidney disease: from concept to practice. *Int J Mol Sci*. (2020) 21. doi: 10.3390/ijms21114066

37. Gulali A, Atiqa K, Ozge K, Tuba TD, Satilmis B, Gizem K, et al. Poorly controlled hypertension is associated with elevated serum uric acid to HDL-cholesterol ratio: a cross-sectional cohort study. *Postgraduate Med*. (2022) 134:297–302. doi: 10.1080/00325481.2022.2039007

38. Novak S, Melkonian AK, Patel PA, Kleinman NL, Joseph-Ridge N, Brook RA. Metabolic syndrome-related conditions among people with and without gout: prevalence and resource use. *Curr Med Res Opinion*. (2007) 23:623–30. doi: 10.1185/030079906X167651

39. Rajiv H, Masahiko Y, Michelle S, Madhu B, Fuad ZA, Paul JT, et al. Non-alcoholic fatty liver and chronic kidney disease: Retrospect, introspect, and prospect. *World J Gastroenterol*. (2021) 27:1864–82. doi: 10.3748/wjg.v27.i17.1864

40. Franco ÁdO, Starosta RT, Roriz-Cruz M. The specific impact of uremic toxins upon cognitive domains: a review. *Jornal Brasileiro Nefrologia*. (2019) 41:103–11. doi: 10.1590/2175-8239-jbn-2018-0033

41. Giacomo Z, Giovanni T, Carlo N, Vincenzo S, Fabrizia P, Michele M, et al. Elevated serum uric acid concentrations independently predict cardiovascular mortality in type 2 diabetic patients. *Diabetes Care*. (2009) 32:1716–20. doi: 10.2337/dc09-0625

42. Yili X, Jiayu Z, Li G, Yun L, Jie S, Chong S, et al. Hyperuricemia as an independent predictor of vascular complications and mortality in type 2 diabetes patients: a meta-analysis. *PLoS One*. (2013) 8:e78206. doi: 10.1371/journal.pone.0078206

43. Jialal I, Adams-Huet B, Remaley AT. A comparison of the ratios of C-reactive protein and triglycerides to high-density lipoprotein-cholesterol as biomarkers of metabolic syndrome in African Americans and non-Hispanic Whites. *J Diabetes Its Complications*. (2022) 36:108231. doi: 10.1016/j.jdiacomp.2022.108231

44. Ma L, Wang J, Ma L, Wang XM. The link between hyperuricemia and diabetes: insights from a quantitative analysis of scientific literature. *Front In Endocrinol*. (2024) 15:1441503. doi: 10.3389/fendo.2024.1441503

45. Katsiki N, Yovos JG, Gotzamani-Psarrakou A, Karamitsos DT. Adipokines and vascular risk in type 2 diabetes mellitus. *Angiology*. (2011) 62:601–4. doi: 10.1177/0003319711409201

46. Chan Seok P, Sang-Hyun I, Hun-Jun P, Woo-Seung S, Pum-Jun K, Kiyuk C, et al. Relationship between plasma adiponectin, retinol-binding protein 4 and uric Acid in hypertensive patients with metabolic syndrome. *Korean Circ J*. (2011) 41:198–202. doi: 10.4070/kcj.2011.41.4.198

47. Mustafa K, Suleyman Hilmi I, Levent K, Ayse Gul K, Huseyin K, Fikret A, et al. Risk factors for diabetes mellitus in women with primary ovarian insufficiency. *Biol Trace Element Res*. (2013) 154:313–20. doi: 10.1007/s12011-013-9738-0

48. Yizhou H, Yifei L, Tongyun Q, Zhou L, Xingjun M, Qian Y, et al. Metabolic profile of women with premature ovarian insufficiency compared with that of age-matched healthy controls. *Maturitas*. (2021) 148:33–9. doi: 10.1016/j.maturitas.2021.04.003

49. Hak AE, Choi HK. Menopause, postmenopausal hormone use and serum uric acid levels in US women–the Third National Health and Nutrition Examination Survey. *Arthritis Res Ther*. (2008) 10:R116. doi: 10.1186/ar2519

frontiers | Frontiers in Immunology

TYPE Original Research
PUBLISHED 16 July 2025
DOI 10.3389/fimmu.2025.1631409

OPEN ACCESS

EDITED BY
Bin Cheng,
Lanzhou University of Technology, China

REVIEWED BY
Tayyaba Zainab,
Pir Mehr Ali Shah Arid Agriculture University, Pakistan
Chayan Munshi,
Ethophilia Research Foundation, India
Hao An,
Lanzhou University, China

*CORRESPONDENCE
Alok Agrawal
avds_99@yahoo.com
Sanjay K. Singh
singhs@etsu.edu

†PRESENT ADDRESS
Alok Agrawal,
Retired, Johnson City, TN, United States

RECEIVED 19 May 2025
ACCEPTED 30 June 2025
PUBLISHED 16 July 2025

CITATION
Agrawal A, Ngwa DN, Simons JP and Singh SK (2025) Protection against prolonged pneumococcal infection involves structural changes in C-reactive protein and subsequent binding to both phosphocholine and amyloids on the bacterial surface. *Front. Immunol.* 16:1631409. doi: 10.3389/fimmu.2025.1631409

Protection against prolonged pneumococcal infection involves structural changes in C-reactive protein and subsequent binding to both phosphocholine and amyloids on the bacterial surface

Alok Agrawal[1*†], Donald N. Ngwa[1], J. Paul Simons[2] and Sanjay K. Singh[1*]

[1]Department of Biomedical Sciences, College of Medicine, East Tennessee State University, Johnson City, TN, United States, [2]Centre for Amyloidosis and Acute Phase Proteins, Division of Medicine, University College London, London, United Kingdom

C-reactive protein (CRP) protects mice during the initial stages of *Streptococcus pneumoniae* infection. In order to be protective against all stages of infection, we hypothesize that CRP binds to two different ligands on pneumococci. In its native form, CRP binds to phosphocholine residues of C-polysaccharide to activate complement. In its altered form, CRP binds to amyloid-like structures (amyloids) formed on complement inhibitors recruited by pneumococci. We employed CRP knockout mice to test this hypothesis. In one approach, both wild-type CRP and E42Q/F66A/T76Y/E81A mutant CRP (E-CRP-1) were administered together. E-CRP-1 does not bind to phosphocholine but binds to amyloids. In another approach, Y40F/E42Q mutant CRP (E-CRP-2) was administered. E-CRP-2 binds to both phosphocholine and amyloids. When CRP was administered to mice 12 h after inoculation, then unlike wild-type CRP by itself, the combination of wild-type CRP and E-CRP-1 was protective and E-CRP-2 alone was protective. We also detected amyloids on pneumococci. The serum levels of the amyloid-binding protein, serum amyloid P component (SAP), were higher in CRP knockout mice than in wild-type mice. Also, the basal SAP levels were higher in female than in male mice and, conversely, male mice were more susceptible than female mice to severe infection. We conclude that the protection against prolonged pneumococcal infection requires structural changes in CRP and binding to both phosphocholine and amyloids on pneumococci. The sources of amyloids can be virulence factors or recruited complement inhibitors or both. Combined data also raise the possibility that SAP cooperates with CRP in reducing bacteremia and bacterial load.

KEYWORDS

C-reactive protein, *Streptococcus pneumoniae*, bacterial amyloids, complement evasion, serum amyloid P component

Introduction

C-reactive protein (CRP) is an evolutionarily conserved protein, which suggests that CRP performs host-defense functions in all organisms from arthropods to humans (1–4). In humans, CRP is a component of the acute phase response; the serum level of CRP increases thousand-fold or more in acute inflammatory states (5). CRP is composed of five identical subunits arranged in a cyclic pentameric symmetry (6). CRP binds to phosphocholine (PCh)-containing substances, such as C-polysaccharide of the cell wall of *Streptococcus pneumoniae*, in a Ca^{2+}-dependent manner (7). All five subunits of CRP have a PCh-binding site consisting of amino acid residues Phe^{66}, Thr^{76} and Glu^{81} (8–10). PCh-complexed CRP activates the classical pathway of the complement system, leading to the destruction of the ligand (11). Human CRP activates mouse complement system also and therefore mice are widely used to investigate the *in vivo* functions of CRP (12–14).

The native pentameric conformation of CRP is altered under experimental inflammatory conditions such as in the presence of acidic pH or reactive oxygen species (15–18). At acidic pH, CRP has been shown to bind to amyloid-β peptide 1-42 (Aβ) (16, 19, 20). Some proteins, when immobilized, express Aβ-like structures (amyloids), and acidic pH-treated CRP binds to such immobilized proteins through the exposed amyloids (21, 22). The existence of non-native CRP *in vivo* and their deposition at sites of inflammation have been demonstrated by employing antibodies specific for non-native CRP (23, 24); however, it is not evident whether CRP seen at the sites of inflammation was monomeric CRP or non-native pentameric CRP. Like the PCh-binding function of CRP, the amyloid-binding function of CRP has also been conserved throughout evolution (25).

Human CRP protects against lethal pneumococcal infection by decreasing bacteremia in mouse models of the disease (26–30). Complement activation by ligand-complexed CRP is necessary for CRP-mediated protection against infection (31–33). In mouse models in which human CRP was passively administered to mice, CRP was protective only when administered 6 h before to 2 h after inoculation with pneumococci (34). It has been shown that pneumococci recruit complement-inhibitory proteins on their surface to become complement attack-resistant (35–42). The presence of complement-inhibitory proteins on pneumococci could be the reason for the inability of CRP to protect when administered 2 h after inoculation (Figures 1A, B).

It remains to be established that the ability of structurally altered pentameric CRP to bind to amyloids contributes to protection against pneumococcal infection (43). Since the acidic pH-induced changes in CRP are reversible at physiological pH, acidic pH-treated CRP cannot be administered to mice for *in vivo* studies (16). Therefore, recombinant CRP mutants have been created that mimic the amyloid-binding property of acidic pH-treated CRP (20, 21, 44). Previously, two such CRP mutants have been used as tools to investigate the host-defense functions of structurally altered CRP *in vivo*: E-CRP-1 and E-CRP-2 (22, 43). The ligand-recognition and effector functions of wild-type (WT) CRP, E-CRP-1 and E-CRP-2 are summarized in Figure 1C. E-CRP-1 (E42Q/F66A/T76Y/E81A CRP mutant) does not bind to PCh due to the mutations in the PCh-binding site (43, 45). E-CRP-1, however, binds to amyloids due to the presence of the E42Q mutation (20, 21). In contrast to E-CRP-1, E-CRP-2 (Y40F/E42Q CRP mutant) retains the ability to bind to PCh and, in addition, also binds to amyloids (20, 21, 43, 46). Biochemical analyses of acidic pH-treated WT CRP and of CRP mutants suggested that CRP gains the amyloid-binding property due to the loss of one Ca^{2+} from CRP and that the cholesterol-binding region of CRP which contains the Ca^{2+}-binding site may be involved (16, 20, 21, 47).

Our earlier findings that immobilized proteins express amyloids (21) prompted us to hypothesize that complement inhibitory proteins recruited by pneumococci may express amyloids. It is not known whether the virulence factors present on pneumococci also express amyloids. In this study, we tested the overall hypothesis that if the amyloid-expressing proteins on the pneumococcal surface are blocked by E-CRP-1/-2, then WT CRP should be able to protect mice against all stages of pneumococcal infection; for example, WT CRP should be able to protect mice against infection even when administered to mice 12 h post-inoculation. Two approaches were employed in this study. In the first approach, both WT CRP (for PCh-binding) and E-CRP-1 (for amyloid-binding) were administered to mice. In this approach, E-CRP-1 can bind to amyloid-expressing proteins and PCh-bound WT CRP can then activate complement and kill the bacteria (Figure 1D). In the second approach, E-CRP-2 (for both PCh-binding and amyloid-binding) was administered to mice, assuming that some E-CRP-2 molecules would bind to amyloids and some to PCh (Figure 1E). PCh-bound E-CRP-2 can then activate complement and kill the bacteria. CRP knockout (KO) mice were used in this study since our hypothesis could only be tested in CRP-deficient mice.

Materials and methods

Preparation of CRP

The cDNAs for E42Q/F66A/T76Y/E81A mutant CRP (E-CRP-1) and Y40F/E42Q mutant CRP (E-CRP-2) were constructed, expressed in CHO cells using the ExpiCHO Expression System (Thermo Fisher Scientific) and purified from the cell culture supernatants, as described previously (43, 46, 48). E-CRP-1 was purified by employing Ca^{2+}-dependent affinity chromatography on a phosphoethanolamine-conjugated Sepharose column, followed by ion-exchange chromatography on a MonoQ column and gel filtration on a Superose12 column. E-CRP-2 from cell culture supernatants and native WT CRP from discarded human pleural fluid were purified by employing Ca^{2+}-dependent affinity chromatography on a PCh-conjugated Sepharose column,

Abbreviations: Aβ, Amyloid-β peptide; Amyloids, amyloid-like structures; cfu, colony-forming units; CRP, C-reactive protein; E-CRP, engineered CRP; KO, knockout; moCRP, mouse CRP; MST, median survival time; PCh, phosphocholine; SAP, serum amyloid P component; *S. pneumoniae*, *Streptococcus pneumoniae*; WT, wild-type.

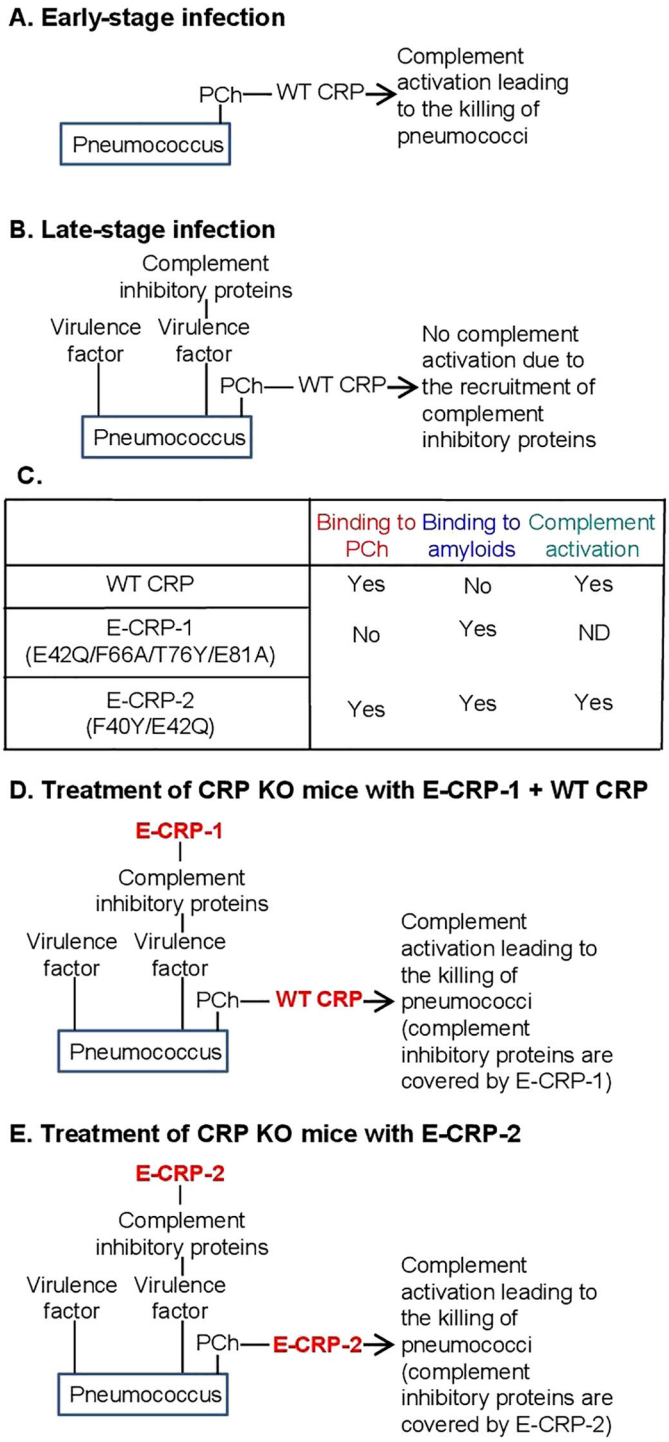

FIGURE 1
(A, B) Suggested mechanism of action of CRP in pneumococcal infection. **(C)** Ligand-recognition and effector functions of CRP molecules employed in this study. **(D, E)** Hypothesis for the mechanism of action of exogenously administered CRP in protecting CRP KO mice against prolonged pneumococcal infection.

followed by ion-exchange chromatography on a MonoQ column and gel filtration on a Superose12 column. The purity of CRP preparations was confirmed by denaturing 4-20% SDS-PAGE under reducing conditions. Purified CRP was dialyzed against 10 mM Tris-HCl, pH 7.2, containing 150 mM NaCl and 2 mM $CaCl_2$, and was subsequently treated with Detoxi-Gel Endotoxin Removing Gel (Thermo Fisher Scientific). The concentration of endotoxin in CRP preparations was determined by using the Limulus Amebocyte Lysate kit QCL-1000 (Lonza). Purified CRP was stored at 4°C and used within a week.

Pneumococci

S. pneumoniae type 3, strain WU2, was obtained from Dr. David Briles (University of Alabama at Birmingham, Birmingham, AL, USA) and used as described previously (43, 45). In brief, pneumococci were made virulent by sequential i.v. passages in mice and were stored in aliquots at -80°C. For each experiment, a separate aliquot of pneumococci was thawed and cultured. Cultured pneumococci were resuspended in normal saline and the concentration of pneumococci (cfu/ml) was adjusted based on the absorbance of the suspension at 600 nm (A_{600} = 1.00 = 1.2 x 10^9 cfu/ml). Within 2 h, 100 µl of pneumococci suspension containing the required number (cfu) of pneumococci, as mentioned in the figures, was injected into mice. The concentration of pneumococci was confirmed next day by plating.

Mice

The method for the generation of pure-line C57BL/6 CRP KO mice has been previously described (49). The breeding colony of CRP KO mice was maintained in the Division of Laboratory Animal Research of our university. Male and female WT C57BL/6 mice were purchased from Jackson Laboratories. Mice were brought up and maintained according to protocols approved by the University Committee on Animal Care. Mice were 8–10 weeks old when used in experiments.

Mouse protection experiments

Mouse protection experiments were performed exactly as described previously (29, 43). In brief, mice were inoculated with pneumococci; the numbers of pneumococci (cfu) are mentioned in the figures. CRP (25 µg) was administered at different time points as mentioned in the figures. The amount of endotoxin in 25 µg of all CRP preparations was <1.0 endotoxin units. Survival of mice was recorded three times per day for 7 days. Survival curves were generated using the GraphPad Prism 9 software. To determine *p*-values for the differences in the survival curves among various groups, the survival curves were compared using the software's Logrank (Mantel-Cox) test.

To determine bacteremia in the surviving mice, blood was collected daily for 5 days from the tip of the tail vein, diluted in normal saline, and plated on sheep blood agar for colony counting. The bacteremia value for dead mice was recorded as 10^9 cfu/ml because mice died when the bacteremia exceeded 10^8 cfu/ml. The scatter plots of the bacteremia data and the median bacteremia value for each group were generated using the GraphPad Prism 9 software. The software's Mann-Whitney test was used to determine *p*-values for the differences in bacteremia among various groups at each time point. The median values shown in the scatter plots for each group of mice were also plotted separately for easier comparison of all groups of mice in a single figure.

Assay for the detection of amyloids on pneumococci

Microtiter wells (Corning, 9018) were coated with increasing numbers of pneumococci in 100 µl TBS, pH 7.2, in duplicate, and incubated overnight at 4°C. The unreacted sites in the wells were blocked with TBS containing 0.5% gelatin for 45 min at room temperature. Both, polyclonal anti-Aβ antibodies (Novus, NBP2-25093) and monoclonal anti-Aβ antibodies (Novus, NBP2-13075) were used to detect the amyloids on the coated pneumococci. Normal rabbit IgG and normal mouse IgG were used as controls for the antibodies. The anti-Aβ antibodies (10 µg/ml) diluted in TBS containing 0.1% gelatin and 0.02% Tween 20 were added to the wells and incubated at 37°C for 1 h. After washing the wells, bound polyclonal anti-Aβ antibodies were detected by using HRP-conjugated donkey anti-rabbit IgG (GE Healthcare) and bound monoclonal anti-Aβ antibodies were detected by using HRP-conjugated goat anti-mouse IgG (Thermo Fisher Scientific). Color was developed, and the OD was read at 405 nm.

Assays for the measurement of mouse CRP and serum amyloid P component

The levels of mouse CRP (moCRP) in the sera obtained from the blood of WT mice were measured by using Mouse CRP Quantikine ELISA Kit (R&D, catalog number MCRP00). The levels of mouse serum amyloid P component (SAP) in the sera from WT and KO mice were measured by using Mouse SAP Quantikine ELISA Kit (R&D, catalog number MPTX20).

Results

Male mice are more susceptible than female mice to infection

To establish a CRP KO mouse model of infection with *S. pneumoniae* type 3, strain WU2, we titrated the dose of bacteria needed for inoculation. In order to determine whether there was any difference between WT and KO mice for their susceptibility to infection and whether there was any difference between male and female mice, both WT and KO mice and both male and female mice were employed. The median survival time (MST, the time taken for the death of 50% of mice) for each dose of bacteria was then determined.

As shown in the survival curves for all four types of mice (Figures 2A–D), and as expected, the MST decreased as the inoculation dose of bacteria increased. To determine the relative susceptibility of each type of mice to infection in terms of the dose of bacteria and the corresponding survival times, the data (Figures 2A–D) were compiled together and presented as MST curves (Figure 2E). The survival time of 50 h and the dose of 3 x 10^7 cfu of bacteria were chosen for comparing the four MST curves. As

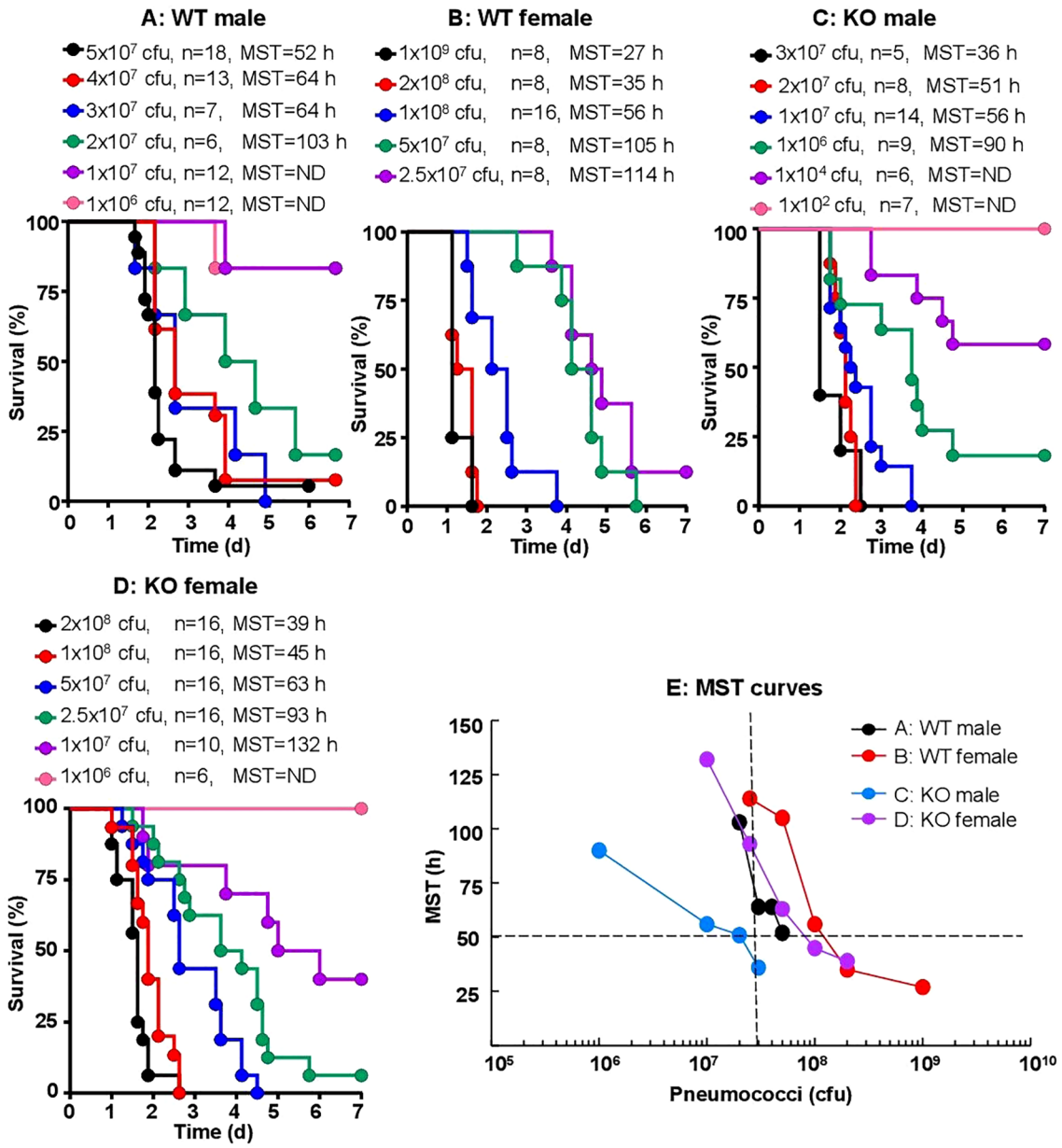

FIGURE 2
Sex-specificity and susceptibility of mice to infection. Mice were injected with 10^2–10^9 cfu of pneumococci, as shown for each group of mice (n, number of mice). The MST values are shown for each dose of pneumococci for each group of mice (ND, MST not determined since >50% mice survived). The data are combined from two separate experiments with six to nine mice for each dose of pneumococci in each group of mice. **(A)** Survival of male WT mice. **(B)** Survival of female WT mice. **(C)** Survival of male CRP KO mice. **(D)** Survival of female CRP KO mice. **(E)** The MST values for each group of mice shown in A-D are plotted together for comparing the susceptibility of all four types of mice. To determine *p*-values for the differences in the MST curves, the curves were subjected to two-way ANOVA followed by Tukey's multiple comparison test. The *p*-values for the differences in the MST curves between groups A B, C D, A C and B D were 0.07, 0.01, 0.03 and 0.31, respectively.

shown, for each type of mice to survive for 50 h after inoculation, the doses of bacteria were 13 x 10^7, 8 x 10^7, 5 x 10^7 and 2 x 10^7 cfu for WT female, KO female, WT male and KO male mice, respectively. Similarly, for mice inoculated with 3 x 10^7 cfu of bacteria, the survival times were 112 h, 86 h, 63 h and 36 h for WT female, KO female, WT male and KO male mice, respectively. These results and the statistical analyses of the MST curves indicated that male mice were significantly more susceptible than female mice to infection. Also, CRP KO mice were more susceptible than WT mice to infection, although the difference between the MST curves for female WT and female KO mice was not statistically significant.

CRP KO male mice inoculated with 10^7 cfu of pneumococci were employed as the mouse model for all CRP-mediated protection experiments, unless otherwise mentioned.

KO mice are most protected when WT CRP is administered prior to or within an hour of inoculation

The protective effects of WT CRP administered 30 min prior to and 15 min to 4 h after inoculation into KO male mice (Figure 3A) were determined first, by analyzing the survival curves of mice. Statistical analysis of the data showed that, when compared to group A mice (bacteria alone), CRP was clearly protective for groups B-F of mice, that is, if injected 30 min before to 2 h after inoculation. The *p*-value between group A and group G (CRP injected 4 h after inoculation), however, was 0.05, suggesting that CRP may still be protective. When compared to group B mice in which CRP was administered 30 min prior to inoculation, CRP was found to be protective only when injected 45 min after inoculation, but not later. Overall, as shown, as the interval between inoculation and CRP administration increased, the MST decreased. Mice survived longest and the MST could not be determined when CRP was given to mice 30 min before inoculation. Mice survived shortest when CRP was given to mice 4 h after inoculation. These results were similar to previously published data on the effects of WT CRP in WT mice: CRP was protective only when administered either prior to inoculation or at most 2 h post-inoculation. To confirm that WT CRP was protective against infection in KO female mice also, the 30 min time point for CRP injection prior to inoculation was chosen. As shown in Figure 3B, CRP protected female mice also. In all subsequent protection experiments, only CRP KO male mice were employed.

WT CRP and E-CRP-1 together protect KO mice even when administered 12 h after inoculation

We determined the protective effects of E-CRP-1 which does not bind to PCh and instead binds to amyloids. WT CRP administered 30 min prior to inoculation was included as a control for the animal model. As shown in Figure 4, and as has been reported earlier (43), WT CRP protected mice when administered 30 min prior to inoculation (group B) but did not protect when administered 12 h after inoculation (group D). The survival curve of mice treated with E-CRP-1, 30 min prior to inoculation (group C), was found to be significantly different from both group A (no CRP) and group B. However, like WT CRP, E-CRP-1 was not protective when administered 12 h after inoculation (group E). Although WT CRP and E-CRP-1 were not protective when either one was administered 12 h after inoculation, the survival curve of mice treated with the combination of WT CRP and E-CRP-1 was significantly different from both groups D and E and also different from group A. The survival times of mice treated with both WT CRP and E-CRP-1 together were longer than the survival times of mice treated with either WT CRP or E-CRP-1 alone and 10% of mice survived at the end of the experiment.

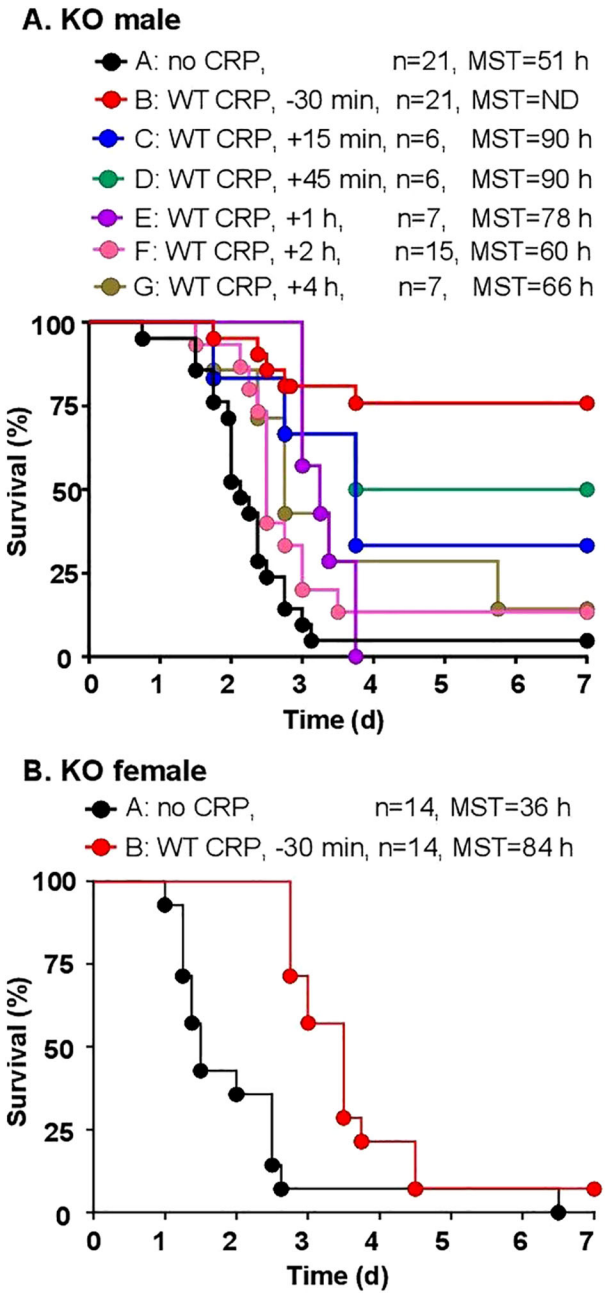

FIGURE 3
Survival of CRP KO mice infected with pneumococci and treated with WT CRP. The data are combined from two to three separate experiments with six to eight mice in each group in each experiment (n, number of mice). The MST values are shown for each group of mice (ND, MST not determined since >50% mice survived). **(A)** Male CRP KO mice. CRP was injected at various time points in different groups of mice, from 30 min before to 4 h after inoculation with pneumococci (10^7 cfu). The *p*-value for the difference in the survival curves between groups A and B was <0.001. The *p*-values for the differences between A C, A D, A E and A F were 0.01. The *p*-value for the difference between A and G was 0.05. The *p*-values for the differences between B C and B D were >0.05. The *p*-values for the differences between B E, B F and B G were <0.005. **(B)** Female CRP KO mice. CRP was injected 30 min prior to inoculation with pneumococci (10^8 cfu). The *p*-value for the difference between groups A and B was <0.05.

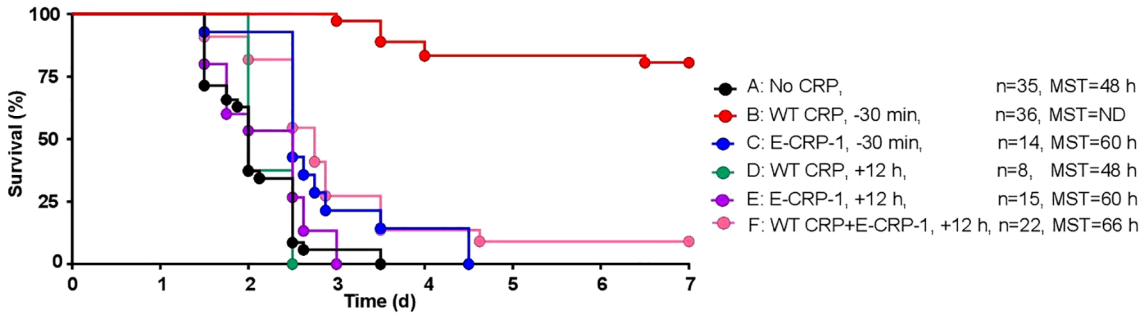

FIGURE 4
Survival of CRP KO mice infected with pneumococci and treated with E-CRP-1. The data are combined from two to four separate experiments with six to nine mice in each group in each experiment (n, number of mice). The MST values are shown for each group of mice (ND, MST not determined since >50% mice survived). CRP was injected 30 min prior to inoculation with pneumococci (10^7 cfu) in groups B and C and 12 h after inoculation in groups D-F. The *p*-values for the differences in the survival curves between groups A B, A C and A F were <0.001. The *p*-values for the differences between A D and A E were >0.05. The *p*-values for the differences between B C, B D, B E and B F were <0.001. The *p*-values for the differences between C D, C E and C F were 0.004, 0.04 and 0.46, respectively. The *p*-value for the difference between E and F was 0.01.

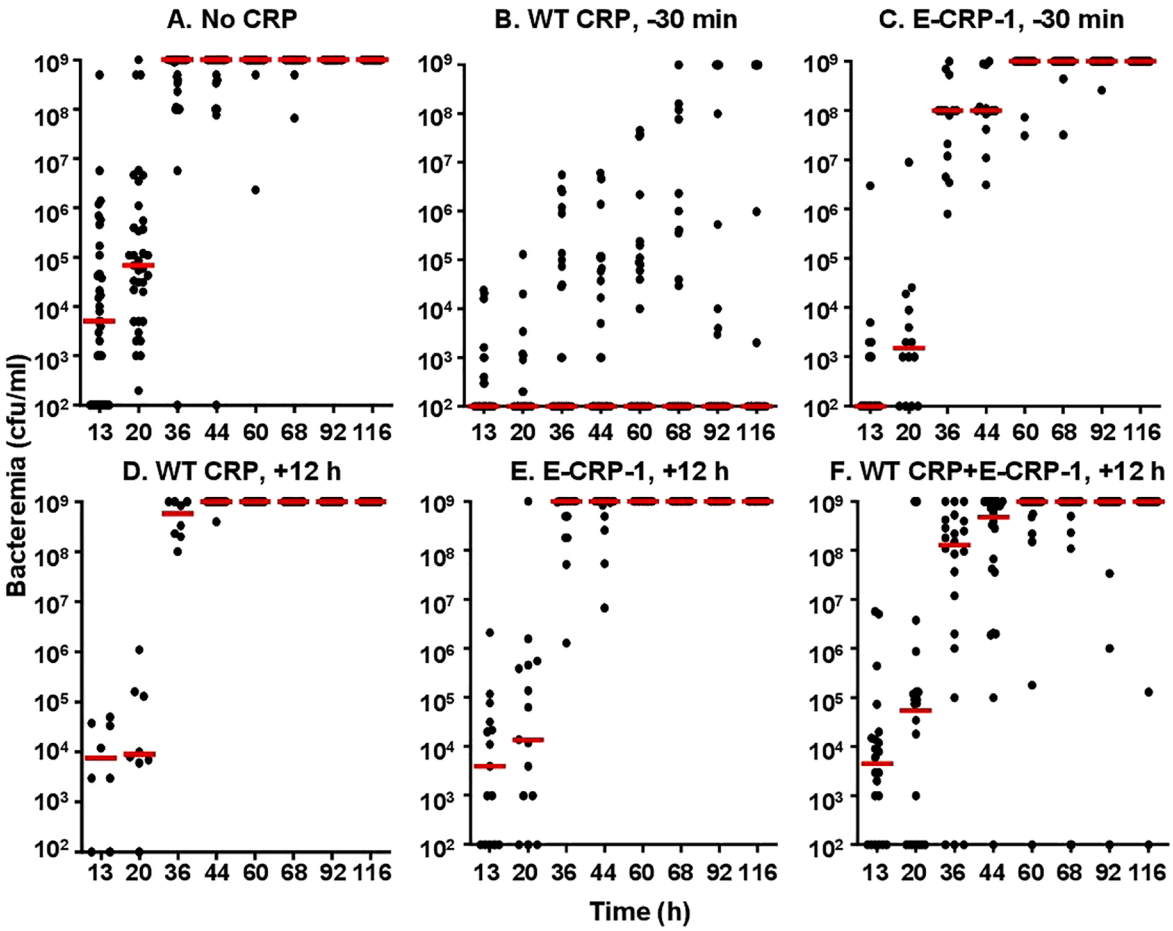

FIGURE 5
Bacteremia in CRP KO mice inoculated with pneumococci and treated with E-CRP-1 **(A–F)**. Blood was collected from each surviving mouse shown in Figure 4. Bacteremia was determined by plating. The bacteremia values for dead mice were recorded as 10^9 cfu/ml. Bacteremia values of 0–100 were plotted as 100 and bacteremia values of >10^8 cfu/ml were plotted as 10^9 cfu/ml. The red horizontal line in each group of mice represents median bacteremia.

To determine whether the increased survival of mice was due to reduced bacteremia, we measured bacteremia in each surviving mouse in all six groups of mice (Figure 5). After 60 h of inoculation, bacteremia reached $>10^8$ cfu/ml in all groups of mice except in mice treated with WT CRP 30 min prior to inoculation. For statistical analysis and to compare bacteremia between any two groups of mice, the median values of bacteremia (Figure 5) for each time point up to 60 h for all groups of mice were plotted together (Figure 6). The bacteremia in mice treated with either WT CRP (group D) or E-CRP-1 (group E) was not significantly different from bacteremia in untreated mice (group A). However, the bacteremia in mice treated with both WT CRP and E-CRP-1 (group F) was found to be significantly lower than bacteremia in untreated mice (group A) at time points 36 h and 44 h. Consistent with the survival curves of mice treated with E-CRP-1 alone 30 min prior to inoculation (Figure 4), these mice had significantly lower bacteremia than in untreated mice and at the same time, significantly higher than mice treated with WT CRP alone 30 min prior to inoculation.

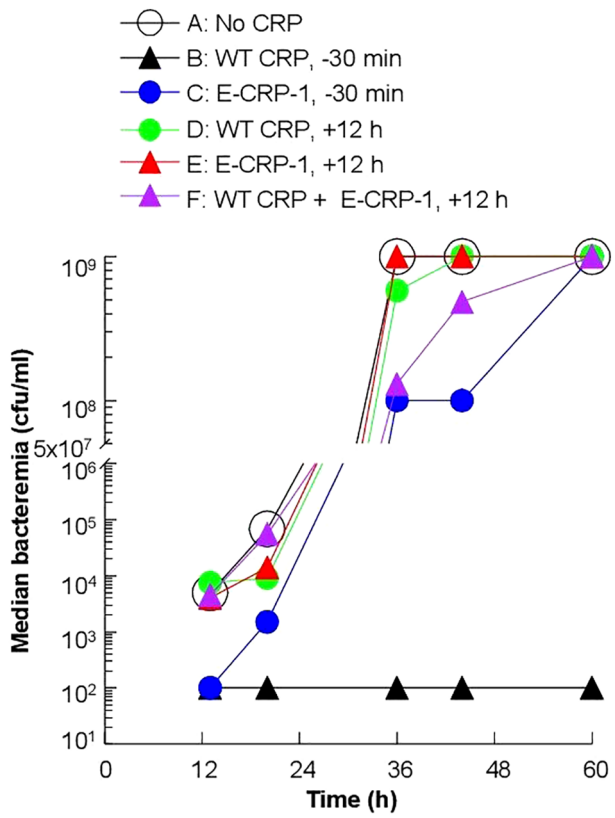

FIGURE 6
Median values of bacteremia in mice inoculated with pneumococci with and without E-CRP-1. The median bacteremia values for all six groups of mice shown in panels **(A-F)** in Figure 5 are plotted together for comparison. For all time points, the *p*-values for the differences between groups A, C were <0.01. For all time points, the *p*-values for the differences between groups A, D and between groups A, E were >0.05. For 36 h and 44 h, the *p*-values for the difference between groups A, F were <0.01.

E-CRP-2 by itself protects KO mice when administered 12 h after inoculation

The protective effects of E-CRP-2 which binds to both PCh and amyloids was determined next. As shown in Figure 7, WT CRP was protective when administered 30 min prior to inoculation (group B) but was not protective when administered 12 h after inoculation (group D). In contrast to WT CRP, E-CRP-2 was protective irrespective of whether E-CRP-2 was administered 30 min prior to inoculation (group C) or 12 h after inoculation (group E). However, the survival curve of mice in which E-CRP-2 was administered 12 h after inoculation was found to be significantly different from both group A (no CRP) and groups B and C. When CRP was administered 12 h after inoculation, the survival times of mice treated with E-CRP-2 were found to be longer than the survival times of mice treated with WT CRP.

Next, we measured bacteremia in each surviving mouse from all five groups of mice (Figure 8). After 66 h of inoculation, bacteremia reached $>10^8$ cfu/ml in all groups of mice except in mice treated with either WT CRP or E-CRP-2, 30 min prior to inoculation. For statistical analysis and to compare bacteremia between any two groups of mice, the median values of bacteremia (Figure 8) for each time point up to 66 h for all groups of mice were plotted together (Figure 9). Bacteremia was significantly reduced in mice treated with either CRP species 30 min prior to inoculation for the entire duration of the experiment. Bacteremia was not reduced in mice treated with WT CRP 12 h after inoculation, except at 36 h time point. In contrast, when E-CRP-2 was administered 12 h after inoculation, bacteremia was significantly reduced sometime after 20 h post-inoculation and remained low till at least 44 h. The bacteremia data were largely consistent with the survival data shown in Figure 7.

Amyloids are present on the pneumococcal surface

First, we determined whether amyloids were present on pneumococci which were cultured *in vitro* in broth and used to inoculate mice. As shown in Figure 10, pneumococci were reactive with both polyclonal and monoclonal anti-Aβ antibodies. These data suggested that amyloids were already present on the surface of pneumococci even if the bacteria were not grown in the serum in the presence of complement inhibitor proteins. For this reason, we did not investigate the presence of amyloids on pneumococci which were grown *in vivo* in mice and then isolated from the blood.

SAP levels are higher in KO mice than in WT mice

In mice, CRP is a minor acute phase protein (50). SAP, an amyloid-binding protein, is the major acute phase protein in mice (51–54). Since the four types of mice (WT female and male, KO female and male) responded differently to the severity of infection

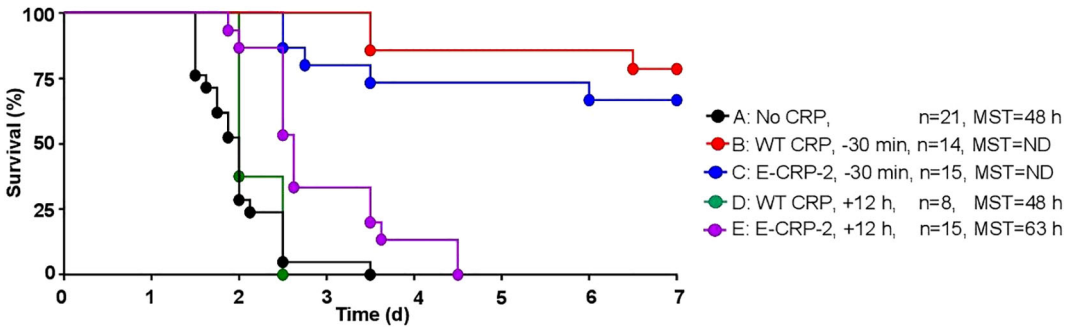

FIGURE 7
Survival of CRP KO mice inoculated with pneumococci and treated with E-CRP-2. The data are combined from two to three separate experiments with six to eight mice in each group in each experiment (n, number of mice). The MST values are shown for each group of mice (ND, MST not determined since >50% mice survived). CRP was injected 30 min prior to inoculation with pneumococci (10^7 cfu) in groups B and C and 12 h after inoculation in groups D, E. The *p*-values for the differences in the survival curves between groups A B, A C and A E were 0.001. The *p*-value for the differences between A, D was 0.22. The *p*-value for the difference between B, C was 0.40. The *p*-values for the differences between B D and B E were <0.001. The *p*-values for the differences between C D, C E and D E were <0.005.

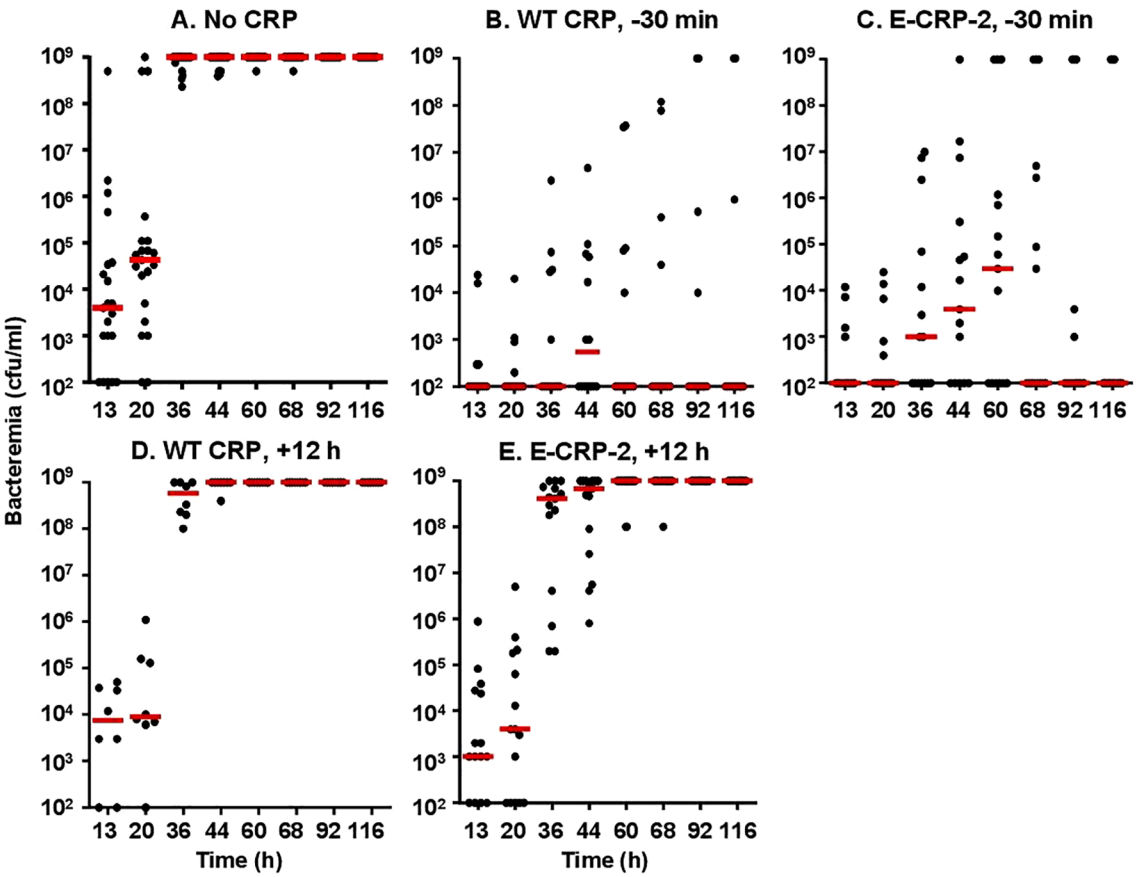

FIGURE 8
Bacteremia in CRP KO mice inoculated with pneumococci and treated with E-CRP-2 **(A–E)**. Blood was collected from each surviving mouse shown in Figure 7. Bacteremia was determined by plating. The bacteremia values for dead mice were recorded as 10^9 cfu/ml. Bacteremia values of 0–100 were plotted as 100 and bacteremia values of >10^8 cfu/ml were plotted as 10^9 cfu/ml. The red horizontal line in each group of mice represents median bacteremia.

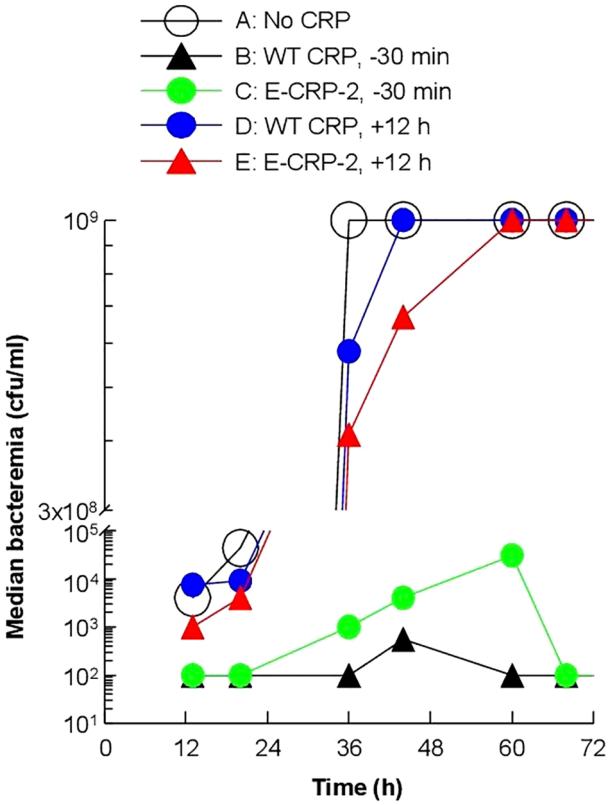

FIGURE 9
Median values of bacteremia in mice inoculated with pneumococci with and without E-CRP-2. The median bacteremia values for all five groups of mice shown in panels **(A-F)** in Figure 7 are plotted together for comparison. For all time points, the *p*-values for the differences between groups A and C were <0.01. For all time points, the *p*-values for the differences between groups A and D were >0.05, except at 36 h where the *p*-value was <0.05. The *p* values for the difference between groups A and E for time points 13 h and 20 h were >0.05 and for 36 h and 44 h were <0.005.

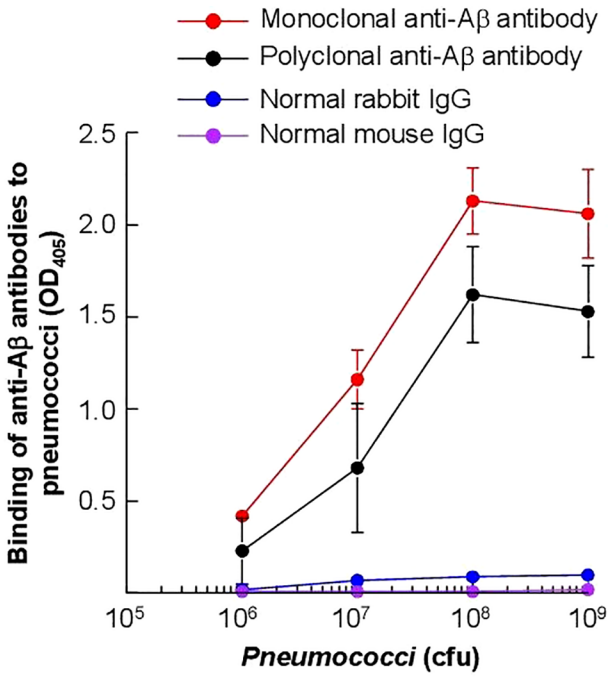

FIGURE 10
Detection of Aβ epitopes on the surface of *S. pneumoniae*. Microtiter wells were coated with pneumococci. Anti-Aβ antibodies, both monoclonal and polyclonal, were then added to the wells. Normal mouse IgG and rabbit IgG were included as controls. Bound monoclonal anti-Aβ antibodies and normal mouse IgG were detected by using HRP-conjugated goat anti-mouse IgG. Bound polyclonal anti-Aβ antibodies and normal rabbit IgG were detected by using HRP-conjugated donkey anti-rabbit IgG. The OD of the developed color was read at 405 nm. Data shown are mean ± SEM of three experiments.

in terms of their MST, we measured the serum levels of moCRP in WT mice and of SAP in WT and KO mice. As shown in Figure 11A, the basal levels of SAP in the sera (0 h) were approximately five-fold higher in KO mice than in WT mice, irrespective of the sex of mice (p = <0.005). The induced levels of SAP in mice after 36 h of inoculation was also higher in KO mice than in WT mice, irrespective of the sex of mice (p = <0.005). These data suggest that the absence of endogenous CRP can trigger acute phase response and that SAP can substitute CRP.

Basal SAP levels are higher in female mice than in male mice

In both WT and KO mice, the basal levels of SAP were significantly higher (p = <0.005) in female mice than in male mice (Figure 11A). At 36 h post-inoculation, however, the levels of SAP were significantly higher in males than in females (p < 0.005), probably due to greater induction of SAP expression in male mice in response to inoculation. In WT mice, the increase in the levels of SAP was ~250-fold in male mice and ~50-fold in female mice. Similarly, in KO mice, the increase in the levels of SAP was ~80-fold in male mice and ~25-fold in female mice. In contrast to SAP, both the basal and induced serum levels of moCRP were not significantly different (p = >0.05) in male and female mice (Figure 11B).

Discussion

WT CRP protects mice against pneumococcal infection if administered to mice prior to inoculation with bacteria and does not protect if administered a few hours after inoculation (30, 34). Thus, WT CRP is not protective against prolonged infection. We tested the hypothesis that the amyloid-binding function of structurally altered CRP is required for CRP-mediated protection against prolonged infection. In this study, we employed CRP KO mice and investigated the effects of the amyloid-binding CRP molecules E-CRP-1 and E-CRP-2 on the survival of and bacteremia in mice when administered 12 h after inoculation. There were three major findings: 1. Amyloids were detected on the surface of broth-cultured pneumococci. 2. Unlike WT CRP alone, the combination of WT CRP and E-CRP-1 was protective

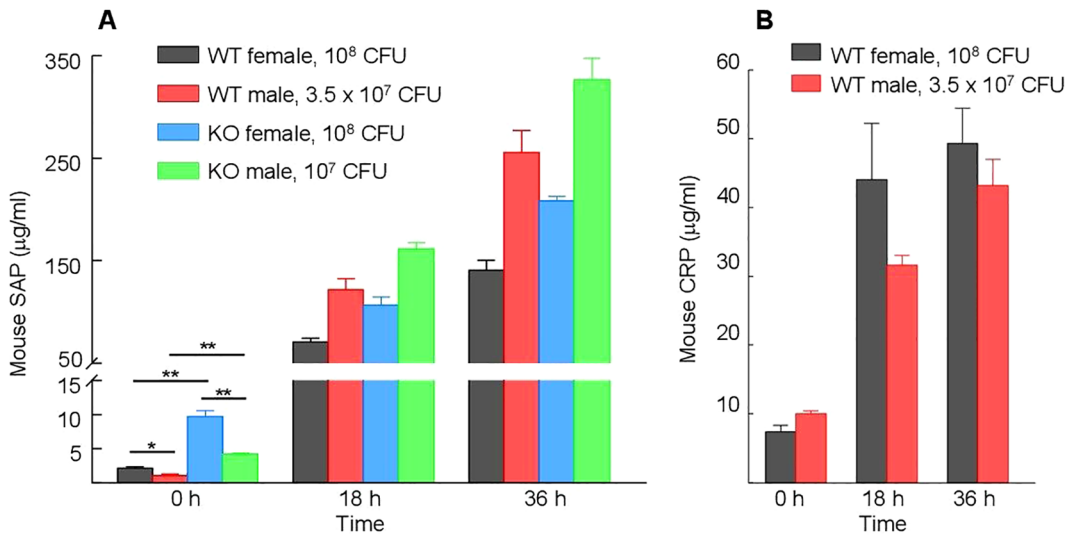

FIGURE 11
Serum levels of endogenous moCRP and SAP. Different types of mice were inoculated with different doses of pneumococci; the doses of pneumococci were chosen based on the relative susceptibility of each type of mouse to infection. Blood was collected just prior to inoculation (time zero) and at 18 h and 36 h post-inoculation. The data shown are mean ± SEM of three assays. At time zero, there were 8 mice in each group. At 18 h and 36 h time points, there were 5 mice in both groups of female mice and 8 mice in both groups of male mice, since 3 WT and 3 KO female mice died after infection. The *p*-values are shown as $*p < 0.05$ and $**p < 0.005$. **(A)** Levels of CRP in WT mice before and after inoculation. **(B)** Levels of SAP in WT and KO mice before and after inoculation.

when administered to mice 12 h after inoculation. E-CRP-2 by itself protected mice when administered 12 h after inoculation. 3. Serum SAP levels were higher in KO mice than in WT mice. Also, the basal SAP levels were higher in female mice than in male mice and, conversely, male mice were more susceptible than female mice to infection. Thus, there was an inverse relationship between the susceptibility of mice to infection and basal SAP levels in their sera.

In a previous study, WT mice were employed to investigate the effects of E-CRP-1 on pneumococcal infection (43). It was reported that E-CRP-1 was protective in WT mice against infection when administered 12 h after inoculation. The explanation was that E-CRP-1 blocked the complement inhibitor proteins recruited by pneumococci and then endogenous moCRP could activate complement by complexing with the PCh groups on pneumococci. Subsequently, it was reported that many proteins, when immobilized on microtiter plates, expressed amyloids (21), which raised the possibility that complement inhibitors expressed amyloids once immobilized on the pneumococcal surface and that the amyloids were the ligands for E-CRP-1. In this study, we found that pneumococci cultured in broth, with no exposure to serum complement inhibitors, had amyloids on their surface. The presence of functional amyloids on bacterial surfaces has been demonstrated previously (55). The sources of the amyloids on broth-grown pneumococci are not known; however, it is possible that the surface virulence factors are amyloidogenic proteins. The possibility that E-CRP-1 directly binds to virulence factors has been raised previously based on the following findings: the binding of E-CRP-1 to pneumococci was 99% less than the binding of WT CRP to pneumococci, and that the residual binding of E-CRP-1 to pneumococci occurred in the absence of Ca^{2+} (43). Since broth-cultured pneumococci were already amyloid-positive, we did not test pneumococci isolated from infected mice for the presence of surface amyloids. However, the possibility that both the virulence factors and the complement inhibitor proteins recruited by virulence factors express amyloids still exists.

In the current study, instead of WT mice, KO mice were employed to investigate the effects of E-CRP-1 on pneumococcal infection. In this animal model, E-CRP-1 by itself was not protective but the combination of exogenous WT human CRP and E-CRP-1 was protective when administered to mice 12 h after inoculation. Like the combination of WT CRP and E-CRP-1, E-CRP-2 by itself was protective. These findings provide a proof of concept that CRP can protect against prolonged infection provided that both PCh and amyloids on the bacterial surface are occupied by either structurally altered CRP molecules mimicking E-CRP-2 or by WT CRP and structurally altered CRP molecules mimicking E-CRP-1, respectively. Although both E-CRP-1 and E-CRP-2 were protective when administered to mice 12 h after inoculation, the protection was not as good as the protection seen when CRP was administered to mice 30 min prior to inoculation. It is possible that multiple injections of WT CRP and E-CRP-1 or E-CRP-2 or higher doses of each CRP species would result in better protection than seen with the single injection of structurally altered CRP reported here.

It is not known whether structurally altered CRP mimicking the ligand-binding properties of E-CRP-1 or E-CRP-2 is formed at sites of inflammation *in vivo* during pneumococcal infection. Since CRP mutants E-CRP-1 and E-CRP-2 mimic the ligand-binding properties of acidic pH-treated CRP and H_2O_2-treated CRP, these mutants provide us with a tool to identify the actual CRP species

present at sites of inflammation. E-CRP-1 and E-CRP-2 can be used to generate a library of monoclonal antibodies which can then be screened to identify the antibodies which neither react with WT CRP nor with monomeric CRP. The antibodies specific for E-CRP-1 and E-CRP-2 can then be employed to detect structurally altered pentameric CRP *in vivo* and to locate the sites where WT CRP is converted to amyloid-binding forms of CRP.

Our data suggest that the recognition of bacterial amyloids by structurally altered CRP is critical for protection against prolonged infection. In theory then, any amyloid-binding protein administered to mice should give the results similar to that of E-CRP-1 and E-CRP-2. Since SAP is an amyloid-binding protein, SAP should be able to bind to bacterial amyloids and contribute to CRP-mediated protection. It is also possible that the binding of SAP to bacterial amyloids reduces the virulence of pneumococci. It has been shown previously that SAP binds to pneumococci and activates complement (56); however, it has been suggested that the ligands of SAP on pneumococci were surface carbohydrates since SAP also binds to carbohydrates.

While developing the KO mouse model for this study, we noted sex-specificity in the expression of the SAP gene, in the susceptibility of both WT and KO mice to infection and in the SAP levels in the sera from both WT and KO mice. There was no sex-specificity in the expression of the moCRP gene, although it has been reported previously that the expression of the human CRP transgene in mice was sex-specific (28, 57). We found that female mice were less susceptible than male mice to infection; these results are consistent with a previously published report that, in both animals and humans, males are generally more susceptible than females to bacterial infections and that women have stronger immune responses to foreign antigens than men (58). We propose that female mice were less susceptible than male mice to infection because female mice had higher basal SAP levels in their sera than in the sera of male mice. The inverse relationship between the susceptibility of mice to infection and the basal levels of SAP in the sera further suggests that SAP plays a role in protecting against pneumococcal infection.

As described above, the capability of SAP to bind amyloids and the relationship between basal SAP levels and susceptibility to infection both suggested the involvement of SAP in protection against pneumococcal infection. Another evidence to support the role of SAP in pneumococcal infection came from the data on SAP levels seen in KO mice which was higher than in WT mice. The higher expression of the SAP gene in the absence of the CRP gene supports our interpretation that SAP plays a role in protecting against pneumococcal infection. Indeed, employing SAP KO mice, it has been shown previously that mouse SAP participates in protection against pneumococcal infection (56).

We conclude that the protection against prolonged pneumococcal infection involves conformational changes in CRP, binding of CRP to both PCh and amyloids on the pneumococcal surface, and complement activation by PCh-complexed CRP. The two recognition functions of CRP, PCh-binding and amyloid-binding, can be exhibited by two different CRP molecules as exemplified here by the combination of WT CRP and E-CRP-1 or by a single structurally altered CRP molecule if the PCh-binding function is retained in the structurally altered form as exemplified here by E-CRP-2. The combined data reported here and published previously (56) suggest that SAP cooperates with CRP in protection against pneumococcal infection. We propose that, in circulation, CRP cooperates with SAP to reduce bacteremia. At sites of inflammation in the organs, where the conformation of CRP can be altered, WT CRP cooperates with structurally altered CRP to reduce bacterial load in the organs. Future investigations employing double SAP KO and CRP KO mice would provide definitive proof for the cooperation between SAP and CRP in controlling pneumococcal infection.

Data availability statement

All data generated for this study is presented in this article. Further inquiries can be directed to corresponding authors.

Ethics statement

The animal study was approved by University Committee of Animal Care, East Tennessee State University. The study was conducted in accordance with the local legislation and institutional requirements.

Author contributions

AA: Conceptualization, Formal analysis, Funding acquisition, Supervision, Writing – original draft. DN: Investigation, Writing – review & editing. JS: Methodology, Resources, Writing – review & editing. SS: Investigation, Writing – review & editing.

Funding

The author(s) declare that financial support was received for the research and/or publication of this article. This work was supported by National Institutes of Health Grant AI151561.

Acknowledgments

We thank Nicole Lewis, Ph.D., for statistical analysis of the data shown in Figure 2E.

Conflict of interest

The authors declare that the research was conducted in the absence of any commercial or financial relationships that could be construed as a potential conflict of interest.

The author(s) declared that they were an editorial board member of Frontiers, at the time of submission. This had no impact on the peer review process and the final decision.

Generative AI statement

The author(s) declare that no Generative AI was used in the creation of this manuscript.

Publisher's note

References

1. Pathak A, Agrawal A. Evolution of C-reactive protein. *Front Immunol.* (2019) 10:943. doi: 10.3389/fimmu.2019.00943

2. Torzewski M. C-reactive protein: Friend or foe? Phylogeny from heavy metals to modified lipoproteins and SARS-CoV-2. *Front Cardiovasc Med.* (2022) 9:797116. doi: 10.3389/fcvm.2022.797116

3. Ji S-R, Zhang S-H, Chang Y, Li H-Y, Wang M-Y, Lv J-M, et al. C-reactive protein: The most familiar stranger. *J Immunol.* (2023) 210:699–707. doi: 10.4049/jimmunol.2200831

4. Saralahti AK, Harjula SE, Rantapero T, Uusi-Mäkelä MIE, Kaasinen M, Junno M, et al. Characterization of the innate immune response to *Streptococcus pneumoniae* infection in zebrafish. *PloS Genet.* (2023) 19:1010586. doi: 10.1371/journal.pgen.1010586

5. Kushner I. The phenomenon of the acute phase response. *Ann N Y Acad Sci.* (1982) 389:39–48. doi: 10.1111/j.1749-6632.1982.tb22124.x

6. Osmand AP, Friedenson B, Gewurz H, Painter RH, Hofmann T, Shelton E. Characterization of C-reactive protein and the complement subcomponent C1t as homologous proteins displaying cyclic pentameric symmetry (pentraxins). *Proc Natl Acad Sci USA.* (1977) 74:739–43. doi: 10.1073/pnas.74.2.739

7. Volanakis JE, Kaplan MH. Specificity of C-reactive protein for choline phosphate residues of pneumococcal C-polysaccharide. *Proc Soc Exp Biol Med.* (1971) 136:612–4. doi: 10.3181/00379727-136-35323

8. Shrive AK, Cheetham GMT, Holden D, Myles DAA, Turnell WG, Volanakis JE, et al. Three-dimensional structure of human C-reactive protein. *Nat Struct Biol.* (1996) 3:346–54. doi: 10.1038/nsb0496-346

9. Agrawal A, Lee S, Carson M, Narayana SVL, Greenhough TJ, Volanakis JE. Site-directed mutagenesis of the phosphocholine-binding site of human C-reactive protein: Role of Thr^{76} and Trp^{67}. *J Immunol.* (1997) 158:345–50. doi: 10.4049/jimmunol.158.1.345

10. Agrawal A, Simpson MJ, Black S, Carey M-P, Samols D. A C-reactive protein mutant that does not bind to phosphocholine and pneumococcal C-polysaccharide. *J Immunol.* (2002) 169:3217–22. doi: 10.4049/jimmunol.169.6.3217

11. Kaplan MH, Volanakis JE. Interaction of C-reactive protein complexes with the complement system. I. Consumption of human complement associated with the reaction of C-reactive protein with pneumococcal C-polysaccharide and with the choline phosphatides, lecithin, and sphingomyelin. *J Immunol.* (1974) 112:2135–47. doi: 10.4049/jimmunol.112.6.2135

12. Suresh MV, Singh SK, Ferguson DA Jr, Agrawal A. Role of the property of C-reactive protein to activate the classical pathway of complement in protecting mice from pneumococcal infection. *J Immunol.* (2006) 176:4369–74. doi: 10.4049/jimmunol.176.7.4369

13. Li H-Y, Tang Z-M, Wang Z, Lv J-M, Liu X-L, Liang Y-L, et al. C-reactive protein protects against acetaminophen-induced liver injury by preventing complement overactivation. *Cell Mol Gastroenterol Hepatol.* (2022) 13:289–307. doi: 10.1016/j.jcmgh.2021.09.003

14. Ma YJ, Parente R, Zhong H, Sun Y, Garlanda C, Doni A. Complement-pentraxins synergy: Navigating the immune battlefield and beyond. *BioMed Pharmacother.* (2023) 169:115878. doi: 10.1016/j.biopha.2023.115878

15. Suresh MV, Singh SK, Agrawal A. Interaction of calcium-bound C-reactive protein with fibronectin is controlled by pH: *In vivo* implications. *J Biol Chem.* (2004) 279:52552–7. doi: 10.1074/jbc.M409054200

16. Hammond DJ Jr, Singh SK, Thompson JA, Beeler BW, Rusiñol AE, Pangburn MK, et al. Identification of acidic pH-dependent ligands of pentameric C-reactive protein. *J Biol Chem.* (2010) 285:36235–44. doi: 10.1074/jbc.M110.142026

17. Singh SK, Thirumalai A, Pathak A, Ngwa DN, Agrawal A. Functional transformation of C-reactive protein by hydrogen peroxide. *J Biol Chem.* (2017) 292:3129–36. doi: 10.1074/jbc.M116.773176

18. Li S-L, Feng J-R, Zhou H-H, Zhang C-M, Lv G-B, Tan Y-B, et al. Acidic pH promotes oxidation-induced dissociation of C-reactive protein. *Mol Immunol.* (2018) 104:47–53. doi: 10.1016/j.molimm.2018.09.021

19. Singh SK, Hammond DJ Jr, Beeler BW, Agrawal A. The binding of C-reactive protein, in the presence of phosphoethanolamine, to low-density lipoproteins is due to phosphoethanolamine-generated acidic pH. *Clin Chim Acta.* (2009) 409:143–4. doi: 10.1016/j.cca.2009.08.013

20. Singh SK, Thirumalai A, Hammond DJ Jr, Pangburn MK, Mishra VK, Johnson DA, et al. Exposing a hidden functional site of C-reactive protein by site-directed mutagenesis. *J Biol Chem.* (2012) 287:3550–8. doi: 10.1074/jbc.M111.310011

21. Ngwa DN, Agrawal A. Structurally altered, not wild-type, pentameric C-reactive protein inhibits formation of amyloid-β fibrils. *J Immunol.* (2022) 209:1180–8. doi: 10.4049/jimmunol.2200148

22. Singh SK, Prislovsky A, Ngwa DN, Munkhsaikhan U, Abidi AH, Brand DD, et al. C-reactive protein lowers the serum level of IL-17, but not TNF-α, and decreases the incidence of collagen-induced arthritis in mice. *Front Immunol.* (2024) 15:1385085. doi: 10.3389/fimmu.2024.1385085

23. Olson ME, Hornick MG, Stefanski A, Albanna HR, Gjoni A, Hall GD, et al. A biofunctional review of C-reactive protein (CRP) as a mediator of inflammatory and immune responses: Differentiating pentameric and modified CRP isoform effects. *Front Immunol.* (2023) 14:1264383. doi: 10.3389/fimmu.2023.1264383

24. Zeller J, Cheung Tung Shing KS, Nero TL, McFadyen JD, Krippner G, Bogner B, et al. A novel phosphocholine-mimetic inhibits a pro-inflammatory conformational change in C-reactive protein. *EMBO Mol Med.* (2023) 15:16236. doi: 10.15252/emmm.202216236

25. Agrawal A, Pathak A, Ngwa DN, Thirumalai A, Armstrong PB, Singh SK. An evolutionarily conserved function of C-reactive protein is to prevent the formation of amyloid fibrils. *Front Immunol.* (2024) 15:1466865. doi: 10.3389/fimmu.2024.1466865

26. Mold C, Nakayama S, Holzer TJ, Gewurz H, Du Clos TW. C-reactive protein is protective against *Streptococcus pneumoniae* infection in mice. *J Exp Med.* (1981) 154:1703–8. doi: 10.1084/jem.154.5.1703

27. Yother J, Volanakis JE, Briles DE. Human C-reactive protein is protective against fatal *Streptococcus pneumoniae* infection in mice. *J Immunol.* (1982) 128:2374–6. doi: 10.4049/jimmunol.128.5.2374

28. Szalai AJ, Briles DE, Volanakis JE. Human C-reactive protein is protective against fatal *Streptococcus pneumoniae* infection in transgenic mice. *J Immunol.* (1995) 155:2557–63. doi: 10.4049/jimmunol.155.5.2557

29. Gang TB, Hanley GA, Agrawal A. C-reactive protein protects mice against pneumococcal infection via both phosphocholine-dependent and phosphocholine-independent mechanisms. *Infect Immun.* (2015) 83:1845–52. doi: 10.1128/IAI.03058-14

30. Ngwa DN, Agrawal A. Structure-function relationships of C-reactive protein in bacterial infection. *Front Immunol.* (2019) 10:166. doi: 10.3389/fimmu.2019.00166

31. Szalai AJ, Briles DE, Volanakis JE. Role of complement in C-reactive protein-mediated protection of mice from *Streptococcus pneumoniae*. *Infect Immun.* (1996) 64:4850–3. doi: 10.1128/iai.64.11.4850-4853.1996

32. Mold C, Rodic-Polic B, Du Clos TW. Protection from *Streptococcus pneumoniae* infection by C-reactive protein and natural antibody requires complement but not Fcγ receptors. *J Immunol.* (2002) 168:6375–81. doi: 10.4049/jimmunol.168.12.6375

33. Singh SK, Ngwa DN, Agrawal A. Complement activation by C-reactive protein is critical for protection of mice against pneumococcal infection. *Front Immunol.* (2020) 11:1812. doi: 10.3389/fimmu.2020.01812

34. Nakayama S, Gewurz H, Holzer T, Du Clos TW, Mold C. The role of the spleen in the protective effect of C-reactive protein in *Streptococcus pneumoniae* infection. *Clin Exp Immunol.* (1983) 54:319–26.

35. Janulczyk R, Iannelli F, Sjoholm AG, Pozzi G, Bjorck L. Hic, a novel surface protein of *Streptococcus pneumoniae* that interferes with complement function. *J Biol Chem.* (2000) 275:37257–63. doi: 10.1074/jbc.M004572200

36. Dave S, Brooks-Walter A, Pangburn MK, McDaniel LS. PspC, a pneumococcal surface protein, binds human factor H. *Infect Immun*. (2001) 69:3435–7. doi: 10.1128/IAI.69.5.3435-3437.2001

37. Jarva H, Janullczyk R, Hellwage J, Zipfel PF, Björck L, Meri S. *Streptococcus pneumoniae* evades complement attack and opsonophagocytosis by expressing the *pspC* locus encoded Hic protein that binds to short consensus repeats 8–11 of factor H. *J Immunol*. (2002) 168:1886–94. doi: 10.4049/jimmunol.168.4.1886

38. Dieudonné-Vatran A, Krentz S, Blom AM, Meri S, Henriques-Normark B, Riesbeck K, et al. Clinical isolates of *Streptococcus pneumoniae* bind the complement inhibitor C4b-binding protein in a PspC allele-dependent fashion. *J Immunol*. (2009) 182:7865–77. doi: 10.4049/jimmunol.0802376

39. Agarwal V, Hammerschmidt S, Malm S, Bergmann S, Riesbeck K, Blom AM. Enolase of *Streptococcus pneumoniae* binds human complement inhibitor C4b-binding protein and contributes to complement evasion. *J Immunol*. (2012) 189:3575–84. doi: 10.4049/jimmunol.1102934

40. Andre GO, Converso TR, Politano WR, Ferraz LFC, Ribeiro ML, Leite LCC, et al. Role of *Streptococcus pneumoniae* proteins in evasion of complement-mediated immunity. *Front Microbiol*. (2017) 8:224. doi: 10.3389/fmicb.2017.00224

41. Du S, Vilhena C, King S, Sahagún-Ruiz A, Hammerschmidt S, Skerka C, et al. Molecular analyses identify new domains and structural differences among *Streptococcus pneumoniae* immune evasion proteins PspC and Hic. *Sci Rep*. (2021) 11:1701. doi: 10.1038/s41598-020-79362-3

42. Gil E, Noursadeghi M, Brown JS. *Streptococcus pneumoniae* interactions with the complement system. *Front Cell Infect Microbiol*. (2022) 12:929483. doi: 10.3389/fcimb.2022.929483

43. Ngwa DN, Singh SK, Gang TB, Agrawal A. Treatment of pneumococcal infection by using engineered human C-reactive protein in a mouse model. *Front Immunol*. (2020) 11:586669. doi: 10.3389/fimmu.2020.586669

44. Pathak A, Singh SK, Thewke DP, Agrawal A. Conformationally altered C-reactive protein capable of binding to atherogenic lipoproteins reduces atherosclerosis. *Front Immunol*. (2020) 11:1780. doi: 10.3389/fimmu.2020.01780

45. Gang TB, Hammond DJ Jr, Singh SK, Ferguson DA Jr, Mishra VK, Agrawal A. The phosphocholine-binding pocket on C-reactive protein is necessary for initial protection of mice against pneumococcal infection. *J Biol Chem*. (2012) 287:43116–25. doi: 10.1074/jbc.M112.427310

46. Agrawal A, Xu Y, Ansardi D, Macon KJ, Volanakis JE. Probing the phosphocholine-binding site of human C-reactive protein by site-directed mutagenesis. *J Biol Chem*. (1992) 267:25352–8. doi: 10.1016/S0021-9258(19)74047-2

47. Lv J-M, Huang X-P, Chen J-Y, Cheng B, Chen W-Z, Yuan P, et al. Cholesterol-binding sequence is a key regulatory motif of cellular folding and conformational activation for C-reactive protein. *Mol Immunol*. (2022) 152:123–8. doi: 10.1016/j.molimm.2022.10.010

48. Thirumalai A, Singh SK, Hammond DJ Jr, Gang TB, Ngwa DN, Pathak A, et al. Purification of recombinant C-reactive protein mutants. *J Immunol Methods*. (2017) 443:26–32. doi: 10.1016/j.jim.2017.01.011

49. Simons JP, Loeffler JM, Al-Shawi R, Ellmerich S, Hutchinson WL, Tennent GA, et al. C-reactive protein is essential for innate resistance to pneumococcal infection. *Immunology*. (2014) 142:414–20. doi: 10.1111/imm.12266

50. Whitehead AS, Zahedi K, Rits M, Mortensen RF, Lelias JM. Mouse C-reactive protein: Generation of cDNA clones, structural analysis, and induction of mRNA during inflammation. *Biochem J*. (1990) 266:283290. doi: 10.1042/bj2660283

51. Pepys MB, Baltz M, Gomer K, Davies AJ, Doenhoff M. Serum amyloid P-component is an acute-phase reactant in the mouse. *Nature*. (1979) 278:259–61. doi: 10.1038/278259a0

52. Pepys MB, Dyck RF, de Beer FC, Skinner M, Cohen AS. Binding of serum amyloid P-component (SAP) by amyloid fibrils. *Clin Exp Immunol*. (1979) 38:284–93.

53. Janciauskiene S, de Frutos PG, Carlemalm E, Dahlbäck B, Eriksson S. Inhibition of Alzheimer β-peptide fibril formation by serum amyloid P component. *J Biol Chem*. (1995) 270:26041–4. doi: 10.1074/jbc.270.44.26041

54. Hamazaki H. Ca^{2+}-dependent binding of human serum amyloid P component to Alzheimer's β-amyloid peptide. *J Biol Chem*. (1995) 270:10392–4. doi: 10.1074/jbc.270.18.10392

55. Van Gerven N, van der Verren SE, Reiter DM, Remaut H. The role of functional amyloids in bacterial virulence. *J Mol Biol*. (2018) 430:3657–84. doi: 10.1016/j.jmb.2018.07.010

56. Yuste J, Botto M, Bottoms SE, Brown JS. Serum amyloid P aids complement-mediated immunity to *Streptococcus pneumoniae*. *PloS Pathog*. (2007) 3:1208–19. doi: 10.1371/journal.ppat.0030120

57. Szalai AJ, van Ginkel FW, Dalrymple SA, Murray R, McGhee JR, Volanakis JE. Testosterone and IL-6 requirements for human C-reactive protein gene expression in transgenic mice. *J Immunol*. (1998) 160:5294–9. doi: 10.4049/jimmunol.160.11.5294

58. Dias SP, Brouwer MC, van de Beek D. Sex and gender differences in bacterial infections. *Infect Immun*. (2022) 90:0028322. doi: 10.1128/iai.00283-22

frontiers | Frontiers in Immunology

TYPE Brief Research Report
PUBLISHED 13 August 2025
DOI 10.3389/fimmu.2025.1652139

OPEN ACCESS

EDITED BY
Yi Wu,
Xi'an Jiaotong University, China

REVIEWED BY
Pengxiang Qu,
Xi'an Jiaotong University, China
Se Jin Oh,
Seoul Metropolitan Government - Seoul National University Boramae Medical Center, Republic of Korea

*CORRESPONDENCE
Yankui Li
yankuili@tmu.edu.cn

†These authors have contributed equally to this work

RECEIVED 23 June 2025
ACCEPTED 28 July 2025
PUBLISHED 13 August 2025

CITATION
Chen B, Zhang T, Wang Y, Li Z, Liu H, Jiang Z, Yang H, Cai Y, Fan G, Wang K, Zhang H, Hu H and Li Y (2025) Elevated C-reactive protein and D-dimer to predict venous thromboembolism in patients with bladder cancer. *Front. Immunol.* 16:1652139. doi: 10.3389/fimmu.2025.1652139

Elevated C-reactive protein and D-dimer to predict venous thromboembolism in patients with bladder cancer

Bo Chen[1,2†], Tonghe Zhang[1,2†], Yisong Wang[1,2], Zhaoyang Li[1,3], Haoyu Liu[1,2], Zhan Jiang[1,2], Huitang Yang[1,2], Yandong Cai[1,2], Guoju Fan[1,2], Kaiqiang Wang[1,2], Hongwei Zhang[1,2], Hailong Hu[4,5] and Yankui Li[1,2*]

[1]Department of Vascular Surgery, The Second Hospital of Tianjin Medical University, Tianjin, China, [2]Center for Cardiovascular Diseases, The Second Hospital of Tianjin Medical University, Tianjin, China, [3]Clinical Medical College, Hebei University, Baoding, Hebei, China, [4]Department of Urology, The Second Hospital of Tianjin Medical University, Tianjin, China, [5]Tianjin Key Laboratory of Urology, Tianjin Institute of Urology, Tianjin, China

Objective: This study evaluated C-reactive protein (CRP) in hospitalized patients with bladder cancer (BC) and explored the predictive value of CRP for venous thromboembolism (VTE), combining CRP and D-dimer (D-D) levels to improve the ability to predict the risk of VTE in BC patients, thereby better guiding clinical prevention and treatment of this disease.

Methods: Clinical data from 4,438 patients with BC admitted between January 2015 and December 2020 were reviewed. After screening, 2,164 patients remained.52 VTE cases were identified, and 104 matched controls were selected (1:2 ratio). Conditional logistic regression, receiver operating characteristic (ROC) curve analysis, stratified analysis, and interaction tests were conducted to assess predictive performance and control for confounding bias.

Results: Conditional logistic regression analysis indicated that elevated CRP and D-D levels were associated with higher risk of VTE in hospitalized patients with BC. Moreover, the areas under the ROC curves were 0.734 for CRP, 0.817 for D-D, and 0.865 for the combined model, indicating that the combined model offers superior predictive performance. Stratified and interaction analyses further revealed that the predictive value of CRP and D-D levels was influenced by the infection status.

Conclusion: Elevated CRP and D-D levels may be potential indicators of VTE in BC patients. Their combined use improves predictive accuracy, and their predictive value may be better in non-infected patients.

KEYWORDS

venous thromboembolism, C-reactive protein, d-dimer, bladder cancer, inflammation, immune system

1 Introduction

Venous thromboembolism (VTE) is a serious clinical condition that includes deep vein thrombosis (DVT) and pulmonary embolism (PE) (1, 2). In cancer patients, the risk of VTE ranges from 3% to 5% in early-stage disease and up to 30% in advanced-stage or metastatic cancer (3, 4). The overall incidence of VTE in patients with bladder cancer (BC) ranges from 0.4% to 4.7% (5, 6). VTE is not only a disorder of coagulation but also a complex immunoinflammatory process (7–9). In patients with BC, the development of VTE involves multiple interrelated factors, such as tumor biology, treatment modalities, and patient-specific characteristics (10–12). Without early identification and prevention, severe VTE events, such as pulmonary embolism, can lead to sudden death or disrupt the course of cancer treatment (13, 14). Therefore, early screening of high-risk individuals and timely initiation of anticoagulant prophylaxis are crucial to reduce VTE incidence, improve patients' quality of life, and enhance clinical outcomes, making them vital components of comprehensive cancer management (15, 16).

VTE is increasingly recognized as a classic example of immunothrombosis, in which systemic inflammation significantly elevates thrombotic risk (17, 18). C-reactive protein (CRP)—a highly conserved member of the pentraxin family—is widely used as a biomarker of infection and inflammation in clinical practice and is typically measured using either traditional or high-sensitivity CRP assays (19–21). CRP possesses both proinflammatory and prothrombotic properties and plays a central role in the pathogenesis of arterial and venous thrombosis (20, 22). D-dimer (D-D)—a soluble fibrin degradation product generated through plasmin-mediated fibrinolysis of cross-linked fibrin—is a well-established biomarker of coagulation activation and secondary fibrinolysis (23, 24). Elevated plasma D-D levels have frequently been associated with the pathophysiology of VTE (25, 26). Research suggests that CRP and D-D may be potential prognostic biomarkers for patients with cancer and for the recurrence of VTE after discontinuation of anticoagulant therapy in cancer-related thrombosis (27–29).

An individualized medical approach that integrates immunological and coagulation markers may offer a superior strategy for preventing and managing VTE in patients with BC (30). However, the current guideline-based evidence for VTE risk assessment in patients with BC remains limited. Therefore, this study aimed to explore the predictive value of CRP and D-D levels, individually and in combination, for VTE in patients with BC. We hypothesize that evaluating these markers in combination will improve the accuracy of early-risk identification and screening, reduce the incidence of VTE and related mortality, and ultimately improve clinical outcomes for patients.

2 Materials and methods

2.1 Patient source

This study initially screened 4,438 patients diagnosed with BC who were admitted to the Department of Urology at our hospital between January 2015 and December 2020. After applying the inclusion and exclusion criteria, 2,164 patients were eligible for further analysis. Of these, 52 patients were selected for the VTE group based on in-hospital imaging results, and patients without VTE (controls) were selected and matched in a 1:2 ratio, considering age, sex, and cancer stage, yielding a final study population of 156 patients (Figure 1).

2.2 Patient screening criteria

The inclusion criteria were as follows: (1) A confirmed diagnosis of BC by pathological examination, (2) color Doppler ultrasound (CDU) and/or computed tomography angiography (CTA) were utilized to ascertain that patients had no VTE upon admission, (3) non-use of anticoagulants or antiplatelet medications within one month, and (4) availability of plasma CRP test results (immunoturbidimetric method was used for CRP detection in our hospital; CRP reference range: 0–10 mg/L). The exclusion criteria were as follows: (1) The patient had other tumors besides BC, (2) patients with VTE upon hospital admission, (3) predicted life expectancy of less than 6 months, (4) presence of active bleeding, (5) immune system-related diseases, and (6) incomplete clinical and imaging data.

2.3 Data collection

Patients' clinical characteristics, including, but not limited to, age, sex, body mass index (BMI), cancer stage, history of lifestyle or related disease (alcohol consumption, smoking, diabetes mellitus, and hypertension), infection, CRP level, D-D level, surgery received, and medications administered, were extracted from the electronic medical record system of our hospital. Patients identified as high risk (Caprini risk score ≥ 5) routinely underwent lower limb venous CDU screening. For those presenting with chest pain, cough, or dyspnea in addition to lower limb DVT, pulmonary CTA was performed to assess for PE.

2.4 Statistical analysis

R software (version 4.4.0; R Foundation for Statistical Computing, Vienna, Austria) was used for statistical analysis. Continuous data are shown as the mean ± standard deviation (SD). Student's t-test was used for normally distributed data and the Mann–Whitney U test for non-normally distributed data. All categorical data are shown as frequencies and rates, and the chi-square (χ^2) test was used to assess comparisons between groups. Conditional logistic regression analysis was applied, and receiver operating characteristic (ROC) curves were constructed to evaluate the discriminatory ability of CRP, D-D, and their combination in predicting VTE. In addition, stratified analysis and interaction

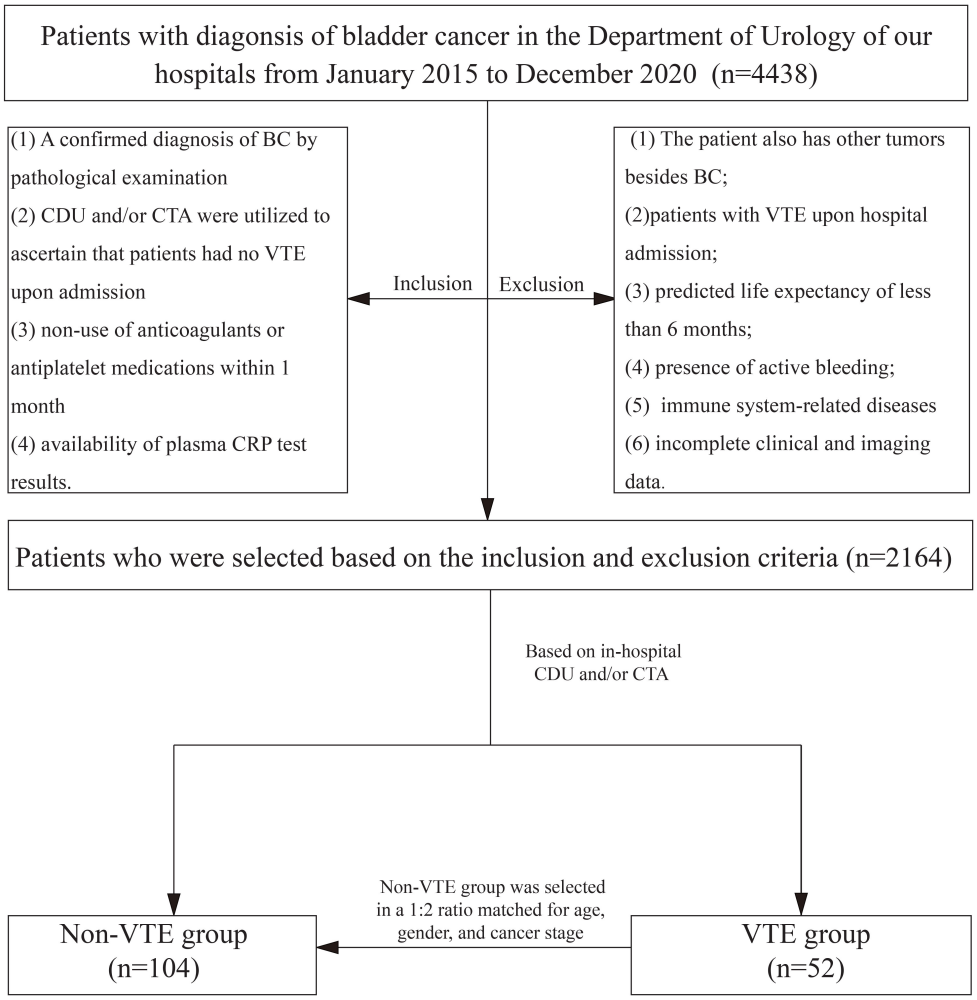

FIGURE 1
Flowchart for the enrolled patients.

testing were performed to assess whether infection status modified the associations between CRP, D-D, and VTE risk.

3 Results

The baseline characteristics of the enrolled patients are summarized in Table 1, along with comparative outcomes between the VTE and non-VTE groups. A total of 156 patients were included in this study: 52 patients with VTE and 104 without VTE. Among the 52 patients with VTE, 3 had PE (with concurrent DVT), and all 52 had DVT: 43 patients had below-knee venous thrombosis (including posterior tibial vein, anterior tibial vein, peroneal vein, and intermuscular vein), 2 had popliteal vein thrombosis, and 7 had femoral vein thrombosis. The VTE and non-VTE groups were similar regarding baseline characteristics, including age, sex, BMI, cancer stage, and history of smoking, alcohol consumption, hypertension, and surgeries and medications received, indicating that the matching method applied was appropriate (Table 1). However, after matching, statistically significant differences remained in the history of diabetes mellitus, CRP level, and D-D level between the VTE and non-VTE groups ($p < 0.05$).

To explore the potential of CRP and D-D as predictive markers of VTE in hospitalized patients with BC, we performed a conditional logistic regression analysis. The clinical data of patients with BC were included in the conditional logistic regression analysis to identify predictors of in-hospital VTE. Age, sex, BMI, cancer stage, alcohol consumption, smoking history, diabetic status, hypertension history, infection status, CRP level, D-D level, surgery received, and medications administered were input as independent variables in the conditional logistic analysis, with the in-hospital VTE incidence as the dependent variable. Elevated CRP and D-D levels were independently associated with an increased risk of VTE ($p < 0.05$). These results suggest that CRP

10.3389/fimmu.2025.1652139

TABLE 1 Baseline characteristics and different treatments of enrolled patients.

Characteristics	Non-VTE group (n=104)	VTE group (n=52)	p
Age, Mean ± SD	71.42 ± 7.67	71.50 ± 7.44	0.952
Sex, n (%)			
male	82 (78.85%)	41 (78.85%)	1.000
female	22 (21.15%)	11 (21.15%)	
BMI, Mean ± SD	23.51 ± 2.82	24.02 ± 2.58	0.259
Smoking history, n (%)	44 (42.31%)	23 (44.23%)	0.954
Alcohol consumption, n (%)	21 (20.19%)	16 (30.77%)	0.206
Hypertension, n (%)	46 (44.23%)	23 (44.23%)	1.000
Diabetes mellitus, n (%)	15 (14.425%)	18 (34.62%)	0.007**
Infection, n (%)	31 (29.82%)	14 (26.92%)	0.851
CRP, Mean ± SD	19.37 ± 30.14	81.58 ± 176.92	0.015*
D-D, Mean ± SD	0.8 ± 1	4.64 ± 11.34	0.018*
Surgery, n (%)			
TURBT	51 (49.08%)	21 (40.38%)	0.577
RC	26 (25.00%)	16 (30.77%)	
Medications, n (%)			
Chemotherapy alone	59 (56.73%)	26 (50.00%)	0.075
Chemotherapy + Immunotherapy	13 (12.50%)	14 (26.92%)	
Cancer stages, n (%)			
I	26 (25.00%)	13 (25.00%)	1.000
II	48 (46.15%)	24 (46.15%)	
III	24 (23.08%)	12 (23.08%)	
IV	6 (5.77%)	3 (5.77%)	

*p<0.05 **p<0.01 BMI, body mass index; CRP, C-reactive protein; D-D, D-dimer; TURBT, transurethral resection of bladder tumor; RC, radical cystectomy; VTE, venous thromboembolism.

and D-D levels may serve as valuable predictive markers of VTE in patients with BC (Table 2).

ROC curves were constructed to evaluate the predictive ability of CRP levels, D-D levels, and their combination for VTE in patients with BC. The area under the curve (AUC) values were 0.734 for CRP, 0.817 for D-D, and 0.865 for the combined model, indicating that the combined index had the highest discriminatory ability. These results suggest that integrating CRP and D-D levels may improve the predictive performance of VTE risk stratification in this population (Figure 2).

TABLE 2 Conditional logistic regression analysis for VTE in patients with bladder cancer.

Variable	Beta.	OR	95% CI	p
CRP	0.023	1.024	0.009–0.038	0.002**
D-D	0.65	1.915	0.287–1.013	<0.001**

**p<0.01 CRP, C-reactive protein; D-D, D-dimer; OR, odds ratio; CI, confidence interval; VTE, venous thromboembolism.

To minimize the potential confounding effect of infection, a stratified analysis was conducted based on the infection status. The results indicated that both CRP and D-D levels were significantly associated with VTE in the non-infected group ($p < 0.05$), whereas no such associations were observed in the infected group ($p > 0.05$). These findings support that CRP and D-D plasma levels may serve as reliable predictive markers for VTE in patients with BC without infection (Supplementary Table S1).

Interaction analysis confirmed the modifying effect of infection on the predictive value of the CRP level. A significant interaction was observed between CRP levels and infection ($p = 0.003$), indicating that the infection status may attenuate the predictive ability of the CRP level for VTE. In contrast, no significant interaction was found between D-D and infection ($p = 0.313$), suggesting that the D-D level remains a relatively stable predictor, regardless of infection status (Supplementary Table S2).

4 Discussion

VTE is not only a manifestation of abnormal coagulation but also a classic process of immunothrombosis, involving complex interactions between the inflammatory and coagulation systems (31, 32). In patients with malignancies, such as BC, the risk of VTE is significantly increased due to tumor-induced hypercoagulability, prolonged immobilization, surgical intervention, and chemotherapy (33, 34). Identifying biomarkers that simultaneously reflect inflammation and coagulation status is crucial for early prediction and prevention of VTE in high-risk populations.

CRP, an acute-phase reactant, is a sensitive marker of systemic inflammation that promotes thrombosis by enhancing endothelial dysfunction, activating coagulation pathways, and impairing fibrinolysis (35, 36). In the present study, elevated CRP level in the absence of infection was statistically significantly associated with VTE in hospitalized patients with BC ($p < 0.01$), suggesting its potential utility as a predictive marker. This finding is consistent with that of a previous report highlighting the predictive role of CRP in thrombogenesis (36). CRP measurement is cost-effective, widely available, and easy to

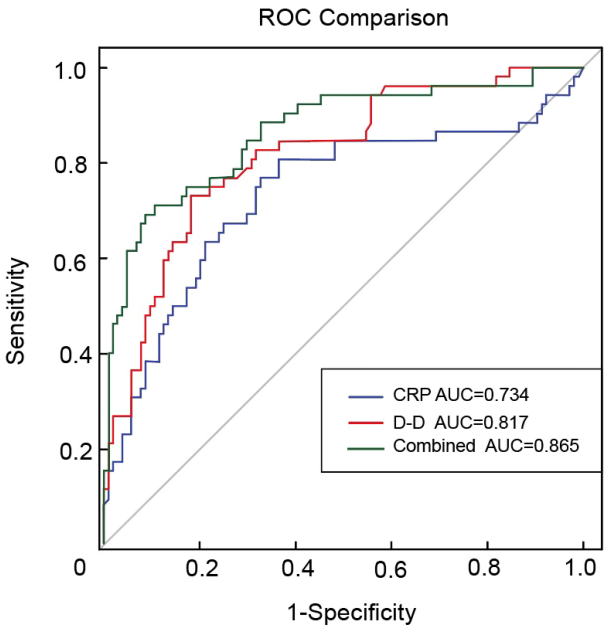

FIGURE 2
ROC curves for CRP, D-D, and their combination in predicting VTE in bladder cancer. ROC, receiver operating characteristic; CRP, C-reactive protein; D-D, D-dimer; VTE, venous thromboembolism.

perform in clinical settings (37, 38). However, in the current study, stratified analysis by infection status showed that infection may attenuate the specificity of CRP ($p > 0.05$), and an interaction test further confirmed the significant modifying effect of infection on the CRP–VTE association ($p < 0.05$). These findings highlight the importance of considering background inflammatory conditions when interpreting CRP levels in clinical practice.

This study is the first to assess the risk of VTE in patients with BC using CRP and D-D levels combined, addressing not only coagulation dysfunction but also the immunoinflammatory aspects of thrombosis. Our study revealed a statistically significant association between elevated D-D levels and VTE incidence, consistent with the findings of previous studies (39, 40). ROC curve analysis revealed AUCs of 0.734 for CRP, 0.817 for D-D, and 0.865 for the combined model. The combination of CRP and D-D significantly improved the predictive performance of the model compared to either marker alone, suggesting that integrating inflammatory and coagulation markers may enhance the clinical utility of risk assessment models. This combined approach may improve the efficiency of VTE screening in patients with BC. This further supports the development of more precise preventive strategies by highlighting the importance of managing thromboinflammatory responses in parallel with anticoagulation therapy, with the aim of lowering the incidence and mortality of VTE.

These findings suggest that CRP and D-D levels are promising biomarkers for individualized VTE risk assessment in patients with BC. However, there are some limitations to this study. First, the retrospective design did not fully exclude patient heterogeneity in reasons for hospitalization. We plan to address this issue further in future research by collecting data from a large number of patients and conducting more rigorous stratified analyses. Second, due to the retrospective nature of the study and limited availability of clinical data, time series data was unavailable for most patients. To enhance the reliability and clinical relevance of these findings, future prospective multicenter studies incorporating dynamic biomarker monitoring are needed.

5 Conclusion

This study demonstrated that elevated CRP and D-D levels were statistically associated with an increased risk of VTE in hospitalized patients with BC. Our findings suggest that integrating CRP and D-D levels may provide a useful strategy for the early identification and risk stratification of VTE in BC, particularly in patients without infection.

Data availability statement

The original contributions presented in the study are included in the article/Supplementary Material. Further inquiries can be directed to the corresponding author/s.

Ethics statement

The studies involving humans were approved by The Ethics Committee of the Second Hospital of Tianjin Medical University (approval number KY2024K211 from 15 April 2024). The studies were conducted in accordance with the local legislation and institutional requirements. The ethics committee/institutional review board waived the requirement of written informed consent for participation from the participants or the participants' legal guardians/next of kin because The Ethics Committee confirmed that the waiver of informed consent would not adversely affect the rights, welfare, or health of the study participants.

Author contributions

BC: Conceptualization, Investigation, Methodology, Writing – original draft. TZ: Data curation, Formal Analysis, Methodology, Writing – original draft. YW: Data curation, Formal Analysis, Writing – original draft. ZL: Formal Analysis, Investigation, Writing – original draft. HL: Visualization, Writing – original draft, Investigation. ZJ: Writing – review & editing, Data curation, Software. HY: Software, Visualization, Writing – original draft. YC: Writing – review & editing, Validation, Investigation. GF: Writing – review & editing, Software, Validation. KW: Project administration, Writing – review & editing, Validation. HZ: Supervision, Writing – review & editing, Project administration. HH: Resources, Supervision, Writing – review & editing. YL: Conceptualization, Funding acquisition, Methodology, Supervision, Writing – review & editing.

Funding

The author(s) declare financial support was received for the research and/or publication of this article. This research was funded by the Tianjin Health Research Project, grant number TJWJ2024ZK002; the Special Project of Beijing-Tianjin-Hebei Basic Research Cooperation (Tianjin Science and Technology Project), grant number 23JCZXJC00160.

Conflict of interest

The authors declare that the research was conducted in the absence of any commercial or financial relationships that could be construed as a potential conflict of interest.

Generative AI statement

The author(s) declare that no Generative AI was used in the creation of this manuscript.

Any alternative text (alt text) provided alongside figures in this article has been generated by Frontiers with the support of artificial intelligence and reasonable efforts have been made to ensure accuracy, including review by the authors wherever possible. If you identify any issues, please contact us.

Publisher's note

Supplementary material

The Supplementary Material for this article can be found online at: https://www.frontiersin.org/articles/10.3389/fimmu.2025.1652139/full#supplementary-material

References

1. Key NS, Khorana AA, Kuderer NM, Bohlke K, Lee AYY, Arcelus JI, et al. Venous thromboembolism prophylaxis and treatment in patients with cancer: ASCO clinical practice guideline update. *J Clin Oncol*. (2020) 38:496–520. doi: 10.1200/JCO.19.01461

2. Key NS, Khorana AA, Kuderer NM, Bohlke K, Lee AYY, Arcelus JI, et al. Venous thromboembolism prophylaxis and treatment in patients with cancer: ASCO guideline update. *J Clin Oncol*. (2023) 41:3063–71. doi: 10.1200/JCO.23.00294

3. Bailey AJM, Luo OD, Zhou SQ, Wells PS. The incidence and risk of venous thromboembolism in patients with active Malignancy and isolated superficial venous thrombosis: a systematic review and meta-analysis (the IROVAM-iSVT review). *J Thromb Haemost*. (2025) 23:1824–37. doi: 10.1016/j.jtha.2025.03.019

4. Wan T, Song J, Zhu D. Cancer-associated venous thromboembolism: a comprehensive review. *Thromb J*. (2025) 23:35. doi: 10.1186/s12959-025-00719-7

5. Zareba P, Duivenvoorden WCM, Pinthus JH. Thromboembolism in patients with bladder cancer: incidence, risk factors and prevention. *Bladder Cancer*. (2018) 4:139–47. doi: 10.3233/BLC-170146

6. Abdullah O, Parashar D, Mustafa IJ, Young AM. Venous thromboembolism rate in patients with bladder cancer according to the type of treatment: A systematic review. *Cureus*. (2022) 14:e22945. doi: 10.7759/cureus.22945

7. Loo J, Spittle DA, Newnham M. COVID-19, immunothrombosis and venous thromboembolism: biological mechanisms. *Thorax*. (2021) 76:412–20. doi: 10.1136/thoraxjnl-2020-216243

8. Dix C, Zeller J, Stevens H, Eisenhardt SU, Shing K, Nero TL, et al. C-reactive protein, immunothrombosis and venous thromboembolism. *Front Immunol*. (2022) 13:1002652. doi: 10.3389/fimmu.2022.1002652

9. Grover SP, Brill A. Editorial: Inflammation and immune factors in venous thromboembolism. *Front Immunol*. (2025) 16:1616253. doi: 10.3389/fimmu.2025.1616253

10. Di Nisio M, Candeloro M, Rutjes AWS, Porreca E. Venous thromboembolism in cancer patients receiving neoadjuvant chemotherapy: a systematic review and meta-analysis. *J Thromb Haemost*. (2018) 16:1336–46. doi: 10.1111/jth.14149

11. Klaassen Z, Wallis CJD, Lavallée LT, Violette PD. Perioperative venous thromboembolism prophylaxis in prostate cancer surgery. *World J Urol*. (2020) 38:593–600. doi: 10.1007/s00345-019-02705-x

12. Girardi L, Wang TF, Ageno W, Carrier M. Updates in the incidence, pathogenesis, and management of cancer and venous thromboembolism. *Arterioscler Thromb Vasc Biol*. (2023) 43:824–31. doi: 10.1161/ATVBAHA.123.318779

13. Felix G, Ferreira E, Ribeiro A, Guerreiro I, Araújo E, Ferreira S, et al. Predictors of cancer in patients with acute pulmonary embolism. *Thromb Res*. (2023) 230:11–7. doi: 10.1016/j.thromres.2023.08.005

14. Starling S., Marshall L. Pulmonary embolism. *Nat Rev Dis Primers*. (2018) 4:18031. doi: 10.1038/nrdp.2018.31

15. O'Connell C, Escalante CP, Goldhaber SZ, McBane R, Connors JM, Raskob GE. Treatment of cancer-associated venous thromboembolism with low-molecular-weight heparin or direct oral anticoagulants: patient selection, controversies, and caveats. *Oncologist*. (2021) 26:e8–e16. doi: 10.1002/onco.13584

16. Lyman GH, Carrier M, Ay C, Di Nisio M, Hicks LK, Khorana AA, et al. American Society of Hematology 2021 guidelines for management of venous thromboembolism: prevention and treatment in patients with cancer. *Blood Adv*. (2021) 5:927–74. doi: 10.1182/bloodadvances.2020003442

17. Potere N, Abbate A, Kanthi Y, Carrier M, Toldo S, Porreca E, et al. Inflammasome signaling, thromboinflammation, and venous thromboembolism. *JACC Basic Transl Sci*. (2023) 8:1245–61. doi: 10.1016/j.jacbts.2023.03.017

18. Heestermans M, Poenou G, Duchez AC, Hamzeh-Cognasse H, Bertoletti L, Cognasse F. Immunothrombosis and the role of platelets in venous thromboembolic diseases. *Int J Mol Sci*. (2022) 23:13176. doi: 10.3390/ijms232113176

19. Rajab IM, Hart PC, Potempa LA. How C-reactive protein structural isoforms with distinctive bioactivities affect disease progression. *Front Immunol*. (2020) 11:2126. doi: 10.3389/fimmu.2020.02126

20. Zhou HH, Tang YL, Xu TH, Cheng B. C-reactive protein: structure, function, regulation, and role in clinical diseases. *Front Immunol*. (2024) 15:1425168. doi: 10.3389/fimmu.2024.1425168

21. Pepys MB, Hirschfield GM. C-reactive protein: a critical update. *J Clin Invest*. (2003) 111:1805–12. doi: 10.1172/JCI200318921

22. Guan Y, Gan Z, Li S, Cao X, Zeng A, Li J, et al. C-reactive protein, genetic susceptibility, and the long-term risk of venous thromboembolism in patients with past cancer. *Thromb Haemost*. (2024). doi: 10.1055/a-2495-1350

23. Kim AS, Khorana AA, McCrae KR. Mechanisms and biomarkers of cancer-associated thrombosis. *Transl Res*. (2020) 225:33–53. doi: 10.1016/j.trsl.2020.06.012

24. Favresse J, Lippi G, Roy PM, Chatelain B, Jacqmin H, Ten Cate H, et al. D-dimer: Preanalytical, analytical, postanalytical variables, and clinical applications. *Crit Rev Clin Lab Sci*. (2018) 55:548–77. doi: 10.1080/10408363.2018.1529734

25. Franchini M, Focosi D, Pezzo MP, Mannucci PM. How we manage a high D-dimer. *Haematologica*. (2024) 109:1035–45. doi: 10.3324/haematol.2023.283966

26. Yang H, Zhang T, Li Z, Cai Y, Jiang Z, Fan G, et al. Risk factors for in-hospital venous thromboembolism in patients with bladder cancer: A retrospective single-center study. *BMC Cancer*. (2025) 25:536. doi: 10.1186/s12885-025-13939-x

27. Jara-Palomares L, Solier-Lopez A, Elias-Hernandez T, Asensio-Cruz MI, Blasco-Esquivias I, Sanchez-Lopez V, et al. D-dimer and high-sensitivity C-reactive protein levels to predict venous thromboembolism recurrence after discontinuation of anticoagulation for cancer-associated thrombosis. *Br J Cancer*. (2018) 119:915–21. doi: 10.1038/s41416-018-0269-5

28. Gon Y, Sakaguchi M, Takasugi J, Kawano T, Kanki H, Watanabe A, et al. Plasma D-dimer levels and ischaemic lesions in multiple vascular regions can predict occult cancer in patients with cryptogenic stroke. *Eur J Neurol*. (2017) 24:503–8. doi: 10.1111/ene.13234

29. Shen Q, Dong X, Tang X, Zhou J. Risk factors and prognosis value of venous thromboembolism in patients with advanced non-small cell lung cancer: a case-control study. *J Thorac Dis*. (2017) 9:5068–74. doi: 10.21037/jtd.2017.11.116

30. Balan D, Vartolomei MD, Magdás A, Balan-Bernstein N, Voidăzan ST, Mártha O. Inflammatory markers and thromboembolic risk in patients with non-muscle-invasive bladder cancer. *J Clin Med*. (2021) 10:5270. doi: 10.3390/jcm10225270

31. Stark K, Massberg S. Interplay between inflammation and thrombosis in cardiovascular pathology. *Nat Rev Cardiol*. (2021) 18:666–82. doi: 10.1038/s41569-021-00552-1

32. Gauchel N, Krauel K, Hamad MA, Bode C, Duerschmied D. Thromboinflammation as a driver of venous thromboembolism. *Hamostaseologie*. (2021) 41:428–32. doi: 10.1055/a-1661-0257

33. Fernandes CJ, Morinaga LTK, Alves JLJ, Castro MA, Calderaro D, Jardim CVP, et al. Cancer-associated thrombosis: the when, how and why. *Eur Respir Rev*. (2019) 28:180119. doi: 10.1183/16000617.0119-2018

34. Mulder FI, Horváth-Puhó E, van Es N, van Laarhoven HWM, Pedersen L, Moik F, et al. Venous thromboembolism in cancer patients: a population-based cohort study. *Blood*. (2021) 137:1959–69. doi: 10.1182/blood.2020007338

35. Rizo-Téllez SA, Sekheri M, Filep JG. C-reactive protein: a target for therapy to reduce inflammation. *Front Immunol*. (2023) 14:1237729. doi: 10.3389/fimmu.2023.1237729

36. Ding J, Yue X, Tian X, Liao Z, Meng R, Zou M. Association between inflammatory biomarkers and venous thromboembolism: a systematic review and meta-analysis. *Thromb J*. (2023) 21:82. doi: 10.1186/s12959-023-00526-y

37. Plebani M. Why C-reactive protein is one of the most requested tests in clinical laboratories? *Clin Chem Lab Med*. (2023) 61:1540–5. doi: 10.1515/cclm-2023-0086

38. Horvei LD, Grimnes G, Hindberg K, Mathiesen EB, Njølstad I, Wilsgaard T, et al. C-reactive protein, obesity, and the risk of arterial and venous thrombosis. *J Thromb Haemost*. (2016) 14:1561–71. doi: 10.1111/jth.13369

39. Chopard R, Albertsen IE, Piazza G. Diagnosis and treatment of lower extremity venous thromboembolism: A review. *Jama*. (2020) 324:1765–76. doi: 10.1001/jama.2020.17272

40. Tikkinen KAO, Craigie S, Agarwal A, Siemieniuk RAC, Cartwright R, Violette PD, et al. Procedure-specific risks of thrombosis and bleeding in urological non-cancer surgery: systematic review and meta-analysis. *Eur Urol*. (2018) 73:236–41. doi: 10.1016/j.eururo.2017.02.025

Frontiers in Immunology

Explores novel approaches and diagnoses to treat immune disorders.

The official journal of the International Union of Immunological Societies (IUIS) and the most cited in its field, leading the way for research across basic, translational and clinical immunology.

Discover the latest Research Topics

See more →

Frontiers

Avenue du Tribunal-Fédéral 34
1005 Lausanne, Switzerland
frontiersin.org

Contact us

+41 (0)21 510 17 00
frontiersin.org/about/contact